Dating the Stones: Developing Software Solutions for Thermoluminescence Dating and Improving Age Estimation of Heated Flint Samples

Inaugural-Dissertation

zur

Erlangung des Doktorgrades

der Mathematisch-Naturwissenschaftlichen Fakultät

der Universität zu Köln



vorgelegt von

David Strebler

aus Brüssel, Belgien

Köln, Dezember 2023

Berichterstatter:	Prof. Dr. Helmut Brückner
	Prof. Dr. Gerd-Christian Weniger
Tag der letzten mündlichen Prüfung:	31. Januar 2022

Diese Arbeit wurde von der Mathematisch-Naturwissenschaftlichen Fakultät der Universität zu Köln im Jahr 2021 als Dissertation angenommenen.

Erklärung zur Dissertation

gemäß der Promotionsordnung vom 12. März 2020

„Hiermit versichere ich an Eides statt, dass ich die vorliegende Dissertation selbstständig und ohne die Benutzung anderer als der angegebenen Hilfsmittel und Literatur angefertigt habe. Alle Stellen, die wörtlich oder sinngemäß aus veröffentlichten und nicht veröffentlichten Werken dem Wortlaut oder dem Sinn nach entnommen wurden, sind als solche kenntlich gemacht. Ich versichere an Eides statt, dass diese Dissertation noch keiner anderen Fakultät oder Universität zur Prüfung vorgelegen hat; dass sie - abgesehen von unten angegebenen Teilpublikationen und eingebundenen Artikeln und Manuskripten - noch nicht veröffentlicht worden ist sowie, dass ich eine Veröffentlichung der Dissertation vor Abschluss der Promotion nicht ohne Genehmigung des Promotionsausschusses vornehmen werde. Die Bestimmungen dieser Ordnung sind mir bekannt. Darüber hinaus erkläre ich hiermit, dass ich die Ordnung zur Sicherung guter wissenschaftlicher Praxis und zum Umgang mit wissenschaftlichem Fehlverhalten der Universität zu Köln gelesen und sie bei der Durchführung der Dissertation zugrundeliegenden Arbeiten und der schriftlich verfassten Dissertation beachtet habe und verpflichte mich hiermit, die dort genannten Vorgaben bei allen wissenschaftlichen Tätigkeiten zu beachten und umzusetzen. Ich versichere, dass die eingereichte elektronische Fassung der eingereichten Druckfassung vollständig entspricht. “

Teilpublikationen

Strebler, D. *et al.* (2017) Using R for TL dating. *Quaternary Geochronology*, 37, 97–107.

Strebler, D. *et al.* (2019) Using DRAC in complex geometries - TL dating of heated flints from Taibeh, Jordan. *Quaternary Geochronology*, 49, 4–7.

Strebler, D. et al. (2019) LumReader: Designing your luminescence experiment with R. *Radiation Measurements*, 129, 106143.

Weitere Publikation

Zander, A. Strebler, D. *et al.* (2019) Roman traces in Germania magna: New thermoluminescence and $pIRIR_{290}$ data from a lime kiln at Bergisch Gladbach, Germany, *Archaeometry*, 61, 506– 518.

Brüssel, den 11. November 2021 Unterschrift



"People assume that time is a strict progression of cause to effect, but actually from a non-linear, non-subjective viewpoint – it's more like a big ball of wibbly-wobbly... timey-wimey... stuff."

The Doctor, *Doctor Who* (TV series), 2007.

In memory of Marie-Jeanne Strebler Burgy (1933-2023)

Abstract

Establishing a robust chronology is key to improving our understanding of the past. It requires not only reliable absolute dating methods but also a proper assessment of the connection between the events of interest and the dated events. There is evidence that the dispersal of anatomically modern humans (AMH), who had evolved around 300 ka to 200 ka in East Africa, occurred in several advances across the Levant, finally reaching central Europe around 45 ka cal BP. Luminescence dating is one of the few absolute dating methods capable of covering the full time range of these migrations. While optically stimulated luminescence (OSL) is more suitable for sediment dating because of faster signal resetting, thermoluminescence (TL) remains the method of choice when dating heated or burnt materials.

In prehistoric settings, most sedimentary deposits are not directly related to anthropogenic activity but are rather the result of natural processes. Heated lithics, and especially heated flint, are common in most human occupation layers, sometimes even ubiquitous. The burning or heating of these artefacts is quite systematically the direct consequence of human activities. Therefore, the dating of these heated flint samples by thermoluminescence provides age estimates for well-defined anthropogenic events.

TL dating of heated flint samples can be challenging. In particular, the lack of user-optimised analysis software for TL data has exacerbated the decline of TL dating in comparison to OSL dating. In this thesis, two new software solutions specifically designed to improve and facilitate TL dating are presented. Initially developed for the dating of heated flint samples, these two software solutions were designed to be easily updated and enhanced. The tools they provide can be used or adapted to most of the settings where TL dating is the method of choice.

LumReader is an **R** package designed to simulate both the detection properties of luminescence readers and the emission properties of materials. It allows the optimisation of the experimental detection window for a given filter and detector combination through comparison of the detection window, the stimulation signal and the luminescence emission of the studied material.

TLdating is an **R** package specifically dedicated to thermoluminescence dating. It allows the processing of all the data needed to estimate an age using thermoluminescence, from the estimation of the equivalent dose (D_e) based on the thermoluminescence curve signals

provided by a semi-automated TL/OSL reader to the estimation of the annual dose rate ($\dot{D}$) using radionuclide concentrations or in-situ dose rate measurements.

This thesis presents several case studies. It also provides new luminescence ages for four archaeological sites:

From the archaeological site of Taibeh 3, Jordan, a series of heated flint samples were collected. The *LumReader* package is used to identify the best filter combination to maximise the luminescence signal and minimise the signal-to-noise ratio. It allows to optimize the signal from the fine grain aliquots that are used to estimate a specific α-efficiency (a-value) for each heated flint sample. The *TLdating* package was used to estimate the equivalent dose, the a-value and the dose rate. It provides an age estimate for five of these heated flint samples. These age estimates were mostly consistent with the radiocarbon ages of charcoal samples coming from the same occupation layers.

From the archaeological sites of Ansab 1 and 2, Jordan, a series of heated flint and sediment samples were collected. OSL age estimates are provided for the sediment samples using the *Luminescence* package. They complete the current chronology of these two open-air sites. The *TLdating* package was used to estimate an equivalent dose for two of the heated flint samples. No final age estimates are proposed due to the lack of reliable dose rate estimates for these samples. However, this fieldwork provides an opportunity to explore the limitations of heated flint dating. Finally, this study presents an improved sample preparation protocol.

In Bergisch Gladbach, Germany, four samples of sediment and one of architectural ceramics were collected. The newly developed *TLdating* package is used to assess an equivalent dose estimation for each of these samples using thermoluminescence. In addition, the equivalent dose values are estimated for each of these samples using post-infrared, infrared stimulated luminescence. The different equivalent dose estimates are largely in agreement with each other and the resulting age estimates agree with the expected chronology.

Zusammenfassung

Die Etablierung einer soliden Chronologie ist essentiell für ein besseres Verständnis der Geschichte. Dafür braucht es nicht nur verlässliche Datierungsmethoden, sondern auch die korrekte Einschätzung des Zusammenhangs zwischen bereits datierten Vorkommnissen und den zu untersuchenden. Es gibt Hinweise darauf, dass die Ausbreitung des anatomisch modernen Menschen (AMH), der sich etwa 300 ka bis 200 ka in Ostafrika entwickelt hatte, in mehreren Vorstößen über die Levante erfolgte und schließlich Mitteleuropa um 45 ka cal BP erreichte. Die Lumineszenzdatierung ist eine der wenigen existierenden Methoden, die den gesamten Zeitraum des AMH abdecken kann. Für die Datierung von Sedimenten eignet sich optisch stimulierte Lumineszenz (OSL) wegen der schnelleren Signal-Rücksetzung besser, aber für erhitzte und gebrannte Materialien ist Thermolumineszenz (TL) die Methode der Wahl.

Prähistorische Sedimentablagerungen wurden nur selten von Menschen verursacht, sondern vielmehr durch natürliche Umstände. Im Gegensatz dazu ist erhitztes und gebranntes Material, vor allem Feuerstein/Flint, eine Folge menschlicher Aktivitäten und in entsprechenden Sedimentschichten weit verbreitet zu finden. Die Datierung erhitzter Feuersteine mittels Thermolumineszenz ermöglicht damit die zeitliche Einordnung derartiger anthropogener Ereignisse.

Eine Problematik der Thermolumineszenz-Datierung ist der Mangel an benutzerfreundlicher Analyse-Software - ein Grund, weshalb immer weniger Gebrauch von TL gegenüber OSL gemacht wird, um Altersabschätzungen zu erhalten. In dieser Dissertation werden zwei Software-Lösungen präsentiert, die entwickelt wurden, um die Datierung mittels TL zu verbessern. Entwickelt für die Feuerstein-Datierung sind die Softare-Pakete leicht zu erweitern und zu aktualisieren. Die damit verfügbaren Tools eignen sich für die Nutzung und Anpassung an die meisten Settings, in denen die TL-Datierung angewandt wird.

LumReader ist ein **R** Package, entwickelt für die Simulation der Detektoreigenschaften von Lumineszenz-Readern und den Emissionseigenschaften von Materialien. Es ermöglicht die Optimierung des experimentellen Nachweisfensters für eine bestimmte Filter- und Detektorkombination durch Vergleich des Nachweisfensters, des Stimulationssignals und der Lumineszenzemission des untersuchten Materials.

TLdating ist ein speziell für die Thermolumineszenz-Datierung entwickeltes **R** Package. Es ermöglicht die Verarbeitung aller Daten, die für die Abschätzung eines Alters mittels Thermolumineszenz erforderlich sind, von der Abschätzung der Äquivalentdosis (D_e)

auf Grundlage der von einem halbautomatischen TL/OSL-Reader gelieferten Thermolumineszenzkurvensignale bis zur Abschätzung der jährlichen Dosisleistung ($\dot{D}$) anhand von Radionuklidkonzentrationen oder in-situ Messungen der Dosisleistung.

In der vorliegenden Dissertation werden mehrere Fallstudien und neue Lumineszenz-Alter für vier archäologische Stätten präsentiert:

Für die archäologische Stätte Taibeh 3 in Jordanien konnte für eine Reihe von erhitzten Feuersteinen mit dem *LumReader* Package die beste Filterkombination identifiziert werden, um das Lumineszenz-Signal zu maximieren und das Verhältnis von Signal und Hintergrundrauschen zu minimieren. Das ermöglichte die Signaloptimierung der Feinkorn-Aliquots zur Einschätzung der spezifischen α-Effizienz der jeweiligen Feuersteinprobe. Mit dem *TLdating* Package wurden Äquivalenzdosis, α-Effizienz und Dosisrate ermittelt. Die fünf untersuchten Feuersteinproben zeigten TL-Alter, die recht gut mit den ^{14}C-Altern von Holzkohlen aus denselben Kulturschichten übereinstimmten.

Aus den archäologischen Stätten Ansab 1 und 2 in Jordanien wurde eine Reihe von erhitzten Feuersteinen und Sedimentproben entnommen. Für die Sedimentproben wurden OSL-Altersabschätzungen unter Verwendung des vorhandenen *Luminescence* Package erstellt. Sie vervollständigen die aktuelle Chronologie dieser beiden Freilandstandorte. Das *TLdating* Package wurde verwendet, um die Äquivalentdosis (D_e) für zwei der erhitzten Feuersteinproben zu berechnen. Aufgrund des Mangels an zuverlässigen Abschätzungen der Dosisleistung für diese Proben werden keine Alter vorgeschlagen. Diese Arbeit bietet dennoch die Möglichkeit, die Grenzen der Datierung mit erhitztem Feuerstein zu erkunden. Außerdem wird ein verbessertes Protokoll zur Aufbereitung von Feuersteinproben vorgeschlagen.

In Bergisch Gladbach, Deutschland, wurden vier Proben von verbranntem Sediment und eine Probe von Baukeramik gesammelt. Auch hier wurde das *TLdating* Pakage verwendet, um eine Abschätzung der Äquivalenzdosis (D_e) für jede dieser Proben mittels Thermolumineszenz vorzunehmen. Darüber hinaus wurden die D_e-Werte für jede dieser Proben mittels post-Infrared IRSL (infrarot-stimulierte Lumineszenz) bestimmt. Diese verschiedenen Bestimmungen der Äquivalenzdosis passen weitgehend zueinander, und die daraus resultierenden Alter stimmen mit der erwarteten Chronologie überein.

Acknowledgements

First and foremost, this project would not have been possible without the *German Research Foundation* (DFG) and the *Collaborative Research Centre* (CRC) *806: "Our way to Europe" – Culture-environment interaction and human mobility in the Late Quaternary*. Through the CRC 806, the DFG not only funded all the field and laboratory work whose results are presented in this PhD thesis, but also allowed me to live and work in Cologne during the first three years of this project. I would also like to thank the Graduate School of Geosciences (GSGS) of the University of Cologne for awarding me a fellowship grant (no. GSGS-2017A-F08), which allowed me to stay in Cologne for a few extra months and complete the final measurements and analyses.

The CRC 806 and the GSGS were not only a source of funding but also a place to learn and develop. The multidisciplinary environment of the CRC 806, where archaeologists met geologists and mathematicians met anthropologists, was unique in many ways. Within the Integrated Research Training Group (IRTG) of the CRC 806, I met many other PhD students from different disciplines. We met during seminars and also in the field. Despite our different approaches, we were all working towards a common goal: to understand and illuminate parts of humanity's past.

Doctoral research leads to a very specific investigation. It is by nature very individual, even if it is not solitary. Often, doctoral students only interact with researchers in their own field of studies. Both the GSGS and the IRTG brought us into contact with completely different ways of thinking. While the GSGS allowed us to present our research to colleagues from other geoscientific disciplines, the IRTG gave us the opportunity to interact with scholars from both the natural and the human sciences. It was the perfect place to continue the path I had started with my Masters in Engineering and Archaeology. I am glad that some of the peers I met in these graduate schools became not only colleagues but also good friends.

Although the IRTG and GSGS were places to learn about other areas of research, it was at the *Cologne Luminescence Laboratory* (CLL) that I spent most of my time. It was there that I developed my theoretical and practical skills in luminescence dating. If it was in the luminescence laboratory of the *Research Laboratory for Archaeology and the History of Art* (RLAHA) at the University of Oxford that I dated my first samples, a series of architectural ceramics, it was at the CLL that I really explored the possibilities of luminescence dating and, in particular, thermoluminescence dating. Team meetings were always an opportunity to explore new ideas, tackle new challenges or share better practices.

On a more personal level, I would like to thank Prof. Dr. Helmut Brückner for giving me the opportunity to work on this project. My departure from Cologne could have meant the end of my PhD thesis, but he continued to believe in me. Now, four years later, I am finally presenting this manuscript. It would not have been possible without his support.

Prof. Dr. Brückner set the course, but Dr. Dominik Brill was always there to answer my questions and help organise my work, sometimes on a day-to-day basis. He was the first to introduce me to the CLL and show me how things worked. He was also a welcoming hand, helping me to find my way around the administration when I moved to Cologne.

The CLL would not be the same without Dr. Anja Zander. She is the heart of the lab and I owe her most of my current practical knowledge of thermoluminescence to her. It is always a pleasure to tackle new challenges with her.

I would also like to thank all the other current and former members of the CLL and, in particular, Christoph Burow for introducing me to **R** and Dr. Georgina King. During her short stay in Cologne as the head of the CLL, Dr. King brought her unique energy to the lab. She created synergies that continue to this day. I count her among those who have shaped my vision of academic research.

It is no secret that this project is a direct continuation of Dr. Christoph Schmidt's doctoral research. He paved the way that led to the original research proposal. The advice he gave me when I visited him in Bayreuth, Germany, helped me to direct my research.

It is the interdisciplinary component that has always attracted me to luminescence dating; the possibility of using my expertise in physics, mathematics and engineering to solve challenges encountered in archaeology, geography or history. I would like to thank Prof. Dr. Jürgen Richter who offered me the opportunity to join his fieldwork in Jordan where I collected my first heated flint samples for dating. I should also mention Prof. Dr. Gerd-Christian Weniger who agreed to be the second reviewer for this dissertation, and Prof. Dr. Tibor Dunai who chaired my thesis defence committee.

The list of people who have supported me over the last eight years is far too long to mention. Colleagues, peers, friends – without them I would never have made it this far. In addition to all the academic colleagues I have already mentioned, I would like to thank my family for all the support they have given me, especially when I have been away and when the temptation to give up has been close. To my late grandmother Marie-Jeanne, my mother Francine, my father Luc, my brothers Killian and Ronan, and my loves Gabrielle, Hélène and Natalie: Thank you!

Contents

Erklärung zur Dissertation i

Abstract iii

Zusammenfassung v

Acknowledgements vii

Contents ix

List of Figures xiii

List of Tables xxii

1 Introduction 1
- 1.1 The CRC 806 - Our way to Europe . . . 1
- 1.2 Objectives of the present study . . . 4
- 1.3 Research design and applied methodology . . . 7
  - 1.3.1 Luminescence dating . . . 7
  - 1.3.2 Field work . . . 8
  - 1.3.3 Outline of this dissertation . . . 10

2 Luminescence dating of heated flint - State of the Art 12
- 2.1 Robust dating of heated flint and implication for the occupation chronology of prehistoric humans . . . 12
  - 2.1.1 Precision, accuracy and time range . . . 13
  - 2.1.2 Typology of dated events . . . 14
  - 2.1.3 Dating methods in prehistorical contexts . . . 15
    - 2.1.3.1 Radiocarbon dating . . . 15
    - 2.1.3.2 OSL dating of sediment . . . 16
    - 2.1.3.3 TL dating of heated flint . . . 17
- 2.2 Principles of thermoluminescence dating . . . 18
  - 2.2.1 The age equation . . . 22
  - 2.2.2 Equivalent dose estimation . . . 24
  - 2.2.3 Dose rate estimation . . . 30
- 2.3 The dating of heated flint . . . 34

2.3.1 History . . . 34
2.3.2 Sample selection and collection . . . 37
2.3.3 Sample preparation . . . 37
2.3.4 Specifics of heated flint samples regarding the age estimation . . . 40
2.4 CLL protocol for heated flint sample TL dating . . . 43
2.4.1 Sample collection . . . 43
2.4.2 Sample preparation . . . 44
2.4.3 Equivalent dose estimation . . . 46
2.4.4 Dose rate estimation . . . 48
2.4.4.1 Radionuclide concentration in the flint matrix . . . 49
2.4.4.2 Radionuclide concentration in the surrounding sediment matrix . . . 49
2.4.5 Age estimation . . . 50
2.5 Software solutions for thermoluminescence dating . . . 51
2.5.1 Historical software solutions . . . 52
2.5.2 R and the luminescence community . . . 56

3 LumReader: Designing your luminescence experiment with R 58
3.1 Introduction . . . 59
3.2 Simulate a TL/OSL experiment using the *LumReader* package . . . 62
3.2.1 Filters . . . 62
3.2.2 Detection units . . . 65
3.2.3 Stimulation unit . . . 66
3.2.4 Reader . . . 67
3.2.5 Material . . . 68
3.2.6 Experiment . . . 69
3.3 Case studies . . . 71
3.3.1 Visualisation of the TL emission from feldspar samples . . . 71
3.3.2 Optimisation of the reader configuration for the dating of heated flint samples . . . 75
3.4 Conclusion . . . 77

4 Using R for thermoluminescence dating 79
4.1 Introduction . . . 80
4.2 *TLdating* package and **R** environment . . . 81
4.3 Thermoluminescence dating using the *TLdating* package . . . 84
4.3.1 Data import and export . . . 84
4.3.2 Pretreatment of TL data . . . 85
4.3.3 Identification of sufficiently heated objects using the heating plateau test . . . 86
4.3.4 Equivalent dose calculation from TL data . . . 88
4.3.4.1 The growth curve and dose plateau approach . . . 88
4.3.4.2 D_e calculation with the MAAD protocol . . . 89
4.3.4.3 D_e calculation with the SAR protocol . . . 92
4.4 Discussion . . . 95
4.5 Conclusions . . . 97

5 Using DRAC in complex geometries: TL dating of heated flints from Taibeh, Jordan 99
5.1 Introduction . . . 100
5.2 Methodology . . . 101
5.2.1 Sample selection and preparation . . . 101
5.2.2 Equivalent dose and a-value estimation . . . 102
5.2.3 Dose rate estimation . . . 103
5.3 Results and discussion . . . 105
5.4 Conclusion . . . 106

6 Another case study: Dating the prehistoric sites of Al-Ansab I and II, Jordan 108
6.1 Introduction . . . 108
6.2 Previous Age estimation for Al-Ansab 1, Jordan . . . 111
6.3 New age estimations for Al-Ansab 1 and 2, Jordan . . . 113
6.3.1 Sediment sample dating . . . 113
6.4 Heated flint sample dating . . . 114
6.4.1 Sample selection and preparation . . . 115
6.4.2 Equivalent dose estimation . . . 119
6.4.3 a-value estimation . . . 121
6.4.4 Dose rate estimation . . . 122
6.4.5 Age estimation . . . 124
6.5 Discussion . . . 124

7 Roman traces in Germania Magna: New thermoluminescence and $pIRIR_{290}$ data from a lime kiln at Bergisch Gladbach, Germany 128
7.1 Introduction . . . 129
7.1.1 Sample and independent age control . . . 130
7.1.2 Sample preparation and measuring equipment . . . 131
7.2 Material and methods . . . 132
7.2.1 Application of the TL-MAAD protocol . . . 132
7.2.2 Application of the TL-SAR protocol . . . 133
7.2.3 Application of the $pIRIR_{290}$ and IR_{50} protocols . . . 134
7.2.4 Determination of dose rate . . . 134
7.3 Results and discussion . . . 136
7.3.1 TL-MAAD . . . 136
7.3.2 TL-SAR . . . 136
7.3.3 $pIRIR_{290}$ and IR_{50} . . . 137
7.4 Conclusions . . . 138

8 Discussion 142
8.1 From the design of the experiment to the age estimation using R . . . 142
8.1.1 The *TLdating* package . . . 143
8.1.2 The *LumReader* package . . . 150
8.2 Age estimations of heated flint samples in the context of the CRC 806: Our Way to Europe . . . 154
8.2.1 Taibeh 3, Jordan . . . 154
8.2.2 Al-Ansab 1 and 2, Jordan . . . 159

8.3 Applying the new TL software solutions to other settings 164
8.3.1 TL emission spectra from feldpar samples 165
8.3.2 Bergisch Gladbach, Germany 165

9 Conclusion and Outlook **169**

A Flint samples preparation for radionuclide content estimation **173**

B LumReader: Designing your luminescence experiment with R - Online supplement **175**
B.1 Source files 175

C Using R for thermoluminescence dating - Online supplement **178**
C.1 Tables 178

D Using DRAC in complex geometries: TL dating heated flints from Taibeh, Jordan - Online supplement **181**
D.1 Calibration of the α-source 181
D.2 Measurement Protocols 182
D.3 Filter combinations for the estimation of the De value and the a-value. . 185
D.4 Radio-element concentration tables 185
D.5 Dose rate table 186
D.6 Radiocarbon ages 186
D.7 Input table for the *TLdating* package in **R** 188
D.8 Selection of plateau and growth curves 192

E Alpha source Calibration **194**

F Roman traces in Germania Magna: New thermoluminescence and pIRIR$_{290}$ data from a lime kiln at Bergisch Gladbach, Germany - Online supplement **197**
F.1 Tables 197
F.2 Figures 200

Bibliography **201**

List of Figures

1.1 **Geographical distribution of the regional projects during the first and second phases of the CRC 806.** The projects of the clusters A-D are related to specific fieldwork areas when the E and F projects follow an integrative approach (figure from `https://www.sfb806.uni-koeln.de/index.php/about?start=3`). 3

2.1 **Age ranges of various dating methods.** Actual limits are dependent on circumstances, i.e. sample preservation (Aitken, 1990, 1998). 13

2.2 **Radioactive decay schemes of the main radionuclide elements naturally present in soil:** Potassium 40 and Rubidium 87 series (Aitken, 1985a). 18

2.3 **Radioactive decay schemes of the main radionuclide elements naturally present in soil:** Uranium 238 and Thorium 232 Series (Lalou and Valladas, 1985). 19

2.4 **Energy-level representation of the eletron trapping and thermoluminescence recombination process.** (i) Ionization due to the exposure of the crystal to radiation and trapping on the electron. (ii) Storage of the electrons in the traps. The energy gap (E) between the trap and the conduction band defines the trap's depth. (iii) Thermal release when the crystal is heated again. The electron travel in the conduction band until it reaches a luminescence centre where it recombines with a hole, emitting light during the recombination process (Aitken, 1985a). . . 20

2.5 **TL glow-curve observed from small sample taken from a terracotta statuette (measurement by D. Stoneham).** (a) light emission during the first heating (at 20 $°C/s$) (b) light emission during the second heating (Aitken, 1985a). 21

2.6 **Representative isothermal thermoluminescence curves**, obtained at 330 $°C$. Dark count rate is shown dotted (log Y axis, sample 992101) (Murray and Wintle, 2000a). 22

2.7 **Basic principle of luminescence dating:** zeroing of the signal when the crystal is heated (or exposed to daylight for OSL) and subsequent accumulation of the signal with time when the material remains at normal temperature (or sealed from daylight for OSL). Each new heating (or exposition to sunlight for OSL) will reset (bleaches) the luminescence signal, including the laboratory's one (Preusser et al., 2008). 23

2.8 **Estimation of the D_e using the SAR protocol.** The natural TL signal (N) is compared with the TL signal resulting from aliquots which have been bleached down then exposed (regenerated) to known β-doses (laboratory doses). The paleodose by regeneration P*, or D_e is read off as indicated (Aitken, 1998). 26

2.9 **Estimation of the D_e using an additive protocol.** At least 2 level of additive dose ($N + \beta$) should be use in order to check for linearity of response above the level of the natural TL signal. The paleodose (P) is usually grater than the linear equivalent dose (Q) because of initial supralinearity of response (Aitken, 1985a) 28
2.10 **Estimation of the supralinearity correction using second-glow growth characteristic.** Bleached aliquots are irradiated using different additive dose. The supralinearity correction (I) is here estimated using a linear regression. To avoid interference by pre-dose effects, a new aliquot is used for each measurement (Aitken, 1985a). 30
2.11 **The heating plateau test:** The ratio between the additive curve ($N+\beta$) and the natural curve (N) should present a plateau around the temperature range used for the D_e estimation (Aitken, 1985a). 31
2.12 **Internal, external, environmental and cosmic dose rate components:** The internal $\dot{D}$ is mostly due to α and β. The external $\dot{D}$ is due to α, β and γ irradiation. Etching the grain with hydrofluoric acid (HF) usually allows to remove the α component. The γ component is often neglected for artefacts smaller than a few centimetres. The α and β component of the environmental $\dot{D}$ are always neglected except when dating sediments where the external and environmental $\dot{D}$ are merged. 32
2.13 **Beta-autoradiography images and color scans of nine selected flint samples.** The exposure duration was 263 h, except for sample N1 (123 h). On the upper left-hand side of A2R, a small dark area is observed which can be attributed to cortex remains. Sample O6 and O7 show the presence of hotspot regions where the flint matrix is darker. (Schmidt, 2013). 42
2.14 **Heated flint sample (TAI 1).** The presence of a pot-lid (red circle) is a strong indication of an heating of this flint sample (the ruler is 5 cm long). 43
2.15 **Removal of the outer surfaces of a burnt flint using a diamond saw** (diagram courtesy of Dr N Debenham) (Duller, 2008). 44
2.16 **(a) Diamond saw and (b) Hydraulic press** used for the heated flint sample's core material extraction and the production of artificial grains (CG and FG). 45
2.17 **(a) Risø TL/OSL DA-20 readers at the CLL. (b) 8 mm coarse grain aliquot deposited onto a stainless steel disc (9.8 mm in diameter)**, photo by AG Prof. Bubenzer. 47
2.18 **HPGe γ-spectrometer** from the CLL: PROFILE M-Series GEM Coaxial P-type HPGe Gamma-Ray Detector (Ortec), photo by Dr. Zander. 50
2.19 **Work-flow for TL age determination of heated flint samples.** Estimating a TL age for a heated flint sample requires to combine multiple measurements. The surrounding sediment sample will provide the environmental (here called external) dose rate. The FG fraction of the core material is used to estimate the *a-value*. The CG fraction is used to estimate the D_e and the remaining material from the core is used to estimated the radionuclide element concentration (Schmidt, 2013). 51
2.20 **Stuart Fleming making TL measurements on equipment from the 1970s** (from the cover of his 1979 book) (Wintle, 2008). 52

3.1 **Transmittance of (a) an absorption filter and (b) an interference filter.** . . . 63
3.2 **Transmission spectrum for (a) the *BG-39* absorption filter and (b) the combination of the *HA-3* (dashed line), *BG-39* (solid line) and *GG-400* (dotted line) filters (grey solid surface).** . . . 64
3.3 **Quantum efficiency of the *EMI 9235QG* bialkani PMT.** . . . 66
3.4 **(a) Black body radiation at 500 °C symbolizing a TL stimulation unit and (b) the emission peak emitted by a *Risø* BSL stimulation unit.** . . . 67
3.5 **(a) Reader configuration for TL dating of burnt flint:** The detection unit is a 9235QB PMT (black line) and is protected by 3 filters: an HA-3 (dashed purple line), a BG-39 (dashed blue line), and a GG-400 (dashed orange line); **(b) Reader configuration for OSL dating of quartz sediment:** the 9235QB PMT (black line) is protected by an U-340 filter (dashed line). In both combinations, the reader detection windows (grey solid surfaces) and the stimulation signal (red dashed surfaces) do not overlap. The green dotted lines are the filter combination transmissions. . . . 68
3.6 **Theoretical thermoluminescence emission properties of quartz** based on Krbetschek et al. (1997) expressed (a) as a level plot and (b) as a 3D plot. . . . 70
3.7 **Simulation of an experiment using the R package *LumReader*.** (a) The experiment use a TL stimulation unit and a 9235QB PMT protected by 3 filters (HA-3, BG-39 and GG-400, see Fig. 3.5 for more details). (b) The material shows one peak in the region of interest (around 300 °C) and two peaks out of the region of interest (around 100 and 400 °C); (c) Nearly all the signal from the emission peak in the region of interest (blue hatched surface) is detected by the reader (black solid surface). If we change our region of interest and focus on the peak at 400 °C which emits in the near-infrared, the actual configuration of the reader will not allow the detecting of any luminescence signal. The red hatched surfaces represent the stimulation signal (see Fig. 3.4 for more details). . . . 71
3.8 **TL emission for the F1 feldspar sample:** (a-c) without any preheat; (b-d) with a preheat. The data are shown using a level plot in (a,b) and a 3D plot in (c,d). . . . 73
3.9 **TL emission for the NB139 feldspar sample:** (a-c) without any preheat; (b-d) with a preheat. The data are shown using a level plot in (a,b) and a 3D plot in (c,d). . . . 74
3.10 **Luminescence signal for (a) 4 coarse grain (100-200 μm) aliquots and (b) 4 fine grain (4-10 μm) aliquots after 100 s of β-irradiation (around 10 Gy)** using a combination of the HA-3, GG-400, BG-39 and 7-59 filters. All the curves were smoothed using the *smooth.spline* function from the *stats* package. . . . 74
3.11 **Luminescence signal for 4 fine grain (4-11 μm) aliquots after 400s of β-irradiation (around 40 Gy)** using a combination of (a) the HA-3, GG-400, BG-39 and 7-59 filters and (b) the HA-3, GG-400 and BG-39 filters (without the 7-59); (c) and (d) being the respective background signals. All the curves were smoothed using the *smooth.spline* function from the *stats* package. . . . 75

3.12 **Simulation of the thermoluminescence experiment using different filter combinations:** (a) the initial HA-3, GG-400, BG-39 and 7-59 filters combination, (b) the same combination without the 7-59 filter and (c) an alternative combination including a KG-3 and a 475/50 interference filter. The orange curve represents the black body radiation at 500 °C, the blue curve represents the thermoluminescence signal between 350 and 400 °C, the green curve is the different detection windows and the black curves is the emission signal detected by the reader. 76

3.13 **Thermoluminescence signal for 4 fine grain (4-11 μm) aliquots after 100s of β-irradiation** using (a) a combination of the HA-3, GG-400, BG-39 and 7-59 filters, and (b) a combination of the RG-3 and a 475/50 filters. The signal intensity is slightly higher with the second filter combination and the peaks are 'clearer' when the signal is smoothed but the order of magnitude remains the same. 77

4.1 **Workflow followed by the different *script_** functions of the *TLdating* package.** First the TL curves are imported into **R**, then they are submitted to a series of pretreatment to prepare the upcoming analysis. Finally, the modified curves can be exported, for use in a different package or software, or they can be combined in **R** to realize the desired analysis. 83

4.2 **Selection of TL curves.** As this package focuses exclusively on TL, all non-TL data are automatically removed from the *.BINX* file. In this figure, it is possible to identify (a) preheat curves (dotted lines), (b) L_x and T_x curves (solid lines) and (c) background curves (dashed lines). The aliquot is composed of 150-200 μm quartz grains, extracted from sample NS2 (flint) that were bleached at 360 °C for 2 h and then irradiated with regenerative doses ranging from 80 to 1200 Gy. 84

4.3 **Pretreatment of the TL data: Separation of (a) the preheat signals from (b) the signals used for dating.** In (a), the solid lines are the preheat signals and the dashed line is the temperature. (c) Creation of the L_x and T_x signal that will be used for dating by subtracting the corresponding background signal. (d) Alignment of the TL peaks of the L_x and T_x signals. The aliquot is composed of 150-200 μm quartz grains, extracted from sample NS2 (flint) that were bleached at 360 °C for 2 h, and then irradiated with regenerative doses ranging from 80 to 1200 Gy. . 85

4.4 **Heating plateau for quartz extracted from sample NS2 (flint).** When a natural signal L_n (a) is divided by an additive dose signal L_x (b), the $\frac{L_n}{L_x}$ ratio should present a plateau around the maximum peak position (c). The *natural* aliquot is composed of 150-200 μm quartz grains that were bleached at 360 °C for 2 h, then irradiated with 80 Gy and preheated at 180 °C for 3 min. The *additive dose* aliquot was prepared as described for the *natural* aliquot and then irradiated with an additive dose of 80 Gy. 87

4.5 **Heating plateau test for (a) two additive dose TL signals (L_x) and (c) the corresponding sensitivity corrected signals ($\frac{L_x}{T_x}$).** In both cases, a heating plateau can be observed between 290 and 360 °C, i.e. around the position of the TL peak (b, d). The *natural* aliquot is composed of 150-200 μm quartz grains from sample NS2 (flint) that were bleached at 360 °C for 2 h, then irradiated with 40 Gy. The *additive dose* aliquots were prepared as described for the *natural* aliquot and then irradiated with additive doses of 30 and 60 Gy. 88

4.6 **Comparison between the growth curve and the dose plateau approach.** In both cases, the same TL data are used (a); in the GC approach the response for each additive/regenerative dose is averaged over the heating plateau before estimating the D_e (b); in the DP approach, a D_e is estimated for each temperature interval before averaging the results (c). This aliquot is composed of 150-200 μm quartz grains from sample NS2 (flint) that were bleached at 360 °C for 2 h, then irradiated with 30 Gy to simulate the natural dose. The aliquot was then irradiated with increasing *regenerative dose* from 20 to 80 Gy. 89

4.7 **The growth curve can be separated into 3 parts (a) the linear region, (b) the saturation region and (c) the supralinear region.** When using the MAAD protocol, the linear approximation (Q) does not take into account this supralinearity. Therefore, a supralinear correction (I) has to be added to obtain a final D_e which reflects the real palaeodose (P). This aliquot is composed of 150-200 μm quartz grains, extracted from sample NS2 (flint) that were bleached at 360 °C for 2 h and then irradiated with doses ranging from 0 to 2400 Gy. 90

4.8 **When there is no sensitivity change during the measurement, the additive and the regenerative dose response curve slopes are identical.** In this example, the first three regenerative dose responses are above the regression line and should not be used to determine the supralinear correction. The 18 aliquots are composed of 150-200 μm quartz grains, extracted from sample NS2 (flint) that were bleached at 360 °C for 2 h. Six aliquots were irradiated with 40 Gy to simulate the natural dose and four of them received extra *additive doses* of 30 and 60 Gy. Eight further aliquots received *regenerative doses* from 10 to 80 Gy. . . . 91

4.9 **Estimation of the D_e with the MAAD protocol using the *TLdating* package.** Two aliquots were irradiated with *additive doses* of 0, 30 and 60 Gy (a). Their test dose response signals allow correction for the very low signal emitted by one of the 60 Gy aliquots. Five regenerative dose steps were used (from 0 up to 80 Gy) to identify the supralinear effect (b). Both the DP (c, d) and the GC (e) approaches provide very similar results, around 40 Gy. D_e values below 20 Gy are very sensitive to variations in the supralinear correction. 93

4.10 **Estimation of the D_e with the SAR protocol for one aliquot using the *TLdating* package.** Six regenerative doses, including a zero dose and a repeated dose point, were administered (a). The test dose responses show a sensitisation of the material with increasing doses (b). The dose plateau (c) and growth curve approach (d) provide a similar D_e estimation, around 27 Gy. The DP approach allows an easy assessment of the temperature interval for D_e estimation whereas the GC approach allows an easy assessment of the regenerative dose interval which avoids the supralinear and the saturation regions. 94

4.11 **D_e estimation for burnt flint from Taibeh, Jordan.** (a) Estimation of the D_e for 5 samples (TAI 1, TAI 15, TAI 18, TAI 19, TAI 20) using different protocols (SAR & MAAD), and software (**R** & *Analyst*); (b) Comparison of the results of the SAR and MAAD protocols using the GC and the DP approach in **R** and using *Analyst* with and without a pretreatment in **R**. For the complete dataset see online supplement (Table C.2). 96

5.1 **(a) Stratigraphic sequence and (b) schematic representation of the staired test trench with geological (A-M) and archaeological (AH 1-5) horizons** (Hussain, 2015a). The flint samples are from the layers B and C. 101
5.2 **Comparison of the age estimation using the MAAD and the SAR protocols.** All the age are in the expected range for Masraqan artefacts except for TAI 15 which seems a little bit older. The TL ages are also in good agreement with the radiocarbon ages. 106

6.1 **Archaeological sites attributed to the Early Ahmarian techno-cultural unit composed of the Northern Early Ahmarian (NEA) and Southern Early Ahmarian (SEA) groups.** SEA sites include the Lagaman regional variant (Goring-Morris and Belfer-Cohen, 2018) known in the Negev Desert and on the Sinai Peninsula (Richter et al., 2020). 109
6.2 **Palaeolithic sites discovered in Wadi Sabra during the CRC 806 archaeological survey from 2009 to 2019.** Coordinate system used: WGS 84/EPSG 4326. (Richter et al., 2020). 110
6.3 **Local geological sequence of the pleistocene wadi fill around the Al-Ansab 1 Early Ahmarian settlement site.** (A) South-to-North schematic section through the Pleistocene sediment remnant bearing the Al-Ansab 1 site, from the base of the present Wadi Sabra dry-river channel to the top of the wadi fill ; (B) Selected data resulting from sediment analysis of geological sections 6 and 3. (Klasen et al., 2013, Richter et al., 2020). 112
6.4 **Heated flint samples from Al-Ansab 1 collected in 2015 for TL dating.** 116
6.5 **Diamond saw and Hydraulic press** used for the sample's core material extraction of the Ansab flint samples. 117
6.6 **Luminescence signal and Growth curve for the F1b stone sample using the MAAD protocol.** The integration interval is $320 - 390°C$. The relative uncertainty on the D_e is above 60%. Only one of the rejection criteria is validated. 120
6.7 **D_e estimation using the dose plateau (DP) and the growth curve (GC) approaches for a representative aliquot from ANS F10.** Both D_e estimation are consistent with each other and the natural dose is in the linear region of the growth curve. 122
6.8 **Age estimation for the sediment and heated flint samples from Al-Ansab.** The green box indicates the time range of the radiocarbon age estimations for Al-Ansab 1 (Richter et al., 2020) when the grey box (and the grey doted lines) indicates the time span of the Ahmarian techno-cultural unit (Goring-Morris and Belfer-Cohen, 2018). 125
6.9 **D_e Estimations for the sediment and heated flint samples from Al-Ansab 1 and 2.** The D_e values estimated using the SAR protocol are in black while those estimated using the MAAD protocol are in red. . 126

7.1 **Cut through the lime kiln dug into the soft weathered Devonian base rock without any further mansoning.** Three samples were taken from the fritted contact area (open circles), two from the soft sediment (filled circles) which was oxidised and fritted by temperature influence, and one typical Roman roof tile (open square). Dose rate samples were also taken from the greyish lime remains from inside the kiln, exposed in the front centre of the picture. 131

7.2 **Typical dose response curve of a polymineral fine grain sample (BGB 3) measured with the multiple aliquot additive dose (MAAD) TL protocol (a) and a single aliquot regeneration dose (SAR) TL protocol (b).** The insets show glow curves after background subtraction (a1 and b1), the associated De plateau (a2 and b2) and the corresponding 2nd glow TL dose response curve after applying low doses to check for supra-linearity (a3 and b3). 133

7.3 **Typical $pIRIR_2 90$ growth curve of sample BGB 1, natural $pIRIR_{290}$ signal intensity of all six samples (a1) and a check for temperature dependence of De and recycling ratio (b)**. Recycling ratios match the 10% acceptance criterion at least for the lower temperature range. 135

7.4 **Preheat plateau test for sample BGB 5 from the soft sediment surrounding the kiln structure using a standard SAR $IRSL_{50}$ protocol with a 60 s preheat and a 200 s IR stimulation.** The D_e shows no dependence on the preheat temperature, but the scatter increases due to reduced signal intensities. Recycling ratios are within the 10% acceptance range. 139

7.5 **Age compilation of OSL and TL results.** Except for sample 5, all age estimates match the expected Roman age range within 1σ confidence interval. They are also in good agreement with two radiocarbon ages (cal. AD, 2σ), obtained for a horse scull which was excavated in a working pit in front of the kiln, and charcoal remains from the kiln area (see Table F.5). 140

8.1 **Workflow for the D_e estimation using the TLdating package.** First, the luminescence signal data are imported into **R**. Second, the luminescence data are reorganised, modified and combined to allow for their analysis. It is the pretreatment step. Third, the data are analysed either to fulfil the desired test or to estimate an equivalent dose using the MAAD or the SAR protocol (Strebler et al., 2017). 144

8.2 **Pretreatment of TL signal from a heated flint sample (NS2).** (a) Preheat curves, (b) Luminescence curves (before any modification), (c) background subtraction and (d) peak alignment (Strebler et al., 2017). . . 145

8.3 **Overview of the workflow for the $\dot{D}$ calculation using the DRAC software.** (Durcan et al., 2015) 147

8.4 **Various components of the total $\dot{D}$.** The total $\dot{D}$ can be separated in four origins: (1) The internal $\dot{D}$ ($\dot{D}_{int}$) is coming from the radionuclide elements present inside the grain. It includes α and β radiations. (2) The *external* $\dot{D}$ ($\dot{D}_{ext}$) is coming from the radionuclide elements present inside flint matrix surrounding the grain. It includes α and β radiations. Its γ component is usually neglected, especially when the artefact is relatively small as it the case in this project. (3) The environmental component is coming from the radionuclide elements present in the sediment surrounding the flint sample. Since the external layer of the flint is removed, it is only composed of γ radiations. (4) The cosmic dose rate ($\dot{D}_c$) is due to the cosmic radiation reaching the earth. It is mostly composed of muon (Blain, 2009). 148

8.5 **The *TLdating* graphical user interface (GUI).** This screenshot shows the third step from the D_e estimation section, here, using the MAAD protocol. This GUI was developed using the *shiny* package. 149

8.6 **Detection windows for the 'usual' reader configuration for BSL and BTL.** The red curves represent the stimulation signal (up) and the black body radiation signal (down). The black continued curves are the PMT quantum efficiency. The green curves are the filters' detection windows. The grey area are the final detection windows for both reader configurations. 151

8.7 **Graphical user interface of the *LumReader* package.** The upper figure shows the visualisation of the TL properties of the material emitting the luminescence signal, i.e. quartz. The lower graph combins the stimulation signal with the reader detection window. The blue dashed area is the emitted signal while the black dashed area is the detected signal. The red dashed area represents the black body radiation signal. . . 152

8.8 **(a) Stratigraphic sequence and (b) schematic representation of the test trench with geological (A-M) and archaeological (AH 1-5) horizons.** The flint samples are from the layers B (AH-1) and C (AH-2). 155

8.9 **Comparison of the age estimates using the MAAD and the SAR protocols.** All of the ages are in the expected range for Masraqan artefacts except for TAI 15 which seems slightly older. The TL ages are also in good agreement with the radiocarbon ages (see Fig. 5.2). 156

8.10 **Local geological sequence of the pleistocene wadi fill around the Al-Ansab 1 Early Ahmarian settlement site.** (A) South-to-North schematic section through the Pleistocene sediment remnant bearing the Al-Ansab 1 site, from the base of the present Wadi Sabra dry-river channel to the top of the wadi fill; (B) Selected data resulting from sediment analysis of geological sections 6 and 3. (Klasen et al., 2013, Richter et al., 2020). 160

8.11 **Age estimation for the sediment and heated flint samples from Al-Ansab.** The green box indicates the time range of the radiocarbon age estimations for Al-Ansab 1 (Richter et al., 2020), while the grey box (and the grey doted lines) indicates the time span of the Ahmarian techno-cultural unit (Goring-Morris and Belfer-Cohen, 2018). 164

8.12 **Archaeological section from Bergish Gladbach, Germany.** Cut through the lime kiln dug into the soft weathered Devonian base rock without any further mansoning. Three samples were taken from the fritted contact area (open circles), two from the soft sediment (filled circles), which was oxidised and fritted by temperature influence, and one typical Roman roof tile (open rectangle). Dose rate samples were also taken from the greyish lime remains from inside the kiln, exposed in the front centre of the image (Zander et al., 2019). 166

8.13 **Age compilation of OSL and TL results for the samples from the Roman lime kiln at Bergisch Gladbach.** Except for sample 5, all age estimates match the expected Roman age range within a 1σ confidence interval. They are also in good agreement with the two radiocarbon ages obtained for a horse skull excavated in a working pit in front of the kiln and charcoal remains from the kiln area (Zander et al., 2019). 167

B.1 **.FLT file for the Huya *U340* filter.** 175

B.2 **.PMT file for the *9235QB* PMT.** 176

B.3 **.EXI file for a TL stimulation** 176

B.4 **.TL file for an imaginary material.** 176

B.5 **.OSL file for an imaginary material.** 177

D.1 **(a) Filter combination for the D_e value estimation (bandwidth 400-470 [nm]) and (b) filter combination for the *a-value* estimation (bandwidth 450-500 [nm]).** 185

D.2 **TL curves for the D_e estimation of the TAI 1 sample using the MAAD protocol:** (a) Average TL signal and heating plateau test curves; (b) D_e plateau and growth curves. 192

D.3 **TL curves for the *a-value* estimation of the TAI 1 sample using the MAAD protocol:** (a) Average TL signal and heating plateau test curves; (b) D_e plateau and growth curves. 192

D.4 **TL curves for the D_e estimation of the TAI 1 sample using the SAR protocol:** (a) Average TL signal and heating plateau test curves; (b) D_e plateau and growth curves. 193

D.5 **TL curves for the *a-value* estimation of the TAI 1 sample using the SAR protocol:** (a) Average TL signal and heating plateau test curves; (b) D_e plateau and growth curves. 193

F.1 **IRSL dose recovery tests obtained for the pIRIR290 protocol (BGB 1, 2, 3) and the IR50 protocol (BGB 4, 5).** # = discs were thermally reset by a $480°C$ TL measurement. & = discs were reset in an SOL2 solar simulator for 24 hr. * = measurements were made by an IR_{50} protocol ($pIRIR_{290}$ unsuccessful). 200

List of Tables

2.1 **Non exhaustive List of software solutions available for luminescence dating** (based on `http://ancienttl.org/software.htm`). 54

2.2 **Non exhaustive list of R packages available for luminescence dating** (based on `http://ancienttl.org/software.htm`). 56

3.1 **Main functions of the *LumReader* package.** 62

4.1 **Summary of the main functions of the *TLdating* package.** (1) Class objects containing the data; (2) functions which convert a class object into another class object; (3) functions that manipulate the data; (4) functions that do the data analysis; and (5) scripts that gather a predefined set of functions. For a list of required input arguments see online supplement (Table C.1). 81

5.1 **D_e, *a-value* an age estimation for the Taibeh heated flints.** For both the D_e and the *a-value* estimation, the MAAD and the SAR protocol produced consistent results. $\dot{D}_{int}$ represents up to 70% of $\dot{D}_{tot}$. 103

6.1 **Age estimation for the sediment sample collected during the 2013 archaeological campaign** (Klasen et al., 2013). 111

6.2 **Radiocarbon age estimations for charcoal samples collected during the 2011 and 2013 archaeological campaigns.** Calibration was conducted using the IntCal13 calibration curve provide by the OxCal 4.3 software package. ^{14}C measurements provided by CologneAMS and realised using a Acid-Alkani-Acid (AAA) pretreatment (Richter et al., 2020). 113

6.3 **D_e, $\dot{D}$ and age estimations for the Al-Ansab sediment samples collected during the 2015 field campaign**. 113

6.4 **List of the burnt and heated samples collected during the 2015 field campaign in Al-Ansab for TL dating.** 115

6.5 **Results of the heating plateau test (HPT) using an additive protocol on 4 aliquots** (2 for the natural signal and 2 for the additive one) **and first estimation of the D_e using a SAR protocol on 3 aliquots.** For four stones samples (ANS F4, F5, F9 and F11), the D_e estimation was above the higher regenerative dose (3200 s or 317.44 Gy). Three of the stone samples (ANS F1b, F5 and F11) present multiple TL peaks around the plateau region ($\sim 270°C$ and $\sim 370°C$) which could be indicative of polymineral samples. 119

6.6 **D_e estimations for the burnt stone sample (ANS F1b) and the two heated flint samples (ANS F10 and F12) showing an archaeological reset.** The D_e were estimated with a SAR and a MAAD protocols and, in both cases, using a dose plateau and a growth curve approach (see Chapter 4). . . . 121
6.7 **A-value estimation for the 2 heated flint samples showing signs of a signal reset during archaeological times.** The β-dose values were estimated using a GC and a DP approaches. Only the CG values are reported here. The DP results are used to defined the integration temperature interval. The a-value obtained using the MAAD protocol for ANS F12 is definitively overestimated. Neglecting its supra-linearity correction brings it down to 0.23 ± 0.02 which is already more consistent with the other a-value estimations. . . . 123
6.8 **Radionuclide concentrations for the heated flint/stone samples and the surrounding sediment material.** . . . 123
6.9 **D_e, $\dot{D}$ and age estimation for the two heated flint samples (ANS F10 and F12) from Al-Ansab 1 showing a archaeological reset.** The D_e were estimated with a SAR protocol on 12 aliquots and a MAAD protocol on 24 aliquots (12 for the Q estimation and 12 for the I estimation). In both case, a DP and a GC approaches are used. The DP results are used to define the temperature integration interval when the GC results are used for the age estimation (Strebler et al., 2017). . . . 124
6.10 **Internal and external $\dot{D}$ components of the Ansab heated flint samples.** . . . 125

7.1 **Compilation of dose rate results and dating results** of polymineral fine grain samples obtained by multiple aliquot additive dose (MAAD) and single aliquot regenerated (SAR) TL protocols and by IRSL. The $pIRIR_{290}$ protocol was used for BGB 1, 2, 3 and the IR_{50} protocol (*) for BGB 4, 5 because the $pIRIR_{290}$ signal intensity was too low for a reliable D_e determination. . . . 141

8.1 **Age of the Taibeh heated flint samples** (see Table 5.1). . . . 156
8.2 **The a-value and the corresponding internal and external $\dot{D}$ components for the Taibeh 3 heated flint samples.** For this table, only the results obtained using the MAAD protocol are presented (see Chap. 5, Table 1 for the SAR data). . . . 158
8.3 **Radionuclide concentrations for the Taibeh heated flint and sediment samples.** . . . 158
8.4 **Age estimation for the sediment samples collected during the 2013 archaeological campaign** (Klasen et al., 2013). . . . 159
8.5 **D_e and age estimates for the Al-Ansab sediment samples collected during the 2015 field campaign in Wadi Sabra** (see table 6.3). . . . 161

8.6 **D_e, $\dot{D}$ and age estimation for the two heated flint samples (ANS F10 and F12) from Al-Ansab 1 showing a archaeological reset.** The D_e were estimated with a SAR protocol on 12 aliquots and a MAAD protocol on 24 aliquots (12 for the Q estimation and 12 for the I estimation). In both cases, a DP and a GC approach are used. The DP results are used to define the temperature integration interval when the GC results are used for the age estimation (Strebler et al., 2017) (see Table 6.9. . 162

8.7 **Internal and external $\dot{D}$ components for the Al-Ansab heated flint samples.** The *a-value* estimated for ANS F12 using the MAAD protocol is clearly overestimated. When the supra-linearity correction is neglected, the value becomes similar to the SAR estimation (~ 0.20). The internal doses represent up to 78% of the total dose rate. Therefore, any $\dot{D}_{int}$ overestimation has a strong effect on the final age estimate. 162

8.8 **Radionuclide concentrations for the heated flint/stone samples from Al-Ansab 1** (see Table 6.8 for the radionuclide concentrations in the surrounding sediments). 163

8.9 **Compilation of the D_e and $\dot{D}$ results for the TL-MAAD and TL-SAR measurements and the resulting ages.** 168

C.1 **Summary of the main functions of the *TLdating* package.** (1) Class object containing the data; (2) functions converting a class object into another one; (3) functions manipulating the data; (4) functions making the data analysis; and (5) scripts gathering a predefined set of functions. 179

C.2 **Comparison of the D_e estimation (in s) for 5 burnt flint sample from Taibeh, Jordan**, using the *TLdating* package (**R**) and *Analyst* (*A*) with the SAR & MAAD protocols. DP = dose plateau approach, GC = Growth curve approach, and PT = pretreatment. 179

C.3 **Comparison of the age estimation using the MAAD and the SAR protocols.** All the age are in the expected range for Masraqan artefacts except for TAI 15 which seems a little bit older. The TL ages are also in good agreement with the radiocarbon ages. (UI0) unweighted average, all doses & independent I; (UQ0) unweighted average, all doses & reusing Q slope; (WI0) weighted average, all doses & independent I; (WQ0) weighted average, all doses & reusing Q slope; (UI150) unweighted average, only higher doses & independent I; (UQ150) unweighted average, only higher doses & reusing Q slope ; (WI150) weighted average, only higher doses & independent I; (WQ150) weighted average, only higher doses & reusing Q slope. For the SAR protocol, there is no supra-linear correction, therefore columns (UI0) and (UQ0), columns (WI0) and (WQ0), columns (UI150) and (UQ150) and columns (WI150) and (WQ150) provide the same results (this is indicated by slashes in the table). All the doses are provided in s, the dose rates are the same as in Table C.2. 180

D.5 **Radio-element concentrations for the Taibeh sediment samples.** The radio-element concentration are relatively low which allows to use an average for the flint $\dot{D}_{ext2}$ estimation. 185

D.6 **Radio-element concentrations for the Taibeh heated flint samples.** 186

D.7 **α, β and γ Dose rates for the Taibeh heated flint samples.** 186

D.8 **Radiocarbon ages.** All samples are charcoal samples. The calibrated radiocarbon ages were estimated using *Calib 7.2* and the *IntCal13 Northern Hemisphere atmospheric radiocarbon calibration curve*. 186

F.1 **Luminescence measuring protocol used for multiple aliquot additive dose (MAAD) TL dating.** Two discs each were measured for the natural signal and additive dose signal. Step 4 works as a reset, step 5 records the signal for normalisation. 197

F.2 **Single aliquot regeneration (SAR) measuring protocols used for IRSL and TL dating.** 198

F.3 **Dose rate determination results using high resolution gamma-ray spectrometry.** To account for potential variations of the different materials, up to 3 dose rate samples were measured. Water contents are given in relation to dry mass. 198

F.4 **Results of the quality check measurements for the TL-SAR and $pIRIR_{50\&290}$ protocols**. $^{\#}$ = discs were thermally reset by a $480°C$ TL measurement $^{\&}$ = discs were reset in an SOL2 solar simulator for 24 hrs * measurements made by an IR50 protocol (pIRIR290 unsuccessful). . . 199

F.5 **Radiocarbon ages were calibrated using OxCal V 4.2.3.** 200

Chapter 1

Introduction

1.1 The CRC 806 - Our way to Europe

The Collaborative Research Centre (CRC) 806 "Our Way to Europe; Culture-Environment Interaction and Human Mobility in the Late Quaternary"[1] started in 2009 and has ended its third phase in September 2021. Funded by the German Research Foundation (Deutsche Forschungsgemeinschaft; DFG SFB 806), the CRC 806 is a multidisciplinary project bringing together geoscientists and archaeologists from the universities of Cologne, Bonn and the RWTH Aachen University. Its purpose was to study the cultural-environmental context of the spread of anatomically modern humans (AMH) from their cradle in Africa to Western Eurasia during the last 190 ka. This investigation of the transcontinental and intercontinental dispersal behaviour was realised by a combination of archaeological and geoscientific methods in order to understand the relationship between the predominant palaeoenvironmental and palaeoclimatic conditions and the migration and dispersal of the AMH (Richter et al., 2012b).

The question of the origin and dispersal of AMH has long driven human evolutionary history. Mitochondrial DNA (mtDNA) analyses place the ancestor of AMH in Africa (Cann et al., 1987). The earliest fossil attributed to *Homo sapiens sapiens* was discovered in Eastern Africa and is approximately 195 ka old (Brown et al., 2012, McDougall et al., 2008). In the Levant, the earliest fossils of *Homo sapiens* are dated to around 100 ka before present (BP) (Mercier et al., 1993, Valladas et al., 1988). However, they are not associated to major changes in the Middle Palaeolithic material culture. Around 45-35 ka BP, a more recent type of *Homo sapiens* appears in this region; this time, associated with a genuine Near Eastern Upper Palaeolithic material culture called the Ahmarian (Goring-Morris and Belfer-Cohen, 2018). Human remains found at Bacho Kiro Cave

[1] http://www.sfb806.uni-koeln.de/

(Bulgaria) link the expansion of Initial Upper Palaeolithic (IUP) technologies with the spread of *Homo sapiens* into Eastern Europe between 47 and 45 ka cal BP (Fewlass et al., 2020, Hublin et al., 2020). There have been claims made of the presence of *Homo sapiens* in both Cavallo (Italy) and Kent's Cave (United Kingdom) dating to 42 ka cal BP (Benazzi et al., 2011, Higham et al., 2011). However, they rely on the dating of the archaeological contexts of the specimens, despite the fact that the exact stratigraphic origin of the fossils is still debated in both cases (Hublin et al., 2020).

Evidence seems to show that the dispersal of AMH started 300 to 200 ka BP in Eastern Africa and has been disrupted in the Levant at least once. This hypothesis of a recent African origin of AMH is called the *Out of Africa II* model (Posth et al., 2016, Stringer, 2003), in reference to the *Out of Africa I* which describes the migration of archaic humans from Africa to Eurasia (1.8-0.5 ma) (Fleagle et al., 2010). Before 45 ka BP, this dispersal reached Central Europe (Hajdinjak et al., 2021, Hublin et al., 2020).

During the European Middle to Upper Palaeolithic transition, *Homo sapiens* populations of African origin replaced and assimilitated native Neanderthal populations (Hublin, 2015). At Bacho Kiro (Bulgaria), the IUP starts before 45 ka cal BP, with possible extension to 47 ka cal BP (Fewlass et al., 2020, Hublin et al., 2020). Mitochondrial DNA analysis of the oldest Bacho Kiro Cave indiviuals indicates that they are more closely related to present-day and ancient populations in East Asia and the Americas than to later west Eurasian populations. All IUP Bacho Kiro Cave individuals also had recent Neanderthal ancestors in their immediate family histories (Hajdinjak et al., 2021). By contrast, an individual found in an upper stratigraphic layer of the same site and dated to around 35 ka cal BP is more similar to later Upper Palaeolithic individuals from Europe, who lived between 37 and 14 ka ago (Fu et al., 2016, Seguin-Orlando et al., 2014). The Bacho Kiro Cave genomes show that several distinct modern human populations existed during the early Upper Palaeolithic in Eurasia (Hajdinjak et al., 2021). Eventually, populations related to the IUP Bacho Kiro Cave individuals desappeared in western Eurasia without leaving a detectable genetic contribution to later populations (Hajdinjak et al., 2021). The cultural background of the later European AMH populations and the links between the Levantine and European early Upper Palaeolithic industries have yet to be explored. The dispersal process appears to have been affected by behavioural variability (Groucutt et al., 2015) and, in addition to the *Eastern Corridor* connecting North-East Africa to Central Europe (Richter et al., 2012a), the existence of a Western path across the Straits of Gibraltar is now suggested (Linstädter et al., 2012, Straus, 2001).

The CRC 806 aims to reconstruct past climates, cultures, population changes and living conditions to understand the push and pull factors of the dispersal and retreat of our

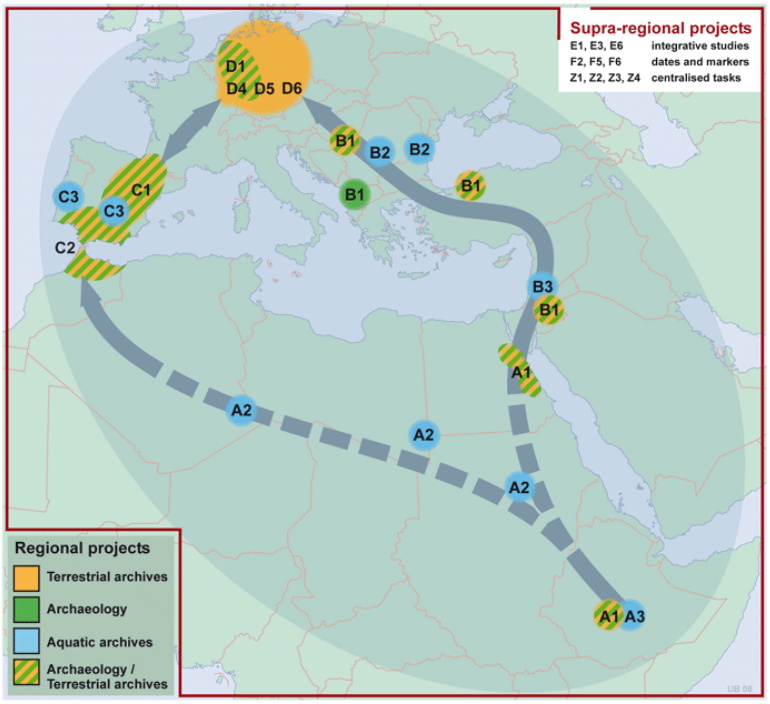


FIGURE 1.1: **Geographical distribution of the regional projects during the first and second phases of the CRC 806.** The projects of the clusters A-D are related to specific fieldwork areas when the E and F projects follow an integrative approach (figure from https://www.sfb806.uni-koeln.de/index.php/about?start=3).

ancestors. It is subdivided into several groups (themselves divided in clusters). The two first groups (R, for regional, and S, for supra-regional) have a strong geographical approach, the third (T, for timeline) has a more methodological approach and the fourth (Z) regroups the administration, teaching and public relation services.

The *regional group* (R) follows the main migration routes of our ancestors out of Africa and into Europe (see Fig. 1.1). It gathers the former clusters A to D from the two first phases of the CRC 806. **Cluster A** focuses on East Africa, the 'source' area of the emergence of Modern Humans. It starts with the first appearance of AMH in Ethiopia about 190 ka ago (during MIS 6) and continues with their dispersal into the Middle East (and to other African regions) during MIS 5 to MIS 3. This dispersal took place in several waves which did not all end successfully, i.e. with the long-lasting dominance of our ancestors in these new regions. **Cluster B** focuses on the so-called *Eastern Corridor* of dispersal into Europe. It includes the Near East, Anatolia and the Balkans. It starts with the "return" of AMH in the Near East during MIS 4 to MIS 3 (60-30 ka BP), when they managed to move forward into SE-Europe, and continues up to MIS 2/1 (10 ka BP) and the resettlement of Central Europe after the second glacial maximum. **Cluster C** explores the possible *Western Corridor* of dispersal into Europe with a focus on Northwest Africa and the Iberian Peninsula. Its time frame is relatively

similar to cluster B, starting from MIS 4/3 (around 60-50 ka BP) and continuing up to MIS 2/1 (10 ka BP). Finally, **Cluster D** is dedicated to Central Europe, one of the sink areas of transcontinental population movement, resettlement and establishment processes. Chronologically speaking, it concentrates on MIS 1 (10-1 ka BP), starting from the dispersal of farming and husbandry and the possible initial migrations from the Near East to Central Europe. It also included comparison with developed farming systems of later times in western Central Europe.

The *timeline group* (former **cluster F** now T) gathers projects specialised in different dating methods. The F2 project is dedicated to electron trap dating, i.e. luminescence and electron spin resonance (ESR) dating. The F3 project focuses on Accelerator Mass Spectrometry (AMS) dating, especially radiocarbon (^{14}C) dating. The F6 project explores palaeomagnetic dating. The reconstruction of human-environment interaction throughout 200 ka requires a chronological framework for both archaeological and geological archives. While radiocarbon is a robust dating technique up to 50 ka BP, optically stimulated luminescence (OSL), thermoluminescence (TL) and electron spin resonance (ESR) dating techniques provide precise and accurate chronometric ages needed to organise the manifold information from these multiple archives while covering the entire age range considered in the CRC 806.

1.2 Objectives of the present study

This PhD thesis is embedded in the **F2 project** of the second phase of the CRC 806, entitled "Application of Luminescence Dating Techniques in Geoarchaeological Studies". The heated flints dated during this project were collected in the frame of the **B1 project** called "The *Eastern Trajectory*: Last Glacial Palaeogeography and Archaeology of the Eastern Mediterranean and of the Balkan Peninsula".

It is in the continuity of the PhD thesis realised by Christoph Schmidt during the first phase of the CRC 806 (Schmidt, 2013). Schmidt explored several aspects of the luminescence dating of heated flint, in particular: (1) the influence of the sample carriers on the luminescence signal (Schmidt et al., 2011); (2) the influence of an heterogeneous distribution of radionuclide on the age estimation (Schmidt et al., 2012); and (3) the use of red TL (Schmidt et al., 2015a) and OSL (Schmidt, 2013) for the dating of heated flint.

Based on Schmidt's results and the challenges encountered, a new set of working hypotheses was defined.

Hypothesis 1 - Developing and improving the thermoluminescence (TL) dating method is relevant.

Luminescence dating is in a phase of vivid diversification. It is related equally to instrumental advances and methodological developments. Moreover, research has been conducted on TL and OSL dating of minerals other than quartz and feldspar.

TL is especially useful to explore the properties of new materials. The basic mechanisms of charge transfer underlying the generation of luminescence are usually explained using an energy band model. Luminescence signal is generated when charges trapped in the defects of the crystal lattice are released. Amongst the properties defining a trap is the average time a charge is expected to be caught in it, which directly depends on the temperature.

TL is the best technique when it comes to dating heated material. Heating a material modifies its luminescence properties. Heated material like burnt flint, ceramics, kiln or meteorite impact sediments already undergo such sensitisation. When heating such material to obtain an age estimation, they follow a process similar to their initial resetting.

Hypothesis 2 - TL dating lacks user-friendly, up-to-date, transparent and freely available software.

TL dating still heavily relies on the use of spreadsheet and proprietary software solutions. Despite its relative efficiency, this approach has strong limitations.

The new software solution should make data processing *easier*, *faster* and *more comprehensible*. It should help to *select the most appropriate parameters* for the age estimation and *identify problematic samples*. It should also *harmonise the protocols*, improve the *reproducibility* and help for the *citation*.

Hypothesis 3 - Dating heated flint is key for a better understanding of prehistoric human settlement contexts.

Flint is amongst the most common material from prehistoric sites. Based on ethnographic studies, organic raw materials represent almost 85-90% of the raw materials used in hunter-gatherer and farming societies (Hurcombe, 2014). Unfortunately, it is rare that those materials survived the ravages of time. Palaeolithic populations are therefore identified by the lithic culture they left behind. The terminology associated with the lithic raw material used for tool production is obfuscating and follows different

criteria and local variations. In this thesis, we will use the term *flint* to speak indistinctly about all varieties of amorphous and microcrystalline siliceous rocks.

Dating heated flint allows the direct dating of an anthropic event. Amongst the flint artefacts, a non-negligible number has been heated. The heating can be done on purpose, during the production of the tool, to modify the raw material properties, or as a by-product of human activities, typically when waste material is discard in a fireplace. Natural heating of flint artefacts could happen, for example during a forest fire. However the duration and intensity of this kind of heating is usually not sufficient to properly reset the luminescence signal.

In some settings it is the only method available for an age estimate. The range of radiocarbon dating is limited to the last 50 ka BP. Not all sediments allow optically stimulated luminescence (OSL) dating, for example due to a poor bleaching. Heated flint artefacts are sometimes the only material left to date lithic cultural contexts.

Hypothesis 4 - Heated flint is the ideal material to develop a new software for TL dating and to validate its applicability.

Heated flint is a complex material to date. It is important to assess if the flint was properly reset. It requires the combination of data from multiple origins. The internal dose rate cannot be neglected and the α-efficiency can strongly vary between samples. The environmental dose rate can also be a challenge to estimate, especially in complex geometries, such as caves, or when there is no sample of the surrounding sediments available.

Heated flint has a solid TL dating record/history. Despite the challenge that can be encountered, the method has proven its efficiency and accuracy. Schmidt has already set up a solid protocol that is used in the Cologne Luminescence Laboratory (CCL). Moreover, there is data available for the calibration of our software solution or for cross-checking new results.

A software for TL dating heated flint should also be applicable for other heated materials. Most of the challenges encountered when TL dating heated flint artefacts are also present in other materials. During a fire, for example in a kiln, the surrounding sediment is rarely heated evenly. Being able to properly identify the heated material that can be dated using TL is mandatory. A sample of the surrounding sediment is not always available, which can affect the estimation of the environmental dose rate and therefore the dating result. Even when the surrounding material can be sampled, the dating of bricks, tiles and other architectural ceramics often requires managing complex geometries for the environmental dose rate estimation.

Based on these different hypotheses, four objectives have been defined:

Objective A Developing a software for TL dating, in particular for heated flint.

Objective B Using the new software in the context of the CRC 806.

Objective C Making this software applicable for other environmental and archaeological settings.

Objective D Developing an additional software to improve the configuration of the TL/OSL reader, in particular for TL dating of heated flint samples.

1.3 Research design and applied methodology

1.3.1 Luminescence dating

Luminescence dating is a chronological method used in archaeology and earth sciences. It is based on the emission of light (luminescence) by commonly occurring minerals, especially quartz and feldspar. For heated material (pottery, burnt flint, heated sediment, etc.), the event being dated is the last heating of the object. It can also be used to date sediments. In this case, the event being dated is the last exposure of the mineral grains to daylight. The age range over which the method can be applied is from a few decades to over 100 ka (Duller, 2008).

The first applications of luminescence dating were developed in the 1960s. The technique was used to date archaeological ceramics and the luminescence was generated by heating the material, hence the name thermoluminescence (TL) dating (Houtermans et al., 1957, Tite and Waine, 1962). Two decades later, it was shown that it is possible to generate luminescence with light. This technique is called optically stimulated luminescence (OSL) dating and extends the range of luminescence dating by allowing to date sediment deposition (Huntley, 1985).

The principles of luminescence, with a focus on thermoluminescence, are developed in Chapter 2.

The Cologne Luminescence Laboratory

The Cologne Luminescence Laboratory (CLL) was set up in 1996 by Prof. Dr. Ulrich Radtke (Janotta et al., 1997) and is currently run by Dr. Dominik Brill, who follows Dr. Georgina King as head of the laboratory, and Dr. Anja Zander, who is in charge of the technical issues. At the Institute of Geography of the University of Cologne, the CLL is

part of the geochronology working group which is chaired by Prof. Dr. Tony Reimann who succeeded Prof. Dr. Helmut Brückner.

One of the main focuses of the CLL is the study of environmental changes during the Quaternary in a range of environmental settings, especially coastal settings. It also investigates a series of other research objectives, including geoarchaeological applications of luminescence dating, the expansion of the age range of luminescence dating using radiofluorescence, the exploration of luminescence-thermochronometry, the constrain of complex environmental dosimetry and the application of ESR dating (Bartz et al., 2020). As such, the laboratory is involved in several research projects including the CRC 806 "Our Way to Europe"[2], the CRC 1211 "Earth - Evolution at the Dry Limit"[3] and the RLum.Network [4].

The CLL is equipped with 7 luminescence readers. All the luminescence measurements that were done during this PhD thesis were realised on a TL-DA 20 TL/OSL reader (Risø) equipped with a β-source. The α-irradiation required to do the a-value estimation were done using the α-source of a Lexsyg Research Imaging TL-OSL-RF-System (Freiberg Instruments). The estimation of the γ dose rate from the sediment samples were realised using a PROFILE M-Series GEM Coaxial P-type HPGe Gamma-Ray Detector (Ortec). Finally, the flint samples were cut using a Isomet 1000 Precision Saw (Buehler).

1.3.2 Field work

In the frame of this PhD, the author has participated in several field campaigns to collect samples for OSL and TL dating. Some of these campaigns successfully provided archaeological material, i.e. heated flint samples suitable for dating with TL; others only provided sediment samples that were dated with OSL. In addition to this set of samples, a series of other heated flint and sediment samples, previously collected by other researchers from the CLL, were also processed in the frame of this research project. In this section, we present the three archaeological sites which provided most of the samples that were analysed and dated, as described in the following chapters.

Taibeh 3, Wadi Musa, Jordan

The archaeological site of Taibeh 3 is located in Wadi Musa, Jordan. The Wadi Musa lies south of Petra, in the neighbourhood of the Jordan Rift Valley. The excavation was

[2] https://www.sfb806.uni-koeln.de
[3] https://sfb1211.uni-koeln.de/
[4] http://www.r-luminescence.de/en/rlum_net_en.html

carried out by Prof. Dr. Jürgen Richter from the University of Cologne in the context of the CRC 806 in 2010. Five layers of human occupations were discovered during the excavation. The material coming from the two upper layers were identified as related to the late Ahmarian, also known as Masraqan, technocomplex (Hussain, 2015a, Hussain and Richter, 2015). The Masraqan is elsewhere connected with the beginning of the intensive use of plant food and with permanent settlements. Taibeh 3 could be the first site to present as much as five successive layers of this cultural unit. The Masraqan is relatively well constrained in time, usually dated between 18 and 25 ka BP (Belfer-Cohen and Goring-Morris, 2007).

The sediment and heated flint samples for OSL and TL dating were collected by Dr. Christoph Schmidt. Simultaneously, charcoal samples were collected for radiocarbon dating. Unfortunately, during transport the sediment samples were exposed to light, which affected their OSL dating. It was decided to only use the sediment samples for the dose rate estimation. Sample preparation, analyses and dating were carried on by the author at the CLL. In Chapter 5, the TL age estimates from the heated flint samples are compared with the radiocarbon age estimates from the charcoal samples (Strebler et al., 2019a).

Al-Ansab I and II, Wadi Sabra, Jordan

The archaeological site of Al-Ansab I and II are located in Wadi Sabra, Jordan. Same as Wadi Musa, Wadi Sabra is located south of Petra, not far from the Jordan Rift Valley. The neighbourhood of the Jordan Rift Valley is one of the focus areas of geoscientific and archaeological research of the CRC 806, more specifically of cluster B (Klasen et al., 2013, Schyle and Richter, 2015). Several excavations have been carried out in Wadi Musa. Those realised in the frame of the CRC 806 started in 2007 and were led by Prof. Dr. Jürgen Richter from the University of Cologne. In 2013, sediment samples were collected by Dr. Nicole Klasen from the CLL. She provided a first series of OSL ages ranging from 30 to 48 ka BP. The archaeological artefacts from Al-Ansab I were identified as related to the Ahmarian technocomplex. The OSL ages from Wadi Sabra provide the first numerical ages and, so far, no other dates exist for the Ahmarian find layer in the study area due to the lack of other datable material (Klasen et al., 2013).

The author took part to the field campaign of 2015 and collected a new series of sediment and heated flint samples to complete the luminescence age estimates already provided by Klassen. Charcoal samples were also collected for radiocarbon dating during this campaign. The results of the TL and OSL dating are presented in Chapter 6.

Bergisch Gladbach, Germany

The city of Bergisch Gladbach, Germany, is located East of Cologne and the Rhine River. Roof tiles remains found in a forest nearby were identified as typical *tegula* tiles from the Roman Iron Age (Dasbach and Selbach, 2015). Subsequent excavations carried out by Dr. Erich Claßen, director of the *LVR-Amt für Bodendenkmalpflege im Rheinland*, revealed an underlying sequence of four lime kilns designed in a typical Roman style (Classen et al., 2016).

In 2015 Dr. Anja Zander collected a series of samples from heated sediments and architectural ceramics, more specifically kiln walls and a tile, found close by in front of the kiln. Age estimates were realised using different methods, including TL dating and $pIRIR_{290}$ OSL dating. The results, presented in Chapter 7, confirm that the kilns were built during the late Roman Period (Zander et al., 2019).

1.3.3 Outline of this dissertation

After this introductory chapter, which includes a presentation of the project and the methodology, and the following chapter, which presents the state of the art in thermoluminescence dating of heated flint (Chapter 2), this PhD thesis is subdivided into two main parts: part I deals with the development of new software solutions for thermoluminescence dating (Chapters 3, 4 and 5), whilst part II focuses on the application of these software solutions to date heated flint (Chapter 5 and 6) but also other heated material, in particular heated sediment and architectural ceramics (Chapter 7). The last part (Chapters 8 and 9) provides an overview of the results and the conclusion.

Chapter 3 presents a new **R** package designed to simulate both the detection properties of luminescence readers and the emission properties of materials. The appropriate configuration of detection equipment is key to designing new experimental studies. This package, called *LumReader*, is used to compare two TL/OSL reader settings for thermoluminescence dating of heated flint proposed by Schmidt (2013) and Schmidt et al. (2015b). These results are published in *Radiation Measurements* (Strebler et al., 2019b).

Chapter 4 presents another new **R** package, this time specifically dedicated to TL dating. In this chapter, the focus is put on the estimation of the equivalent dose (D_e) using two different protocols (SAR and MAAD protocols, see Chapter 2).The functionality of this package, called *TLdating*, is evaluated using heated flints from Taibeh 3, Jordan. These results are published in *Quaternary Geochronology* (Strebler et al., 2017).

Chapter 5 continues with the presentation of the *TLdating* package. The focus is now put on the estimation of the dose rate ($\dot{D}$) using a modified version of DRAC (Durcan et al.,

2015). This chapter also presents the final age estimates obtained for the heated flints collected in Taibeh 3, Jordan. These results are published in *Quaternary Geochronology* (Strebler et al., 2019a).

Chapter 6 reviews the dating of heated flints coming from Wadi Sabra, Jordan. At Wadi Sabra (SW Jordan) human occupation dates back to the Palaeolithic and Epipalaeolithic. A first age estimate of 30-48 ka was obtained using OSL dating on coarse-grained quartz (Klasen et al., 2013). This chapter presents a new method to prepare heated flint samples and the complications encountered when trying to date those collected in Wadi Sabra, Jordan.

Chapter 7 generalises the use of the software solution presented previously. Samples coming from a lime kiln at Bergisch Gladbach, Germany, the attached silty sediments and a roof tile found close by were dated. The dating was made by using a post-infrared infrared stimulated luminescence ($pIRIR_{290}$) protocol (al Khasawneh et al., 2015) and two different thermoluminescence (TL) protocols: a single aliquot regeneration (SAR) and a multiple aliquot additive dose (MAAD). The results for all three protocols are consistent together and the resulting ages are in agreement with the expected time range (Roman Iron Age) and with independent age control provided by radiocarbon ages (Classen et al., 2016). These results are published in *Archaeometry* (Zander, Strebler et al., 2019).

Chapter 8 discusses the various results in relation to the working hypotheses set out in Chapter 1.2. Finally, conclusion and outlook are provided in Chapter 9 of this cumulative PhD thesis.

Chapter 2

Luminescence dating of heated flint - State of the Art

2.1 Robust dating of heated flint and implication for the occupation chronology of prehistoric humans

The question of the succession and/or contemporaneity of (pre)historical events and occupation layers is ubiquitous in archaeology. Dating methods are usually separated in two categories: relative and absolute dating methods. The *relative* dating methods provide information concerning the chronology of layers, objects or events relative to each other. Among the relative dating methods are the study of the stratigraphy and the typology. The *absolute* dating methods provides an age estimation for a specific layer, object or event. Their development is intricately related to the development of modern physics. Radiometric dating methods compare the abundance of a naturally occurring radioactive isotope within the dated material to either the abundance of another element also present in the material at the same time, typically its decay product, or the abundance of the same element at a specific moment. It includes techniques like uranium-thorium, potassium-argon, argon-argon and radiocarbon dating. Trapped charge dating uses natural dosimeter to assess a burial or exposition age. It gathers luminescence dating techniques, i.e. thermoluminescence (TL), optically stimulated luminescence (OSL) and radioluminescence (RL) dating, and electron spin resonance (ESR) dating techniques. Numerous other (relative and absolute) dating methods are used in archaeology including dendrochronology, tephrachronology, palaeomagnetic dating or palaeolimnology (see Fig. 2.1).

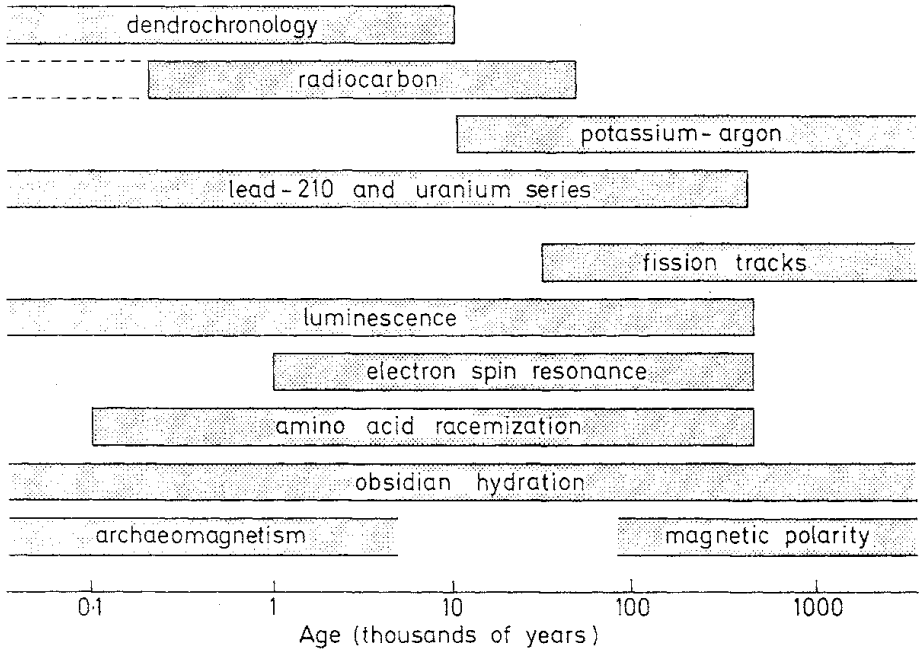


FIGURE 2.1: **Age ranges of various dating methods.** Actual limits are dependent on circumstances, i.e. sample preservation (Aitken, 1990, 1998).

Relative and absolute dating methods should not be seen as opposite but as complementary. Different dating methods are not affected by the same disrupting phenomena, carbon contamination does not affect luminescence dating, and disequilibrium in the uranium series has no influence on the radiocarbon dating. The applicability of dating methods is limited to the available material. Such availability differs among archaeological periods and cultures but is also restricted by the environmental conservation condition. Organic material has a shorter life span than lithic or ceramic artefacts, especially in acidic soil. Each technique has its own advantages and disadvantages (Aitken, 1990).

2.1.1 Precision, accuracy and time range

As any measurement results, age estimation are not pure numbers. They always comes with a confidence interval. Usually, a Gaussian distribution of the measurement results is expected, and increasing the confidence interval increases the likelihood that the true age lies within the cited range. A 1σ interval means that there is roughly a 68% probability that the *true* age lies within the uncertainty boundaries when a 2σ means that this probability goes up to 95.5%. Rather than being considered as absolute ages, chronometric dates should be seen as a statements on *probabilities*. *Precision* is defined by the scatter of the data. *Accuracy* is a measured of the deviation of the estimation

from the *true* value (which is, of course, unknown). Low precision is usually related to random and undirected error when a poor accuracy is the results of systematic and directed errors. It also means that precise results are not always accurate and, vice versa, accurate results can suffer from a low precision. To determine the final uncertainties on an age estimation, both the precision and the accuracy need to be taken into account too.

Dendrochronology is among the most precise dating methods. Its precision reaches the year and sometimes the season. However, it is dependant on the existence of a reference database. Securely dated tree-ring data for the northern hemisphere are available going back 12 ka (Reimer et al., 2020).

Radiometric dating methods rely on the presence of specific radionuclide elements. The half-life of the radionuclide element influences the dating range of the methods. The diminishing level of the radionuclide concentration via decay means that, after a time, there is little if any left. Radiocarbon dating is well adapted to date organic material, especially bones, wood or charcoal, but finding datable carbon in a pottery is quite uncommon, and less so for lithic material. The limit for radiocarbon dating is usually set around 50,000 years (Weninger and Jöris, 2008). Above this limit, most detectable ^{14}C atoms will most likely originate from contamination. For recent material (less than a few ka), the precision of an uncalibrated radiocarbon age estimation is usually below 1% (at 2σ) (Svetlik et al., 2019).

With a precision (at 1σ) ranging roughly from 5 to 10 %, TL and OSL age estimation are definitively less precise than radiocarbon dating (Wintle, 2008). However, luminescence dating of quartz sample, more specifically OSL, has been shown to be accurate over an age range from the last century to at least 350 ka when the right conditions are gathered (Murray and Olley, 2002). Age estimations above 1 Ma have been obtained using red thermoluminescence (RTL) of quartz embedded in volcanic deposits (Fattahi and Stokes, 2000).

2.1.2 Typology of dated events

Different dating methods do not only date different material, they also date different events. Dendrochronology provides an age estimation for the cutting of the tree. OSL dating of aeolian sediment provides an age estimation for the last exposition to sunlight. TL dating of a pottery provides an age estimation for the last intense heating. Radiocarbon dating provides an age estimation for the organism's death. All these events are usually correlated but rarely identical to the event that the archaeologists want to date. For example, the trees used for the framework of a building can have been cut

years, if not decades, before the building construction. A pottery can have been used for decades before being discarded. The charcoal can have been produced by the burning of a centuries old tree.

The typology of dated events introduced by Dean (1978) and discussed in Richter et al. (2009) provides a useful theoretical framework to address this situation. The distinction is made between the *dated event* which the date actually applies, and the *target event* that is the event or process of archaeological relevance. These two events are not necessarily simultaneous and can show considerable temporal offsets. They are linked by the *bridging event*. Knowing this bridging event is a prerequisite for establishing any temporal and causative relation between the obtained age and the archaeological question.

2.1.3 Dating methods in prehistorical contexts

2.1.3.1 Radiocarbon dating

Radiocarbon dating is, by far, the dating method which is the most commonly used in archaeology. The expected dated event is the death of the organism from which the material originates. For example, dating human bones should provide an age estimation for the individual's death. As seen previously, radiocarbon dating has a technical limit of $\sim$ 50 ka due to the half life of ^{14}C (Weninger and Jöris, 2008). However, such limit can only be reached using specific techniques and uncontaminated samples.

Contamination of the sample with modern carbon is an important issue, especially for older samples. A bulk sample can be subject to post-depositional mixing when charcoal absorbes humic acids. In both cases, the dated event will be an average between the death event and the contamination event, resulting in a systematic underestimation of the target event age (Scharpenseel and Becker-Heidmann, 1992). New preparations techniques, like ultrafiltration, appears to overcome some of the difficulties associated with degraded collagen of bones samples (Higham et al., 2006). However, most of the archaeological work and interpretation still rely on dates obtained using older preparation techniques, leading once again to an underestimation of the age assessment (Higham, 2011, Weninger and Jöris, 2008). Generally speaking, all radiocarbon ages older than 30 ka should be treated carefully and such ages should probably be interpreted as minimum age.

Atmospheric ^{14}C concentration is not constant over time. It leads to temporal changes in the initial $^{14}C/^{12}C$ ratio during the last 50 ka. This variation needs to be taken into account. Radiocarbon ages have to be calibrated in order to convert the *radiocarbon*

scale into a *calendar time scale*. This calibration is based on the reconstruction of past ^{14}C levels using dendrochronologic dataset up to 12 ka, or marine, atmospheric and terrestrial archives up to 60 ka (Fairbanks et al., 2005, Weninger and Jöris, 2008). Different calibration curves and algorithms exist. They are combined in several calibration programs including OxCal[1] and CALIB[2]. When calibrated age estimations slightly differ depending on the programs, especially for older ages (more than 10 ka), such difference is negligible compared to the offset between calibrated and uncalibrated ages that can reach several thousand years. The study of the calibration curves also shows the presence of *plateau* regions. The time interval spanning from the Middle to Upper palaeolithic transition ($>$ 35 ka) which is of major archaeological relevance, is characterized by one of these plateau in the calibration curve (Reimer et al., 2020). These plateaux heavily reduce the accuracy of radiocarbon dating for these time periods, limiting its capacity to answer some archaeological questions.

2.1.3.2 OSL dating of sediment

OSL provides an age estimation for the last exposition to intense light or heat. It is largely used to estimate the age of deposition for aeolian or alluvial sediment layers. It is expected that these sediments were properly reset before, or during, the deposition. When the deposition is indeed the target event for geological studies, the target event for archaeological settings is usually the human occupation time. Sediment deposition depends on complex mechanisms and is usually not homogeneous through time, deposition can speed up or slow down depending on multiple factors, it sometimes stops for long period of time or includes erosion phases (Aitken, 1998).

With some exceptions, i.e. when the sediment movement is directly or indirectly caused by human action, the dated event (the sediment deposition) is not directly related to the target event (the human occupation). Knowing the bridging event between both can be challenging, even when the dated sediment are directly coming from an occupation layer. The interest for an isolated OSL age estimation coming from a single sediment sample is therefore limited in an archaeological setting. However OSL dating of multiple samples combined with a strong stratigraphy can provide unrivalled results, especially when radiocarbon dating is not possible. Rather than trying to associate each target event to single dated event, the target event is bounded using the dated events. Such approach reduces the precision but improves the accuracy and strongly reinforces the confidence in the results.

[1] https://c14.arch.ox.ac.uk
[2] http://calib.org/calib/

Without surprise, the assumption that the dated event is the last exposure to sunlight of all the grains from a sediment sample might be an oversimplification. A sediment layer can be subject to a heterogeneous bleaching or bioturbation (Bateman et al., 2003). Moreover, due to the size of the sampling tube, the grains from a single sample usually deposit during multiple events or a continuous process rather than a single deposition event (Duller, 2008). Small aliquot and Single Grain (SG) OSL dating are some of the solutions proposed to tackle this challenge (Duller and Murray, 2000). They allow to multiply the D_e estimations for a single sediment sample and to apply statistical analysis to extract the most likely value for the target event.

Dose rate estimation can also be quite challenging when dating sediment sample with OSL. Water content variation through time is especially difficult to quantify. The two most common approaches are either to consider it as constant in time or to estimate maximum and minimum values. Disequilibrium of the Uranium series is another of the challenges that can cause an overestimation of the $\dot{D}$ and therefore an underestimation of the age (Lahaye et al., 2012).

2.1.3.3 TL dating of heated flint

The TL dating of a heated flint artefact provides an age estimation for its last heating. To properly reset the TL signal from the whole artefact, the core grains should have been exposed to a temperature above 300 $°C$ for a few hours or above 400 $°C$ for a few seconds. On one hand, rapid heating of flint material often generates mechanical damages. It increases brittleness and can strongly degrade the raw material. For these reasons, it is usually associated with the discarding of heated flint samples. The presence of cracks and pot-lids is usually the sign of such fast heating (see Chap. 2.3). On the other hand, slow heating can be used to modify the mechanical properties of the raw material. It is, for example, used to improve the knapping quality of some raw lithic material (Weiner et al., 2015). Such heating is usually done at a temperature between 150 and 300 $°C$ (Agam et al., 2021) and is insufficient to properly reset the TL signal when not applied long enough. Of course, the possibility of natural fires exists. However, the temperatures of most wood and grassland fires are too low to allow for complete signal resetting. When traces of fire are available, they are usually spatially confined, and can therefore be associated to campfires, rather than vastly spread, which would be indicative of more natural causes (Richter, 2007). In both cases, fast or slow heating, once the signal is properly reset, heated flint dating benefits from a direct connection between the target event, i.e. human occupation or activities, and the dated event, i.e. the heating.

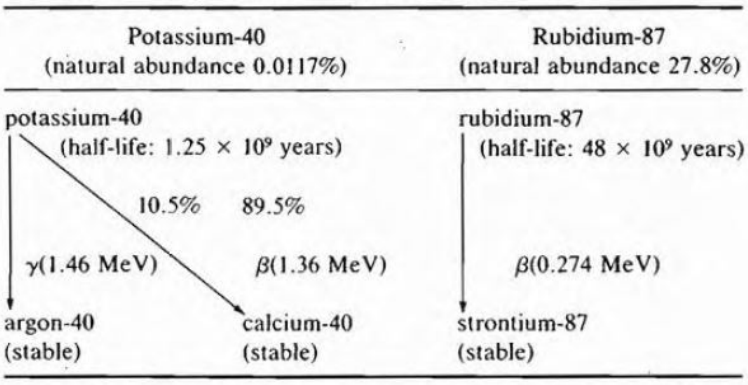


FIGURE 2.2: **Radioactive decay schemes of the main radionuclide elements naturally present in soil:** Potassium 40 and Rubidium 87 series (Aitken, 1985a).

The $\dot{D}$ estimation when using TL dating on heated flint samples can be challenging. Among the challenges specific to the heated flint dating is the influence of potential hot-spots (Schmidt et al., 2012). However, some of the factors impacting the OSL dating of sediment have a limited impact on the TL dating of heated flint. The environmental $\dot{D}$ represents only a fraction of the total $\dot{D}$. Water content variation or disequilibrium of the uranium series will therefore have a more limited impact on the uncertainty of the age estimation (Richter, 2007).

TL dating of heated flint samples is a powerful and essential tool to provide reliable age estimation in prehistoric contexts. Contrary to OSL ages of sediment samples, TL ages of heated flint samples already provide important information even in isolation. They become even more meaningful once combined with other age estimations, i.e. age estimation for other heated flint samples but also OSL age estimations for the surrounding sediment layers or, when possible, radiocarbon age estimations for associated artefacts, bones and charcoal remains. Each dating techniques is subject to different sources of uncertainties, multiple age estimations allow for cross calibration of results which improves our confidence on the final age sequence.

2.2 Principles of thermoluminescence dating

Thermoluminescence (TL) is the capacity of some minerals to produce light when they are heated. Every mineral is continuously submitted to radioactivity ; it comes from the radionuclide elements naturally present in the soil, mainly U, Th their daughter elements and ^{40}K (see Fig. 2.2 and 2.3), but also from cosmological sources (*cosmic ray*). Some minerals act as *natural* dosimeters, storing within their structure a small portion of the energy delivered over time, and releasing this energy as light, when exposed to heat

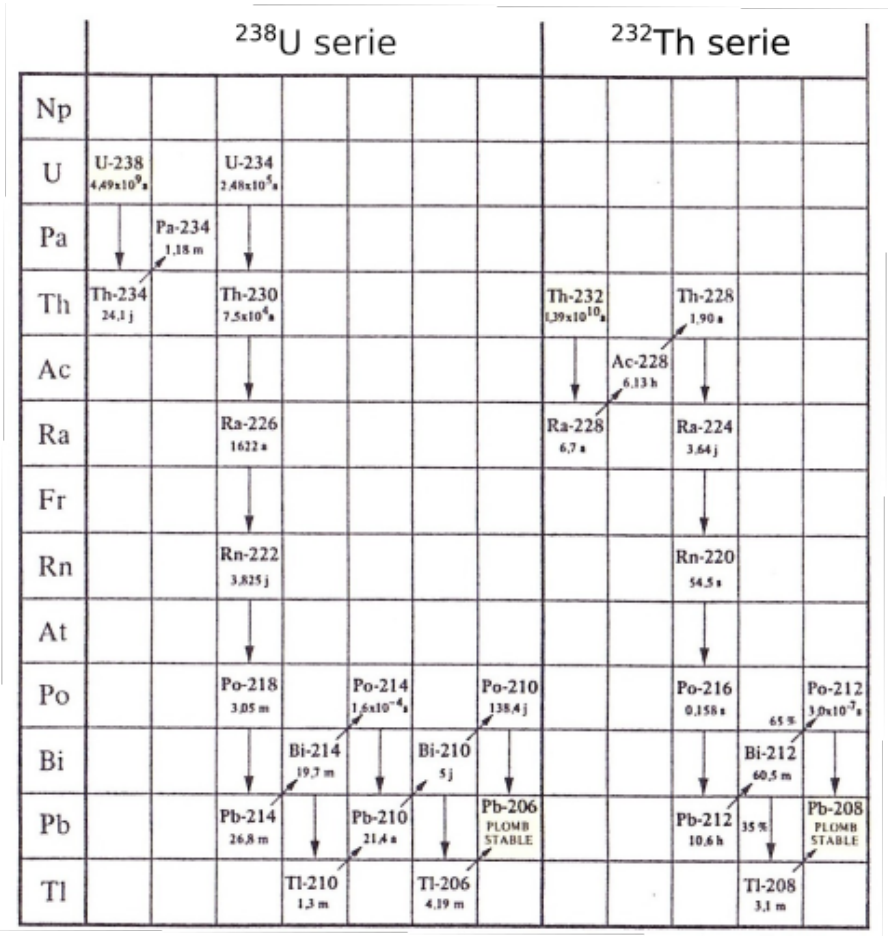


FIGURE 2.3: **Radioactive decay schemes of the main radionuclide elements naturally present in soil:** Uranium 238 and Thorium 232 Series (Lalou and Valladas, 1985).

(Lalou and Valladas, 1985). The light signal is proportional to the irradiation absorbed by the mineral. The heating resets the TL signal and the mineral must be irradiated again before it emits more light (Urbach, 1930).

TL emission can be explained using an energy band model and described using an energy level diagram (see Fig. 2.4). Radionuclide elements emit α, β and γ particles that ionise the atoms that make up the crossed material. Each released electron travels in the crystal lattice, leaving a *hole* behind them. Most of these *travelling* electrons quickly recombines with another hole but some are *trapped* by crystal deflects. A new income of energy will released the trapped electrons, allowing them to recombine with holes sometimes long after the initial irradiation. Some of these recombination are non radiative but others emit light during the process. The sites where the latter take place are called *luminescence centres*. Thermoluminescence is the result of a four steps process: (1) ionisation, (2) trapping, (3) releasing and (4) recombination (Aitken, 1985a).

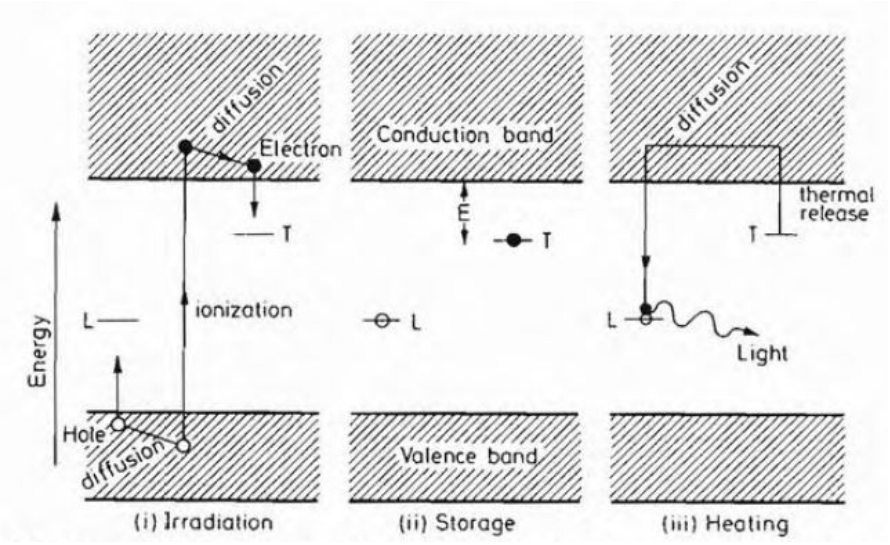


FIGURE 2.4: **Energy-level representation of the eletron trapping and thermoluminescence recombination process.** (i) Ionization due to the exposure of the crystal to radiation and trapping on the electron. (ii) Storage of the electrons in the traps. The energy gap (E) between the trap and the conduction band defines the trap's depth. (iii) Thermal release when the crystal is heated again. The electron travel in the conduction band until it reaches a luminescence centre where it recombines with a hole, emitting light during the recombination process (Aitken, 1985a).

Not all the trapped electrons need the same amount of energy to be *released* (reach the conduction band). Thermal agitation is enough to release some of them when other need much more energy. The latter are in *deeper* traps. The time needed for a trap to be emptied at a given temperature is defined by its thermal stability:

$$\tau = \frac{1}{s}.e^{-\frac{E}{k_B \cdot T}} \tag{2.1}$$

τ is the half-life of the trapped electrons, s is the frequency factor (specific to each crystal), k_B is the Boltzmann constant, T is the temperature (in K) and E is the energy needed to release the electron. To be considered as stable at a given temperature, the half-life (τ) of a trap should be several times greater than the duration which is estimated. In archaeology, τ needs to be several time greater than the age of the last reset to produce a reliable age estimation, i.e. around $10^5 - 10^6$ years.

The easiest way to produce a thermoluminescence signal is to linearly increase the temperature (usually up to 450-500 $°C$). This method will produce a series of peaks, each of them being associated to one or more traps. The traps are usually defined by the temperature at which they emit a maximum of luminescence, i.e. the temperature such as τ becomes smaller than the measurement integration time (usually around 1 s). It is

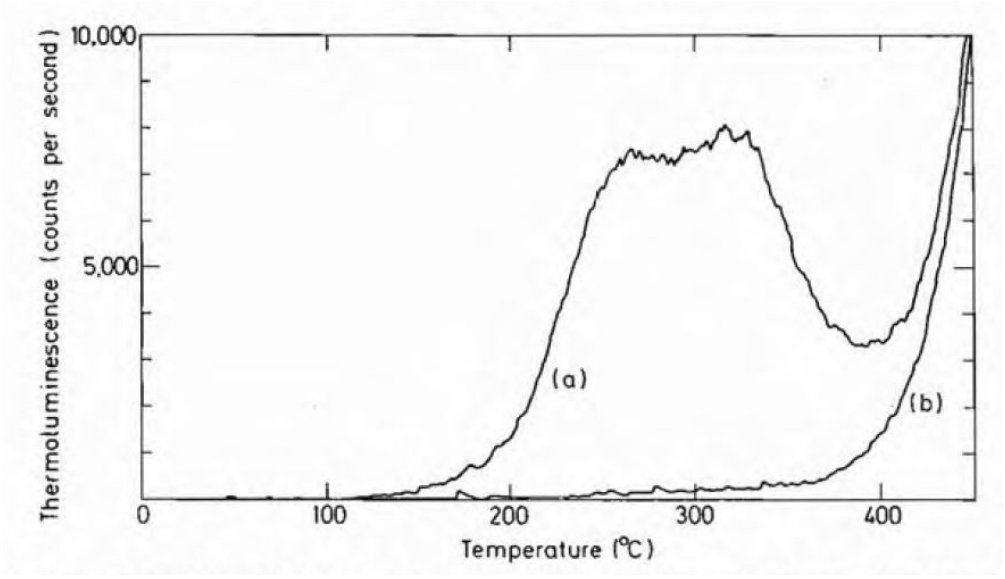


FIGURE 2.5: **TL glow-curve observed from small sample taken from a terra-cotta statuette (measurement by D. Stoneham).** (a) light emission during the first heating (at 20 $°C/s$) (b) light emission during the second heating (Aitken, 1985a).

the most commonly used method for thermoluminescence dating (see Fig. 2.5) (Aitken, 1985a).

Another method is heating the sample at a defined temperature and recording the luminescence signal emitted over time. The emitted thermoluminescence signal is a combination of exponential curves, each corresponding to an electron trap (see Eq. 2.1 and Fig. 2.6). It is called Isothermal Thermoluminescence (ITL) dating (Jain et al., 2005, Murray and Wintle, 2000a, Tribolo and Mercier, 2012).

The heating temperature depends on the TL peak we want to study (usually around 250-300 $°C$). It needs to be low enough to not deplete the selected trap too fast, i.e. the associated τ remains larger than the measurement integration time, but high enough for allowing the complete depletion of the trap during the TL signal recording, i.e. τ should be around a tenth of the experiment time.

On one hand, ITL allows working at a lower temperature. It has the advantage of reducing the heat sensitisation (Bowman and Seeley, 1978) and lowering the signal-interference due to the black-body radiation. On the other hand, data processing is more challenging because it requires the deconvolution of a series of exponentials. For the rest of this section, we will only consider thermoluminescence signal produced using linearly increasing temperatures (LM-TL or simply TL). The heating rate used in thermoluminescence dating is usually between 2 and 10 $°C/s$ (Aitken, 1985a).

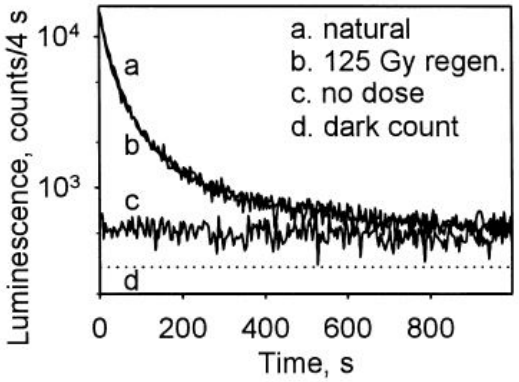


FIGURE 2.6: **Representative isothermal thermoluminescence curves**, obtained at 330 $°C$. Dark count rate is shown dotted (log Y axis, sample 992101) (Murray and Wintle, 2000a).

For this dating application, the minerals that are the most used are quartz and feldspar (Wintle, 2008). They are present in most sediments and therefore most ceramic artefacts and architectural ceramics. The electron traps used for the age estimation are between 300 and 450 $°C$. Below this temperature, the traps are not considered stable enough. Above this temperature, the signal is dominated by the black-body radiation.

It must be noted that other minerals can also be dated using luminescence, including zircon (van Es et al., 2002b, Hanh et al., 2013), gypsum (Aydas et al., 2011, Mahan and Kay, 2012, Nagar et al., 2010), halite (Zhang et al., 2005), apatite (Kitis et al., 2013), calcium carbonate from different origins like shells (Stirling et al., 2012), rizoliths (Polymeris et al., 2016), marble (Pagonis et al., 2009, Polikreti et al., 2003) and even extraterrestrial materials (Blair et al., 2007, Detschel and Lepper, 2009, Jain et al., 2006, McKeever et al., 2010, O'Connor et al., 2011). In particular, the dating of zircon grains embedded in archaeological ceramics was used to overcome the absence of surrounding sediments and to identify forgery (Aitken, 1985a, Sutton and Zimmerman, 1976, Zimmerman and Yuhas, 1974). Burnt flint artefacts (Göksu, 1972) are mostly composed of quartz and were among the first heated material to be dated using TL (see Section 2.3).

2.2.1 The age equation

The thermoluminescence signal is time dependent. There is a *zero*, a moment in time when there is no signal. Then the signal slowly grows due to the cumulative action of the radionuclide elements surrounding the mineral. Finally, the luminescence recording and the associated heating resets the signal (see Fig. 2.7).

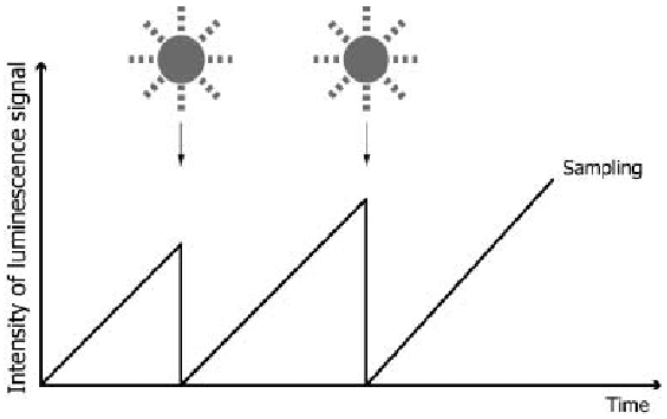


FIGURE 2.7: **Basic principle of luminescence dating:** zeroing of the signal when the crystal is heated (or exposed to daylight for OSL) and subsequent accumulation of the signal with time when the material remains at normal temperature (or sealed from daylight for OSL). Each new heating (or exposition to sunlight for OSL) will reset (bleaches) the luminescence signal, including the laboratory's one (Preusser et al., 2008).

The dose *absorbed* by the crystal since its last resetting event (D_{tot}) can be expressed using the expression:

$$D_{tot} = \int_0^t \sum_i \dot{D}_i(t)dt \tag{2.2}$$

Where the $\dot{D}_i(t)$ are the different dose rates. The absorbed dose is a combination of α, β and γ doses. The recording of a luminescence signal does not allow to make such differentiation. When recording the luminescence signal, we estimate what is called an *equivalent* dose (D_e), i.e. the equivalent β dose[3] that produces a luminescence signal similar to the absorbed dose.

When we only consider the D_e and the β dose rate ($\dot{D}$) equivalent to the sum of the various real dose rates, this equation becomes:

$$D_e = \int_0^t \dot{D}(t)dt \tag{2.3}$$

$\dot{D}(t)$ depends on multiple factors. Some of these factors, like moisture, sediment cover or disequilibrium of U and Th series are time dependent. However, moisture variation is usually seasonal. Once the sediment cover becomes sufficient, its influence on the $\dot{D}$ stays constant. Under good conditions, the U and Th daughter element's concentrations

[3] γ or α equivalent dose are also possible. However most TL/OSL readers are equipped with a β source (typically a ^{90}Sr source), hence the β equivalent dose (Risø, 2015).

reach equilibrium relatively quickly compared to the burial age. Most of the times, the effect of the $\dot{D}(t)$ variations is considered negligible compare to the age and an average value is used. The equation 2.3 can be simplified as:

$$D_e = \dot{D}.\Delta t \tag{2.4}$$

Neglecting the time dependency of $\dot{D}$ is not always possible. In this case, more complex models have to be taken into account (Olley et al., 1996, Vieillevigne et al., 2007). In the context of luminescence dating, Δt is the *Age* of the sample. D_e is usually expressed in Gy and $\dot{D}$ in Gy/ka which provides an *Age* in ka. The so called *Age equation* is obtained by isolating the age:

$$Age = \frac{D_e}{\dot{D}} \tag{2.5}$$

To produce an age using thermoluminescence dating, two parameters have to be estimated and combined: (1) the equivalent dose (D_e) and (2) the (equivalent) dose rate ($\dot{D}$). Both measurement suffers from their own uncertainties that combines to affect the age estimation. When using the root sum of squares (RSS) method, the relative uncertainty on the age ($\frac{\delta A}{A}$) is given by:

$$\frac{\delta A}{A} = \sqrt{\left(\frac{\delta D_e}{D_e}\right)^2 + \left(\frac{\delta \dot{D}}{\dot{D}}\right)^2} \tag{2.6}$$

2.2.2 Equivalent dose estimation

The estimation of the D_e is the first step for the estimation of an age using TL. It is also the part on which most publications, including this one, focus. Thermoluminescence signal does not allow a direct measurement of the D_e. Several techniques have been proposed to estimate the D_e. All of them combine multiple TL recording to produce a single D_e estimation (Aitken, 1985a, Wintle, 2008).

D_e estimation are usually done either on fine grain, i.e. grains with a diameter between 4 and 11 μm (Zimmerman, 1967), or on coarse grains, i.e. grains with a diameter between 63 and 250 μm (Fleming, 1966). The size of the grain has no influence on the protocol used to estimate the D_e. However the conversion of the irradiation time into a dose depends on the distance between the sample and the irradiation source, therefore on the grain size. Moreover, the grain size will influence the estimation of the dose rate ($\dot{D}$) as seen in section 2.2.3

Three types of thermoluminescence signals can be recorded: (1) *natural* signals are generated by heating a sample that has only been exposed to the *natural* dose, i.e. the dose absorbed over time, (2) *additive* signals are generated by heating a sample that has been exposed to a known laboratory dose in addition to the natural dose, and (3) *regenerative* signals are generated by heating a sample that has been irradiated using a known laboratory dose after being *reset*.

Thermoluminescence protocols are usually divided in two families: the *additive* and *regenerative* protocols.

Additive protocols divide the sample in several *aliquots* before any luminescence measurement. One of the aliquot provides the *natural* dose signal (1) while the others are irradiated with increasing known laboratory doses, providing a series of different *additive* dose signals (2). The D_e is then estimated using a regression curve. The multiple aliquot additive dose (MAAD) protocol was the first to be developed and is still the most used for thermoluminescence dating (see Fig. 2.9).

The regenerative protocol does not required to subdivide the sample. It determines the D_e on thermally depleted and redosed (*regenerated*) aliquots (3) after the recording of their respective natural dose signals (1). Unlike the classical additive method, it measures the signal for only one aliquot at a time, providing a D_e estimation for each of them. Nowadays, the most commonly used regenerative protocol is the *Single Aliquot Regenerative* (SAR) measurement protocol (Murray and Wintle, 2000b).

It must be noted that some measurement protocols, like the Single aliquot regeneration and added dose (SARA) protocol (Mejdahl and Botter-Jensen, 1994), combine an additive with a regenerative approach.

The SAR measurement protocol

Most artificial dosimeters are standardized and made of material with stable and reproductive properties. Their *dose-response* curve is well known and can be determined *a priori*. A single recording of the light signal can provide a D_e estimation (Knoll, 2010). It is not the case for *natural* dosimeters like quartz and feldspar. Every crystal, and therefore every aliquot, reacts differently. Direct estimation of the D_e only using the light emitted when a crystal or an aliquot is excited for the first time is not possible. The idea behind the SAR measurement protocol is to determine the dose-response curve of each aliquot *a posteriori* and to compare the initial natural dose signal to this *dose-response* curve.

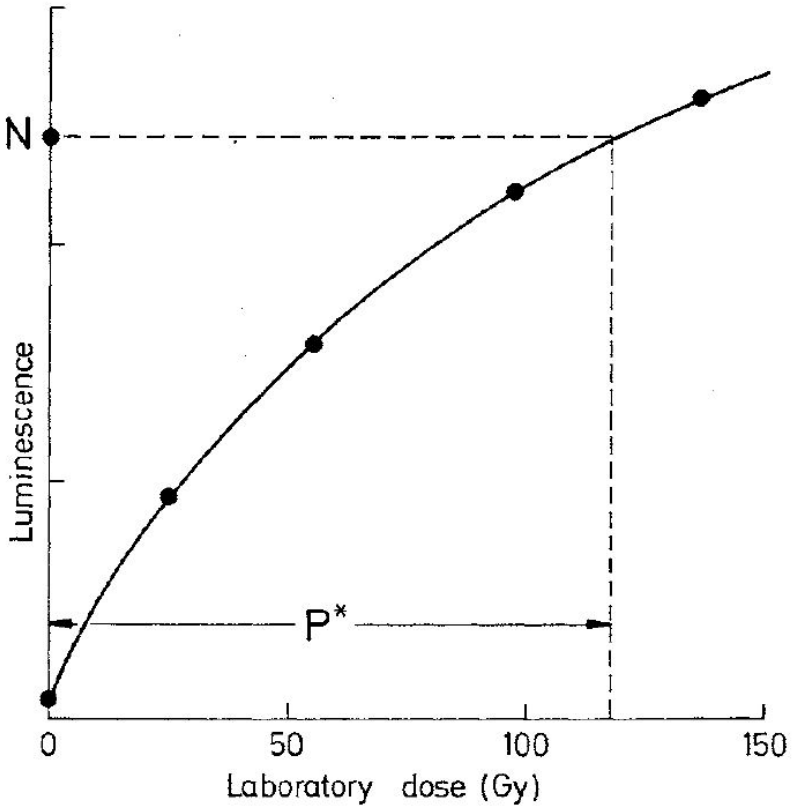


FIGURE 2.8: **Estimation of the D_e using the SAR protocol.** The natural TL signal (N) is compared with the TL signal resulting from aliquots which have been bleached down then exposed (regenerated) to known β-doses (laboratory doses). The paleodose by regeneration P*, or D_e is read off as indicated (Aitken, 1998).

The SAR protocol was developed to routinely date quartz grain from sediment using optically stimulated luminescence (OSL). Initially proposed by Duller (1991), it was later improved by Murray and Wintle (2000b). It was quickly applied to TL (Bluszcz and Bøtter-Jensen, 1995, Murray and Wintle, 2000a, Richter and Krbetschek, 2006).

First, the signal for the natural dose is recorded. Then the sample is bleached (reset) and submitted to increasing known doses. Each time, the luminescence signal is recorded and the sample bleached again. Finally, the first signal is compared to the response curve generated by the laboratory doses. The evolution of the dose sensitivity of the sample is also recorded. Between each luminescence measurement, the sample is submitted to a small *test-dose*. When the luminescence for this test-dose changes, the sensitivity changes and the response curve must be corrected (see Fig. 2.8).

Once all the regenerative doses have been recorded, the recording of one of the lowest laboratory dose is repeated. It is called the *recycled dose test*. The recycled signal should be similar to the one initially obtained for this laboratory β dose (taking into account

the test-dose normalisation). This *recycled* dose allows to determine a *recycling ratio* that should be close to 1.

When a proper bleaching of the signal is required after each OSL measurement, recording the TL signal up to 450-500 $°C$ already induces a reset of the signal. A second bleaching is therefore not required and can even increase the sensitisation of the sample. Some protocols still keep this *bleaching* step after each TL signal recording while others only include a single *bleaching* step after the recording of the *test-dose* signal (Richter and Krbetschek, 2006). Heat sensitisation seems to mainly occur after the first heating, i.e. during the recording of the *natural* signal (Bowman and Seeley, 1978). This initial heat sensitivity change is difficult to record (Singhvi et al., 2011, Wintle and Murray, 2006). Extra heatings are expected to have a limited impact on the sensitivity for most samples while ensuring a proper resetting of the signal between each recording step.

The SAR measurement protocol is currently the most used for sediment dating using OSL. It was also successfully applied to other settings, including ceramics (Duller, 2008, Wintle, 2008), architectural ceramics (Bailiff, 2007, Bailiff and Holland, 2000, Blain et al., 2010) and heated flint (Richter and Krbetschek, 2006, Schmidt, 2013) dating. One of the main interests of the SAR measurement protocol is that a small amount of material can generate a D_e estimation. Each single aliquot produces an estimation for the D_e value. Increasing the number of aliquots improves the quality of the D_e estimation and reduces the random uncertainty of the final D_e estimation.

When dating sediment using OSL, luminescence signal and properties can strongly vary inside a single sample (Galbraith, 2003, Rodnight, 2008). It could generate an important dispersion of the D_e estimation of each aliquot. It leads to the development of the single grain (SG) measurement technique (Duller and Murray, 2000, Jacobs and Roberts, 2007, Olley et al., 2006.) and several approaches for the estimation of the D_e based on how the aliquot's D_e are dispersed (Fuchs and Lang, 2001, Galbraith, 2005, Galbraith et al., 1999, Galbraith and Roberts, 2012, Woda and Fuchs, 2008).

For heated material, the aliquot's D_e are usually much more consistent with each other (Pagonis et al., 2011), especially when the aliquot are standardized. It can be explained by the initial reset which is more homogeneous and the resulting heat-sensitisation. Increasing the number of aliquots still improves the confidence on the D_e estimation and reduce the random uncertainty. A reliable D_e estimation can already be obtained by using 4 to 6 aliquots with some heated samples. However, the use of 12 up to 24 aliquots is recommended when possible (Richter and Krbetschek, 2006, Schmidt, 2013).

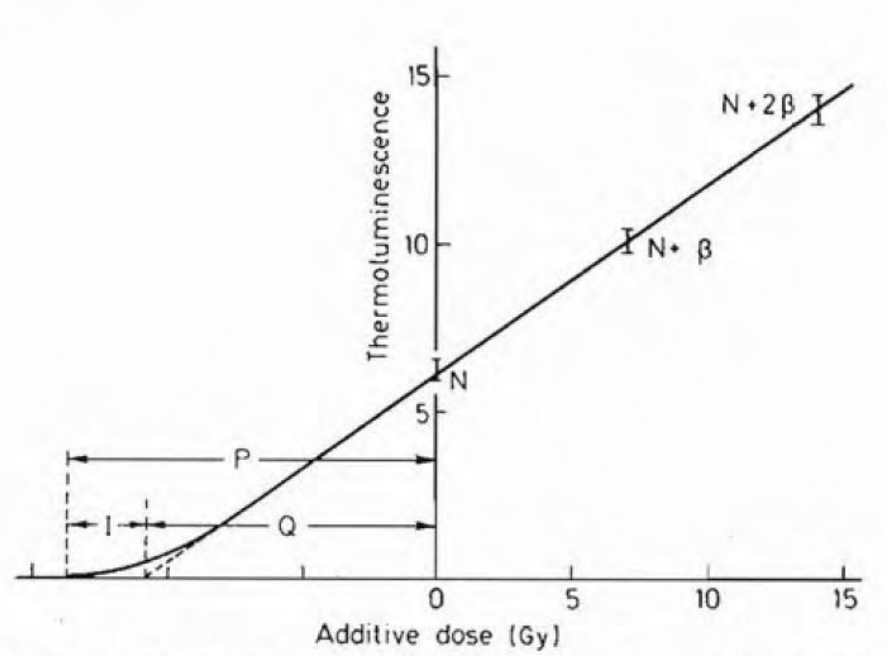


FIGURE 2.9: **Estimation of the D_e using an additive protocol.** At least 2 level of additive dose ($N + \beta$) should be use in order to check for linearity of response above the level of the natural TL signal. The paleodose (P) is usually grater than the linear equivalent dose (Q) because of initial supralinearity of response (Aitken, 1985a)

The MAAD protocol

Additive protocols were the first to be developed (Aitken, 1985a). Before any measurement, the samples are divided into sub-samples called aliquots. Some of these aliquots are left untouched while the others are irradiated with increasing known laboratory doses. All the aliquots are then left to rest for a few weeks which allows for the unstable traps to naturally empty themselves. When only the stable signal remains, the luminescence signal of each of the aliquots are recorded (Aitken, 1985a, Dutkiewicz and Prescott, 1997, Lalou and Valladas, 1985). The aliquots that were not irradiated in the laboratory provide *natural* dose signals. The aliquot that were irradiated in the laboratory provide *additive* dose signals, i.e. the signal due to the natural dose enhanced by the known laboratory doses. Finally, the signals from all the aliquots is reported on a graph with, on the x-axis, the value of the added laboratory dose (0 for the natural signal) and, on the y-axis, the intensity of the signal (in an arbitrary unit). A first estimation of the D_e, called *paleodose*, is given by the intersection of a regression curve (usually linear) with the x-axis (see Fig. 2.9).

This protocol has the advantages to only require one TL signal recording per aliquot and is therefore not influenced by heat sensitisation (Bowman and Seeley, 1978). It is also much faster to be realised than the SAR protocol, especially when D_e is quite

high (which require multiple time consuming β-irradiation steps). However, the MAAD protocol also has its own challenges.

Additive protocols requires homogeneous aliquots. The standardization of the preparation of the aliquots, by reducing the size range of the grains, controlling the weight and the size of the aliquots and only having a single layer of grain on the discs, helps but is not always sufficient. Grains from a natural sample do not have identical luminescence properties. A few very bright grains can produce most of the luminescence signal (Ganzawa et al., 2005). A solution is to expose every aliquots which provide a natural or an additive dose signal to a small known laboratory dose. The luminescence signal generated by this *test dose* can be used to normalise the different additives and natural signals. However, this *test dose signal*, being a regenerative signal, is influenced by heat sensitisation (Bowman and Seeley, 1978).

Regenerative protocols and the modelling of the electron trap and release mechanisms show that the growth curve is not linear at low doses (Aitken, 1985a). This *supra-linearity* is due to competing mechanisms and has to be corrected for. The supra-linearity correction can be estimated using aliquots that are bleached before being irradiated with different known laboratory doses. Once again, the results are reported on a x-y graph with, on the x-axis the added doses and on the y-axis the luminescence signal (see Fig. 2.10). The supra-linearity correction is provided by the intersection of the new regression curve with the x-axis. The supra-linearity correction can be estimated using the same aliquot that were used for the paleodose estimation. It reduces the amount of material needed but heat sensitisation can influence the correction factor. It can also be estimated using material reset at a lower temperature (and for a longer time), which avoids heat sensitisation but requires more material.

The storage of the aliquot after the additive dose irradiation allowing the unstable signal to naturally deplete before the recording of the luminescence signal is often replaced by the heating of the aliquots at a lower temperature (usually around 200 $°C$) for a few seconds (Dutkiewicz and Prescott, 1997, Feathers, 1997). This *preheat* is especially useful when the supra-linearity correction is estimated using the same aliquot as the paleodose and when the natural and additive dose signals are followed by a test dose to normalise the signal of the different aliquots. It allows to speed up the process and to record all the luminescence signal required to estimate a D_e during a single measurement sequence on a semi-automated TL/OSL reader.

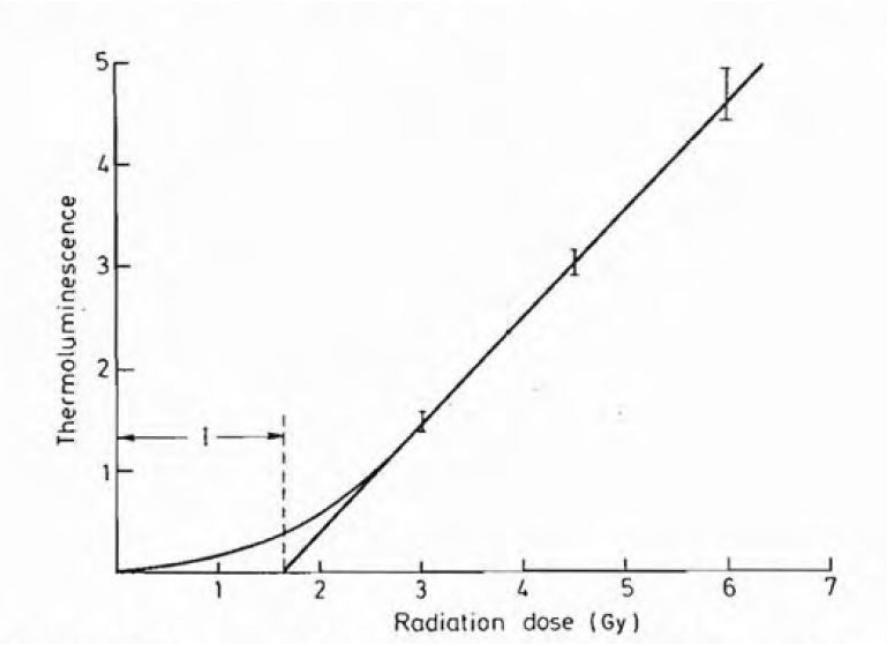


FIGURE 2.10: **Estimation of the supralinearity correction using second-glow growth characteristic.** Bleached aliquots are irradiated using different additive dose. The supralinearity correction (I) is here estimated using a linear regression. To avoid interference by pre-dose effects, a new aliquot is used for each measurement (Aitken, 1985a).

The heating plateau test

Thermoluminescence dating requires the integration of the luminescence signal over a defined range of temperature. Over this temperature range, the luminescence properties need to be homogeneous. Otherwise, any shift of the temperature range used to estimate the D_e will influence its value (Aitken, 1985a).

The *heating plateau test* allows to identify the maximum temperature range that could be used for the D_e estimation. It consists of plotting the ratio between the additive (or regenerative) luminescence signal and the natural luminescence signal for each temperature channel (Aitken, 1985a, Duller, 2008). The region where this ratio forms a plateau is the region where the luminescence properties should be homogeneous (see Fig. 2.11).

2.2.3 Dose rate estimation

The estimation of the dose rate ($\dot{D}$) is the second half of any age estimation. As we previously stated, the annual dose comes from the radionuclide elements naturally present in the environment, especially U, Th, their daughter elements and ^{40}K. These radionuclide elements emit a combination of α, β and γ particles to which we have to add

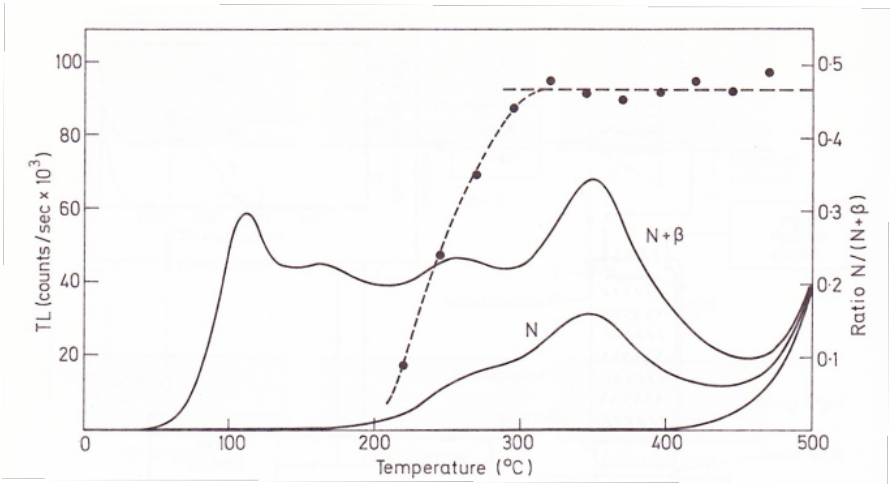


FIGURE 2.11: **The heating plateau test:** The ratio between the additive curve $(N + \beta)$ and the natural curve (N) should present a plateau around the temperature range used for the D_e estimation (Aitken, 1985a).

the cosmic ray radiation (Aitken, 1985a). They can also be separated in three groups, based on their proximity with the mineral grain (Blain, 2009).

- *Internal doses* are due to the radionuclide elements present inside the grain.
- *External doses* are due to the radionuclide elements present around the dated grain but still inside the matrix containing them, i.e. the ceramic or the heated flint artefact.
- *Environmental doses* are due to the cosmic ray and the radionuclide elements far from the dated grains, for example, those present in the sediment surrounding the dated artefact.

The dose rate ($\dot{D}$) is therefore a combination of 10 elements: (1) the internal α dose rate ($\dot{D}_{int,\alpha}$), (2) the internal β dose rate ($\dot{D}_{int,\beta}$), (3) the internal γ dose rate ($\dot{D}_{int,\gamma}$), (4) the external α dose rate ($\dot{D}_{ext,\alpha}$), (5) the external β dose rate ($\dot{D}_{ext,\beta}$), (6) the external γ dose rate ($\dot{D}_{ext,\gamma}$), (7) the environment α dose rate ($\dot{D}_{env,\alpha}$), (8) the environment β dose rate ($\dot{D}_{env,\beta}$), (9) the environment γ dose rate ($\dot{D}_{env,\gamma}$) and (10) the cosmic dose rate ($\dot{D}_c$). The range of the α and β particles being limited, $\dot{D}_{env,\alpha}$ and $\dot{D}_{env,\beta}$ can generally be considered as null. The range of the γ being much larger than the grain size, $\dot{D}_{int,\gamma}$ is also considered as null most of the time (see Fig. 2.12) (Aitken, 1985a, 1998). It has to be noted that, when dating sediment samples, no distinction is usually made between the external and the environmental dose rate which reduce the numbers of elements that have to be combined to 6 ($\dot{D}_{int,\alpha}$, $\dot{D}_{int,\beta}$, $\dot{D}_{ext,\alpha}$, $\dot{D}_{ext,\beta}$, $\dot{D}_{ext,\gamma}$ and $\dot{D}_c$) (Durcan et al., 2015).

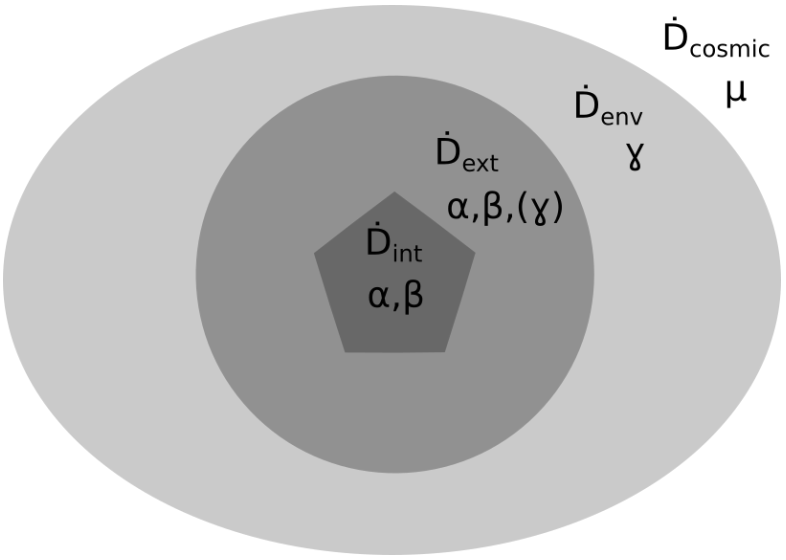


FIGURE 2.12: **Internal, external, environmental and cosmic dose rate components:** The internal $\dot{D}$ is mostly due to α and β. The external $\dot{D}$ is due to α, β and γ irradiation. Etching the grain with hydrofluoric acid (HF) usually allows to remove the α component. The γ component is often neglected for artefacts smaller than a few centimetres. The α and β component of the environmental $\dot{D}$ are always neglected except when dating sediments where the external and environmental $\dot{D}$ are merged.

Alpha efficiency and dose rate equation

β and γ particles have a similar efficiency when it comes to estimating the actual dose absorbed by the material. It is not the case for α particles that deposit most of their energy in a very short region of the crystal. It induces a saturation effect which reduces the efficiency of the absorbed α dose compared to the absorbed β and γ doses (Aitken, 1985a, Bell, 1980).

The combination of the different components of the dose rate and the alpha efficiency provides the following equations for the equivalent β dose rate ($\dot{D}$):

$$\dot{D} = k.\dot{D}_{int,\alpha} + \dot{D}_{int,\beta} + k.\dot{D}_{ext,\alpha} + \dot{D}_{ext,\beta} + \dot{D}_{ext,\gamma} + \dot{D}_{env,\gamma} + \dot{D}_c \tag{2.7}$$

Where k is the corrective factor called the *alpha efficiency value*, or a-value, which is used to take into account the lower efficiency of the α compared to the β particles during the trapping of the electrons.

The estimation of the a-value (k) is done on fine grains to assure that the full grains are α irradiated and not only the top part of them. First the grains are reset (by heat). They are then irradiated by a known dose using a calibrated α source (D_α). Finally an

equivalent β-dose (D_β) is estimated using an additive or a regenerative protocol. The a-value (k) is the ratio between the known α-dose and the estimated equivalent β-dose.

$$k = \frac{D_\alpha}{D_\beta} \tag{2.8}$$

Grain sizes and dose rate estimation

Depending on the size of the grains used to estimate the D_e and the mineral which is dated, some of the dose rate components can be neglected.

When dating fine grains (FG), i.e. grains with a diameter between 4 and 11 μm, the internal dose rates are often neglected. This simplification is only possible for minerals with low or no radionuclide contents, like most quartz. For those with a high radionuclide content like K-feldspar and zircon, $\dot{D}_{int,\alpha}$ and $\dot{D}_{int,\beta}$ still have to be taken into account (Aitken, 1985a, Furetta, 2008). For quartz grains, the equation 2.2.3 becomes:

$$\dot{D} = (k.\dot{D}_{ext,\alpha} + \dot{D}_{ext,\beta} + \dot{D}_{ext,\gamma}) + \dot{D}_{env,\gamma} + \dot{D}_c \tag{2.9}$$

When dating coarse grains (CG), i.e. grains with a diameter larger than 63 μm, it is $\dot{D}_{int,\gamma}$ and the $\dot{D}_{ext,\alpha}$ which are neglected, especially when the grains were etched with hydrofluoric acid (HF) before the D_e estimation. The equation 2.2.3 becomes:

$$\dot{D} = (k.\dot{D}_{int,\alpha} + \dot{D}_{int,\beta}) + (\dot{D}_{ext,\beta} + \dot{D}_{ext,\gamma}) + \dot{D}_{env,\gamma} + \dot{D}_c \tag{2.10}$$

Most of the time, there is no radionuclide embedded into the quartz grains. Therefore, the internal dose rate can also be neglected and the equation 2.10 becomes:

$$\dot{D} = (\dot{D}_{ext,\beta} + \dot{D}_{ext,\gamma}) + \dot{D}_{env,\gamma} + \dot{D}_c \tag{2.11}$$

The D_e is rarely estimated on middle size grains (between 11 and 63 μm). They do not allow such simplifications and require estimation of the proportion of the internal and external dose rate that are actually absorbed by the material.

It must be noted that the matrix containing the grains is usually smaller than the γ range. $\dot{D}_{ext,\gamma}$ can be neglected for small artefacts when an additional corrective factor may be required for larger flint artefacts (Blain, 2009, Wintle, 2008).

Several methods can be used to estimate the different dose rate components. Historically, α and β spectrometry were used to estimate the $\dot{D}_{int}$ and $\dot{D}_{ext}$ but nowadays it is Inductively coupled plasma mass spectrometry (ICP-MS) which is most often used. ICP-MS allows to directly estimate the radionuclide element concentrations. Those are then converted into dose rate using standardized tables (Adamiec and Aitken, 1998, Bell, 1976, Guerin et al., 2011, Liritzis et al., 2013).

The environmental dose rate is often estimated using high precision (HP-Ge) γ spectrometry on a large sample (usually $\sim 1\ kg$) of the sediment surrounding the dated sample in a 30 cm (the γ range in sediment) sphere (Guibert and Schvoerer, 1991). It can also be estimated by burying a dosimeter (TLD) for several month at the initial position of the sample (Erlach and Vana, 1988, Lalou and Valladas, 1985) or by using an in-situ (NaI) γ-spectrometer (Veronese et al., 2008, Vieillevigne et al., 2007).

The cosmic ray component can be calculated theoretically (Grün, 2009, Prescott and Hutton, 1994) or included in the environmental dose estimated using a TLD (Aitken, 1985a) or a NaI spectrometer (Prescott and Clay, 2000).

2.3 The dating of heated flint

2.3.1 History

Around 1630 AD, thermoluminescence was observed for the first time by Vincenzo Cascariolo, a Bolognese alchemist, who reported that the heating of barytes produces light (Goldberg, 1989). Sir Roberts Boyles made the same observation in 1664 when heating diamond (Boyle, 1664). The development of solid-state physics in the beginning of the 20th century provided some understanding of the phenomenon and Daniels et al. (1953) were the first to propose to use it for the dating of archaeological material.

The first material to be dated using thermoluminescence was not archaeological but a meteorite (Houtermans et al., 1957). Five years later, the first article on the dating of archaeological ceramic was published in *Archaeometry* (Tite and Waine, 1962). Multiple protocols for the D_e estimation were developed during the following years including the quartz inclusions (Fleming, 1966), fine grains (Zimmerman, 1967), predose (Fleming, 1973a), subtraction (Fleming, 1973b) and zircon inclusion (Sutton and Zimmerman, 1976) techniques. The determination of the annual dose rate was also studied and several challenging phenomena were enlightened including the non uniformity of the radio-element repartition around and inside the ceramic and the effect of moisture (Aitken, 1969), the anomalous fading of feldspar (Wintle, 1973) and the *supra-linearity*

of the TL growth curve (Bowman, 1975, Fleming, 1975). It is also during this period that the first application of TL to date other heated materials than ceramic was proposed, starting by burnt quartz (Wintle and Oakley, 1972) and burnt flint (Göksu, 1972, Göksu et al., 1974) artefacts.

To avoid triboluminescence, initial TL measurements on heated flint sample were conducted on thin slices of the sample core (Aitken and Wintle, 1977, Göksu, 1972, Göksu et al., 1974, Melcher and Zimmerman, 1977, Wintle and Aitken, 1977). However, the technique suffers from the slice's heterogeneity in terms of opacity and dosimetry (Aitken and Wintle, 1977) and fell into disuse when (1) Valladas (1978) showed that the spurious TL is generated by residual carbonates within the sample and is eliminated by acid treatment with diluted HCl and (2) Huxtable and Jacobi (1982) detected no effect on the luminescence signals from mechanical treatments (grinding, crushing). The preparation protocol for heated flint sample presented in Aitken (1985a) remains the standard.

The identification of the flint samples that have been properly heated can be challenging. An insufficient heating means that the luminescence signal has not been completely reset despite the presence of indication of firing. Several methods to estimate the firing temperature were proposed (Göksu et al., 1989, Koul and Chougaonkar, 2011, Melcher and Zimmerman, 1977, Michab et al., 1998, Valladas, 1981).

Heated flint samples are usually TL dated using multiple aliquot additive dose (MAAD) protocols (Aitken, 1985a, Wintle, 2008). However, a single aliquot regenerative (SAR) protocol, initially developed for sediment dating (Duller, 1991, Mejdahl and Botter-Jensen, 1994, Murray and Wintle, 2000b) was also successfully applied (Richter and Krbetschek, 2006). The possibilities of using the orange-red emission peak (Bailiff et al., 1977, Martini et al., 1999, Richter and Krbetschek, 2006, Richter et al., 1999, Schmidt, 2013, Wintle and Aitken, 1977) and optically stimulated luminescence (OSL) dating (Poolton et al., 1995, Richter and Temming, 2006, Schmidt and Kreutzer, 2013, Tribolo et al., 2003) were also explored with mix results.

Most flint samples present a relatively high internal dose rate component. It has the advantage of reducing the effect of variation of the environmental dose rate and moisture content of the surrounding sediments (Aitken, 1985a). However, the estimation of the dose rate for flint samples encountered its own challenges. The determination of the α-efficiency (*a-value*) was studied by Valladas (1988) and Tribolo et al. (2001). The internal radionuclide distribution is not always homogeneous. The presence of *hot-spots* affects the age estimation (Schmidt et al., 2012, 2013a).

Despite the challenges, being able to date heated flint samples using luminescence dating had an important impact on our understanding of prehistoric populations. It was largely

used in the Levant to date multiple archaeological sites including Quafzeh Cave (Israel, ∼90-100 ka) (Valladas et al., 1988), Es-Skhul (Israel, ∼120 ka) (Mercier et al., 1993), Kebara and Amud Cave (Israel, ∼50-60 ka) (Valladas et al., 1987, 1999), Tabun Cave (Israel) (Mercier and Valladas, 2003), Hayonim Cave (Israel) (Mercier et al., 2007a), Jerf al-Ajla (Syria, ∼36-31 ka) (Richter et al., 2001) and Sodmein Cave (Egypt, ∼120 ka) (Mercier et al., 1999, Schmidt et al., 2015b). All theses studies show a temporal overlap of AMH and Neanderthals of tens of thousands of years in the region.

Multiple other archaeological sites around the Meditarranean were also dated, including Theopetra Cave (Greece, ∼130 ka) (Valladas et al., 2007) and Rhafas Cave (Marocco, ∼60-90 ka) (Mercier et al., 2007b). Direct age estimations were made for archaeological sites around Europe, including Combe Grenal (France, ∼44-113 ka) (Bowman and Seeley, 1978, Bowman and Sieveking, 1983), Saint-Cézaire (France, ∼39-33 ka) (Mercier et al., 1991), Les Forêts (France, ∼93 ka) and Jiboui (France, ∼52 ka) (Duttine et al., 2005), Berigoule (France, ∼54-111 ka) (Richter et al., 2007), Pech de l'Azé IV (France, ∼100-45 ka) (Richter et al., 2013), but also Longmoor (UK, ∼8-10 ka) (Huxtable and Jacobi, 1982), Geissenklösterle Cave (Germany) (Richter et al., 2000), Gruta da Oliveira (Portugal, ∼77-55 ka) (Richter et al., 2014), Piekary IIa (Poland, ∼38 ka) (Mercier et al., 2003), Brno-Bohunice (Czech Republic, ∼59-48 ka) (Richter et al., 2009), Bistricioara-Lutărie (Romania, ∼28-15 ka) (Schmidt et al., 2019) and Românești-Dumbrăviţa I (Romania, ∼39-45 ka) (Schmidt et al., 2013b, Sitlivy et al., 2012). It provides important information on the temporal and spatial distribution of Neanderthals and their progressive replacement by AMH.

TL dating was also used to date African archaeological sites, showing once again the antiquity of modern human behaviour for example in Blombos Cave (South Africa, ∼74 ka) (Tribolo et al., 2006), Rose Cottage Cave (South Africa, ∼62-54 ka) (Valladas et al., 2005) and the Diepkloof rockshelter (South Africa, ∼55-65 ka) (Rigaud et al., 2006).

The TL dating of heated flint samples also allowed to date much older human occupation layers including Schöningen (Germany, ∼337-300 ka) (Richter and Krbetschek, 2015) and La Grande Vallée (France, ∼500-400 ka) (Hérisson et al., 2016). Jebel Irhoud (Morocco, ∼350-280 ka) provides the earliest fossil attributed to a modern form of *Homo sapiens* (Richter et al., 2017a) .

A summary of the state of the art of TL dating can be found in Aitken (1985a) and Wintle (2008) when Mercier et al. (1995b), Richter (2007) and Valladas (1985b, 1992) are specifically dedicated to the TL dating of heated flint samples.

2.3.2 Sample selection and collection

As previously mentioned, what we are calling *flint* in this manuscript covers in fact different materials. From a petrological point of view, flint is a form of chert which occurs in chalk or marly limestone. It can be defined as a sedimentary cryptocrystalline form of quartz, categorized as a variety of chert, which occurs mainly as nodules and masses in sedimentary rocks, such as chalks and limestones. In archaeology, scholars often subsume all varieties of amorphous/microcrystalline siliceous rocks under the expression 'flint' including hornstone, chert, radiolarite and even quartzite. For this reason, some scholars prefer to use the French term 'silex' which is less specific than flint (Schmidt, 2013). All these minerals have colors that can vary from white and nearly translucent to black and opaque, passing by dark grey, green, brown or red.

The identifying and selection of heated flint samples suitable for luminescence dating can be challenging. The colour of a flint (or silex) sample that has been heated often switches to darker shades, usually into black or red tones. Cracks and pot-lids tend to appear at the surface when such material is heated at high temperatures. Unfortunately, only TL analysis can confirm that the heating was sufficient to reset the luminescence signal. Flint can be *naturally* black or reddish and the pot-lids can be the result of a long exposition to sunlight in an arid environment (Martini and Sibilia, 2001). Despite of the presence of heat indicators (red/black, pot-lids, cracks,...), it is not uncommon to discard half of the collected flints because the geological luminescence signal was not fully reset (Aitken, 1985b, Tribolo et al., 2013).

The second important parameter which has to be taken into account when collecting flint samples for luminescence dating is their size. During the sample preparation, it is required to discard any material that could have been partially bleached or that was submitted to a different $\dot{D}$. Typically, it includes material directly exposed to sunlight or to $\alpha-$ and $\beta-$radiations coming from the surrounding sediments.

Fortunately, since most flints that were submitted to a heating treatment are opaque, exposition to sunlight should not affect the luminescence signal from the core material. It is particularly true for TL dating. However, cases of translucent flints for which the core material was partially reset by a long exposition to sunlight have been reported (Bowman and Sieveking, 1983, Huxtable, 1981, Martini et al., 2001).

2.3.3 Sample preparation

The physical and chemical preparation of samples used for luminescence dating has to be done in a red light environment. Some laboratories also used yellow-orange light for

preparing both quartz and feldspar (Duller, 2008, Fattahi and Vahdani motlagh, 2016).

There are two main approaches to the preparation of flint samples for luminescence dating: (1) the slice and (2) the grain methods. The slice method was developed to overcome the problem of triboluminescence generated during sample preparation (Göksu et al., 1974). It was then discovered that triboluminescence is due to the presence of carbonates inside the flint and can be excluded with an acid treatment (Valladas, 1978). The grain method has multiple advantages on slices when estimating the D_e using a standard TL/OSL reader. However, the recent development of the EM-CCD camera and the possibility of spatially resolved TL/OSL (Clark-Balzan and Schwenninger, 2012, Greilich et al., 2015, Kook et al., 2015) generated renewed interest for the use of flint slices. Both methods will destroy the flint artefact. It is therefore important to properly document all samples before starting the preparation.

The slice method

Once the flint sample has been cleaned and any external material deposition removed, it is cut in slices using a water cooled diamond saw. A core drill is then used to extract thin flint discs out of these slices. Those discs should not include any material that was part of the 2 mm external layer of the initial flint sample (Martini et al., 2001).

Finally, the flint discs are cleaned using HCl (10%) to remove potential carbonates that have been exposed by the cutting and the remaining core material is crushed to produce fine grains that will be used for the *a-value* estimation.

The flint discs should be around 0.5 mm thick (Aitken and Wintle, 1977, Bowman and Seeley, 1978, Göksu et al., 1974) with a diameter of maximum 9.7 mm (the standard sample disc size) (Risø, 2015). The flint disks measuring 9.7 mm (diameter) will be placed directly on the sample wheel of the TL/OSL reader when smaller discs have to be placed on sample cups. The top layer of the flint discs will generally be closer to the β source than any quartz grains used for D_e estimation. A specific calibration of the source is therefore required for flint disc dating.

Nowadays, the slice technique has no real advantage when it is not combined with spatially resolved TL/OSL. However, when combined with the measurement of the radionuclide element spatial distribution, it could allow the identification of potential hot spots (Schmidt et al., 2013a, Tribolo et al., 2006).

The grain method

This approach is the most commonly used. The use of quartz grains for heated flint dating was first proposed by Huxtable and Jacobi (1982) and then improved by Valladas (1992).

The first step is to remove the flint's external layer, especially the cortex, which could be partially bleached and exposed to a different $\dot{D}$ than the core material (Aitken, 1985a, Martini et al., 2001). Once the external layer is removed, the core material has to be separated in two. The largest part will be used for the D_e and *a-value* estimations while the remaining part will be collected for estimating the internal radionuclide concentration values. Some scholars use material from the external layer for estimating the radionuclide concentrations, rather than core material. However, such material could have been contaminated by exogenous elements during the burial.

The next step is to crush the core material to produce the coarse grains (CG) and the fine grains (FG) that are respectively used for the D_e and the *a-value* estimations (Huxtable and Jacobi, 1982). The artificially created grains are sieved using two different mesh sizes. Those with a diameter between the 2 mesh sizes are collected for the CG preparation. The smaller grains are collected for FG preparation. Working with mesh size up to 250 μm and down to 80 μm should not influence the final D_e estimation. However, a larger variation between the mesh sizes will increase the uncertainty on the D_e, while a narrower interval will decrease the amount of CG and increase the quantity of FG material.

The last step of the CG preparation is to treat the grains with hydrochloric acid (HCl) for removing any trace of carbonates (Valladas, 1978).

The finer grains requires extra steps for producing proper FG material. The estimation of the *a-value* is done on grains between 4 and 11 μm (Aitken, 1985a). The grains need being crushed again, this time using a pestle and a mortar, until a fine and homogeneous powder is obtained.

A first wet settling, using either deionized H_2O or acetone, allows for selecting the grains that are finer than 11 μm. The fine material remaining in suspension is then dried before being treated with HCl for carbonate removal. A second wet settling allows for removing the silt, i.e. the grains smaller than 4 μm. Acetone, rather than deionized H_2O, is usually used during this last step. The settling times are defined using the Stokes law (Weida and Junding, 1989).

2.3.4 Specifics of heated flint samples regarding the age estimation

Equivalent dose estimation

As seen in the previous section, when dating heated flint, D_e estimation can be done either on flint slices or on flint grains. There is no advantage for using slice except if both the D_e and the $\dot{D}$ estimation are spatially resolved. The luminescence light intensity of heated flint is relatively dim compared to other luminescence materials which makes spatially resolved D_e estimation even more challenging.

When the flint sample is crushed to artificially create grains, the D_e estimation is usually done using the coarse grain (CG) fraction when the fine grain (FG) fraction is dedicated to the *a-value* estimation. Obviously, the D_e estimation could also be done on the FG fraction but it requires crushing the complete flint sample core into fine material, which is more time consuming.

Both the MAAD and SAR measurement protocols can be used for the D_e estimation. The MAAD protocol remains the most used for TL dating of archaeological samples and heated flint samples are no exception (Wintle, 2007, 2008). Recent studies show that using a SAR protocol can also provided reliable age estimations for heated flints (Richter and Krbetschek, 2006, Schmidt, 2013). Removing the external layer of the heated flint artefact can induce the lost of most of the flint material available. It is not uncommon that there is not enough material left for estimating both the D_e and the *a-value* using MAAD measurement protocols. Being able to date smaller heated flint artefacts was amongst the main reasons motivating the use of the SAR measurement protocol for heated flint dating (Richter and Krbetschek, 2006, Schmidt, 2013).

The impact of heat sensitisation is minimum when using the MAAD protocol. It only impacts the test-dose signal which is used to normalise the different aliquot (Bowman and Seeley, 1978). When the material has been properly homogenised before the deposit of the grains on the discs and all the aliquots contain the same quantity of material, heat sensitisation should impact all aliquot in a similar way. Therefore, when using the MAAD protocol, heat sensitisation should not add any systematic uncertainty to the measurement.

During the SAR protocol, the recording of the test-dose signal after each regenerative dose signal allows to take into account the impact of heat sensitisation. However, the *initial* heat sensitisation, generated by the natural dose signal recording, cannot be taken into account. When present, such heat sensitisation may induce a systematic uncertainty on the D_e estimation. However, a significant number of heated flint samples shows no sign of heat sensitisation (Richter, 2007, Schmidt, 2013). Some scholars also

propose to used a isothermal thermoluminescence (ITL) rather than linearly modulated thermoluminescence (TL) to reduce the impact of the heat sensitisation when using the SAR and SARA measurement protocols (Tribolo and Mercier, 2012).

When the large majority of the age estimation made on heated flint were done using blue thermoluminescence (BTL), i.e. the light emitted in the violet-blue spectrum (400-450 nm), red thermoluminescence (RTL), i.e. the emission made in the orange-red spectrum (600-650 nm) was also explored (Bailiff et al., 1977, Martini et al., 1999, Richter and Krbetschek, 2006, Richter et al., 1999, Schmidt, 2013, Wintle and Aitken, 1977). When RTL allows to reach deeper traps and therefore a signal more stable in time, some publications seems to indicate that such signal is not present for all heated flint samples (Schmidt, 2013). Moreover, when the recording of the violet-blue signal is the standard when dating quartz using TL or OSL and, therefore, most of the luminescence laboratories are already equipped to record BTL, RTL requires the use of a specific photomultiplier (PMT) to record the luminescence signal.

Dose rate and a-value estimation

When arriving to $\dot{D}$ estimation, one of the main specificity of heated flint is that the dose rate internal to the flint sample cannot be neglected. In fact, for some samples, this internal dose rate represents most of the dose absorbed by the grains (up to 80 %) (Richter, 2007, Wintle, 2008). When fine and coarse grains are used to estimate the D_e and the *a-value*, the fact that they were created artificially needs to be taken into account. For flint samples with a homogeneous distribution of radionuclide elements, it is done by considering that the the radionuclide concentration inside the grains is equal to the radionuclide concentration of the surrounding flint matrix.

As for the D_e, the *a-value* can be estimated using both a SAR or a MAAD protocol. When the procedure is similar to the D_e estimation, it requires a calibrated α source. This *a-value* estimation should be done on FG to assure the homogeneous α-irradiation of the sample. Some automated TL/OSL readers, like the *Lexsyg Research* can include an α source unit which simplifies the process (it only requires to include a first α irradiation step into the automated measurement protocol). Most of the time however, the aliquots are, often simultaneously, irradiated by an α-source which is independent from the TL/OSL reader.

Not all flint samples have a homogeneous matrix. Some of them also present localised regions with a high concentration of impurities, including radionuclide elements. Those *hot spots* will influence the intensity of the TL signal of the surrounding quartz *grains* (see Fig. 2.13). It will therefore have an impact on the D_e estimation. When such

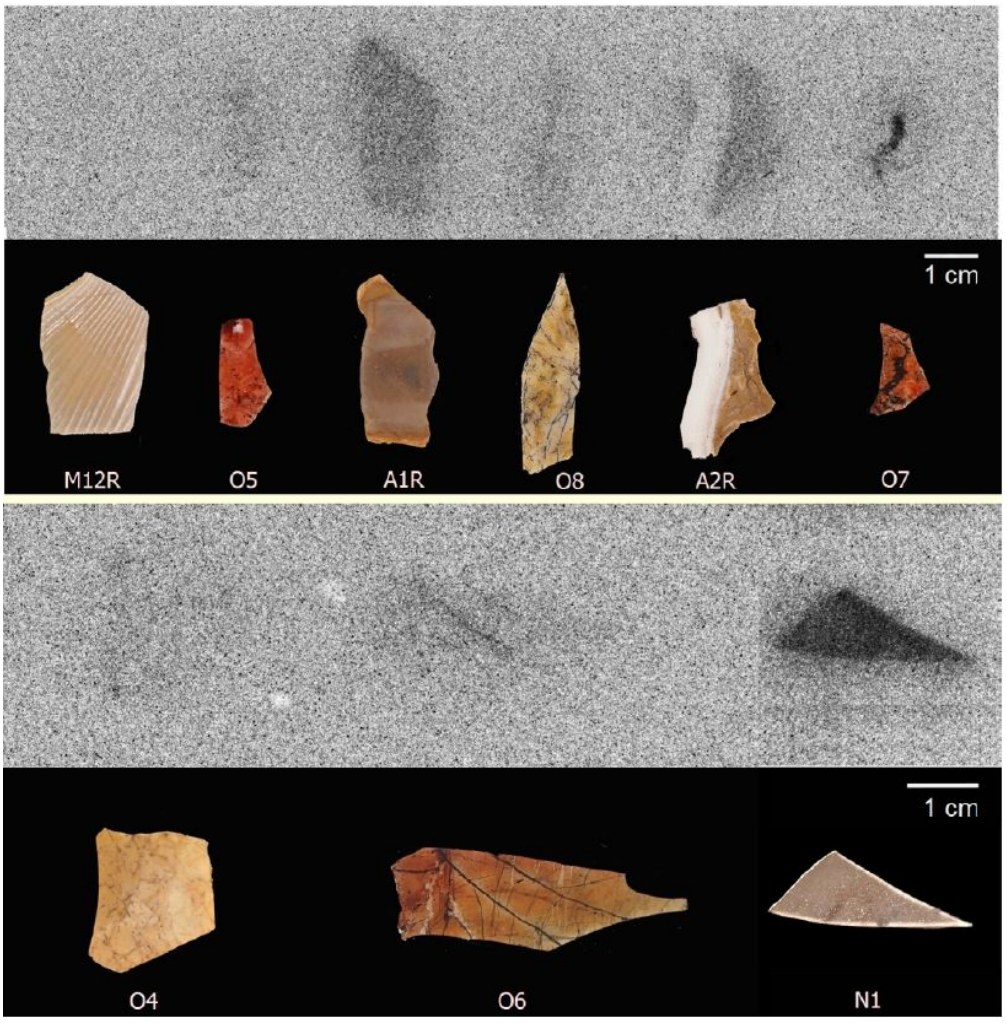


FIGURE 2.13: **Beta-autoradiography images and color scans of nine selected flint samples.** The exposure duration was 263 h, except for sample N1 (123 h). On the upper left-hand side of A2R, a small dark area is observed which can be attributed to cortex remains. Sample O6 and O7 show the presence of hotspot regions where the flint matrix is darker. (Schmidt, 2013).

hot spots are included in the material used to estimate the radionuclide contents of the sample, it will influence the $\dot{D}_{int}$ estimation.

Identifying the presence of hot spots in a flint sample remains a challenging problem. Schmidt (2013) showed that they are often correlated with the present of darker inclusions or veins into the flint matrix . Unfortunately, a visual inspection of the inside of the flint core is generally impossible. However, once the external layer of the flint is removed, a visual inspection of the core's surface provides useful information. When it looks homogeneous, it is usually assumed that it is the case for all the core material. When it already presents sharp colour variation (distinctive inclusions or veins), hot spots may be expected. In that case, the use of flint slices combined with spatially resolved D_e and $\dot{D}_i$ should be considered. Unfortunately, when this manuscript was



FIGURE 2.14: **Heated flint sample (TAI 1).** The presence of a pot-lid (red circle) is a strong indication of an heating of this flint sample (the ruler is 5 cm long).

written, no paper reporting a successful age estimation using such technique had yet been published.

Another solution could be to create a statistical model of the distribution of the radionuclide element inside the flint. Such approach was developed by the Research Institute on Archeomaterial (IRAMAT) from the University of Bordeaux-Montaigne (Martin et al., 2015). However, this approach is time consuming and cannot yet be standardized. It requires access to specific equipment which are not common in most luminescence laboratories, for example 3D scanner. Therefore, samples are usually discarded when the presence of hot spots is suspected.

2.4 CLL protocol for heated flint sample TL dating

The protocol that was applied at the Cologne Luminescence Laboratory (CLL) during the first phase of the CRC 806 for heated flint samples TL dating is presented in Schmidt (2013). This protocol is based on Aitken (1985a) and improved using Mercier et al. (1995a).

2.4.1 Sample collection

As previously mentioned in section 2.3.2, identifying and selecting heated flint samples suitable for luminescence dating can be challenging. In the field, the presence of pot-lids combined with darker colours is considered the most reliable indicator of flint sample heat treatment (see Fig. 2.14).

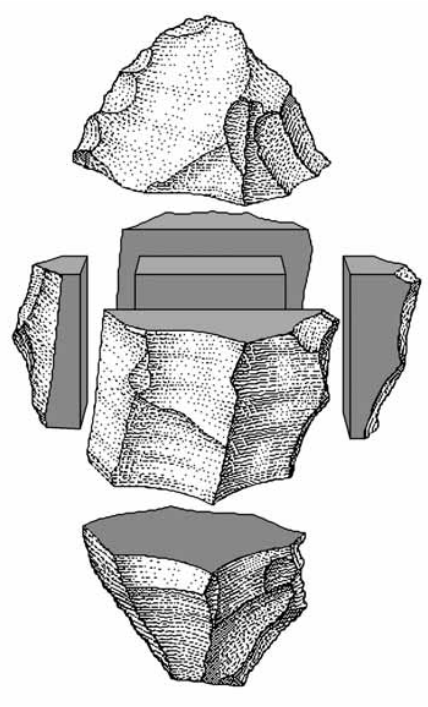


FIGURE 2.15: **Removal of the outer surfaces of a burnt flint using a diamond saw** (diagram courtesy of Dr N Debenham) (Duller, 2008).

Concerning the size of the sample, a rule of thumb used by the CLL is to collect flint samples that are at least 8-10 mm thick and weights more than 10 g. When the flint sample is a few centimetres thick, corrective factors based on the sample geometry must be taken into account for the $\dot{D}$ estimation (Valladas, 1985a). Therefore, for luminescence dating it is recommended to collect heated flint samples that are thinner than 2 cm and shorter than 5 cm when possible.

The samples are stored in black sample bag or protected with aluminium foil as soon as possible for minimising the exposition to sunlight and reducing the risk of a partial reset of the luminescence signal.

2.4.2 Sample preparation

The CLL used the grain method for the sample preparation (see section 2.3.3). First, the flint's external layer, especially the cortex, is removed (see Fig. 2.15). For most opaque flints, removing 2 mm of material is enough (Martini et al., 2001). The cutting is done using a water cooled diamond saw (Mercier et al., 1995a).

At least 200 mg of material has to be collected for the $\dot{D}_{int}$ estimation while using ICP-MS for measuring the radionuclide concentration values (Schmidt, 2013). Material from the flint core is used to avoid contamination by exogenous elements during the burial. It

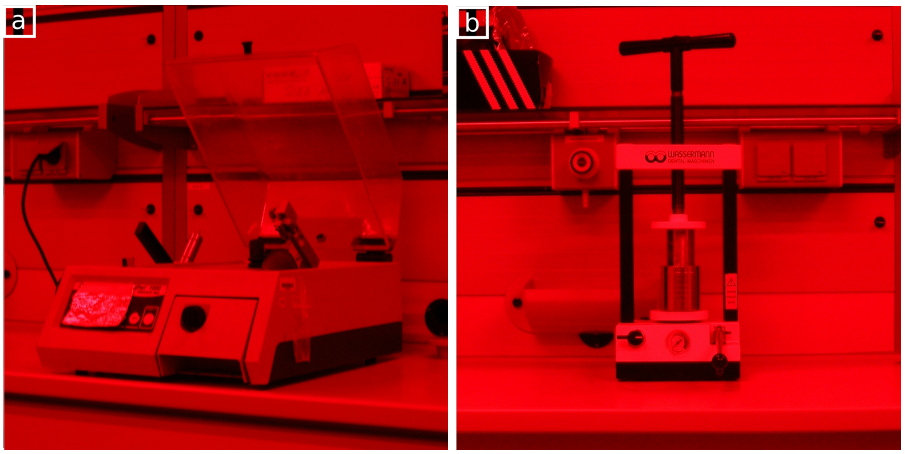


FIGURE 2.16: **(a) Diamond saw and (b) Hydraulic press** used for the heated flint sample's core material extraction and the production of artificial grains (CG and FG).

can be done directly by cutting the core in two using the cooled diamond saw (see Fig. 2.16), or by collecting the material remaining after the first wet sieving of the fine grain preparation (see infra). The first method assures that the right amount of material is collected for the $\dot{D}$ estimation while leading to core material loss. The second method allows for the reuse of core material that would otherwise be lost, but it also requires preparation of the fine grain before any chemical treatment of the coarse grains. The first method should therefore be limited to the largest samples.

The (remaining) core material is crushed to produce the coarse grains (CG) and the fine grains (FG) that will respectively be used for the D_e and the *a-value* estimation (Huxtable and Jacobi, 1982). An hydraulic press and a maximum pressure of 2 to 3 bar is commonly used to gently crush the core material (see Fig. 2.16b) (Mercier et al., 1995b, Schmidt, 2013, Valladas, 1992). After each crushing, the grains are sieved using two different mesh sizes. The grains with a diameter between the 2 mesh size are collected for the CG preparation. The smaller grains are collected for the FG preparation. The bigger grains are crushed again until all the grains are smaller than the bigger mesh size. For our experiments, meshes of 100 and 200 μm are used. Working with mesh size up to 250 μm and down to 80 μm should not influence the final D_e estimation. However, a larger variation between the mesh sizes will increase the uncertainty on the D_e, while a narrower interval will decrease the amount of CG and increase the quantity of FG material.

For the coarse grain fraction, the last step of the process is to treat the grains with HCl to remove any trace of carbonates (Valladas, 1978). For our experiments, HCl (10%) was used and the acid treatment was followed by the washing of the CG several times with deionized H_2O and drying them at 50 $°C$.

The finer fraction (<100 μm) requires extra steps to produce proper FG material. First, the grains are crushed again, this time using a pestle and a mortar, until a fine and homogeneous powder is obtained. The FG material is the fraction between 4-11 μm, i.e. the fine silt. Clay and larger silt fractions are removed by settling processes.

After a HCL (10%) treatment to remove the carbonates, the sample is washed several times, first with water, then with Ethanol, and finally with Acetone. The first settling is made in Acetone (Zimmerman, 1972) and allows for the removal of the larger silt fractions ($> 11\mu m$). The settling time is defined using the Stokes' law:

$$t = \frac{18\nu h}{(\rho_s - \rho_l)gd^2} \tag{2.12}$$

Where t is the settling time, ν the viscosity coefficient, h the height of liquid in the beaker, ρ_s the density of the grains, ρ_l the density of the liquid, g the gravitation acceleration and r the radius of the grain (Weida and Junding, 1989).

For our experiment, the finer material is place in a test tube ($h = 7\ cm$) filled with acetone ($\nu = 0.306\ mPa.s$). The solution is shake using an ultrasonic bath prior to the deposition process. A settling time of 2'40" allows for the deposition of the larger silt fractions ($> 11\mu m$). The suspension ($\leq 11\mu m$) containing the FG fraction is collected in another test tube. The settling material is dried at 50 $°C$ in a oven during one night and can be used for the estimation of the radionuclide concentration values (see supra).

A second settling is required for removing the clay ($< 4\mu m$). A settling time of 21' in acetone ($h = 7\ cm$) allows for the deposition of the fine silt fraction ($> 4\mu m$). Once again the solution is shake using a ultrasonic bath prior to the settling process. The clay is removed by discarding the material still in suspension at the end of the process. The settling material, i.e. the FG ($4 - 11\mu m$), is collected and dried at 50 $°C$ in a oven during one night.

2.4.3 Equivalent dose estimation

The D_e is estimated using the coarse grains (CG) artificially generated from the flint core material during the sample preparation. During the first phase of the CRC 806, the MAAD protocol was the standard for the D_e estimation using TL dating at the CLL (Aitken, 1985a, Wintle, 2007). Experiments were done by Schmidt (2013) to also apply the SAR protocol. However, those were mostly limited to the use of optically stimulated luminescence to date heated flint samples (Schmidt and Kreutzer, 2013).

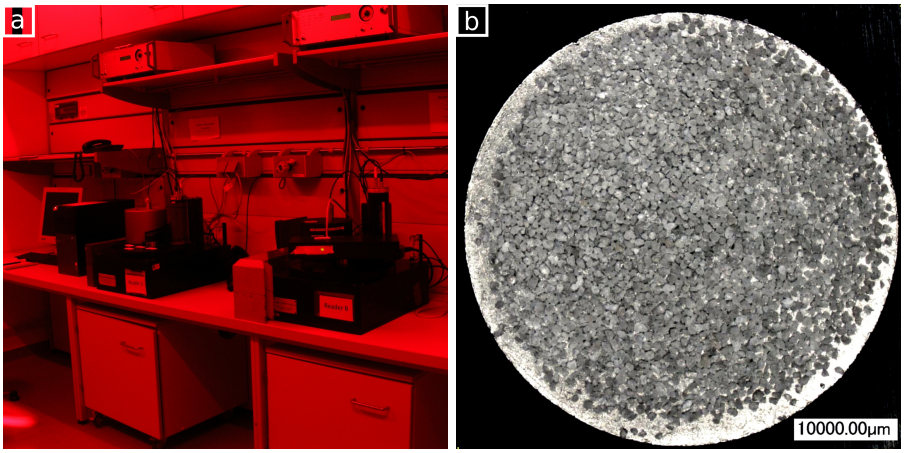


FIGURE 2.17: **(a) Risø TL/OSL DA-20 readers at the CLL. (b) 8 mm coarse grain aliquot deposited onto a stainless steel disc (9.8 mm in diameter)**, photo by AG Prof. Bubenzer.

The impact of heat sensitisation is minimum when using the MAAD protocol. It only impacts the test-dose signal which is used to normalise the different aliquots (Bowman and Seeley, 1978). It is essential to properly homogenise the sample before depositing the grains on the discs and all the aliquots must contain the same amount of material for heat sensitisation to impact them all equally.

Standard stainless steel discs (9.8mm in diameter) are used for the D_e estimation (Schmidt et al., 2011). For the typical aliquots, the central 8 mm (diameter) of the discs is covered with silicone spray using a mask. When the amount of material available is limited, smaller masks (6 to 2 mm) can be used. A monolayer of grains is then deposited onto the discs.

The MAAD protocols rely on LM-TL measurements. The samples are heated to 450 °C with a heating rate of 2 °C.s^{-1}; the background is recorded afterwards and subtracted for each measurement. Natural and additive dose signal measurements are followed by the measurement of a fixed test-dose signal for normalisation (Galloway and Hong, 1996).

TL measurements are performed on Risø TL/OSL DA-15 or TL/OSL DA-20 readers, equipped with EMI 9235QB photomultiplier tubes, in an N_2 atmosphere, using either a UV-blue filter package (BG-39 + GG-400 + Corning 7-59 + Chance Pilkington HA-3) or a blue-transmitting Semrock BrightLine HC 475/50 interference filter (FWHM of 50 nm). The transmission maximum is around 410 nm for the UV-blue combination with a FWHM of $\sim$ 60 nm, but asymmetrically shaped towards higher wavelengths. Samples are β-irradiated in the Risø readers with ^{90}Sr/^{90}Y-sources (Schmidt, 2013).

2.4.4 Dose rate estimation

As seen in Section 2.3.4, the impact of the internal component of the dose rate cannot be neglected. Since the D_e estimation was made using (artificially created) coarse grains, equation 2.10 is used for the dose rate estimation:

$$\dot{D} = (k.\dot{D}_{int,\alpha} + \dot{D}_{int,\beta}) + (\dot{D}_{ext,\beta} + \dot{D}_{ext,\gamma}) + \dot{D}_{env,\gamma} + \dot{D}_c$$

For flint samples with a homogeneous distribution of radionuclide elements, the radionuclide concentration inside the grains can be considered equal to the radionuclide concentration of the surrounding flint matrix. Both the $\dot{D}_{int}$ and the $\dot{D}_{ext}$ are estimated using the radionuclide concentrations in the flint matrix when the $\dot{D}_{env}$ is estimated using radionuclide concentrations in the surrounding sediment.

The cosmic dose rate component is calculated using the dedicated *calc_CosmicDoseRate* function from the *Luminescence* package (Kreutzer et al., 2021) using the flint sample burial depth and geographical position.

a-value

α-efficiency can vary from sample to sample (Mercier et al., 1995a, Zimmerman, 1972). The stopping power of the flint matrix was assumed to be identical to that of quartz for the $\sim$ 3.7 MeV α-particles used for irradiation (Aitken, 1985a). The *k-value* is therefore set equal to the *a-value* (Schmidt, 2013).

The *a-value* of each flint sample is estimated using the FG produced during the sample preparation (see supra). This estimation is performed using a MAAD protocol as a standard. The use of a SAR protocol was explored during the first phase of the CRC 806 (Schmidt et al., 2013b).

The FG are first heated in a furnace at 350 °C for 90 minutes to reset the natural luminescence signal (Mercier et al., 1995a). They are then suspended in water and a drop (1 ml) of the mixture is deposited on aluminium discs (9.8mm in diameter) using a pipette (Schmidt, 2013). Water is used instead of acetone due to its higher surface tension. For the *a-value* estimation, it is essential that the sample deposited on the disk are not too thick. Grain monolayers are ideal. The amount of FG material deposited on each disc should therefore not exceed 1 mg, giving a maximum concentration of 1 mg/ml. Lower concentrations can be used depending on the amount of FG material available and the number of discs that are prepared.

α-irradiations are performed at the University of Bayreuth with a Littlemoore irradiation facility (^{241}Am-foils, $\sim$ 200 MBq) in a vacuum (10^{-2} mbar) or in a Lexsyg research TL/OSL reader (Freiberg Instruments) equipped with a ^{241}Am-source at the CLL ($\sim$ 0.197 Gy/s in 2016). A first calibration of the Cologne ^{241}Am-source was carried out against the Littlemoore source of the Heidelberg luminescence laboratory, which, in turn, has been calibrated against an α-source in Oxford (Schmidt, 2013). TL measurements for the estimation of the equivalent β-dose are made using the same equipment and configuration than for the D_e estimation (see supra).

2.4.4.1 Radionuclide concentration in the flint matrix

The radionuclide concentrations in the flint matrix are estimated using Inductively Coupled Plasma Mass Spectrometry (ICP-MS).

To reduce the risks of contamination, the measurement is performed on core material collected either before the crushing of the sample or after the first wet sieving from the FG preparation (see supra). Depending on the treatments that this core material has already undergone, it may have to be crushed with the hydraulic press then using a mortar and a pestle for obtaining a powder as fine as possible.

200 mg from this powder is prepared using a protocol specifically designed to separate the trace elements from the quartz matrix (see Annexe A). The resulting solution is sent to the laboratory from the Institute of Geology and Mineralogy of the University of Cologne that performs the ICP-MS measurements.

2.4.4.2 Radionuclide concentration in the surrounding sediment matrix

The environmental $\dot{D}$ is estimated based on the radionuclide concentrations in the sediment matrix surrounding the heated flint sample. A sediment sample is usually collected for each heated flint sample (Schmidt, 2013). When the sediment matrix is not homogeneous, it may be required to collect several sediment samples for a single heated flint sample. When multiple heated flint samples are extracted from a single archaeological unit containing an homogeneous sediment matrix, a single sediment sample may be collected for the whole unit.

The collection of the sediment sample starts as soon as an artefact that could potentially be dated is detected, allowing for the collection of sediment material from all around the artefact. Each sediment sample contains $\sim$ 1 kg of material. They are stored in plastic bags that are sealed in the field for keeping the moisture content.



FIGURE 2.18: **HPGe γ-spectrometer** from the CLL: PROFILE M-Series GEM Coaxial P-type HPGe Gamma-Ray Detector (Ortec), photo by Dr. Zander.

In the laboratory, the sediment samples are weighed then dried in an oven at 50 °C for at least one night before being weighed again. The sample water content is estimated using the ratio between both weights (before and after drying). The sediment samples are then stored in sealed 200 to 800 g PP capsules (depending on the amount of material available) for 4 weeks to compensate for radon loss induced by sample preparation.

The radionuclide concentration in the sediment sample is estimated using high resolution γ-spectrometry (Schmidt, 2013). The γ-dose rate measurements are made on a PROFILE M-Series GEM Coaxial P-type HPGe Gamma-Ray Detector (Ortec) at the CLL (see Fig. 2.18).

2.4.5 Age estimation

The calculation of an age estimate is done using a dedicated spreadsheet combining all the data previously estimated (see Fig. 2.19). Conversion factors for gamma and beta dose rates are based on Guerin et al. (2011). Alpha and beta grain size attenuation factors of Brennan et al. (1991) and Guerin et al. (2012), respectively, are applied. The uncertainties are calculated based on Aitken (1985a).

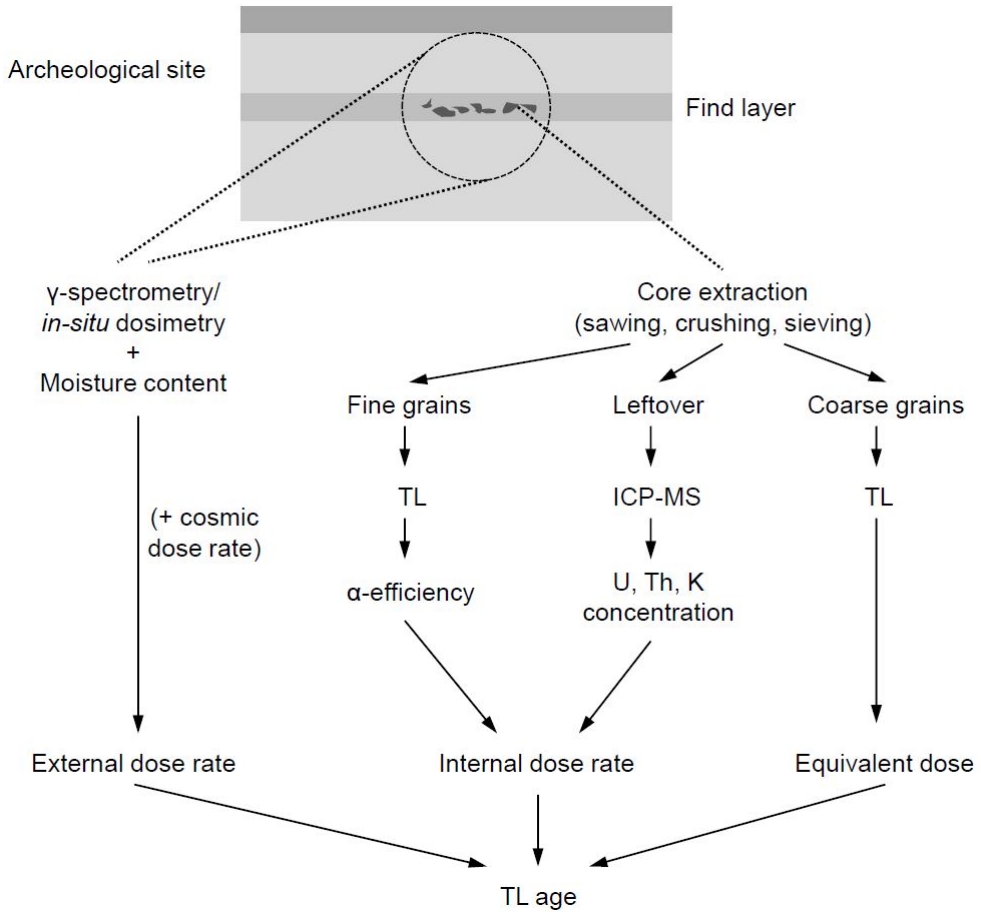


FIGURE 2.19: **Work-flow for TL age determination of heated flint samples.** Estimating a TL age for a heated flint sample requires to combine multiple measurements. The surrounding sediment sample will provide the environmental (here called external) dose rate. The FG fraction of the core material is used to estimate the *a-value*. The CG fraction is used to estimate the D_e and the remaining material from the core is used to estimated the radionuclide element concentration (Schmidt, 2013).

2.5 Software solutions for thermoluminescence dating

As we have seen in the previous section, an age estimation using thermoluminescence dating requires combining multiple measurements and processing a large amount of data. Measurements suffer from uncertainties. These uncertainties propagate through the calculation and needs to be taken into account. The data are coming from various sources and may be encoded in different formats. The estimation of the $\dot{D}$ required conversion factors whose values evolved through time (Adamiec and Aitken, 1998, Guerin et al., 2011, Liritzis et al., 2013). Several publications were dedicated to their determination and it is possible that new conversion factors may be proposed in the future. The selection of these factors influence the $\dot{D}$ and therefore the age estimation. The combination of natural, additive and regenerative luminescence signals to generate a

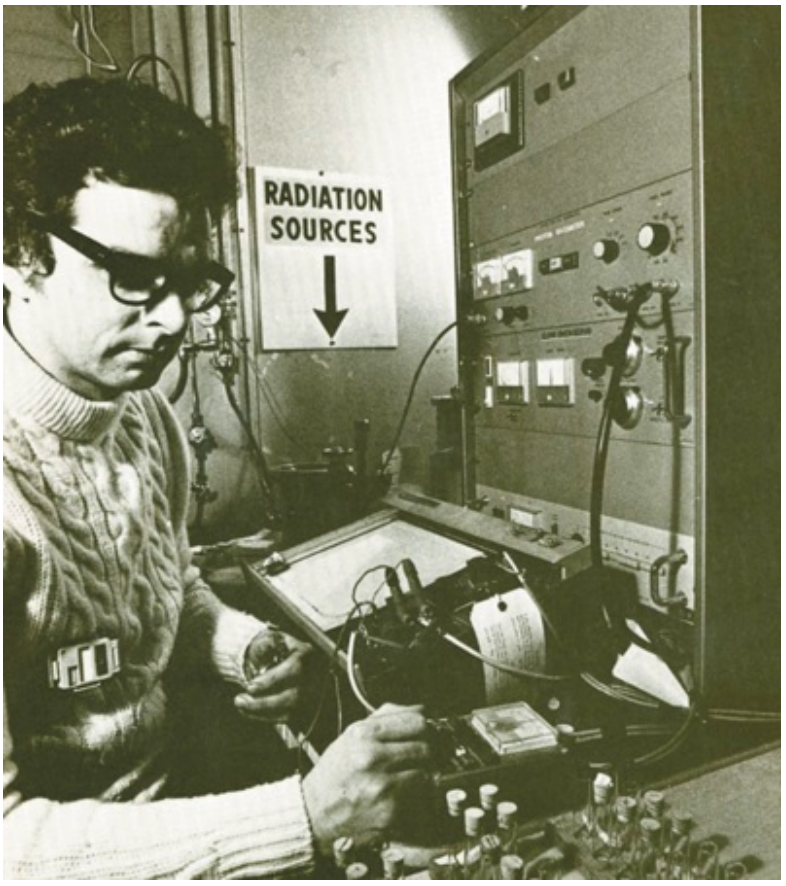


FIGURE 2.20: **Stuart Fleming making TL measurements on equipment from the 1970s** (from the cover of his 1979 book) (Wintle, 2008).

D_e estimation was greatly speeded up and improved by the development of dedicated software solutions.

Data processing is not the only reason that motivates the development of software solutions. In general, the software solutions used for luminescence dating can be separated in three main categories: (1) machine control (MC), (2) data processing and visualisation (DPV), and (3) modelling (MO) software solutions.

2.5.1 Historical software solutions

The first software solutions that were specifically developed for thermoluminescence dating were machine control software (Wintle, 2008). As said by the name, a machine control (MC) software solution is used for controlling the TL/OSL reader. It defines its settings and runs the chosen measurement protocol. It control the duration of the irradiation, the duration, intensity and evolution (linearly modulated or constant) of the heating but also all the other measurement parameters, like the nitrogen flows. In semi-automated TL/OSL reader, they select the aliquot which is process. For some devices,

MC software solution even include the selection of the filters, detection, stimulation and irradiation units used at each step of the measurement.

The first luminescence dating experiments were done completely manually (see Fig. 2.20), from the control of the heating to the processing of the data (Wintle, 2008). However, software solutions quickly appeared to help control the device and process the data. The development of machine control (MC) software strongly improves the reproducibility of the measurements. On one hand, it allows the creation of measurement sequences longer and more complex, and therefore the development of new measurement protocols, like the SAR protocol. On the other hand, it make the development of semi-automated TL/OSL readers possible. New measurement techniques, like spatially resolved luminescence dating, heavily depend on the development of specific machine control software solution.

Among the MC software solutions, we can cite the *Control program* and *Sequence Editor* from *Risø*[4]; *LexStudio 2.0* from *Freiberg Instruments*[5] and *FirstLight Editor* and *Console* from *Daybreak Nuclear*[6]. The measurement devices that are use for the determination of the dose rate also have their own MC software solutions. For example, *ORTEC* provides the *GammaVision*[7] all-in-one application to control its HPGe γ-spectrometer together with the LVis Counting Laboratory Application Manager[8]. MC software solution are usually developed and provided by the manufacturers.

When it comes to data processing and visualisation (DPV) software solutions, we have to distinguish between, on one hand, the DPV software solutions dedicated to the D_e estimation and, on the other hand, those dedicated to the $\dot{D}$ and the age estimations. For the estimation of the D_e, the most famous is probably *Analyst*[9] that is developed by Duller (2015b). It is currently the default DPV software solution for the semi-automated *Risø TL/OSL reader*. However, it is far from the only or even the first DPV software solution developed. For example, the *TLapplic*, and later *FirstLight*, from *Daybreak Nuclear* also include DPV tools (Daybreak, 2001). More recently, *Freiberg instrument* provides its own DPV software solution for D_e estimation: *LexEva*[10]. Some DPV software solutions, like *Viewer* from *Risø*, are exclusively dedicated to the visualisation of the data when others may be exclusively dedicated to data processing, with no graphical output (see table 2.5.1)

[4] https://www.nutech.dtu.dk/english/products-and-services/radiation-instruments/tl_osl_reader/software
[5] https://www.lexsyg.com/software/lexstudio-20-operating-software.html
[6] http://www.daybreaknuclear.us/downloads/downloads.html
[7] https://www.ortec-online.com/products/application-software/gammavision
[8] https://www.ortec-online.com/products/application-software/lvis
[9] https://users.aber.ac.uk/ggd/
[10] https://www.lexsyg.com/software/lexeva-evaluation-software.html

Age Calculation	
Adele	Degering and Degering (2020)
AGE	Grün (2009)
DRAC	Durcan et al. (2015)
DRc	Tsakalos et al. (2015)
Dose rate modelling	
DosiVox	Martin et al. (2015)
Luminescence data analysis	
Analyst	Duller (2015b)
FirstLight	Daybreak (2001)
PTanalyse	Lapp et al. (2009)
RLanalyse	Lapp et al. (2012)
Luminescence data visualisation	
Viewer+	Risø (2015)
Machine control	
Sequence Editor	Risø (2015)
Control	Risø (2015)

TABLE 2.1: **Non exhaustive List of software solutions available for luminescence dating** (based on http://ancienttl.org/software.htm).

The DPV software solutions dedicated to the $\dot{D}$ are usually separated from those dedicated to the D_e estimation. They are often the one that include the tools for the final age estimation. In that case, the value of the D_e estimation, including its uncertainty, is usually encoded 'manually'. Among the most known and commonly used we can cite AGE (Grün, 2009) and DRAC (Durcan et al., 2015) but also Adele (Degering and Degering, 2020). Once again, these are not the only software solutions available. Not all DPV software use the same approach for $\dot{D}$ estimation. DosiVox (Martin et al., 2015), for example, works with a more complex dose rate modelling (see table 2.5.1).

Finally there is a whole new category of software solutions which has developed recently: the data modelling (DM) software solutions dedicated to dating application. We can cite for example *ChronoModel*[11]. Most of these DM software solutions are not directly dedicated to estimate an age but provide new insight on luminescence dating. They can be used, for example, to do 'big data' analysis on existing luminescence age data set or to emulate the electron trapping and releasing mechanisms.

In the previous paragraphs, only stand-alone software solution were presented. Most of them are available for free but a large number are not open source. A non-accessible closed source tool is not, by default, better or worse than a freely available open source tool. When provided by the measurement device manufacturer, it may even provide some security about the quality of the software solution. However, it can make bug

[11] https://chronomodel.com/

tracking and independent validation of the source code more difficult. When disagreements between the results from different sources appear, the ability to track down errors is reduced. Worse, problematic bugs can remain hidden and uncorrected for long periods of time. Once a closed software is not supported by its manufacturer, updates and corrections are not possible and the software often needed to be completely discarded.

When it comes to the D_e estimation, most stand-alone software solutions allow application of the existing measurement protocols. However, creating a new protocol is often challenging. It is not a problem for commercial works but it can become a limitation for research applications. When it comes to the $\dot{D}$ estimation, is it not always easy to know how the different measurements and factors are combined together. Sometimes, strong assumptions are made. It makes the application of the software rather specific. Those assumptions are often required to reduce the number of parameters needed to provide an age estimation. Once again, they are rarely a problem for commercial works but become a limitation for research applications.

For all these reasons, many scholars develop their own DPV tools. Some are made completely from scratch. It allows an unrivalled liberty for the developer. However, it also required to 'reinvent' the wheel. It increases the risk of implementing bugs in functions that already have a reliable version. In the end, coding a new stand-alone software will have the same reliability, flexibility and transparency issues as the already existing ones.

Most of the currently available DPV tools rely on application such as *Excel* or *Matlab* to run. They are composed of open source scripts that can be easily accessed but also modified. When a user identifies a bug or a mistake in the code, they can easily correct it. Such tools are passed on from lab to lab. However, for lot of them, there is no version tracking. It means that, over time, 2 laboratories that get their tool from a single source, and therefore believe to use the exact same one, may work in fact with quite different codes. Some laboratories may have decide to change the values of the conversion factors when other do not. In the absolute, it should not be a problem as long as all the tools that are used for the age estimation are specified. Unfortunately, it is rarely the case (Kreutzer et al., 2017).

Open-source software provides transparency but it also encourages code recycling. Tailored solutions can be built on existing code. Reusing and extending existing codes have a profound impact on how research is carried out. However, it also comes with new challenges that have to be accessed. As seen previously reproducibility and reliability need to be continuously checked. When specifying the measurement devices that were used is a standard for scientific publications, these self-written tools, and more generally, the different software solutions used for the D_e, $\dot{D}$ and age estimations are rarely properly

Chronological modelling	
ArchaeoPhases	Philippe and Vibet (2018)
BayLum	Philippe et al. (2019)
Dose rate modelling	
RCarb	Kreutzer et al. (2019)
Dosimetry	
gamma	Lebrun et al. (2020)
Luminescence data analysis	
Luminescence	Kreutzer et al. (2012)
numOSL	Peng et al. (2013)
tgcd	Peng et al. (2016)
Modelling	
KMS	Peng and Pagonis (2016)
RLumModel	Friedrich et al. (2016)

TABLE 2.2: **Non exhaustive list of R packages available for luminescence dating** (based on http://ancienttl.org/software.htm).

reported (Kreutzer et al., 2017). A non exhaustive, but regularly updated, list of the software solutions commonly used in luminescence dating can be found on the *Ancient TL* website[12].

2.5.2 R and the luminescence community

R is a programming language and environment for statistical computing and graphics. It provides a wide variety of statistical and graphical techniques and is highly versatile (R Core Team, 2015). In 2012, an **R** package especially designed for luminescence data was published (Dietze et al., 2013, Fuchs et al., 2015, Kreutzer et al., 2012). This package, called *Luminescence*, is a marked change in the possibility for statistical analysis, data treatment and plotting of luminescence data. Since its publication, we have observed a rising trend of published software solutions, or more exactly *packages*, using **R** (see table 2.5.2).

Multiple factors can explain the success of the statistical programming language R in the luminescence community, especially when we compare it to historical framework like *Matlab* and *Excel*. First, it is a free and open source software. *Matlab* is a standard in Engineering and Sciences faculties. However it remains a closed software with an expensive licence. There are multiple open source alternatives to *Excel*, for example *LibreOffice*. However compatibility problems remain between different spreadsheet software solutions, especially for *macros* management.

[12] http://ancienttl.org/software.htm

Second, the **R** programming language is very similar to other programming language, including **C**. A programmer used to *Matlab* will have no problem to apply their skills to **R**. A script embedded in an Excel spreadsheet is often difficult to 'read'. It can make bug tracking and correction quite complex. Some Excel macros do not work with all versions of the software or on different operating systems.

The statistical programming language **R** provides a very robust and popular environment. The popularity of **R** has risen not only among the luminescence community but in the academic and scientific world in general. This development can be seen by the Comprehensive R Archive Network (CRAN) statistics. The first R package on CRAN was released in 1997. In 2012, there were around 4000 packages. In 2017, there were more than 10,000 packages and this number grows exponentially with time. This growth brings to another advantage to **R**. Every package published on CRAN is well integrated in the R environment (convenient download and installation). The source code is easily accessible and the package is available for all three major platforms (*Windows*, *MacOS* and *Linux*). Each package also includes a reference manual and can be easily cited in scientific publications.

R natively includes a version control system. Currently, the source codes of the packages published on CRAN are mirrored on *Github*. *Github* is a commercial repository to maintain, develop and host source codes. It is free of charge as long as the source code is made public and open-source. It uses the version control system *Git*[13] (Chacon and Straub, 2014). CRAN automatically archives all packages ever published on the network. It means that package that are renamed, updated or removed remain available. A package which is not supported by its original programmer can therefore be forked when needed. The quality of the data from a publication using an old version of a package can be assessed. Finally, automatic checks are not only run by CRAN before every package submission but also regularly after the first submission, especially when a new version of R will be published. Packages that fail the test are removed until they are updated. It assures that the available package will be installed without error.

The last but not least, interest of **R** for the luminescence community resides in the number of tools already existing. As said previously, open-source software encourages code recycling, allowing tailored solutions to be built on existing code. The *Luminescence* package includes all the tools needed to read and convert the binary files generated by most currently existing TL/OSL readers (Kreutzer et al., 2012). When this project started, all the tools needed for the estimation of an age using OSL and the SAR protocol were already implemented in the *Luminescence* package. Therefore it provides a good starting point to develop new tools dedicated, this time, to TL dating.

[13] https://git-scm.com/

Chapter 3

LumReader: Designing your luminescence experiment with R

David Strebler[1,2], *Svenja Riedesel*[3] , *Georgina King*[4], *Dominik Brill*[2] and *Helmut Brückner*[2]

Notes: The content of this chapter has been published in *Radiation Measurements* **129** (October 2019), 106143. DOI: 10.1016/j.radmeas.2019.106143 (Strebler et al., 2019b). This article was fully written by the main author with the exception of section 3.3.1 that was partially provided by the second author. The remaining co-authors provided valuable input including, but not limited to, content of the **R** package, comments, formatting and (multiple) proofreading. Formatting changes were made to adopt the format of this Thesis.

Keywords: *R, Luminescence dating, TL/OSL reader, filter, Luminescence*

Highlights: *The **R**-package LumReader has been designed to simulate both the detection properties of luminescence readers and the emission properties of materials. Specifically designed for the Luminescence community, it allows easy assessment of the expected characteristics of any luminescence experiment. Not only does it determine the optimal detection window once it is combined with the desired filters, but also compares this detection window with the excitation signal and the expected luminescence signal. A web interface was also developed to make the utilisation of LumReader as simple as possible.*

[1]Corresponding author: david.strebler@outlook.com
[2]Institute of Geography, University of Cologne, Germany
[3]Department of Geography and Earth Sciences, Aberystwyth University, United Kingdom
[4]Institute of Earth Surface Dynamics, University of Lausanne, Switzerland

Abstract

In the last two decades, luminescence dating has entered a phase of diversification. This evolution is strongly linked to a series of technical advances, including but not limited to the improvement of Electron Multiplying Charge-Coupled Device (EMCCD) cameras and the use of violet and yellow LEDs. New measurement techniques have been developed, such as post infra-red infra-red stimulated luminescence (postIR-IRSL) measurement protocols and thermally-transferred OSL (TT-OSL), and the luminescence properties of new materials, such as gypsum and apatite, have been reinvestigated.

The appropriate configuration of detection equipment is key to the design of new experimental investigations. The **R**-package *LumReader* has been designed to simulate both the detection properties of luminescence readers and the emission properties of materials. It allows optimisation of the experimental detection window for a given filter and detector (PMT or EMCCD camera) combination through comparison of the detection window, the stimulation signal and the luminescence emission of the studied material. With the development of a reference database and its flexibility for accommodating user defined functions, this package will allow the spectral information of any luminescence experiment to be simulated, also facilitating experimental design.

3.1 Introduction

More than three decades ago, the first article on the use of *optically stimulated luminescence* (OSL) dating was published (Huntley, 1985). The following fifteen years were dedicated to the improvement of the technique. The development of the *single aliquot regenerative dose* (SAR) protocol (Murray and Wintle, 2000b) induced a phase of measurement protocol standardisation and routine application. However, over the past ten years, research on luminescence dating has entered a new phase of diversification.

The diversification of OSL is related equally to instrumental advances such as the introduction of violet stimulated luminescence (VSL) (Ankjaergaard et al., 2016, 2015, 2013, Jain, 2009), yellow stimulated luminescence (YSL) (Lauer et al., 2011, 2012, Lüthgens et al., 2011) and the use of electron multiplying charge-coupled device (EMCCD) cameras for spatially resolved OSL (Clark-Balzan and Schwenninger, 2012, Greilich et al., 2015, Kook et al., 2015) and spectrally resolved OSL (Demuro et al., 2016, Kook et al., 2016), and to methodological developments, with the introduction of new measurement protocols including the post Infra-Red IRSL (postIR-IRSL) (Buylaert et al., 2009, Roberts, 2012, Thiel et al., 2011, Thomsen et al., 2008), thermally-transferred OSL (TT-OSL) (Chapot et al., 2016, Duller and Wintle, 2012, Wang et al., 2006) or thermally

assisted OSL (TA-OSL) (Polymeris et al., 2016). Thermoluminescence (TL) dating also experienced a renewed interest. Promising results have been obtained for red TL (RTL) of burnt flint (Schmidt et al., 2015b) and volcanic quartz (Tsukamoto et al., 2007). New research has been conducted on TL and OSL dating of minerals other than quartz and feldspar like zircon (van Es et al., 2002a,b, Hanh et al., 2013), gypsum (Aydas et al., 2011, Mahan and Kay, 2012, Nagar et al., 2010), halite (Zhang et al., 2005), apatite (Kitis et al., 2013), calcium carbonate from different origins like shells (Stirling et al., 2012), rizoliths (Polymeris et al., 2016), marble (Pagonis et al., 2009, Polikreti et al., 2003), and even on the dating of polymineral samples of extraterrestrial origins (Blair et al., 2007, Detschel and Lepper, 2009, Jain et al., 2006, McKeever et al., 2010, O'Connor et al., 2011).

Readers with very different configurations are used by the luminescence community. Portable battery-powered IRSL/OSL readers were developed at *SUERC*. They combine IR and blue light stimulations and are designed to analysed bulk sediment samples (Sanderson and Murphy, 2010). *Daybreak Nuclear* produces several TL/OSL readers including a high capacity OSL reader using four Electron Tubes P30CWAD-5 detectors (Bortolot, 2000).

The *Lexsyg* from *Freiberg instruments* and the *Risø TL/OSL reader* from *DTU Nutech* are two semi-automated systems which are widely used. Beside a different design, both devices can include similar equipment and allow equivalent research possibilities. Usually, they are equipped with an EMI 9235QB Bialkali photomultiplier tube (PMT) and three different filters are provided: a Hoya U-340 (7.5 mm), a Schott BG-39 (2 mm) and a Schott BG-3 (3 mm). For multi-grain aliquot measurements, the optical stimulation unit includes infrared (IR) and blue and/or green light emitting diodes (LED). Finally, there is a heating unit enabling measurement of thermoluminescence.

Quartz is sensitive to blue stimulation (BSL) and has a strong emission peak around 375 nm (UV). Feldspar is sensitive to blue (BSL) and IR stimulation (IRSL) and has an emission peak around 410 nm (violet). Therefore, a combination of blue LEDs, for stimulation, and an U-340 filter, in front of the PMT, is commonly used to measure quartz luminescence for dating purposes, whereas IR LEDs with a combination of the BG-39 and BG-3 filters are used to measure feldspar luminescence (Krbetschek et al., 1997, Risø, 2015). The main TL emission peak for quartz is not in the UV but in the blue, around 425 nm. Quartz has a TL peak in the UV at low temperature (110 °C) but it is thermally unstable. It also has a TL peak around 625 nm but the EMI 9235QB PMT sensitivity to the red emission is very low. TL dating of feldspar is even more complicated with peaks ranging from less than 300 nm up to more than 700 nm

depending on the chemical composition and structure of feldspar present in the aliquot (Krbetschek et al., 1997).

Whilst the default filters provided with the readers are well optimized for routine OSL dating of quartz and feldspar from sediment, TL dating and research applications often require the selection of more specific filters. Different PMTs may also be needed to optimize the detection windows, as for RTL. Selecting the best combination of filters for an application can be challenging, especially when different filters have to be combined. When the detection window partially matches the stimulation wavelength, the signal to noise ratio rises (due to the detection of the stimulation signal) and there is a risk of damaging the PMT. Combining too many or inappropriate filters can lead to the loss of most of the luminescence signal.

Most manufacturing companies provide technical descriptions for their products, at least in graphic form and increasingly as spreadsheets. Some even distribute software solutions on how filters and optics can be combined [5]. However these applications or spreadsheets are usually limited to a specific product range. They do not allow the combination of elements from different providers. Neither do they include old products that are no longer available or offer the option to integrate new products/materials. These software solutions are usually free but are not open source. They cannot be modified or updated to extend their databases. It is also difficult to include them in a larger automated process. Due to these limitations, we developed the R package *LumReader*. A software tool focussed on the use of filters in luminescence research applications.

R is a programming language and environment for statistical computing and graphics. It provides a wide variety of statistical and graphical techniques and is highly versatile (R Core Team, 2015). The last five years have seen the publication of different **R** packages dedicated to luminescence dating, including the *Luminescence* package (Dietze et al., 2013, Fuchs et al., 2015, Kreutzer et al., 2021, 2012), the more specific *NumOSL* package (Peng et al., 2013) or the recent *TLdating* package (Strebler et al., 2017) and *BayLum* package (Combès and Philippe, 2017). These packages mainly focus on the analysis of luminescence data to provide an age estimation. **R** can also be used to explore more theoretical aspects of luminescence dating like modelling trap and recombination centre behaviour and generating theoretical luminescence curves (Friedrich et al., 2016, Peng and Pagonis, 2016).

We present here a package designed to optimize the set-up of appropriate combinations of stimulation units, detection units and filters. The *LumReader* package helps to estimate the luminescence detection window of your experiment based on the filters and the

[5] It is the case for example of *SCHOTT Advanced Optics* who provide an *excel* file that allows to combine their filters (see www.schott.com/advanced_optics).

detection unit. It then estimates the emission signal based on the stimulation unit and the investigated material's theoretical properties. Finally, it compares the results and estimates the proportion of the emitted signal that is detected. The package also allows the creation, export and import of text files containing the properties of all of the elements that an instrument or experiment is composed of: filters, stimulation unit, detection unit and materials. The flexibility in terms of implementation of new elements, combination of stimulation unit, filter and material as well as visualisation of data offers considerable advantages over spreadsheet solutions.

3.2 Simulate a TL/OSL experiment using the *LumReader* package

Class objects	Filter	Object containing the properties of a filter
	FilterStack	Object containing the properties of a series of filters
	Stimulation	Object containing the properties of a stimulation unit
	PMT	Object containing the properties of a detection unit
	Material	Object containing the TL and OSL properties of a material
User functions	create_*	Generate a new object directly in **R**
	default_*	Import an object from a file included in the *LumReader* package
	import_*	Import an object from any file
	export_*	Create a file containing the object properties
	plot_*	plot the object properties
Internal functions	combine_Filters	Combine the properties of two filters
	add_Filter	Add a *Filter* to a *FilterStack*
	remove_Filter	Remove a *Filter* from a *FilterStack*

TABLE 3.1: **Main functions of the *LumReader* package.**

A typical luminescence reader is mainly composed of four elements: a stimulation unit, a detection unit, a series of filters, and an irradiation unit. As already seen, the stimulation unit is either optical, LED or laser, for OSL applications, or thermal, for TL applications. Historically, the detection unit is a PMT. Some laboratories are also equipped with EMCCD cameras for spatially and spectrally resolved luminescence. Filters are required to protect the detection unit and select the luminescence wavelengths which will be measured. Filters are also used to reduce the range of stimulation wavelength from the optical stimulation unit. In the following paragraph we will focus on how these different units are described by the *LumReader* package (Table 3.1).

3.2.1 Filters

The optical properties of an absorption filter are determined by the thickness and the wavelength-dependent refractive index $n(\lambda)$ of the glass. At the air-glass interface, a part of the initial luminescence signal will be reflected. This reflection loss is known as the *Fresnel loss* (R). The reflection factor $P(\lambda)$ includes Fresnel loss happening when

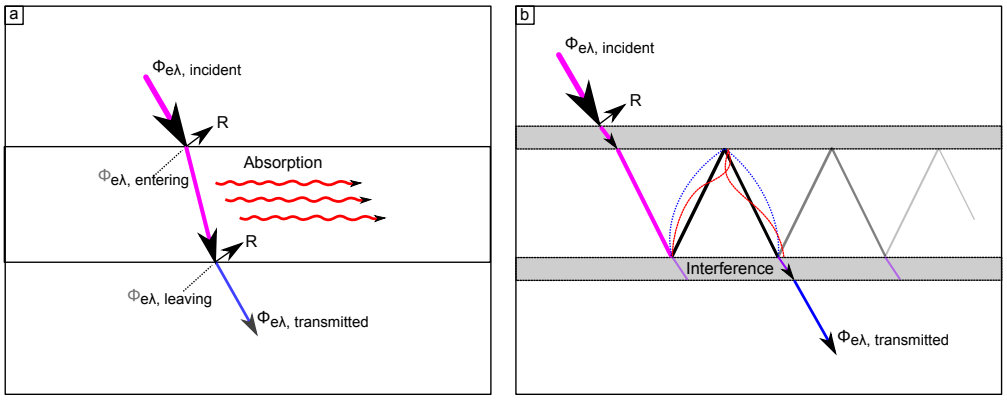


FIGURE 3.1: **Transmittance of (a) an absorption filter and (b) an interference filter.**

both entering and leaving the filter. The most important property of an optical filter is its internal transmittance $\tau_i(\lambda)$. It is the ratio between the spectral flux leaving the filter ($\Phi_{e\lambda,leaving}$) and the spectral flux entering the filter ($\Phi_{e\lambda,entering}$). Internal transmittance is strongly dependent on the wavelength. The total transmittance $\tau(\lambda)$ is the ratio between the transmitted spectral flux ($\Phi_{e\lambda,transmitted}$) and the initial spectral flux ($\Phi_{e\lambda,incident}$) (see Fig. 3.1). Internal transmittance is defined as $\tau(\lambda) = P(\lambda).\tau_i(\lambda)$.

For absorption filters, the reflection factor can usually be considered as wavelength independent and all wavelength dependency integrated into the internal transmittance $\tau_i(\lambda)$, therefore:

$$\tau(\lambda) = P.\tau_i(\lambda) \tag{3.1}$$

$\tau_i(\lambda)$ is dependent on the thickness of the filter. If we assume a perpendicular radiation angle and homogeneous absorption, the Beer–Lambert law allows us to describe the dependence of $\tau_i(\lambda)$ on the glass thickness as $\tau_{i,d_f}(\lambda) = \tau_{i,d_i}(\lambda)^{d_f/d_i}$ where d_i is the initial thickness and d_f is the final thickness. By combining the two equations, we can estimate the spectral transmittance of a filter of thickness d based on the property of a reference filter of thickness d_r as:

$$\tau_d(\lambda) = P.\tau_{i,d_r}(\lambda)^{d/d_r} \tag{3.2}$$

Interference or dichroic filters are composed of a succession of thin-film layers on a glass substrate and use the principle of interference. The transmitted wavelengths depend on the thickness and sequence of the coatings, not on the filter thickness. The total transmittance of an interference filter can still be described using Eq. 3.1. However, the reflection factor P is no longer related to the reflected spectral flux. The transmittance

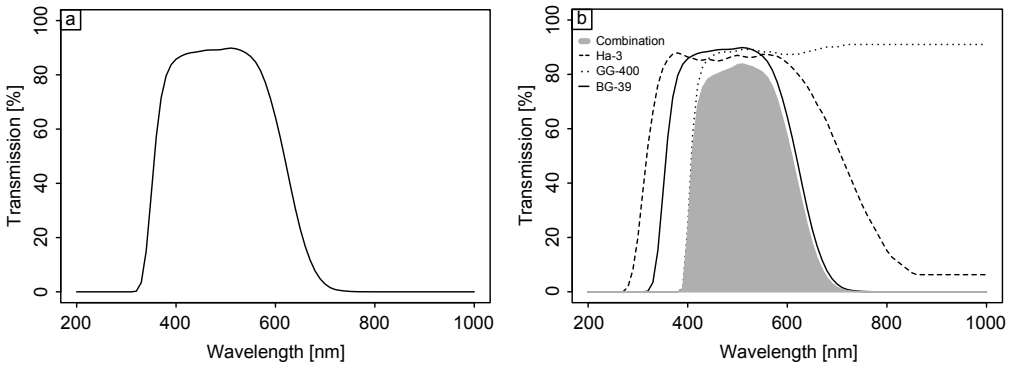


FIGURE 3.2: **Transmission spectrum for (a) the *BG-39* absorption filter and (b) the combination of the *HA-3* (dashed line), *BG-39* (solid line) and *GG-400* (dotted line) filters (grey solid surface).**

of an interference filter is dependent on the incident angle. $\tau_i(\lambda)$ is always defined for light ($\Phi_{e\lambda,incident}$) entering perpendicular to the filter.

In the *LumReader* package, a *Filter* object is described by seven parameters: (1) name, (2) description, (3) *reference* thickness and (4) *effective* thickness, (5) reflection factor, (6) *reference* internal transmission matrix and (7) *effective* internal transmission matrix. The internal transmission matrices are x-y matrices where x is the wavelength, ranging from 200 up to 1000 nm in 10 nm steps, and y is the corresponding internal transmittance.

Create_Filter allows direct creation of a filter in **R**. The internal transmission matrix is systematically resampled. Therefore, the function works with any matrix as long as the first column contains the wavelength and the second column contains the corresponding internal transmission. The *effective* internal transmission matrix is automatically estimated using Eq. 3.2 based on the *reference* internal transmission matrix, the *reference* thickness and the *effective* thickness provided. By default, the *effective* thickness is considered as equal to the *reference* thickness. *Import_Filter* allows an existing filter to be loaded using a *.FLT* file which contains the filter name, description, *reference* thickness and *reference* internal transmission matrix (see online supplement, Fig. B.1). *Default_Filter* allows filters, which are already included in the package, to be imported. It generates a list containing the selected filters and allows an *effective* thickness to be specified for each of them. As indicated by its name, the *plot_Filter* function enables the transmission spectrum of a filter to be plotted. (Fig. 3.2a).

In most experiments, it is necessary to combine different filters to select the appropriate wavelength for the detection unit. In the *LumReader* package, a combination of filters is called a *FilterStack* and is defined by four parameters: (1) name, (2) description, (3) *list* of *Filters* and (4) *resulting Filter*.

Create_FilterStack enables creation of a new *FilterStack*. It automatically generates the *resulting filter*. When filters with the same name are combined, Eq. 3.2 is used to estimate the resulting transmittance. When different filters are combined, the resulting reflection factor will be the higher of the two reflection factors and the resulting internal transmittance will be the product of the internal transmittances. *Plot_FilterStack* allows the transmittance of the filters composing the stack and the resulting filter to be plotted (Fig. 3.2b).

3.2.2 Detection units

The spectral response of a PMT is described by its quantum efficiency, which is the ratio of the number of photoelectrons emitted to the number of initial photons. Most PMTs used in OSL applications have a bialkali photocathode with a spectral response in the 160-650 nm range and a peak radian sensitivity around 400 nm. However, as previously described, some luminescence applications, like RTL, require a completely different detection range.

Charge-Coupled Devices (CCD) are position-sensitive light detectors which offer low dark current, low noise, low-voltage operation, good linearity and good dynamic range (Sze and Ng, 2006). A CCD can be used for OSL measurements enabling spatial resolution (OSL imaging) or wavelength resolution (OSL emission spectroscopy). Luminescence imaging maps OSL and TL intensity as a function of position on the sample. Applications include simultaneously measuring the luminescence from multiple bright grains within the sample (Clark-Balzan and Schwenninger, 2012) and imaging larger objects such as opercula (Duller et al., 2015). In principle, the luminescence image can then be compared with other imaging techniques, such as elemental mapping, to better characterize the source of the luminescence signal or to identify dose rate hot spots. In luminescence emission spectroscopy, the signal is collected and focused into a diffraction grating to disperse the light spatially according to its wavelength. The dispersed light is focused onto the CCD with different wavelengths falling onto different spatial regions of the CCD (Yukihara and McKeever, 2011). Usually, CCD cameras are less sensitive to low light intensity than PMTs but they are sensitive to a much larger range of wavelengths. As for a PMT, the spectral response of a CCD device can be described using a *quantum efficiency* matrix.

The *LumReader* package only focuses on the spectral response of the detection unit. It is expected that the minimum signal threshold for detection will be reached during the experiment and that the detection unit was properly set up to maximise the signal to noise ratio (S/N).

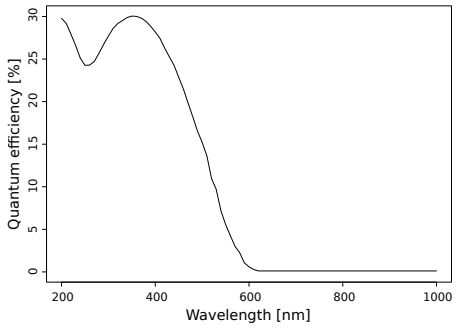


FIGURE 3.3: **Quantum efficiency of the *EMI 9235QG* bialkani PMT.**

In the *LumReader* package, a detection unit is described by a *PMT* class object containing three parameters: (1) name, (2) description and (3) *quantum efficiency* matrix. The *quantum efficiency* matrix is an x-y matrix where x is the wavelength, ranging from 200 up to 1000 nm in 10 nm steps, and y is the corresponding quantum efficiency.

Following the same commands as previously, *create_PMT* allows direct creation of a detection unit in **R**; *import_PMT* allows a detection unit to be loaded using a *.PMT* file which contains the detection unit name, description and quantum efficiency matrix (see online supplement, Fig. B.2); *default_PMT* allows a detection unit already included in the package to be loaded; and *plot_PMT* allows the *quantum efficiency* of a detection unit to be plotted (Fig. 3.3).

3.2.3 Stimulation unit

Usually, stimulation units can be separated in two categories: the heating unit required for TL and the light sources required for OSL. It has to be noted that OSL measurements are rarely done at room temperature therefore they also require the use of a heating unit.

Historically, the first luminescence dating technique to be developed was TL dating. It requires a stimulation unit capable of homogeneously heating the sample up to c.500 °C. A heating unit can be approximated as a black body and its spectral radiance can be described using the Planck's law.

The light sources can be separated into three subcategories: lamps, light-emitting diodes (LEDs) and lasers. The light source selection for an experiment depends on the stimulation wavelength needed and the mode of stimulation, i.e. continuous wave OSL (CW-OSL), linearly modulated OSL (LM-OSL) or pulsed OSL (P-OSL) (Yukihara and McKeever, 2011). Lamps are easy to operate and can provide a large and continuous spectrum in the visible and near-IR for halogen lamps, extending into the UV for arc and gas discharge lamps. However, most of the light output must be filtered to retain only the desired stimulation band, which can result in low efficiency. LEDs are smaller, more

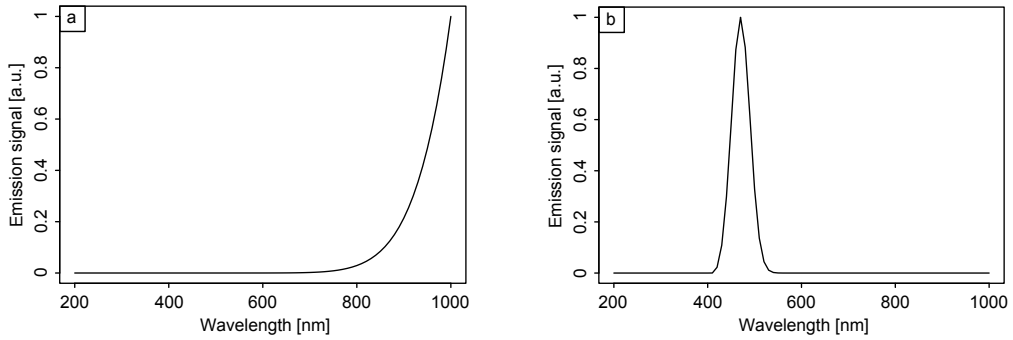


FIGURE 3.4: **(a) Black body radiation at 500 °C symbolizing a TL stimulation unit and (b) the emission peak emitted by a *Risø* BSL stimulation unit.**

efficient and have a much longer operating life. It is possible to obtain LEDs emitting in the IR to the UV range which can be pulsed in the microsecond range (Yukihara and McKeever, 2011). Laser light is highly monochromatic, directional and can be pulsed with high frequency and short pulse duration. Lasers are available in a variety of media and species in wavelengths ranging from the UV to the IR. The narrow beam and highly directional light produced by a laser can be focused to stimulate the OSL from narrow regions of a material. Focused down to a spot of 20 μm in diameter, they can be used for OSL stimulation of single grains (Duller et al., 1999). Most recent TL/OSL readers use LEDs for multi-grain applications and lasers for single-grain applications.

In the *LumReader* package, *stimulation* class objects contain three parameters: (1) name, (2) description and (3) *emission* matrix. The emission matrix is an x-y matrix where x is the wavelength, ranging from 200 up to 1000 nm in 10 nm steps, and y is the corresponding emission intensity in arbitrary units.

As always, *create_Stimulation* allows direct creation of a stimulation unit in **R** and the emission matrix is systematically resampled. It has to be noted that the effects of the filters included in the stimulation unit have to be directly included in the emission matrix. *Import_Stimulation* allows loading of a stimulation unit using a *.EXI* file containing the stimulation unit name, description and emission matrix (see online supplement, Fig. B.3); *default_Stimulation* allows a stimulation unit included in the package to be imported; and *plot_Stimulation* allows the emission spectrum of a stimulation unit to be plotted (Fig. 3.4).

3.2.4 Reader

A luminescence reader is composed of a stimulation unit, a detection unit and a series of filters placed in front of the detection unit to select the wavelength reaching it.

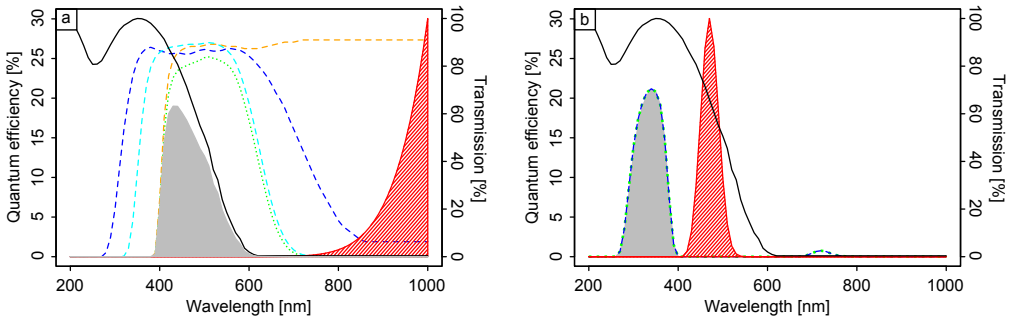


FIGURE 3.5: **(a) Reader configuration for TL dating of burnt flint:** The detection unit is a 9235QB PMT (black line) and is protected by 3 filters: an HA-3 (dashed purple line), a BG-39 (dashed blue line), and a GG-400 (dashed orange line); **(b) Reader configuration for OSL dating of quartz sediment:** the 9235QB PMT (black line) is protected by an U-340 filter (dashed line). In both combinations, the reader detection windows (grey solid surfaces) and the stimulation signal (red dashed surfaces) do not overlap. The green dotted lines are the filter combination transmissions.

In the *LumReader* package, *Reader* class objects contain six parameters: (1) name, (2) description, (3) *Stimulation* unit, (4) *Detection* unit, (5) *FilterStack* containing the *Filters* and (6) *detection window*. To create a new reader, the user must first generate the elements composing it (*Stimulation* unit, *Detection* unit and *FilterStack*) using the corresponding *create_**, *import_** and/or *default_** functions. Those objects are then combined using the *create_Reader* function. The *detection window* is automatically generated and combines the properties of the *Detection* unit and the *FilterStack*. *Plot_Reader* plots the total transmittance from the different filters and from their combination, the quantum efficiency of the detection unit and the detection windows resulting from the combination of the detection unit with the filters. It also plots the stimulation signal, allowing comparison with the detection window to ensure that they do not overlap (Fig. 3.5).

3.2.5 Material

The *LumReader* package enables definition of the OSL and TL properties of a material. Materials react differently when being stimulated by heat or light (Krbetschek et al., 1997). Not all materials are sensitive to the same stimulation wavelengths, for example feldspar is sensitive to IR whereas quartz is not (Duller, 2003, Smith et al., 1990). Some materials emit at different wavelengths when they are stimulated, such as quartz which can emit in the blue (BTL) and in the red (RTL). Finally, similar materials can sometimes have very distinct luminescence behaviour based on their origin, chemical composition and history.

Several papers have studied the relationship between the TL emission wavelength and the stimulation temperature (Krbetschek et al., 1997). Unfortunately, much less has been done on the relation between the OSL emission and stimulation wavelength. Indeed, these kind of studies require specific equipment including a stimulation unit able to shift its stimulation wavelength. Therefore, most papers focus on the emission spectra of VSL/BSL or IRSL independently (Hütt et al., 1988, Krbetschek et al., 1997, Spooner, 1994a,b).

In the *LumReader* package, *Material* objects contain five parameters: (1) name, (2) description of the TL properties, (3) description of the OSL properties, (4) TL emission matrix and (5) OSL emission matrix.

The TL matrix is a matrix where the first column contains the emission wavelength, ranging from 200 up to 1000 nm in 10 nm steps, the second column contains the stimulation temperature, ranging from 0 to 800 °C in 10 °C steps, and the last column contains the intensity in arbitrary units. The OSL matrix is a matrix where the first column contains the emission wavelength, ranging from 200 up to 1000 nm in 10 nm steps, the second column contains the stimulation wavelength, ranging from 200 to 1000 nm in 10 nm steps, and the last column contains the intensity in arbitrary units.

Create_Material allows direct creation of a material in **R**. The TL and OSL matrices are systematically resampled. Therefore, the function works with any matrix as long as the first column contains the emission wavelength, the second column contains the stimulation temperature/wavelength and the third column contains the corresponding emission intensity. *Import_Material* allows loading of a material using a *.TL* and a *.OSL* file (see online supplement, Figs. B.4 and B.5). A .TL file contains the material name, the description of the TL properties and the TL emission matrix. A .OSL file contains the material name, the description of the OSL properties and the OSL emission matrix. It is also possible to create a material containing only TL or OSL properties. *Default_Material* allows the properties of a material which is already included in the package to be imported and *plot_Material* allows the TL and OSL emission properties of a material to be plotted (Fig. 3.6). This function generates surface plots of the TL and the OSL emission intensities using the *levelplot* function from the *lattice* package (Sarkar, 2008). It then generates 3D plots of these emission intensities using the *plot_ly* function from the *plotly* package (Sievert et al., 2016).

3.2.6 Experiment

An *Experiment* is the combination of a *Reader* with a *Material*. As seen previously, the TL and OSL properties of a material can be very different. Therefore, the first step of

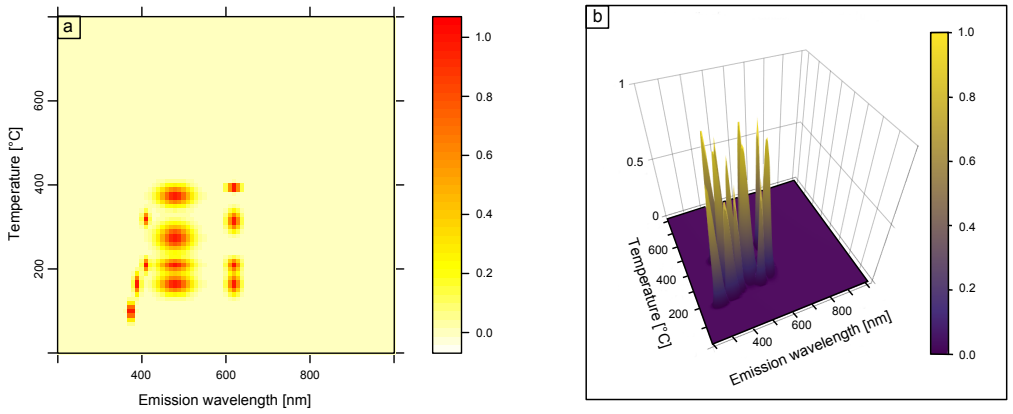


FIGURE 3.6: **Theoretical thermoluminescence emission properties of quartz** based on Krbetschek et al. (1997) expressed (a) as a level plot and (b) as a 3D plot.

an experiment is to choose which luminescence emission will be explored, TL or OSL. The second step is to select a stimulation interval of interest for the experiment. For OSL dating, this interval is determined by the *Stimulation* unit included in the *Reader*. For TL dating, is it usually around the position of the brightest *stable* TL peak. The trapped-electron lifetimes of some minerals and luminescence emissions can be explained by the Arrhenius relationship:

$$\tau = s^{-1} e^{E/k_B T} \tag{3.3}$$

where s is the frequency factor, E (eV) the trap depth, T the absolute temperature and k_B the Botzmann's constant (Aitken, 1985a). The lifetime depends on the trap depth but also on the temperature. When increasing the stimulation temperature, progressively deeper traps become unstable and start to produce luminescence. Therefore, the traps are usually defined by the temperature at which they emit a maximum of luminescence.

In the *LumReader* package, *Experiment* class objects contain eight parameters: (1) name, (2) description, (3) *Reader*, (4) *Material*, (5) *type* of experiment (TL or OSL), (6) stimulation interval of interest, (7) *Emission* spectra for this interval, and (8) the part of this signal which is actually *Detected* by the reader.

In the same way as for the *Reader*, the elements composing a new *Experiment* have to be generated before being combined using the *create_Experiment* function. For TL dating, *create_Experiment* considers that the default stimulation interval of interest is between 320 and 400 °C. For OSL, the default stimulation interval of interest is the stimulation unit peak position ±20 μm. These values can be modified using the *interval* parameter. The *Emission* and *Detected* spectra are automatically generated when the *Experiment* is created.

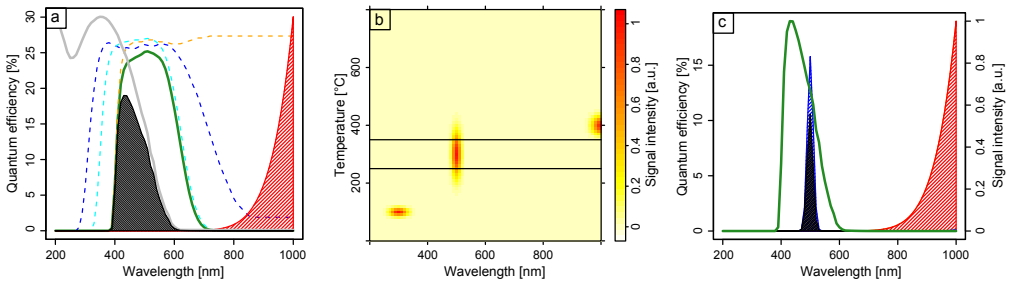


FIGURE 3.7: **Simulation of an experiment using the R package *LumReader*.** (a) The experiment use a TL stimulation unit and a 9235QB PMT protected by 3 filters (HA-3, BG-39 and GG-400, see Fig. 3.5 for more details). (b) The material shows one peak in the region of interest (around 300 °C) and two peaks out of the region of interest (around 100 and 400 °C); (c) Nearly all the signal from the emission peak in the region of interest (blue hatched surface) is detected by the reader (black solid surface). If we change our region of interest and focus on the peak at 400 °C which emits in the near-infrared, the actual configuration of the reader will not allow the detecting of any luminescence signal. The red hatched surfaces represent the stimulation signal (see Fig. 3.4 for more details).

Plot_Experiment allows the properties of an *Experiment* object to be plotted. First this function plots the emission and detection properties of the reader and its components (Fig. 3.7a). It allows any overlap between the detection windows and the stimulation signal to be identified and avoided. It then generates a level plot of the TL or OSL emission intensity (depending on the experiment *type*) of the *Material* using the *levelplot* function (Sarkar, 2008) and indicates the *stimulation interval of interest* for this Experiment (Fig. 3.7b). It allows the user to check that the stimulation unit was properly selected for the material analysed. Finally, The *plot_Experiment* function compares the *Detection* windows from the reader to the signal emitted by the material in the stimulation interval of interest and indicates how much of this *Emission* signal is actually detected. It ensures that the detection unit and the filter combination are appropriately selected for the material under analysis (Fig. 3.7c).

3.3 Case studies

3.3.1 Visualisation of the TL emission from feldspar samples

Most software solutions available online focus only on the selection of filter combinations or on the visualisation of the luminescence properties of a material. The *LumReader* package enables the user to do both and to combine the results. Examples of possible filter combinations have been given earlier in the paper. A case study will now show the applicability of *LumReader* to analysis of TL emission spectra of two feldspar samples, F1 and NB139.

Both samples have been studied previously (Clark and Sanderson, 1994, King et al., 2016, Riedesel et al., 2019, Sanderson and Clark, 1994). The samples under investigation are sand-sized perthitic alkali feldspar, with chemical compositions of 61.3% Orthoclase, 33.4% Albite and 5.4% Anorthite (F1) and 89.3% Orthoclase, 9.4% Albite and 1.4% Anorthite (NB139), when assuming 100% feldspar, determined using the risøXRF OSL/TL reader attachment (Kook et al., 2015). F1 is an International Atomic Energy Agency (IAEA AQCS) secondary reference feldspar (IAEA, 1999), whereas NB139 is a bedrock sample taken from the Namche Barwa massif in the Himalaya (King et al., 2016).

The TL spectra were measured using a risøTL/OSL DA-20 Reader (Bøtter-Jensen et al., 2010, Lapp et al., 2015), equipped with a $^{90}Sr/^{90}Y$ beta source (delivering $\approx 0.1\ Gy/s$ at the sample position) and a risøhigh-sensitive EMCCD-based spectrometer (Thomsen et al., 2018).

Prior to measurement the samples were mounted in aluminium cups as large aliquots of sand-sized material. A blank aluminium cup was measured to allow background correction of the recorded sample spectra. Two different experiments were conducted for both samples. First, after irradiation with a 500 Gy beta dose, the sample material was heated to 450 $°C$ using a heating rate of 5 $°C/s$ and a temperature step of 1.8 $°C$ (resulting in a total of 251 steps). In a second experiment, the same aliquot was irradiated with 500 Gy once more, before being preheated to 250 $°C$ to remove the TL signal which is unstable over laboratory timescales. The aliquot was then heated to 450 $°C$ using the same heating rate of 5 $°C/s$ and temperature step of 1.8 $°C$ as in the previous experiment. Emission spectra were recorded between 300 and 740 nm and the system corrected spectra are shown in Figures 3.8 and 3.9.

Sample F1 is dominated by an emission peak between 520 and 600 nm, from 90 to 270 $°C$ (Fig. 3.8). In contrast, the low temperature peak that dominates the TL emission from sample NB139 is more localized, extending from 470 to 540 nm between 90 and 150 $°C$ (Fig. 3.9). The differences in the emission characteristics of these samples may relate to their chemical compositions. Krbetschek and Rieser (1995) found that Albite emits brightly at 330 nm and 560 nm, with intensities up to two orders of magnitude greater than orthoclase. In contrast orthoclase has a broad blue emission at 420 nm and a green emission at 510 nm (Krbetschek and Rieser, 1995). The data presented here for F1 and NB139 are consistent with these earlier results, F1 contains a relatively high concentration of Albite (33.4%) and its spectra is dominated by the yellow emission at 560 nm. In contrast sample NB139 contains less Albite (9.4%), and its spectrum is dominated by the orthoclase emission.

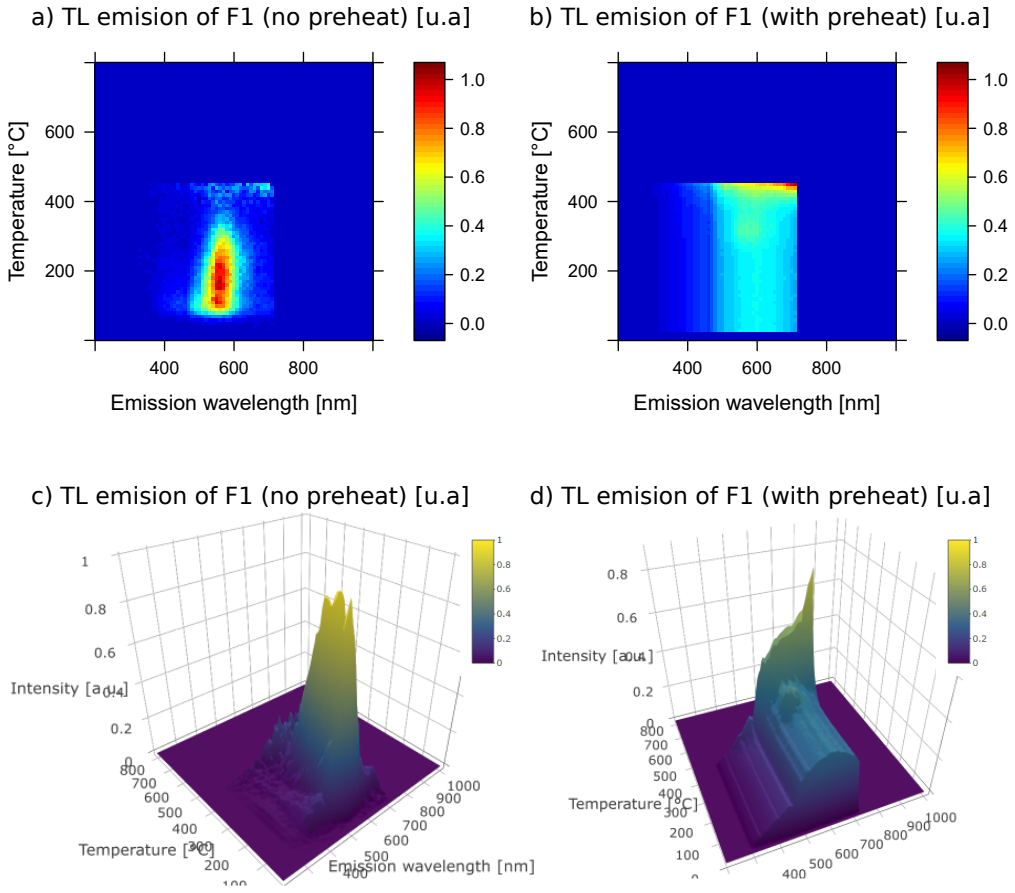


FIGURE 3.8: **TL emission for the F1 feldspar sample:** (a-c) without any preheat; (b-d) with a preheat. The data are shown using a level plot in (a,b) and a 3D plot in (c,d).

Sohbati et al. (2013) explored the potential of Na-rich feldspars for rock surface dating. They used a filter combination of a Schott BG39 and Corning 7-59 to isolate a blue emission, and a filter combination of an OG 515, 730 IK, 2 x 660 IK and a band-pass interference filter with FWHM 511-563 nm to isolate a yellow emission from their samples. They determined that the blue emission originated from K-feldspar contamination of the Na-feldspar, which was dominated by a yellow emission. The equivalent dose that Sohbati et al. (2013) obtained for the blue emission was larger than that obtained for the yellow emission, related to the higher dose rate of K-feldspars due to their internal K-content. Their study highlights the importance of isolating the emission of different feldspar minerals where multi-grain sedimentary samples are investigated, to avoid age bias caused by the application of inappropriate dose rate.

Using LumReader the filter stack combinations proposed by Sohbati et al. (2013) were applied to the emission spectra of samples F1 and NB139. Whereas only a low luminescence sensitivity of sample F1 can be obtained within the blue-filter stack window, a brighter yellow emission could be isolated which could be used for dating purposes, providing that no internal K-content is assumed. In contrast a bright blue emission

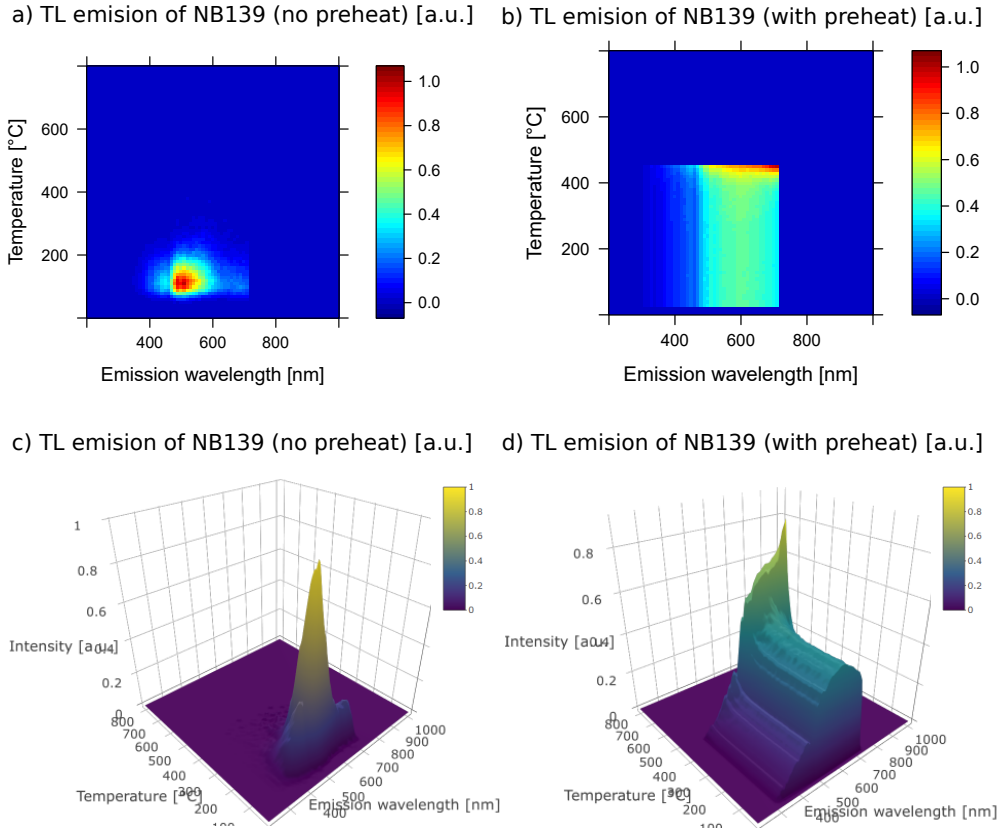


FIGURE 3.9: **TL emission for the NB139 feldspar sample:** (a-c) without any preheat; (b-d) with a preheat. The data are shown using a level plot in (a,b) and a 3D plot in (c,d).

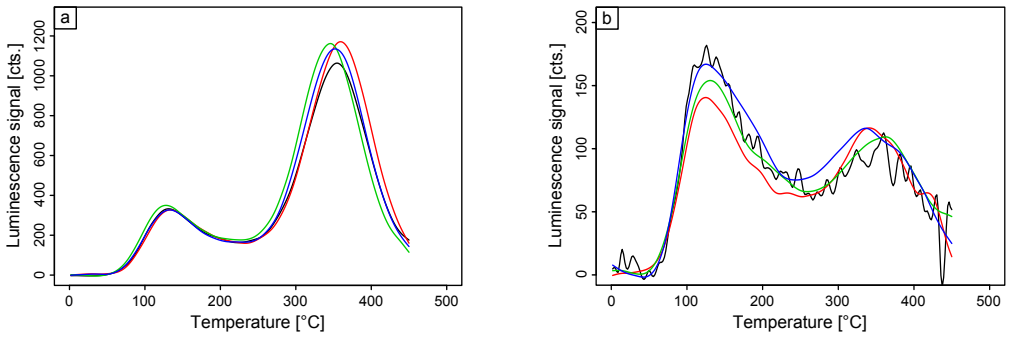


FIGURE 3.10: **Luminescence signal for (a) 4 coarse grain (100-200 μm) aliquots and (b) 4 fine grain (4-10 μm) aliquots after 100 s of β-irradiation (around 10 Gy)** using a combination of the HA-3, GG-400, BG-39 and 7-59 filters. All the curves were smoothed using the *smooth.spline* function from the *stats* package.

can be isolated for sample NB139, for which an internal dose rate from K_2O should be assumed.

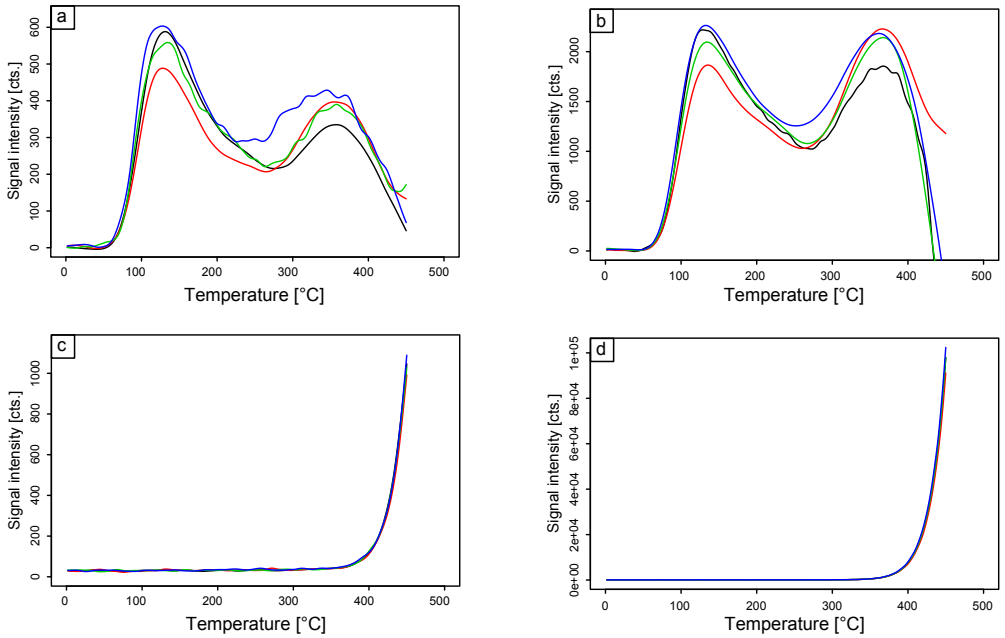


FIGURE 3.11: **Luminescence signal for 4 fine grain (4-11 μm) aliquots after 400s of β-irradiation (around 40 Gy)** using a combination of (a) the HA-3, GG-400, BG-39 and 7-59 filters and (b) the HA-3, GG-400 and BG-39 filters (without the 7-59); (c) and (d) being the respective background signals. All the curves were smoothed using the *smooth.spline* function from the *stats* package.

3.3.2 Optimisation of the reader configuration for the dating of heated flint samples

The *LumReader* package was used to optimize the filter selection for burnt flint dating. Based on Schmidt (2013), we initially measured a sample using a combination of a Schott HA-3 (3 mm), a heat-absorbing filter, a Schott GG-400 (1 mm) to reduce the signal coming from the 110 $°C$ peak, a Schott BG-39 (1 mm) and a Corning 7-59 (1 mm) filters. This filter combination provided reliable and reproducible signals for coarse grain (100-200 μm) aliquots (Fig. 3.10a). However, when we started to measure fine grain (4-11 μm) aliquots for a-value estimation, the signal became very dim, especially for β-doses below 10 Gy (Fig. 3.10b). To increase the detected signal, we removed the 7-59 filter. For a β-dose of 40 Gy, this new combination multiplied the signal around the peak position by 5 (see Fig. 3.11a, b). However, the black body radiation at 450° increased by 50 times, from less than 2000 up to 10^5 counts (Fig. 3.11c, d). This increase of the background signal strongly increases the uncertainties on the final results.

Using the *LumReader* package, an imaginary quartz material was simulated based on the table provided in Krbetschek et al. (1997, p.707) (Fig. 3.6). Even if this model is not quantitatively correct, it shows that the initial detection window of our reader only allows us to detect a small part of the quartz blue TL emission (Fig. 3.12a). The

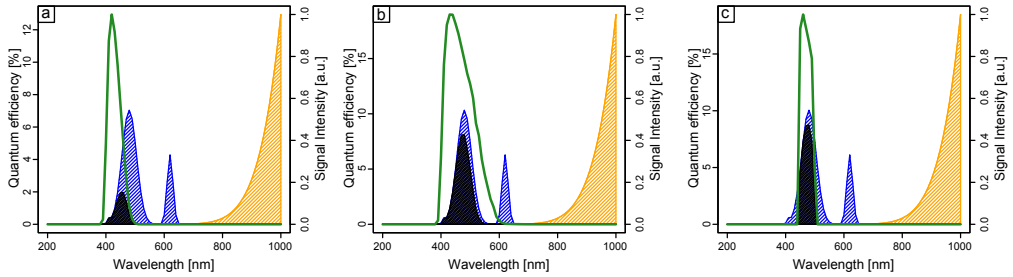


FIGURE 3.12: **Simulation of the thermoluminescence experiment using different filter combinations:** (a) the initial HA-3, GG-400, BG-39 and 7-59 filters combination, (b) the same combination without the 7-59 filter and (c) an alternative combination including a KG-3 and a 475/50 interference filter. The orange curve represents the black body radiation at 500 °C, the blue curve represents the thermoluminescence signal between 350 and 400 °C, the green curve is the different detection windows and the black curves is the emission signal detected by the reader.

second filter combination, without the Corning 7-59, allows us to detect all of the BTL signal but also the tail of the quartz red TL emission (Fig. 3.12b). Black body radiation increases with wavelength and with this second combination, it is the PMT itself that defines the maximum wavelength detected, not the filters. The ideal detection windows for quartz TL should be between 450 and 500 nm (Krbetschek et al., 1997). For a combination of a Semrock Brightline HC 475/50, as used in Schmidt et al. (2015b), and a heat-absorbing Schott KG-3 (1 mm) filter our simulation indicates detection of most of the blue TL peaks while avoiding the red TL emission and reducing the background signal (Fig. 3.12c).

In practice, the intensity of the signal measured with the last combination (475/50 and KG-3) had the same magnitude as the intensity measured using the first combination (HA-3, GG-400, BG-39, 7-59) which seems to contradict our simulation (see Fig. 3.13). However, the HC 475/50 and KG-3 filters used in our measurement only have a diameter of 25 mm, relative to 44 mm for the HA-3, 7-59, BG-39 and GG-400. On the *Risø TL/OSL reader*, the distance between the sample and the PMT is around 55 mm (Risø, 2015). Therefore, the solid angle of the detector was roughly divided by 3 when we exchanged the filters[6]. We can conclude that the new filter combination has a better detection windows but the gain was nearly neutralized by the reduction of the detection solid angle.

As we can see, even with a simplistic model for material properties, the *LumReader* package allows an easy comparison of different filter combinations and can explain the difference between results obtained using different measurement conditions. It has to be noted that the intensity of the luminescence signal reaching the detector unit also depends on parameters which are not simulated by this package, like the detection unit

[6] $R = \frac{\Omega_1}{\Omega_2}$ where $\Omega_i = 2\pi(1 - \cos\theta_i)$, $\theta_i = \frac{h}{r_i}$ and $r_i = \sqrt{(\frac{d_i}{2})^2 + h^2}$ with $h = 55$ mm, $d_1 = 25$ mm and $d_2 = 44$ mm.

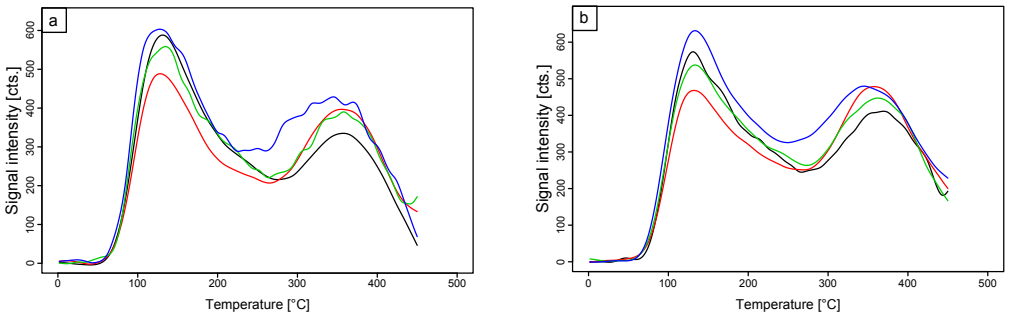


FIGURE 3.13: **Thermoluminescence signal for 4 fine grain (4-11 μm) aliquots after 100s of β-irradiation** using (a) a combination of the HA-3, GG-400, BG-39 and 7-59 filters, and (b) a combination of the RG-3 and a 475/50 filters. The signal intensity is slightly higher with the second filter combination and the peaks are 'clearer' when the signal is smoothed but the order of magnitude remains the same.

diameter or the presence of optical lenses that concentrate the luminescence signal. The *LumReader* results are therefore qualitative rather than quantitative.

3.4 Conclusion

Most software solutions that calculate the effect of combining filters are provided by the filter manufacturers. Therefore, they often include only a limited selection of filters. The *LumReader* package is completely independent and open source. It allows users to combine any filters, as long as their properties, especially the transmission matrix, are known. It also allows the creation of new filters when necessary.

Specifically designed for the Luminescence community, the **R**-package *LumReader* allows easy assessment of the expected characteristics of any luminescence experiment. Not only does it determine the optimal detection window once it is combined with the desired filters, but also compares this detection window with the excitation signal and the expected luminescence signal. The package relies heavily on the existence of a reference database, especially concerning the luminescence properties of the studied materials. Numerous studies have already been done concerning the TL properties of the materials usually encountered in luminescence dating (Krbetschek et al., 1997). Unfortunately, this is not yet the case for the OSL properties. Until now, most research has focused solely on the properties of blue/green and infrared stimulation. In research using other stimulation wavelengths, like VSL and YSL, the filter and PMT combinations are usually similar to those encountered in BSL or IRSL. However, the recent development of EMCCD cameras for spectral analysis (Kook et al., 2016) should allow this gap to be filled in the near future.

The package was developed with two main applications in mind: research and teaching. The files containing the filters, detection and stimulation unit properties are text files and can be easily modified. The *LumReader* package can therefore be used to visualise the usual reader configurations but also to show the consequence of an unintentional modification of them, like forgetting a filter or using a damaged one.

The **R**-package *LumReader* is available on GitHub (https://github.com/dstreble/Lumreader) and on CRAN (http://cran-r-project.org/package=LumReader). A web interface was also developed, using the **R**-package *shiny* (Chang et al., 2016), to make the utilisation of *LumReader* as simple as possible (https://dstreble.shinyapps.io/shinyLumReader/). This web-based application allows anybody, even those with no knowledge of **R**, to use *LumReader* for the simulation of their own luminescence experiments.

Acknowledgement

This project was realized in the context of the CRC 806 "Our Way to Europe" (http://www.sfb806.uni-koeln.de/) which is funded by the German Research foundation (DFG) - Projektnummer 57444011 - SFB 806. D. Strebler gratefully acknowledges fellowship grant No. GSGS-2017A-F08 of the Graduate School of Geosciences, University of Cologne. During the experimental stage, S. Riedesel was funded by the Deutschlandstipendium of the Bundesministerium für Bildung und Forschung and received an ERASMUS+ scholarship, which enbaled her research stay at DTU Nutech. S. Riedesel acknowledges funding by an AberDoc PhD scholarship. G. King ackowledges support from Swiss National Science Foundation grant number PZ00P2_167960

Chapter 4

Using R for thermoluminescence dating

David Strebler[1,2], *Christoph Burow*[2],*Dominik Brill*[2] and *Helmut Brückner*[2]

Notes: The content of this chapter has been published in *Quaternary Geochronology* **37** (February 2017), pp. 97-107. DOI: 10.1016/j.quageo.2016.09.001 (Strebler et al., 2017). This article was fully written by the main author. The remaining co-authors provided valuable input including, but not limited to, content of the **R** package, comments, formatting and (multiple) proofreading. Formatting changes were made to adopt the format of this Thesis.

Keywords: *R, TL, Thermoluminescence dating, burnt flint*

Abstract

Whilst optically stimulated luminescence (OSL) is commonly more suitable for sediment dating because of faster signal resetting, thermoluminescence (TL) remains important for dating burnt material, e.g. in archaeological contexts, or for studying the luminescence properties of different materials. A lack of user-optimized analysis software for TL data has exacerbated the decline of TL dating in comparison to OSL. However, exciting developments in TL dating of flint and calcite indicate a rise in application of this underused method.

R is a programming language and environment for statistical computing and graphics. It provides a wide variety of statistical and graphical techniques and is highly extendable.

[1]Corresponding author: david.strebler@outlook.com
[2]Institute of Geography, University of Cologne, Germany

A package specifically designed for luminescence data analysis is available. However, it mainly includes functions for the analysis of OSL data. The *TLdating* package is a new **R** package specifically dedicated to TL dating. This package is designed to be fully compatible with the existing *Luminescence* package and is user-friendly. It includes functions for TL data pretreatment and palaeodose estimation using the MAAD and the SAR protocols. The functionality of the *TLdating* package is evaluated using heated flints from Taibeh, Jordan.

4.1 Introduction

Thermoluminescence (TL) dating has been used since the end of the 1950s to date archaeological material (Houtermans et al., 1957, Tite and Waine, 1962). Although less commonly applied in sedimentary settings than optically stimulated luminescence (OSL) dating because of the presence of an unbleachable residual component (Aitken, 1985a, 1998), there are some instances where TL dating remains the method of choice, e.g. for burnt flint (Mercier et al., 2003, Richter et al., 2009, Schmidt et al., 2013b), ceramic (Blain et al., 2007, Fraser and Price, 2013, Veronese et al., 2008), and calcite dating (Polikreti et al., 2003, Stirling et al., 2012). It has been demonstrated that the *Single Aliquot Regenerative Dose* (SAR) protocol (Murray and Wintle, 2000b), which is routinely used in OSL dating, is also applicable to TL (Bassinet et al., 2006, Fattahi and Stokes, 2000, Hong et al., 2006) and the use of red rather than blue TL provides promising results for burnt flint (Schmidt et al., 2015b) and volcanic quartz (Tsukamoto et al., 2007), although this signal is not always present (Krbetschek et al., 1997). Moreover, TL has some general advantages compared to OSL. TL is not, or less, sensitive to light (Aitken, 1985a), which is particularly interesting for archaeological samples excavated in bright sunlight. Furthermore, the TL signal is more directly linked to the physical properties of the sample. Each TL peak can be assigned to a specific luminescence trap, which is especially interesting for investigating the use of new materials for dating (Krbetschek et al., 1997). While recent developments demonstrate the relevance of TL dating, its application is still limited by a lack of user-optimized analysis software for TL data.

R is a programming language and environment for statistical computing and graphics. It provides a wide variety of statistical and graphical techniques and is highly versatile (R Core Team, 2015). In 2012, an **R** package especially designed for luminescence data was published (Dietze et al., 2013, Fuchs et al., 2015, Kreutzer et al., 2012). This package, called *Luminescence*, marked a step change in the possibility for statistical analysis, data treatment and plotting of luminescence data. Whereas previously much

	Functions	Description
(1)	*TLum.BIN.file*	Object containing the information present in *.BINX* file
	TLum.Data.Curve	Objet gathering the information linked to a record
	TLum.Analysis	List of *TLum.Data.Curve*.
	TL.Results	Results provided by *Analyse_** function
(2)	*Risoe.BINfileData2TLum.BIN.file*	Converts *Risoe.BINfileData* object into *TLum.BIN.file* object
	Tlum.BIN.file2Risoe.BINfileData	Converts *TLum.BIN.file* object into *Risoe.BINfileData* object
	Tlum.BIN.file2Tlum.Analysis	Converts *Tlum.BIN.file* object into *TLum.Analysis* object
	RLum.Analysis2TLum.Analysis	Converts *RLum.Analysis* object into *TLum.Analysis* object
(3)	*mod_extract.TL*	Extracts TL curve from *TLum.Analysis*
	mod_identify.dType	Updates *data-type* metadata of *TLum.Analysis*
	mod_remove.aliquot	Removes specified aliquots from *TLum.Analysis*
	mod_remove.preheat	Removes preheat curves from *TLum.Analysis*
	mod_subtract.background	Subtracts background from associated TL curve in *TLum.Analysis*
	mod_align.peaks	Aligns TL peaks from *TLum.Analysis*
(4)	*analyse_TL.plateau*	Performs the heating plateau test for *TLum.Analysis* object
	analyse_TL.MAAD	Estimates D_e using the MAAD protocol for *TLum.Analysis* object
	analyse_TL.SAR	Estimates D_e using the SAR protocol for *TLum.Analysis* object
(5)	*script_TL.import*	Creates *TLum.Analysis* from *.BINX* file
	script_TL.export	Creates *.BINX* file from *TLum.Analysis*
	script_TL.pretreatment	Gathers series of data pretreatments
	script_TL.plateau	Gathers heating plateau test estimation and series of data pretreatments
	script_TL.MAAD	Gathers complete workflow to estimate D_e using MAAD protocol
	script_TL.SAR	Gathers complete workflow to estimate D_e using SAR protocol

TABLE 4.1: **Summary of the main functions of the *TLdating* package.** (1) Class objects containing the data; (2) functions which convert a class object into another class object; (3) functions that manipulate the data; (4) functions that do the data analysis; and (5) scripts that gather a predefined set of functions. For a list of required input arguments see online supplement (Table C.1).

analysis was done using the established stand-alone software *Analyst* (Duller, 2015a), the *Luminescence* package has enabled the incorporation of the latest statistical and plotting approaches shared by the luminescence dating community (Dietze et al., 2016, Smedley, 2015). In 2013, a second **R** package called *numOSL* was published (Peng et al., 2013). However, these packages focus almost solely on OSL. The *Luminescence* package includes only a few functions dedicated to TL dating. More generally, most software currently available for luminescence dating seems to neglect TL dating. Whilst *Analyst* (which is bundled with the commonly used *Risø TL/OSL Readers*) still includes functionality to perform the analyses associated with the *Multiple Aliquot Additive Dose* (MAAD) protocol commonly used in TL dating (Aitken, 1985a), researchers have to use their own code to perform more advanced analysis of TL data. To close this gap, we present a new **R** package called *TLdating*, which focuses exclusively on the analysis of TL data. It is fully compatible with the existing *Luminescence* package and has been designed to be as easy to use as possible. It is freely available for the community and offers the functionality to perform the entire dose calculation for TL samples, including the import of measurement data, data pretreatment, and palaeodose estimation with both the MAAD and SAR protocols.

4.2 *TLdating* package and R environment

One of the main differences between this package and the *Luminescence* package is the way the uncertainties are treated. Rather than estimating the uncertainty at the end of the dose estimation process, uncertainties are generated as soon as the data are

imported into **R**. Indeed, TL dating requires the combination of different luminescence curves prior to any dose estimation.

Uncertainties on TL measurements can have various origins including purely statistical fluctuations in the number of photons detected by the PMT or fluctuation in the conditions under which the curves are measured (solid angle of light collection, sample orientation, thermal contact,etc.). These uncertainties can be categorised as systematic and random uncertainties. The systematic uncertainties can usually be discarded as long as an experiment uses the same reader with the same radiation source, the time required to take all necessary luminescence curves is not excessively long and the doses are expressed in terms of irradiation time and not in Gy. Therefore, this package considers all uncertainties as random. Errors are propagated in quadrature. Different hypotheses can be used for estimation of TL signal uncertainty. If signal counts obey a Poisson distribution, the initial standard uncertainties on the signal are the square root of the number of counts (Adamiec et al., 2012). When two signals, a and b, are added or subtracted, the resulting absolute uncertainty δs is calculated as $\delta s = \sqrt{(\delta a)^2 + (\delta b)^2}$. When a signal a is divided by a signal b, the resulting relative uncertainty $\frac{\delta s}{s}$ is calculated as $\frac{\delta s}{s} = \sqrt{(\frac{\delta a}{a})^2 + (\frac{\delta b}{b})^2}$. When a weighted average of the elements i from a signal x is made, $s = \frac{\sum_i (w_i.x_i)}{\sum_i w_i}$ and the resulting absolute uncertainty is: $\delta s = \frac{1}{\sqrt{\sum_i w_i}}$ where $w_i = \frac{1}{(\delta x_i)^2}$. This approach allows a more systematic and homogeneous uncertainty estimation when different steps of data pretreatment and measurement protocols are used and combined.

Another difference between the *Luminescence* and the *TLdating* packages is related to the use of some of the metadata accompanying the luminescence data. Both the *sequence editor* software, used with *Risø TL/OSL readers*, and the *Lexstudio* software, used with *Freiberg Instruments Lexsyg TL/OSL readers*, provide the results of luminescence measurements as a *.BINX* file. This file does not only contain the luminescence response data from the measurements but also a series of *metadata* containing the characteristics of these measurements comprising the irradiation time and sometimes the irradiation dose rate, the type of luminescence signal produced (e.g. TL, OSL, etc.), the heating rate and the maximum temperature, the presence of a temperature plateau and its duration, and the measurement *data-type*. It also includes a comment section that can contain extra information (Duller, 2015a). When discs are analyzed using a single aliquot approach, the *data-type* is directly linked to the order of the curves in the measurement sequence. The first curve is always the *Natural*, the second its *Test Dose* response, and then a succession of *Regenerative Dose* and *Test Dose* responses follow. When several discs are combined in a multiple aliquot approach, this is no longer possible, especially if the palaeodose estimation and sub-linearity correction are included in

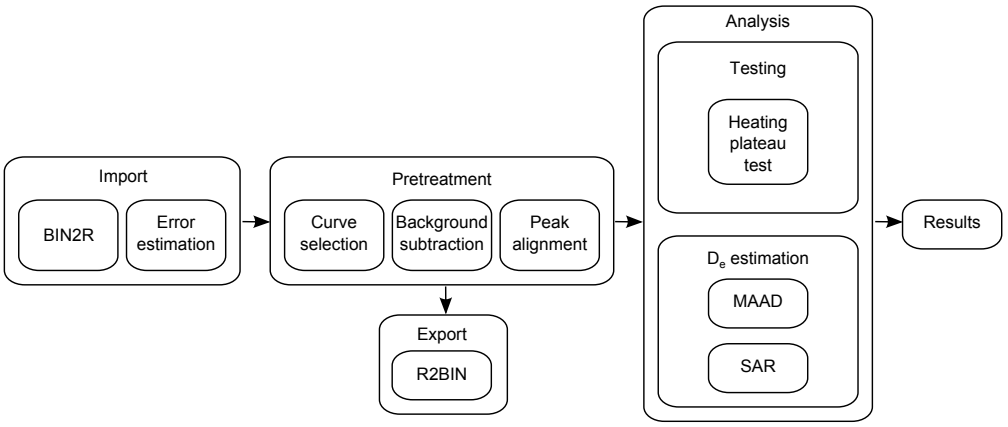


FIGURE 4.1: **Workflow followed by the different *script_** functions of the *TLdating* package.** First the TL curves are imported into **R**, then they are submitted to a series of pretreatment to prepare the upcoming analysis. Finally, the modified curves can be exported, for use in a different package or software, or they can be combined in **R** to realize the desired analysis.

the same sequence. The *data-type* of each measurement is therefore a key feature of the package and it is used by most of the functions, including those for the SAR protocol. the *data-type* has to be defined properly when writing the sequence (or afterwards with *Analyst*). The main existing *data-types* are *Natural*, *Natural+Dose*, *Dose*, *Background*, *Bleach* and *Bleach+Dose*. To make the analysis of luminescence data easier, the package introduces two new *data-types*: *Preheat* and *Testdose*.

The functions of the package can be separated into five categories: (1) the class objects that store the data (*TLum.**); (2) the conversion functions, identified by a 2 between two class names following the *Luminescence* package nomenclature; (3) the data manipulation functions (*mod_**); (4) the analysis functions (*analyse_**); and (5) the predefined scripts (*script_**) (Table 4.1). The easiest way to use the package is to call the *script_** functions, which gather a complete workflow to produce the desired results (Fig. 4.1). The *script_** functions also select the most relevant data for output. For more flexibility, users can create their own scripts using the *mod_** and *analyse_** functions. However, this generally requires more advanced knowledge of **R**.

The *mod_** functions are used for the modification of a *TLum.Analysis* object and create a new *TLum.Analysis* object that can be used for further analysis. All the pretreatment functions are *mod_** functions. The *analyse_** functions combine the curves of a *TLum.Analysis* object to extract information, producing a *TLum.Results* object rather than modifying the original *TLum.Analysis* object. The estimation of an equivalent dose (D_e) is performed using an *analyse_** function. The *TLdating* package also contains a series of *calc_** functions which are internal functions used by the *mod_** and *analyse_** functions. These functions can be used by advanced users who want to develop their own functions.

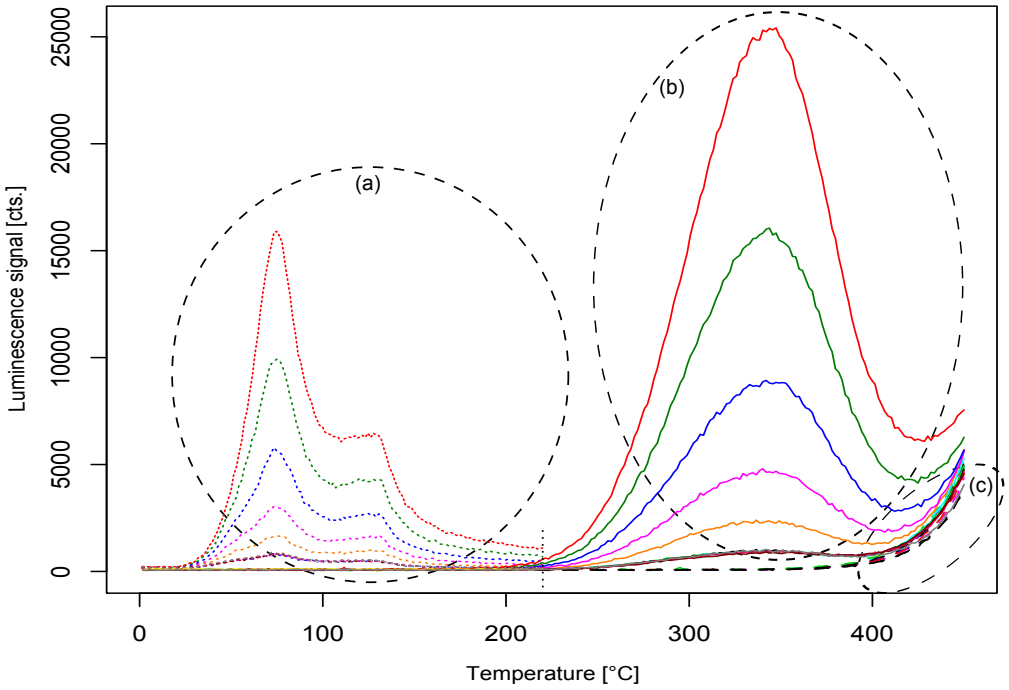


FIGURE 4.2: **Selection of TL curves.** As this package focuses exclusively on TL, all non-TL data are automatically removed from the *.BINX* file. In this figure, it is possible to identify (a) preheat curves (dotted lines), (b) L_x and T_x curves (solid lines) and (c) background curves (dashed lines). The aliquot is composed of 150-200 μm quartz grains, extracted from sample NS2 (flint) that were bleached at 360 °C for 2 h and then irradiated with regenerative doses ranging from 80 to 1200 Gy.

4.3 Thermoluminescence dating using the *TLdating* package

4.3.1 Data import and export

The *script_TL.import* function allows the import of TL data measured on standard *Risø* and *Lexsyg* readers in the form of *.BINX* files into **R**. The only mandatory parameter is the file name. The function will successively call the functions *read_BIN2R*, adopted from the *Luminescence* package (Kreutzer et al., 2012), *Risoe.BINfileData2TLum.BIN.file*, *TLum.BIN.File2TLum.Analysis*, *mod_extract.TL* and *mod_identify.dType*. The creation of the error matrix is fulfilled by *Risoe.BINfileData2TLum.BIN.file* during the conversion of the data created by *read_BIN2R*. This matrix contains an absolute random uncertainty for each data point from the original *Risoe.BINfileData* object. The function default setting is that the initial signal uncertainty is equal to the square root of the intensity. This default can be modified using a corrective factor, k, provided by the user (Adamiec et al., 2012). The function calls a *.BINX* file from the **R** *working directory* unless an alternative path is specified using *file.parameters*.

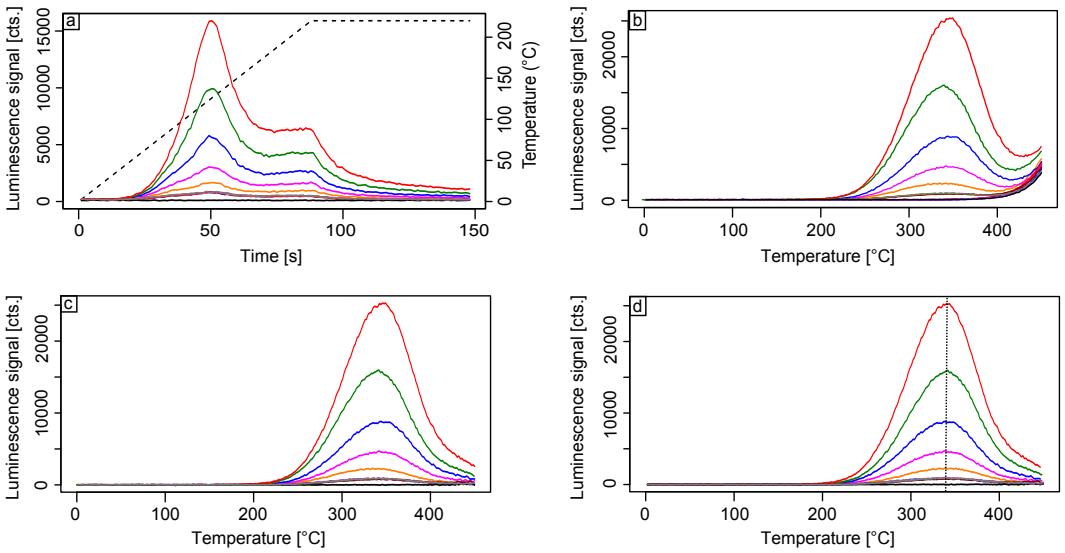


FIGURE 4.3: **Pretreatment of the TL data: Separation of (a) the preheat signals from (b) the signals used for dating.** In (a), the solid lines are the preheat signals and the dashed line is the temperature. (c) Creation of the L_x and T_x signal that will be used for dating by subtracting the corresponding background signal. (d) Alignment of the TL peaks of the L_x and T_x signals. The aliquot is composed of 150-200 μm quartz grains, extracted from sample NS2 (flint) that were bleached at 360 °C for 2 h, and then irradiated with regenerative doses ranging from 80 to 1200 Gy.

Once the data are imported, the script calls *mod_extract.TL*, which removes all the data that are not indicated as TL curves (Fig. 4.2), and *mod_identify.dType*, which updates the *data-type* information of the *TLum.Analysis* object. This function is required to generate the two new *data-types* introduced by the package. These *data-types* are specified using the *comment* metadata of the *.BINX* file. When the data are imported into **R**, this metadata is scanned and the *data-type* section of the *TLum.Analysis* object is automatically updated when it contains the words *Preheat* or *Testdose*. At the same time, the old *data-type* is saved separately for backward compatibility.

The *script_TL.export* function allows the export of TL data stored in a *TLum.Analysis* object as a standard .BINX file. The only mandatory parameter is the file name. The function will successively call the functions *TLum.Analysis2TLum.BIN.File*, *TLum.BIN .File2Risoe.BINfileData* and *write_R2BIN*, from the *Luminescence* package. During the process, the original *data-type* of each curve is restored to avoid a compatibility problem with *Analyst*.

4.3.2 Pretreatment of TL data

Due to thermal effects, it is generally not possible to directly use measured TL curves to estimate a D_e. A series of data pretreatments are required. *script_TL.pretreatment* gathers a series of the most often used pretreatments: (1) the removal of selected aliquots;

(2) the removal of the preheat curves; (3) the subtraction of the background signal; and (4) the alignment of the main TL peak. To make its use easier, the script directly calls *script_TL.import*. Therefore, the only input parameter which is required is the file name. Although the function can automatically detect the TL peak used for the D_e estimation, specifying an initial temperature interval including the TL peak maximum can improve the analysis, especially in case of TL curves with multiple peaks or a strong black body radiation signal. This can be done using the user defined *aligning.parameters* option.

First, the script calls *mod_remove.aliquot*, which allows the removal of specified aliquots. These aliquots are generally identified after a first estimation of the D_e and may not fulfil the selection criteria or be outliers. Secondly, it calls *mod_remove.preheat*. This function removes the preheat curves from the data object (Figs. 4.3a, b). It relies on their prior identification in the *data-type* metadata to work properly. Afterwards, *mod_subtract.background* subtracts the background curve associated with each of the TL curves (Fig. 4.3c). Once again, it relies on a prior identification of the background curves in the *data-type* metadata to work properly. Finally, *mod_align.peaks* is called. This last function will align the main peak of each luminescence curve. It realizes a polynomial smoothing of the curves, using *smooth.spline* from the *stats* package (R Core Team, 2015), to identify the position of the maximum in the interval specified by the user. If the protocol includes a test dose response, it uses the average position of their maxima as the alignment reference point, otherwise it uses the average position of all the maxima. Once the alignment reference point has been defined, it shifts the original TL curves to align their maxima with the reference point (Fig. 4.3d).

Once all the pretreatment has been completed, the script calls *script_TL.export* to save the results into a new *.BINX* file. This allows *Analyst*, or any other compatible software, to be used to visualize the results or estimate the D_e separately.

4.3.3 Identification of sufficiently heated objects using the heating plateau test

The heating plateau test was proposed to verify if a TL signal of a ceramic sample has been properly reset throughout heating (Aitken, 1985a). Initially designed for the MAAD protocol, the test consists of dividing the signal emitted from a natural sample (N) by the signal emitted from a natural sample that has received an additive dose ($N + \beta$). If the natural sample has not been fully reset by heating, the shape of the two curves will be different. If the sample was completely reset, the shape of the curves should be the same and the signals proportional. Therefore $N/(N + \beta)$ should present a plateau in the region of the peak maximum (Fig. 4.4). This plateau defines the region

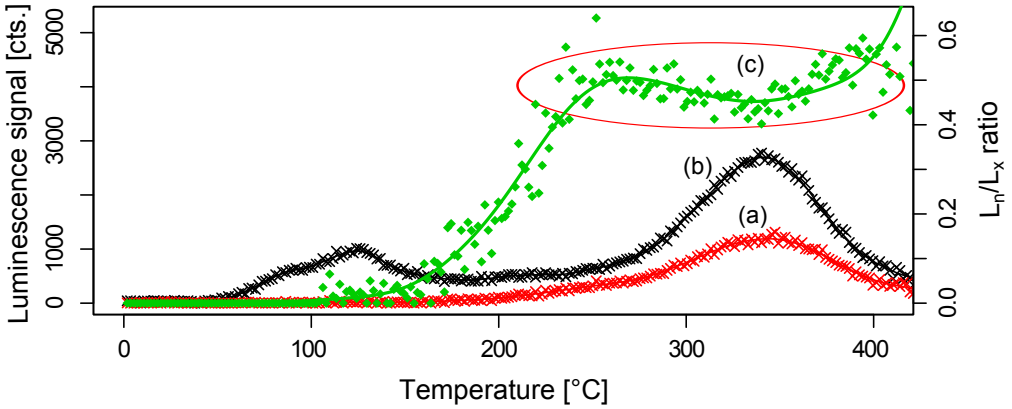


FIGURE 4.4: **Heating plateau for quartz extracted from sample NS2 (flint).** When a natural signal L_n (a) is divided by an additive dose signal L_x (b), the $\frac{L_n}{L_x}$ ratio should present a plateau around the maximum peak position (c). The *natural* aliquot is composed of 150-200 μm quartz grains that were bleached at 360 °C for 2 h, then irradiated with 80 Gy and preheated at 180 °C for 3 min. The *additive dose* aliquot was prepared as described for the *natural* aliquot and then irradiated with an additive dose of 80 Gy.

suitable for D_e estimation. Although the heating plateau forms a robust test, second order kinetics may exhibit an effect similar to partial resetting of the signal (Grün, 1994). Furthermore, if the natural signal is close to saturation, $N/(N+\beta)$ will tend towards 1, preceding any inference of partial resetting.

A similar approach can be used when applying the SAR protocol. If the signal has been properly reset and presents no second order kinetic effects, N/β should form a plateau. Once again, this plateau defines the region that could be used for the D_e estimation. It must be noted that for regenerative doses smaller than the natural dose the ratio will be greater than 1, which is impossible when using additive doses.

When the natural, additive and regenerative dose responses are followed by test dose responses, these can be used to normalize the results. This may be necessary when the aliquots have heterogeneous luminescence properties or when successive irradiations modify their sensitivity.

script_TL.plateau first calls *script_TL.pretreatment* to prepare the TL data. Once again, only the name of the *.BINX* file is required. It then calls *analyse_TL.plateau*. For each temperature channel $\frac{L_n}{L_x}$ is estimated, where L_n is the average natural signal and L_x is the average signal obtained for each additive or regenerative dose. When the dose responses are followed by test dose responses, T_x, the function will also estimate $\frac{(L_n/T_n)}{(L_x/T_x)}$ for each temperature channel (Fig. 4.5).

It has to be noted that having a heating plateau does not guarantee the accuracy of the final D_e. However, when a sample does not fulfil this test, it is a strong indication that it will not provide any meaningful D_e.

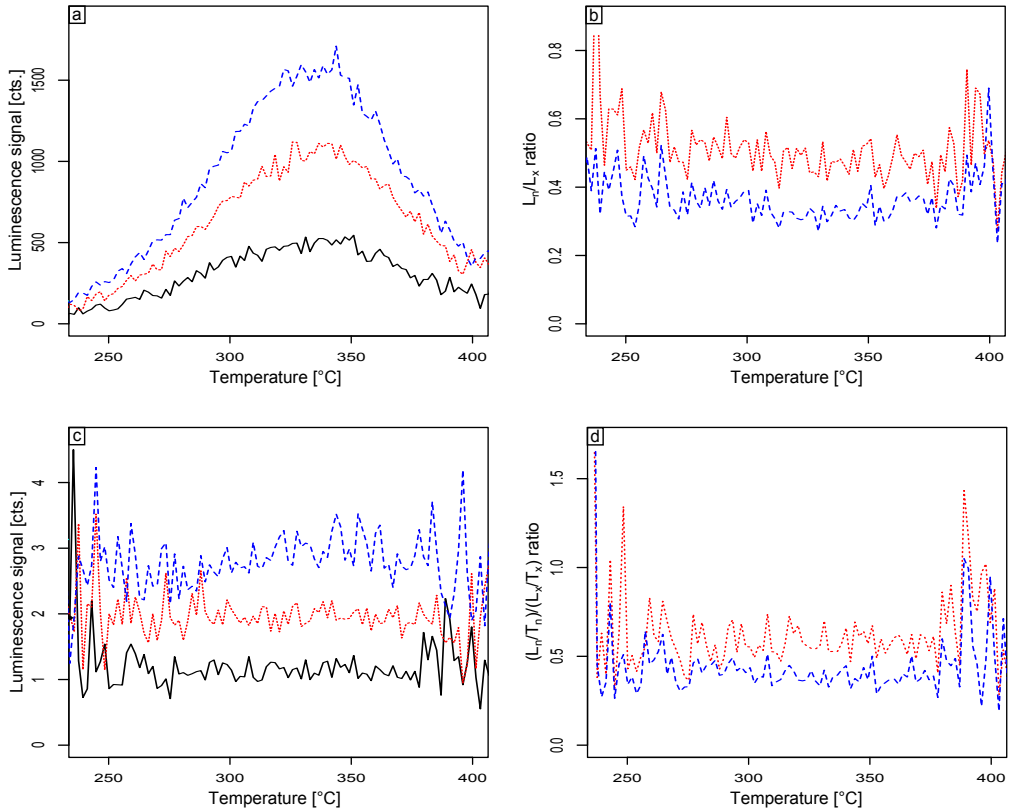


FIGURE 4.5: **Heating plateau test for (a) two additive dose TL signals (L_x) and (c) the corresponding sensitivity corrected signals ($\frac{L_x}{T_x}$).** In both cases, a heating plateau can be observed between 290 and 360 °C, i.e. around the position of the TL peak (b, d). The *natural* aliquot is composed of 150-200 μm quartz grains from sample NS2 (flint) that were bleached at 360 °C for 2 h, then irradiated with 40 Gy. The *additive dose* aliquots were prepared as described for the *natural* aliquot and then irradiated with additive doses of 30 and 60 Gy.

4.3.4 Equivalent dose calculation from TL data

4.3.4.1 The growth curve and dose plateau approach

In TL dating, the usual approach for extracting luminescence signals from TL curves is to integrate the signal over a given temperature interval which is centered on the luminescence peak maximum (Figs. 4.6 a, b). As previously seen, an appropriate interval can be estimated using the heating plateau test. These integrals define the luminescence response for each of the measured additive and regenerative doses. A single regression curve then allows the determination of the D_e; this approach is called the growth curve (GC) approach (Wintle, 1997).

Another approach is to define a D_e value for each data channel or temperature interval. This second approach generally requires the realization of many more regression curves. Once we have a D_e for each temperature interval, we can average the results

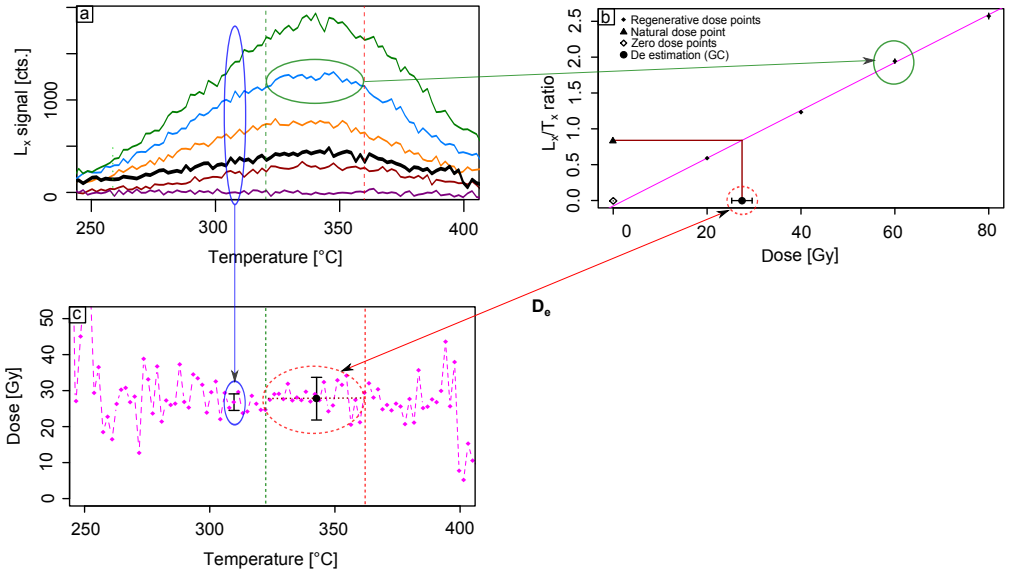


FIGURE 4.6: **Comparison between the growth curve and the dose plateau approach.** In both cases, the same TL data are used (a); in the GC approach the response for each additive/regenerative dose is averaged over the heating plateau before estimating the D_e (b); in the DP approach, a D_e is estimated for each temperature interval before averaging the results (c). This aliquot is composed of 150-200 μm quartz grains from sample NS2 (flint) that were bleached at 360 °C for 2 h, then irradiated with 30 Gy to simulate the natural dose. The aliquot was then irradiated with increasing *regenerative dose* from 20 to 80 Gy.

over the same temperature interval as used in the previous approach (Figs. 4.6a, c). This approach is called the dose plateau (DP) approach (Wintle, 1997).

As previously shown for the heating plateau test, the signal is proportional to the absorbed dose if it does not saturate. Therefore, a D_e plateau should form around the peak maximum position. The plateau obtained with the DP approach is generally shorter than the one obtained with the heating plateau test. Therefore, it is generally a better indicator for defining the temperature interval for the D_e estimation.

4.3.4.2 D_e calculation with the MAAD protocol

Since the development of SAR protocols, the MAAD protocol remains widely used only for TL dating (Zöller et al., 2014). The luminescence signal can be considered as linear before starting to saturate and is relatively well described by an exponential function with a linear term. However, for low doses, this signal also exhibits non-linear behavior that must be corrected for. The dose received by the sample after the last resetting event is called the palaeodose, P. Its best estimation is usually called the equivalent dose, D_e.

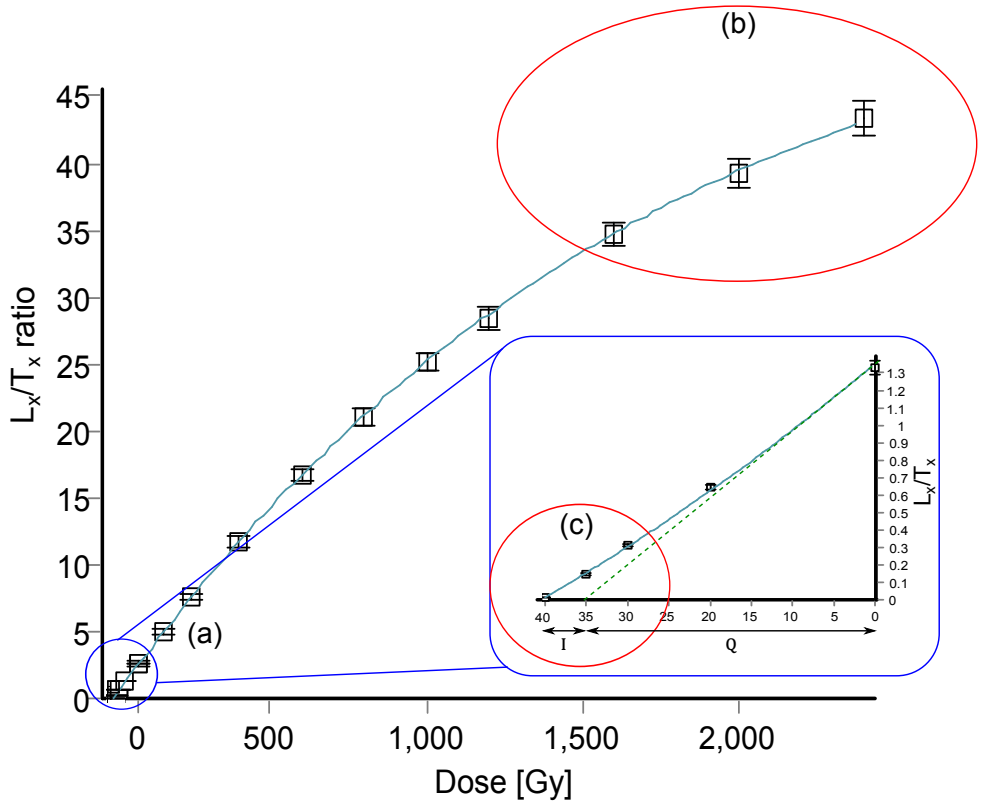


FIGURE 4.7: **The growth curve can be separated into 3 parts (a) the linear region, (b) the saturation region and (c) the supralinear region.** When using the MAAD protocol, the linear approximation (Q) does not take into account this supralinearity. Therefore, a supralinear correction (I) has to be added to obtain a final D_e which reflects the real palaeodose (P). This aliquot is composed of 150-200 μm quartz grains, extracted from sample NS2 (flint) that were bleached at 360 °C for 2 h and then irradiated with doses ranging from 0 to 2400 Gy.

When using the MAAD protocol, the D_e can be separated into two components, the *extrapolated* equivalent dose (Q) and the supralinear correction (I) (Fig. 4.7). Q is estimated using a series of natural aliquots irradiated with different *additive* doses. A luminescence response is evaluated for each of these *additive* doses and a regression function enables determination of Q. I is estimated using bleached aliquots irradiated by different *regenerative* doses. Once again, the luminescence response is evaluated for each of these *regenerative* doses and a regression function can be used to determine I. The final D_e is the sum of Q and I, both of which produce an uncertainty which is propagated in quadrature on the D_e. For TL, in most cases, the regression function is a simple linear fit. Indeed, the MAAD protocol is not applicable beyond the linear dose region.

It is possible to estimate a *test dose* response after each *additive* and *regenerative* dose. Since the MAAD protocol combines signals from different discs, this *test dose* does not allow sample sensitivity change to be tracked. However, it does allow normalization of the results, especially when the aliquots are heterogeneous.

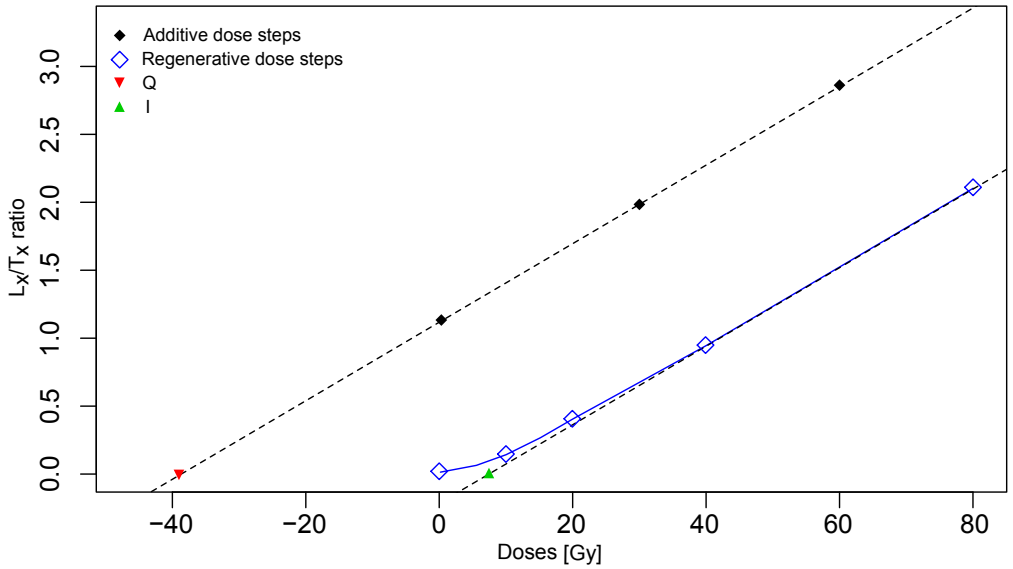


FIGURE 4.8: **When there is no sensitivity change during the measurement, the additive and the regenerative dose response curve slopes are identical.** In this example, the first three regenerative dose responses are above the regression line and should not be used to determine the supralinear correction. The 18 aliquots are composed of 150-200 μm quartz grains, extracted from sample NS2 (flint) that were bleached at 360 °C for 2 h. Six aliquots were irradiated with 40 Gy to simulate the natural dose and four of them received extra *additive doses* of 30 and 60 Gy. Eight further aliquots received *regenerative doses* from 10 to 80 Gy.

The initial MAAD protocol requires that the samples rest for several weeks before estimation of the dose response; this enables thermally unstable signal components to decay (Aitken, 1985a). However, it has been shown that this step can be replaced by preheating at lower temperature, as done in SAR measurement protocols (Dutkiewicz and Prescott, 1997, Feathers, 1997). It allows a more routine application of the MAAD protocol since the aliquots do not have to be removed from the luminescence reader in the middle of the procedure.

The *script_TL.MAAD* function calculates an estimation of the D_e using both the DP and the GC approaches. In theory, both approaches should provide similar results. Once again, it starts by calling *script_TL.pretreatment* to prepare the curves for the D_e estimation. Then it calls *analyse_TL.MAAD*. This function requires two extra parameters: *eval.Tmin* and *eval.Tmax*, which are the temperature boundaries for signal integration. A series of complementary parameters enable improvement of the fitting: (1) the type of fitting, at present only linear fitting is supported; (2) whether the fitting should be weighted; (3) the additive dose interval used for the estimation of Q, which is required when the highest dose signals are in saturation or when the natural signal is in the supralinear region; (4) the regenerative dose interval used for I estimation, which allows exclusion of the regenerative dose signals in the supralinear region; and (5) if the slope defined for Q should be reused to estimate I. The method relies on the hypothesis

that all the aliquots should have the same dose response curve (Aitken, 1985a), i.e. the *additive* and *regenerative* growth curves must have the same slope (Fig. 4.8). Therefore, option (5) will produce more coherent results. Another solution would have been to combine all the aliquots to estimate the slope of the growth curve (Prescott et al., 1993). However this approach has not been implemented as it can mask differences of slope when heating induced sensitivity changes occurs.

The function starts by identifying the dose responses (L_x) and the *test dose* response (T_x) to calculate $\frac{L_x}{T_x}$. The average L_x and T_x for each additive/regenerative dose is estimated before plotting the heating plateau test of all the resulting curves. Finally, the function estimates the D_e using both the DP and GC approaches (Fig. 4.9). When the measurement protocol does not include *test doses*, the function considers that $T_x = 1$ and $\frac{L_x}{T_x} = L_x$. When the measurement protocol does not include *regenerative* doses, only Q is estimated. When the measurement protocol does not include *additive* doses, only I is estimated.

4.3.4.3 D_e calculation with the SAR protocol

Initially developed for OSL dating, the SAR protocol can also be applied in TL dating (Bluszcz and Bøtter-Jensen, 1995, Richter and Krbetschek, 2006). This protocol has the advantage of requiring less sample material and allows D_e estimation for samples close to saturation, using non-linear fit. Moreover, the supralinear correction is no longer required. For this protocol, the D_e is estimated by comparing the natural signal L_n to the dose response curve created by irradiating the aliquot with a series of *regenerative* doses L_x. However, the successive heatings that are required to reset the material between each *regenerative* dose may influence its sensitivity. This sensitivity change can be partially corrected for by the monitoring of a *test dose* response T_x after each *regenerative* dose irradiation. However, common to most SAR protocols, the initial sensitivity change between measurement of the *natural* and the first *regenerative* dose cannot be detected (Wintle and Murray, 2006). Modified SAR protocols were developed to overcome this problem, for example the Natural Sensitivity Corrected-SAR (NSC-SAR) which uses the 110 °C peak present in the preheat signal when the sample is submitted to a pre-dose before the recording of L_n (Singhvi et al., 2011), but they are not yet included in the *TLdating* package.

Since we estimate a D_e for each aliquot, this method is far less sensitive to the heterogeneous luminescence behaviour between aliquots. The final D_e is estimated by averaging the D_e obtained for each aliquot.

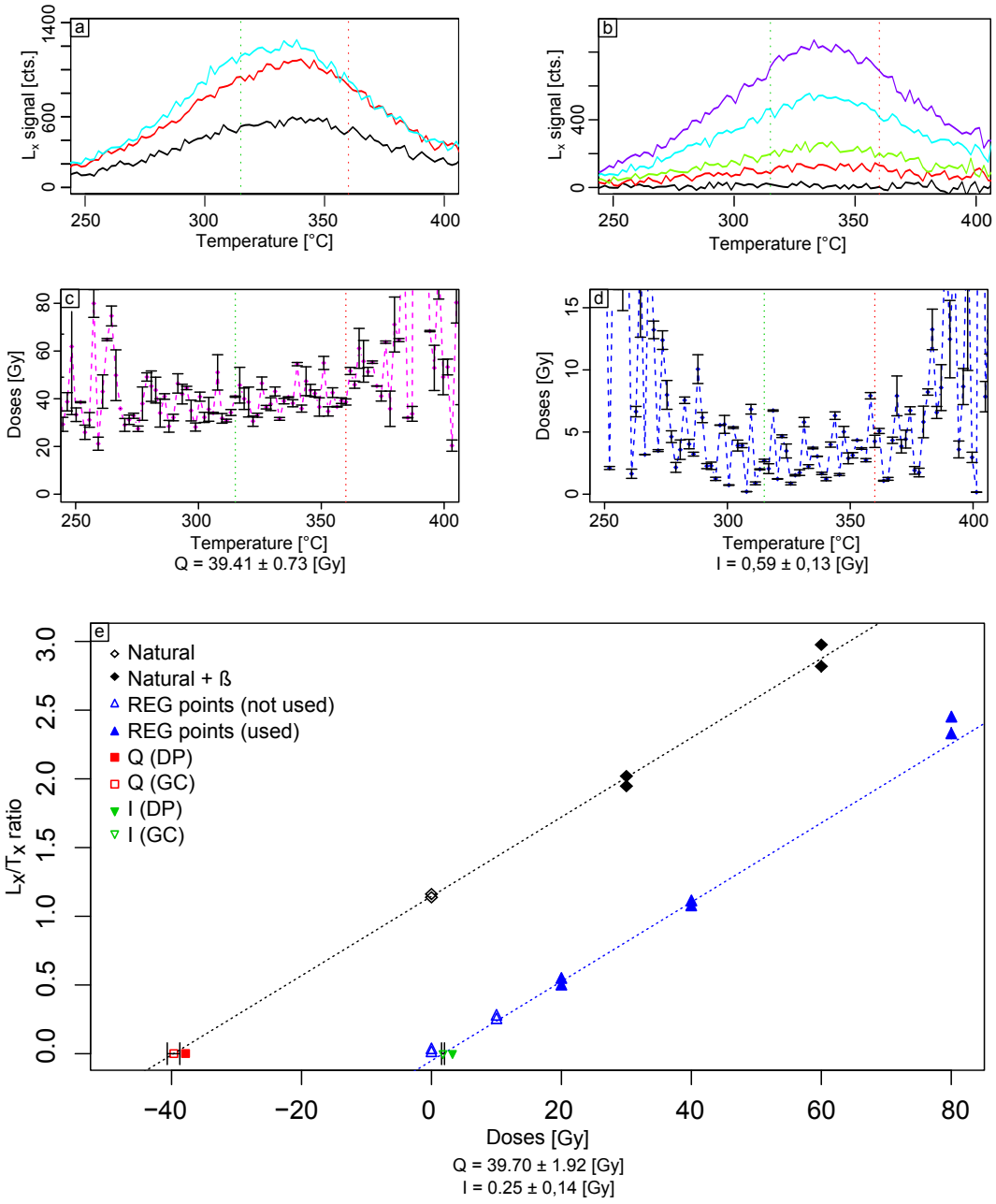


FIGURE 4.9: **Estimation of the D_e with the MAAD protocol using the *TLdating* package.** Two aliquots were irradiated with *additive doses* of 0, 30 and 60 Gy (a). Their test dose response signals allow correction for the very low signal emitted by one of the 60 Gy aliquots. Five regenerative dose steps were used (from 0 up to 80 Gy) to identify the supralinear effect (b). Both the DP (c, d) and the GC (e) approaches provide very similar results, around 40 Gy. D_e values below 20 Gy are very sensitive to variations in the supralinear correction.

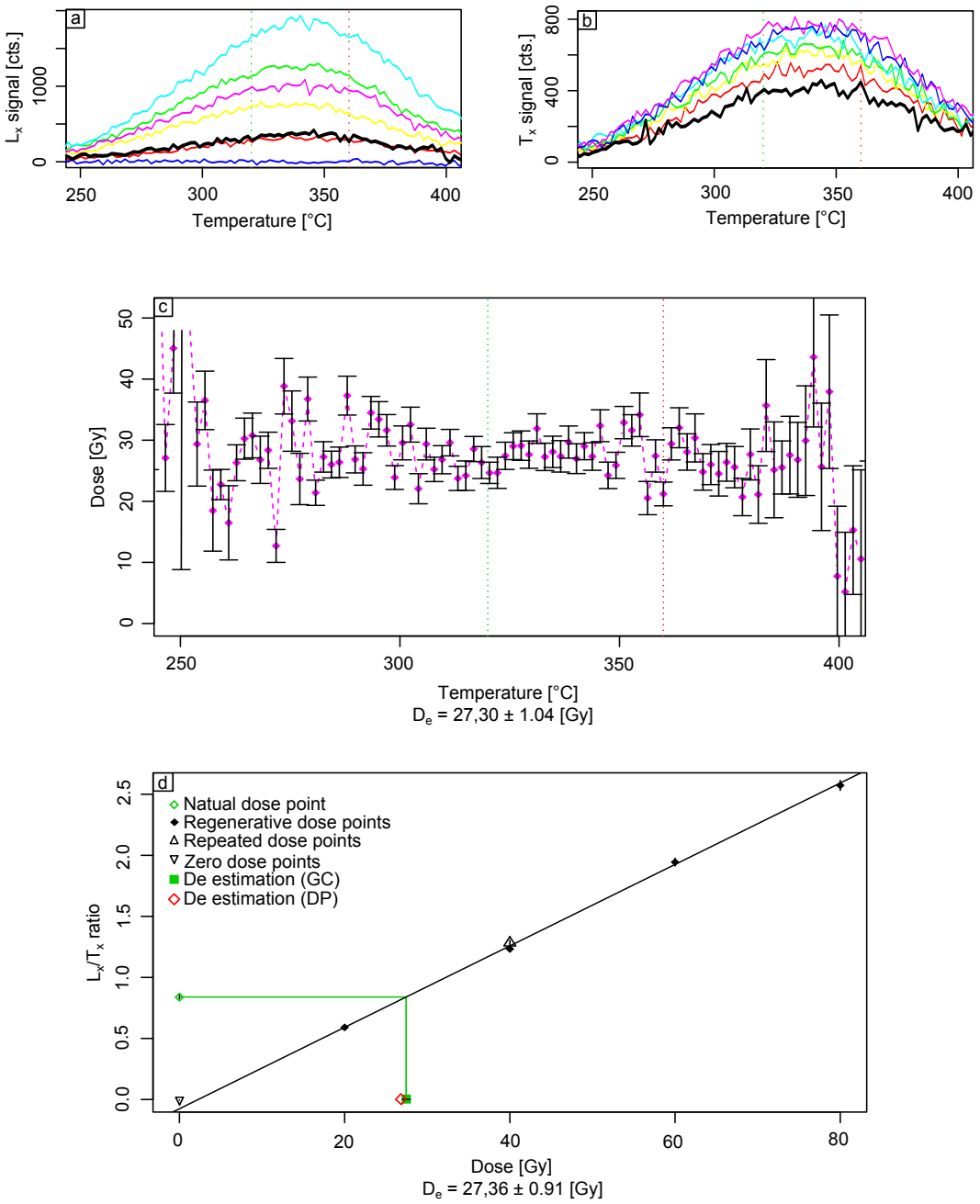


FIGURE 4.10: **Estimation of the D_e with the SAR protocol for one aliquot using the *TLdating* package.** Six regenerative doses, including a zero dose and a repeated dose point, were administered (a). The test dose responses show a sensitisation of the material with increasing doses (b). The dose plateau (c) and growth curve approach (d) provide a similar D_e estimation, around 27 Gy. The DP approach allows an easy assessment of the temperature interval for D_e estimation whereas the GC approach allows an easy assessment of the regenerative dose interval which avoids the supralinear and the saturation regions.

Like *script_TL.MAAD*, *script_TL.SAR* starts with calling *script_TL.pretreatment*. Once again, two parameters, *eval.Tmin* and *eval.Tmax*, are required to define the temperature boundary between which the signal will be integrated. A series of other parameters enables refinement of the final result: (1) fitting type, although at present only a linear fit has been implemented; (2) whether the fitting should be weighted; and (3) dose interval used to define the fitting. As for the MAAD protocol, the function starts by separating L_x and T_x and calculating $\frac{L_x}{T_x}$ for each regenerative curve. It then realizes the heating plateau test for all of the curves before estimating the D_e using both the GC and the DP approach (Fig. 4.10).

4.4 Discussion

The package was used to estimate the D_e values of a series of burnt flint samples from the palaeolithic site of Taibeh, Jordan. These artefacts are associated with the Masraqan technocomplex, currently dated between 25 and 20 ka BC (MIS2) (Belfer-Cohen and Goring-Morris, 2007). All the aliquots were measured on a Risø TL/OSL-DA-20 reader equipped with the optical filters BG39, GG400, 7-59 and HA3. The results obtained with **R** were compared with the results obtained with *Analyst 4.14.6* before and after using the pretreatment script.

For the results obtained with the *TLdating* package, we used a weighted linear fitting. To avoid the supralinear region, we removed the first *regenerative* dose points from the fitting, i.e. *regenerative* doses below 16 Gy. For the MAAD protocol, we reuse the slope obtained when estimating Q to determine I. The same aliquots were used for estimation of Q and I. To calculate a D_e value using the SAR protocol in *Analyst* it is necessary to provide a channel interval for the background estimation, even if it has already been subtracted from the signal. We decided to use the first channels of the TL peaks (channel 120 to channel 125 of 250, i.e. from 216 to 225 °C), to provide background signals as low as possible whist ensuring that values remain positive.

For the SAR protocol, the **R** package provides results very similar to those obtained with *Analyst*. However, for the MAAD protocol, the results are sometimes very different (Fig. 4.11a). Within the **R** package, the difference between the SAR-TL and the MAAD-TL is generally below 5 %; both protocols provide similar results (Fig. 4.11b). The only notable exception is the sample TAI 20. This sample presents all the characteristics of a flint that was heated at lower temperature or during a shorter period. The significantly lower D_e obtained using the SAR protocol can be explained by a sensitivity change which occurs after the recording of the natural signal. The difference between the GC and the DP results are generally below 2 %. However, within *Analyst*, the difference

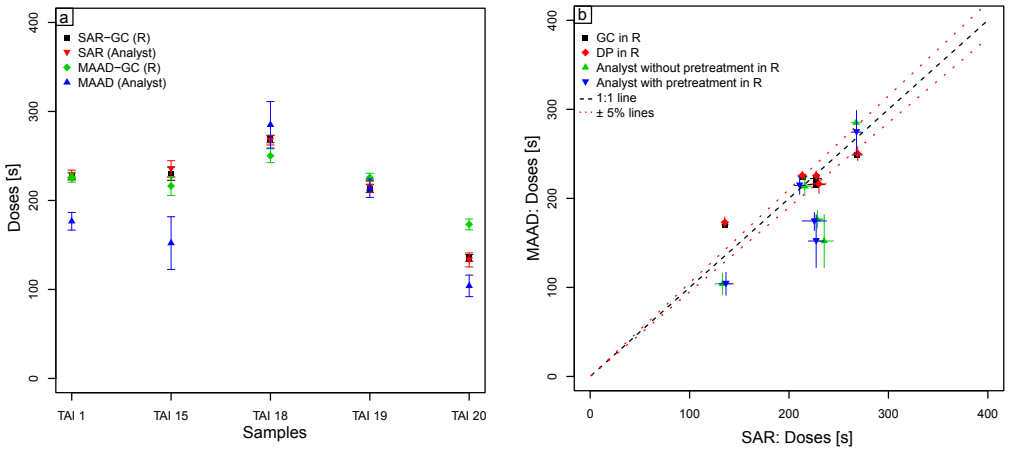


FIGURE 4.11: D_e **estimation for burnt flint from Taibeh, Jordan.** (a) Estimation of the D_e for 5 samples (TAI 1, TAI 15, TAI 18, TAI 19, TAI 20) using different protocols (SAR & MAAD), and software (**R** & *Analyst*); (b) Comparison of the results of the SAR and MAAD protocols using the GC and the DP approach in **R** and using *Analyst* with and without a pretreatment in **R**. For the complete dataset see online supplement (Table C.2).

between the SAR-TL and the MAAD-TL can be above 33 %. These differences can be easily explained by the heterogeneous luminescence properties of the aliquots, each of them containing only a small amount of material. The use of a test dose allows the **R** package to partially correct for this heterogeneity. This feature is not supported by *Analyst* where problematic samples can be easily identified by the user but have to be removed manually.

One of the main strengths of the *TLdating* package is the ability to easily modify the fitting parameters. We compared results using different fitting parameter combinations: (1) unweighted average using all dose responses and an independent I estimation; (2) unweighted average using all dose responses but reusing the Q slope for I estimation; (3) weighted average using all dose responses and an independent I estimation; (4) weighted average using all dose responses but reusing the Q slope for I estimation; (5) unweighted average using only the higher dose responses and independent I estimation; (6) unweighted average using only the higher dose responses but reusing the Q slope for I estimation; and (7) weighted average using only the higher dose responses but with an independent I estimation (for the complete dataset see online supplement, Table C.3).

For these samples, the SAR protocol provides relatively similar results despite the parameter changes. However, using a weighted average systematically underestimates the high dose values when all of the dose responses are taken into account. It is not a problem for low D_e values, as presented in the example data, but it can become problematic for higher D_e values with the deviation being directly proportional to dose.

For the MAAD protocol, using all the dose response values systematically underestimates the D_e. Indeed, most of the *regenerative* doses are still in the supralinear region. Moreover, the zero dose response has the lowest absolute uncertainty and, therefore, the greatest weight, which forces the linear regression to pass near zero and annihilates the supralinear correction. The difference between the DP and GC results are maximized when the Q slopes are not reused for estimation of I. Indeed, once again, when averaging I in the DP approach, the lowest values are overweighted which induces an underestimation of I. This effect is not as strong within the GC approach which therefore provides a more robust D_e.

Finally, it seems that combining the three parameters provides the most robust D_e estimation. The limitation of the dose interval ensures that all the doses used are within or near the linear region. The weighting of the fitting ensures a better mathematical coherence throughout the complete process and finally the reuse of the Q slope smooths the results obtained for the I estimation, especially in the DP approach. The order of the operations should not have an impact on the results. Therefore, a divergence between the DP and the GC approach results is a good indication of problematic samples or parameter selection.

For the Taibeh samples, the SAR protocol seems to provide more robust results despite potential sensitivity changes. It is probably linked to the properties and heterogeneity of the aliquots. The main exception is the TAI 20 sample for which the D_e obtained using the MAAD protocol is more consistent with the D_e obtained for the other samples. This can be explained by a significant sensitivity change between the natural doses and the regenerative doses due to a laboratory heating higher than the archaeological resetting event. It must be noted that the reuse of the same aliquots to estimate I could also introduce an unwanted sensitivity change. Using different aliquots for the Q and I estimation is therefore recommended.

4.5 Conclusions

The new **R** package allows the estimation of a D_e from TL data with both the MAAD and the SAR protocols. It provides a series of tools to pre-process the data but also to evaluate the validity of the results.

The package relies on an extended documentation of the sequence, especially the dose and *data-type* of all luminescence curves. Moreover, extra information, saved in the *comment* metadata, are required. However, well-documented .BINX files facilitate easy

identification of the protocol used and of the *test dose*, *zero dose* and *repeated dose* curves, which is especially important for unconventional protocols.

The *script_** functions make the package easy to use for people without programming experience. However, advanced users can still utilize the specific functions to implement their own scripts which makes the package versatile.

Future development of the package will comprise: (1) implementing more functions to manipulate the .BINX file, especially the *data-type* metadata, and merging different .BINX files; (2) implementing more fitting types, especially exponential and exponential plus linear fitting; (3) supporting the *Single Aliquot Regenerated and Added Dose* (SARA) protocol (Mejdahl and Botter-Jensen, 1994); and (4) implementing functions for isothermal decay data analysis, once again for MAAD, SAR and SARA measurement protocols.

The *TLdating* package is available on GitHub (`https://github.com/dstreble/TLdating`) and on CRAN (`http://cran.r-project.org/package=TLdating`).

Acknowledgements

This project is realized in the context of the CRC 806 “Our Way to Europe” (`http://www.sfb806.uni-koeln.de/`) which is funded by the German Research foundation (DFG). We would like to thank Prof. Dr. Jürgen Richter, Cologne, and Shumon T. Hussain, Cologne, for assistance with sampling the Taibeh site; Dr. Christoph Schmidt, Bayreuth, who collected the samples; Dr. Anja Zander, Cologne, for having been our first beta tester; Dr. Sebastian Kreutzer, Bordeaux, from the **R** *Luminescence* package, for helpful advice and comments; and Dr. Georgina King, Cologne, for numerous corrections of the manuscript.

Chapter 5

Using DRAC in complex geometries: TL dating of heated flints from Taibeh, Jordan

David Strebler[1,2], *Dominik Brill*[2], *Jürgen Richter*[3] and *Helmut Brückner*[2]

Notes: The content of this chapter has been published in *Quaternary Geochronology* **49** (February 2019), pp. 4-7. DOI: 10.1016/j.quageo.2018.07.002 (Strebler et al., 2019a). This article was fully written by the main author. The remaining co-authors provided valuable input including, but not limited to, content of the **R** package, archaeological background, comments, formatting and (multiple) proofreading. Formatting changes were made to adopt the format of this Thesis.

Keywords: *R, Luminescence dating, TL, burnt flint, Jordan, Taibeh.*

Abstract

The archaeological site of Taibeh located south of Wadi Musa, Jordan, incorporates at least two, maybe even five, successive layers associated with the Late Ahmarian, also known as Masraqan, technocomplex. The Masraqan is elsewhere connected with the beginning of the intensive use of plant food and with permanent settlements. Taibeh could be the first site to present as much as 5 successive layers of this cultural unit. The Masraqan is relatively well constrained in time, usually dated between 18 and 25 ka BP.

[1]Corresponding author: david.strebler@outlook.com
[2]Institute of Geography, University of Cologne, Germany
[3]Institute of Prehistory and Early History, University of Cologne, Germany

A series of heated flints was collected at Taibeh to be dated using TL. Two informations are required for the estimation of a TL age: the equivalent dose (D_e) which is the dose accumulated in the flint since it had been heated, and the dose rate ($\dot{D}$) to which the flint is exposed during the burial time. The D_e estimation was done applying two different protocols, and both produced consistent results. The $\dot{D}$ estimation was realised using a modified version of DRAC (Durcan et al., 2015) which allows to use different radio-element concentrations for the flints and the surrounding sediment.

5.1 Introduction

One of the principal topics of the *Collaborative Research Centre CRC 806: Our Way to Europe, Human-environment interaction and Human mobilty in the Late Quaternary* is the dispersal of Early Modern Humans from East Africa to Eurasia (Richter et al., 2012b). The neighbourhood of the Jordan Rift Valley is one of its focus areas of geoscientific and archaeological research (Klasen et al., 2013, Schyle and Richter, 2015). The Taibeh excavation carried out by one of the authors (J. Richter) in 2010 has contributed to a long-term geo-archeological survey with the excavation programme concentrating on the MIS 3 and MIS 2 prehistoric occupation and landscape evolution south of Petra in Southern Jordan. The artefacts from the two upper layers of this site were identified as related to the Masraqan or late Ahmarian technocomplex (Hussain, 2015a, Hussain and Richter, 2015).

The Masraqan comprises a group of early Epipaleolithic assemblages within a settlement area stretching from Northern Israel to the Sinai Peninsula, and from the West Banks to Jordan. As yet, ca. 11 Masraqan sites have been radiocarbon-dated. Settlements of the Masraqan cultural unit occurred preferably 18-25 ka cal BP (26 radiocarbon ages from Ohalo II/Israel, with a mean around 23 ka cal BP). Some settlements have securely been dated to a late occupation phase around 18-19 ka cal BP (Urkan er-Rub IIa/West Banks; Shunera XVI/Israel) whereas a few relatively old radiocarbon dates around 26-28 cal BP appear somewhat isolated and should be used with caution (Shunera XI/Israel, Buhira Spring/Jordan, Yutil-Al-Hasa/Jordan, Uweinid 18/Jordan) (Goring-Morris and Belfer-Cohen, 1998, 2017).

Within the Masraqan, Taibeh has a unique stratigraphy, displaying at least two (AH-1 and 2), maybe even five (AH-1 to 5), successive layers with this technotypological signature (Hussain, 2015a) (see Fig. 5.1). Despite the Masraqan beeing time-wise well defined, reliable dates are required to improve our understanding of the site. Thus, charcoal samples were collected for radiocarbon dating in 2010. In addition, heated flint samples were collected from Taibeh's Masraqan layers B and C. Dating heated flints can

be complex, especially when it comes to the estimation of the dose rate ($\dot{D}$). With the Masraqan being relatively well constrained in time, dating the Taibeh artefacts provides the opportunity to validate tools dedicated to TL dating that we recently implemented and regrouped in an **R** package called *TLdating* (Strebler et al., 2017).

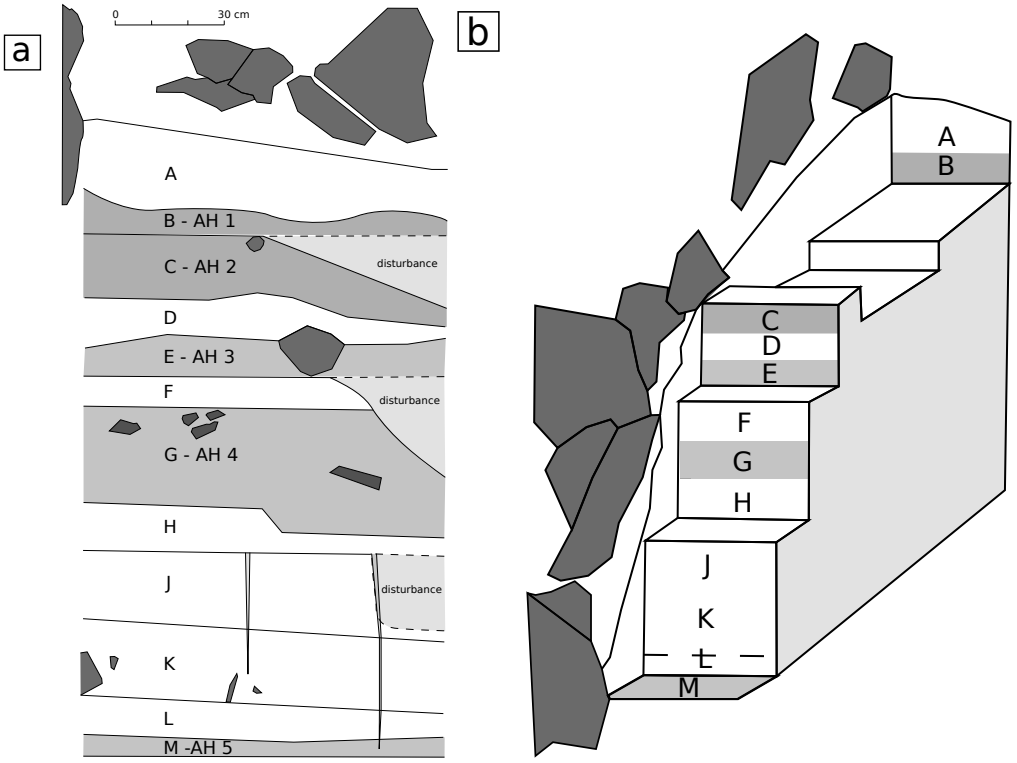


FIGURE 5.1: **(a) Stratigraphic sequence and (b) schematic representation of the staired test trench with geological (A-M) and archaeological (AH 1-5) horizons** (Hussain, 2015a). The flint samples are from the layers B and C.

5.2 Methodology

5.2.1 Sample selection and preparation

The main indication for a former heating of a flint is the presence of pot-lids and cracks on its surface (Schmidt, 2013). Twenty samples of heated flint were collected at Taibeh. For their preparation, we followed the procedure proposed by Schmidt (2013) and based on Aitken (1985a).

The first step is to discard the material partially bleached by sunlight and affected by α and β radiation coming from the surrounding sediment. This is done by removing the flint's external layer (2 mm) using a diamond saw. At the end, only five of the heated flints were large enough to generate core material (TAI 1, TAI 15, TAI 18, TAI 19 and TAI 20).

The second step is to crush of the core material. It separates the quartz *grains*[4] which are used for the estimation of the equivalent dose (D_e) and the *a-value*. This is done using a hydraulic press at a pressure of 2-3 bar. The procedure is repeated until all *grains* are smaller than 200 μm. The 100 to 200 μm fraction is separated by dry sieving and treated with HCl (10%) to remove the remaining carbonates. These coarse grains (CG) are taken for the D_e estimations. The smaller grains are crushed again, using a pestle and a mortar, then treated with HCl (10%) to remove the carbonates. A first settling in acetone allows the collection of the grains bigger than 11 μm. These medium grains (MG) are used for the estimation of the radio-element concentration in the flints. A second settling in acetone allows the collection of the grains between 11 and 4 μm. These fine grains (FG) are used for the *a-value* estimation.

5.2.2 Equivalent dose and a-value estimation

The D_e is the dose that accumulated in the quartz grains since the last heating of the flint. For the 5 remaining samples, dose estimation was made on the CG (100-200 μm) by applying the multiple aliquot additive dose (MAAD) (Aitken, 1985a) and the single aliquot regenerative dose (SAR) protocols (Bluszcz and Bøtter-Jensen, 1995) (see D.2 in the online supplement for the complete protocols). All the TL data were analysed with the *TLdating* **R** package (Strebler et al., 2017). The MAAD protocol is not influenced by an initial sensitivity change but suffers from scattering between the aliquots, which often limits its precision. The SAR protocol estimates a D_e for each aliquot. Their combination reduces the overall uncertainty (Botter-Jensen et al., 1995). The recording of test doses allows to correct for sensitivity changes that occur between the regenerative doses, but cannot detect initial sensitivity changes between the natural dose and the first regenerative dose.

The *a-value* is the ratio between an α dose and the β dose required to produce the same amount of luminescence. The estimation of the *a-value* was made on the FG (4-11 μm). All the FG aliquots were bleached by heating them up to 450 $°C$ at 5 $°C/s$. They were then α-irradiated for 400 s at 0.197 Gy/s. Once again, the MAAD and the SAR protocols were applied to estimate the D_e corresponding to the laboratory α irradiation, and therefore the *a-value* (see D.2 in the online supplement for the complete protocols and information on the α-source calibration).

The α-irradiation were done in a *lexsyg research imaging TL-OSL-RF system* from *Freiberg Instruments*. All measurements were carried out on a *Risoe 20 TL/OSL reader*

[4]The quartz *fragments* that are produced are not real grains. They are rarely made of one single natural grain. However, we are using this term by analogy with sediment dating.

Sample	Protocol	D_e [Gy]	*a-value* [Gy]	$\dot{D}_{flint}$ [Gy/ka]	$\dot{D}_{tot}$ [Gy/ka]	Age [ka]
TAI 1	MAAD	23.9 ± 0.5	0.24 ± 0.01	1.01 ± 0.18	1.48 ± 0.18	16.2 ± 2.0
	SAR	24.2 ± 0.1	0.20 ± 0.01	0.91 ± 0.18	1.38 ± 0.18	17.5 ± 2.3
TAI 15	MAAD	22.5 ± 1.4	0.14 ± 0.02	0.44 ± 0.12	0.92 ± 0.12	24.6 ± 3.6
	SAR	24.1 ± 0.8	0.19 ± 0.01	0.56 ± 0.11	1.04 ± 0.12	23.1 ± 2.8
TAI 18	MAAD	26.5 ± 0.9	0.2 ± 0.01	0.94 ± 0.19	1.42 ± 0.19	18.7 ± 2.6
	SAR	28.7 ± 0.5	0.24 ± 0.01	1.07 ± 0.19	1.54 ± 0.19	18.6 ± 2.3
TAI 19	MAAD	23.9 ± 0.5	0.22 ± 0.01	1.07 ± 0.19	1.55 ± 0.20	15.4 ± 2.0
	SAR	22.5 ± 0.1	0.22 ± 0.01	1.07 ± 0.19	1.55 ± 0.20	14.5 ± 1.8
TAI 20	MAAD	16.8 ± 0.5	0.17 ± 0.01	0.45 ± 0.11	0.93 ± 0.11	18.1 ± 2.3
	SAR	14.1 ± 0.8	0.18 ± 0.01	0.46 ± 0.11	0.94 ± 0.11	15.0 ± 2.0

TABLE 5.1: **D_e, *a-value* an age estimation for the Taibeh heated flints.** For both the D_e and the *a-value* estimation, the MAAD and the SAR protocol produced consistent results. $\dot{D}_{int}$ represents up to 70% of $\dot{D}_{tot}$.

equipped with an *EMI 9235QG* bialkani photomultiplier. For the D_e estimation, a filter combination with *Schott HA-3*, *Schott BG-39*, *Schott GG-400* and *Corning 37-59* was applied (bandwidth 400-470 *nm*) (Schmidt, 2013). For the *a-value* estimation, a filter combination with *Semrock Brightline HC 475/50* and *Schott BG-3* was applied to slightly improve the signal quality (bandwidth 450-500 *nm*, see D.3 in the online supplement) (Schmidt et al., 2015b). The D_e and *a-value* estimations are reported in Tab. 5.1 (see D.8 in the online supplement for a selection of plateau and growth curves).

5.2.3 Dose rate estimation

The Dose Rate and Age Calculator (DRAC) is an open access, web-based programme which enables rapid dose rate calculation (Durcan et al., 2015). The principles behind DRAC are simple: (1) the sediment surrounding the grains is homogeneous; (2) the annual dose rate ($\dot{D}_{tot}$) can be separated into (a) the internal dose rate ($\dot{D}_{int}$) coming from the grain itself, (b) the external dose rate ($\dot{D}_{ext}$) coming from the surrounding sediment, and (c) the cosmic dose rate ($\dot{D}_c$) coming from outer space (Prescott and Hutton, 1994); (3) both $\dot{D}_{int}$ and $\dot{D}_{ext}$ can be separated into their α, β and γ dose components. A series of parameters (like U, Th and K concentrations) is used for the estimation of the emitted α, β and γ dose rates and other parameters (including water content, grain size, etching depth, a-value, etc.) are used to quantify which amount of each dose rate component is actually absorbed by the grains.

By assuming a homogeneous matrix around the grain, DRAC is designed for sedimentary applications; it cannot be used to calculate $\dot{D}$ when complex geometries are encountered as it is the case when dating flints. On the other hand, DRAC is easy to use and allows for a complete control over the input and output parameters. Moreover, the **R** package *Luminescence* (Kreutzer et al., 2021) includes a function allowing the use of DRAC directly within **R**.

When performing the dating of heated flint, it is possible to split the $\dot{D}_{tot}$ into (a) an internal dose rate ($\dot{D}_{int}$) coming from the grain itself, (b) a *first* external dose rate ($\dot{D}_{ext1}$) coming from the surrounding flint, (c) a *second* external dose rate ($\dot{D}_{ext2}$) coming from the surrounding sediment, and (d) the *cosmic* dose rate ($\dot{D}_c$). These *internal* and *external* dose rates can be subdivided into their α, β and γ components. Thus, $\dot{D}_{tot}$ can be divided into ten components ($\dot{D}_{int,\alpha}$, $\dot{D}_{int,\beta}$, $\dot{D}_{int,\gamma}$, $\dot{D}_{ext1,\alpha}$, $\dot{D}_{ext1,\beta}$, $\dot{D}_{ext1,\gamma}$, $\dot{D}_{ext2,\alpha}$, $\dot{D}_{ext2,\beta}$, $\dot{D}_{ext2,\gamma}$ and $\dot{D}_c$). A series of complementary assumptions can be made: (1) Since the flint size is negligible compared to the γ range, the flint γ dose does not interact within the flint; (2) and each grain can be considered as surrounded by an infinite matrix of sediment; (3) removing the flint's external layer assures that only the γ coming from the sediment reaches the grains; (4) the flint size being much larger than the β range, the infinite matrix assumption can be used for the flint β dose; and (5) since the *natural* quartz grains are very small (crypto-cristalin) and the radio-element concentration is considered as homogeneous in the flint, the radio-element concentration in the *artificially* created grains is identical to the one of the flint. These assumptions simplify the $\dot{D}_{tot}$ estimation and make the use of DRAC possible by running it twice and combining the outputs. The first assumption assumes that $\dot{D}_{int,\gamma}$ and $\dot{D}_{ext1,\gamma}$ are zero, the third that $\dot{D}_{ext2,\alpha}$ and $\dot{D}_{ext2,\beta}$ are zero. During the first run, the flint radio-element concentration is used both as the *grain* and the *external* radio-element concentration. It provides an estimation for $\dot{D}_{int,\alpha}$, $\dot{D}_{int,\beta}$, $\dot{D}_{ext1,\alpha}$ and $\dot{D}_{ext1,\beta}$. During the second run, it is the sediment radio-element concentration which is used as *external* radio-element concentration. It provides an estimation for $\dot{D}_{ext2,\gamma}$. $\dot{D}_c$ does not depend on the radio-element concentration but depends on the sediment density. It is therefore also estimated during this second run. The flint's mass and shape also influence $\dot{D}_{ext1,\gamma}$ and $\dot{D}_{ext2,\gamma}$ (Valladas, 1985a), but this corrective factor was not taken into account (it is close to 1 for samples lighter than 10 g).

For our experiment, the radio-element concentrations (U, Th, K) from the surrounding sediment were determined by γ-spectrometry using a High-purity germanium (HPGe) detector at the Cologne Luminescence Laboratory (CLL). Dose rate samples were collected from different layers around the heated flints and it was not possible to link the available surrounding sediment samples to specific flints. However, the sediment radio-element concentrations are relatively low which allows to use an average value of all samples for the estimation of the flint $\dot{D}_{tot}$ (see Tab. D.5 in the online supplement). The radio-element concentration (U, Th, K, Rb) of the heated flint was estimated using Inductively Coupled Plasma Mass Spectrometry (ICP-MS) (see Tab. D.6 in the online supplement) at the Institute of Geology and Mineralogy of the University of Cologne. The analysis was performed on the MG (>11 μm) after these grains were crushed again

using a mortar and a pestle. The $\dot{D}_{tot}$ was calculated with the *use_DRAC4Flint* function from the *TLdating* **R** package (see Tab. 5.1 and D.7 in the online supplement). This function relies on DRAC and the procedure previously presented to provide an estimation of the $\dot{D}_{tot}$ for heated flint.

5.3 Results and discussion

The D_e was estimated using a *dose plateau* (DP) and a *growth curve* (GC) approach (Strebler et al., 2017), both providing nearly identical results. We decided to use the GC results for the age estimation when relying on the DP results to define the integration interval. Similarly, both the SAR and the MAAD protocols gave a consistent estimation of the D_e. The temptation is strong to systematically use the SAR protocol rather than the MAAD protocol when dating heated flint, as it is done when dating sediment. However, the SAR protocol cannot detect an initial sensitivity change, while such changes do not affect the MAAD protocol. The fact that both the MAAD and the SAR protocols provide consistent results indicates that there are no initial sensitivity changes for the Taibeh heated flints. Therefore, the SAR results of this study can be used with confidence. Even if the uncertainty on the D_e is improved by using the SAR protocol, the uncertainty on the age is similar for both protocols. For the Taibeh samples, the age uncertainty is mainly defined by the uncertainty on the $\dot{D}$ estimation. Most of the radiation to which the flint's core grains are exposed originates from the flint itself. $\dot{D}_{int}$ and $\dot{D}_{ext1}$ form 50 to 70 % of $\dot{D}_{tot}$ (0.44 ± 0.12 to 1.09 ± 0.19 Gy/ka). $\dot{D}_{\alpha}$ counts for 70 to 80 % of this $\dot{D}_{flint}$. The dose rate which originated from the surrounding sediments (0.25 ± 0.04 Gy/ka) is equivalent to the dose rate due to the cosmic radiation (0.22 ± 0.02 Gy/ka), each representing 15 to 25 % of $\dot{D}_{tot}$.

Using an average radio-element concentration of the surrounding sediment rather than values specific to each flint has a low influence on the age estimation. On the other hand, the ages are very sensitive to the estimation of the flint radio-element concentrations and the *a-values*. The Taibeh flints have very low radio-element concentrations. We often reached the detection limit of the ICP-MS (see Tab. D.6). The *a-values*, which range from 0.14 to 0.25, are significantly higher than what is usually found in literature (Schmidt, 2013). An overestimation of the *a-value* can be due to an increase in the sensitivity of the flints to α radiation when they were bleached or to a problem in the calibration of the α-source. Both the MAAD and SAR protocols provide consistent results. A sensitivity change occurring after the α-irradiation is therefore very unlikely. α-source calibration has always been a complex issue (see D.1 in the online supplement for the calibration protocol we used). An underestimation of the α-dose-rate cannot be

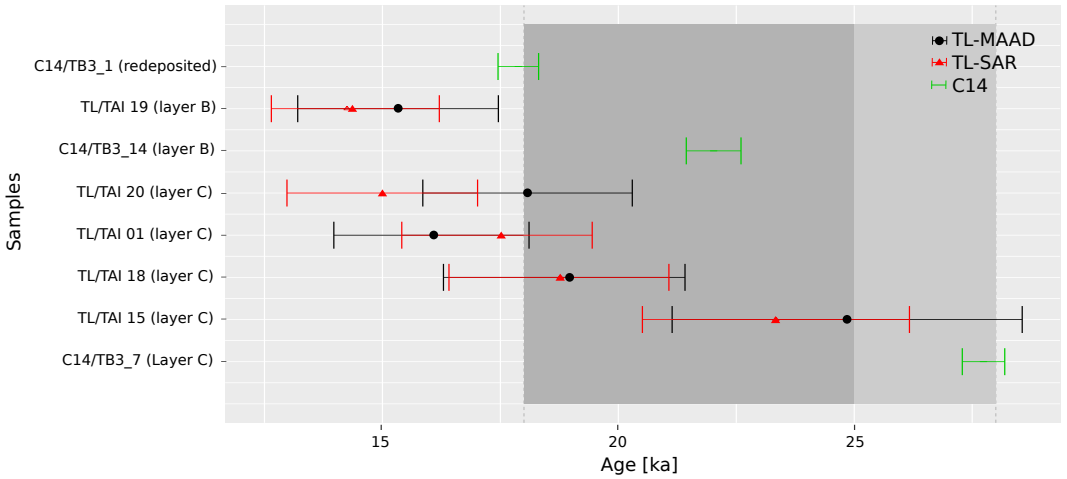


FIGURE 5.2: **Comparison of the age estimation using the MAAD and the SAR protocols.** All the age are in the expected range for Masraqan artefacts except for TAI 15 which seems a little bit older. The TL ages are also in good agreement with the radiocarbon ages.

fully excluded. However, the same measurement equipment was successfully used for *a-value* estimation of unrelated feldspar samples which indicates that the α-dose-rate estimation should be accurate (Bösken et al., 2017). In addition to their very high *a-value*, the Taibeh flint samples also seems to saturate at a very high doses (above $\approx 60\ Gy$), much higher than what is usually published.

The radiocarbon ages are consistent with the expected age for Masraqan artefacts (Goring-Morris and Belfer-Cohen, 2017) and three heating events can be identified (see Tab. D.8 in the online supplement). The TL ages can also be separated between three heating events: (1) TAI-19, which is from layer B, is the youngest; (2) TAI-1, TAI-18 and TAI 20, which are from layer C, are a little bit older; and (3) TAI-15, which is also from layer C, is the oldest (see Fig. 5.2). Unfortunately, except for TAI-15, the TL ages are not fully consistent with the expected age for Masraqan artefacts. There seems to be an offset between the radiocarbon ages and the TL ages which are systematically younger.

5.4 Conclusion

The *Luminescence* and the *TLdating* **R** packages provide all the tools needed for the analysis and the combination of the measurements required for the estimation of an age using TL dating. The dating of the Taibeh artefacts shows that both the SAR and the MAAD protocols can provide a reliable D_e estimation when using TL for the dating of heated flints as long as there is no initial sensitivity change. The consistence

of the results obtained with different protocols (MAAD and SAR) and approaches (dose plateau and growth curve) assures the reliability of the tools that were used.

Despite its relative simplicity, our modified version of DRAC allows to estimate the dose rate for heated flint using the same amount of information needed for sediment dating. With a similar reasoning it is possible to adapt DRAC for other situations encountered in archaeology, like TL-dating of ceramic samples.

When dating heated flint, properly determining the $\dot{D}_{flint}$ is compulsory. It can sometimes represent up to 80% of $\dot{D}_{tot}$. It is therefore important to estimate an *a-value* for each heated flint. Extremely high or low values can be encountered; those reported in literature vary up to one order of magnitude. The dating of the Taibeh heated flints shows a clear offset between the radiocarbon and TL-ages which is consistent with a systematic overestimation of the *a-values*. The next step of this study will therefore be to properly identified the origin of this systematic error and correct for it.

Acknowledgements

This project was realized in the context of the *CRC 806: Our Way to Europe* (http://www.sfb806.uni-koeln.de/) which is funded by the German Research Foundation (DFG). D. Strebler gratefully acknowledges having received the fellowship grant No. GSGS-2017A-F08 of the Graduate School of Geosciences, University of Cologne.

We would like to thank S. T. Hussain for providing valuable informations on the Taibeh archaeological background, resulting from his M.A. thesis about the lithic technology at the site, C. Schmidt for collecting the samples during the first phase of the CRC 806, Dr. H. U. Kasper for realising the ICP-MS measurements and J. Rethemeyer for sharing with us the radiocarbon dating results.

Chapter 6

Another case study: Dating the prehistoric sites of Al-Ansab I and II, Jordan

6.1 Introduction

The Early Ahmarian is the first fully upper Palaelothic techno-cultural unit exclusively related to AMH in the Near East. It was defined more than 30 years ago as a Early Upper Palaeolithic industry characterized by the presence of so-called *El-Wad points* and some other typo-technological features in the lithic assemblages (Gilead, 1991, Marks and Rose, 2014). Based on radiocarbon dating, it developed during a time range between 45 ka BP and 37 ka BP, i.e. during Marine Isotope Stage (MIS) 3. More than 50 sites have been identified as belonging to this techno-cultural unit. They are located in the areas today known as the Sinai Peninsula, the Negev Desert, the Wadi Araba, western Transjordan, the Lebanon Mountains and the souther Syrian Desert (see Fig. 6.1). The Early Ahmarian has been subdivided into the Northern Early Ahmarian (NEA) and the Southern Early Ahmarian (SEA). This subdivision is motivated by slight but systematic variations in the lithic assemblages between the two variants (Goring-Morris and Belfer-Cohen, 2018).

Al-Ansab is located in the Jordan Rift Valley, more specifically in the Lower Wadi Sabra, 15 km South of Petra (Jordan) (see Fig. 6.2). Extensive archaeological surveys in and around the Wadi Sabra from 2009 to 2014 detected a few Middle Palaeolithic surface sites and numerous Middle Palaeolithic single finds, all lacking stratigraphic context (Richter et al., 2020). Numerous Upper Palaeolithic sites were also identified including one Initial Upper Palaeolithic (IUP) site embedded in redeposited sediments, Al-Ansab 2 (Hussain,

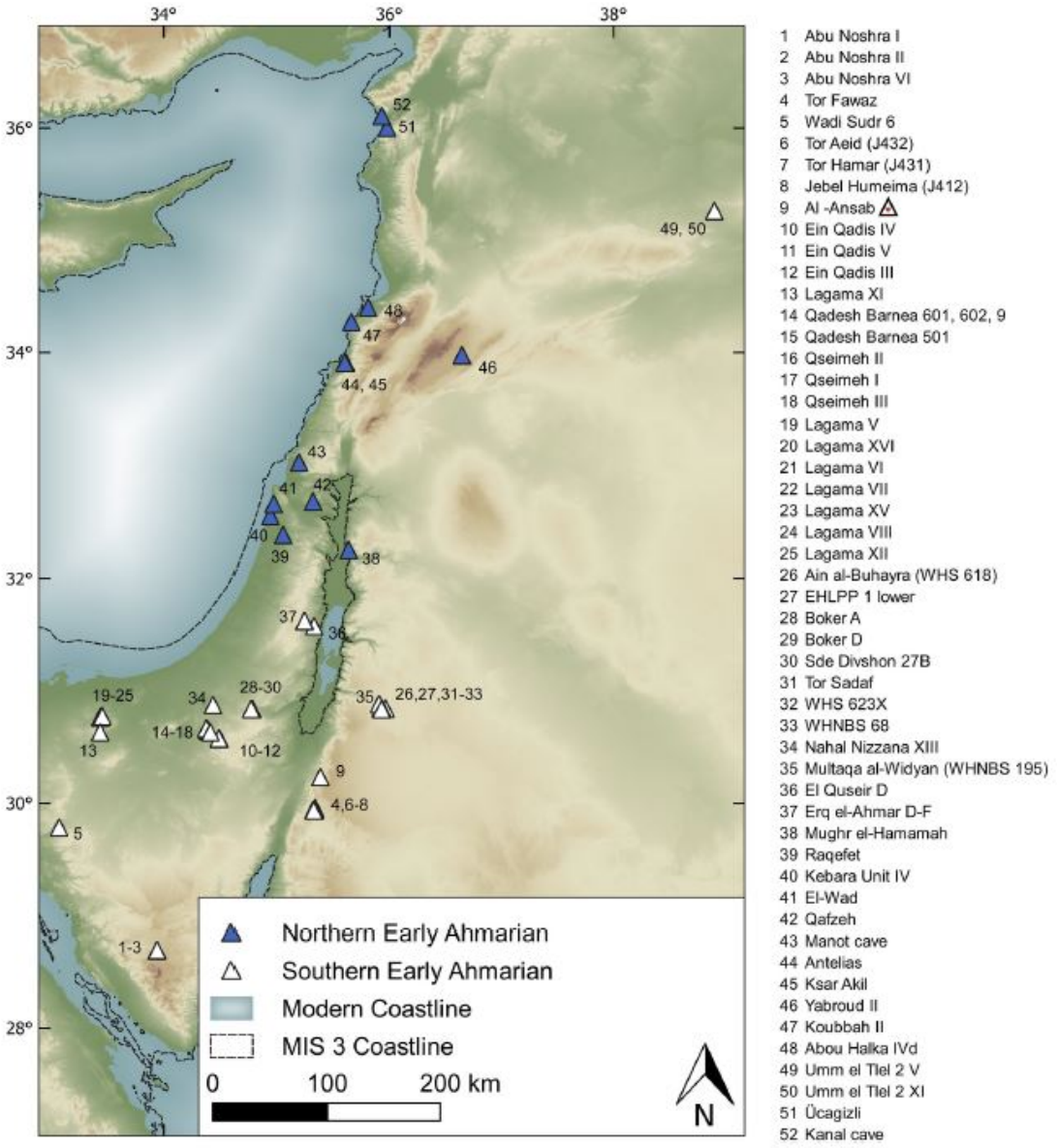


FIGURE 6.1: **Archaeological sites attributed to the Early Ahmarian techno-cultural unit composed of the Northern Early Ahmarian (NEA) and Southern Early Ahmarian (SEA) groups.** SEA sites include the Lagaman regional variant (Goring-Morris and Belfer-Cohen, 2018) known in the Negev Desert and on the Sinai Peninsula (Richter et al., 2020).

2015b, Richter and Schyle, 2015), and, nearby, one Early Upper Palaeolithic site still in primary stratigraphic context and already known from a 1983 survey, Al-Ansab 1 (Schyle and H.P., 1988).

Al-Ansab 1 is a well stratified Early Ahmarian occupation embedded in consolidated sand layers of fluvial and aeolian origin. It is among the few known stratified Early Ahmarian open air settlements available to modern excavation (Richter et al., 2020). It is situated on a Pleistocene sediment promontory at 618 m asl, c. 25 m above the narrow wadi bed which was preserved due to an adjacent limestone crest that protects

the site from erosion. Since 2009, a series of field campaigns were conducted to the site in the context of the CRC 806 (Hussain, 2015b, Klasen et al., 2013, Schyle, 2015). They include sediment studies, radiometric dating and techno-typological analyses of the lithic material.

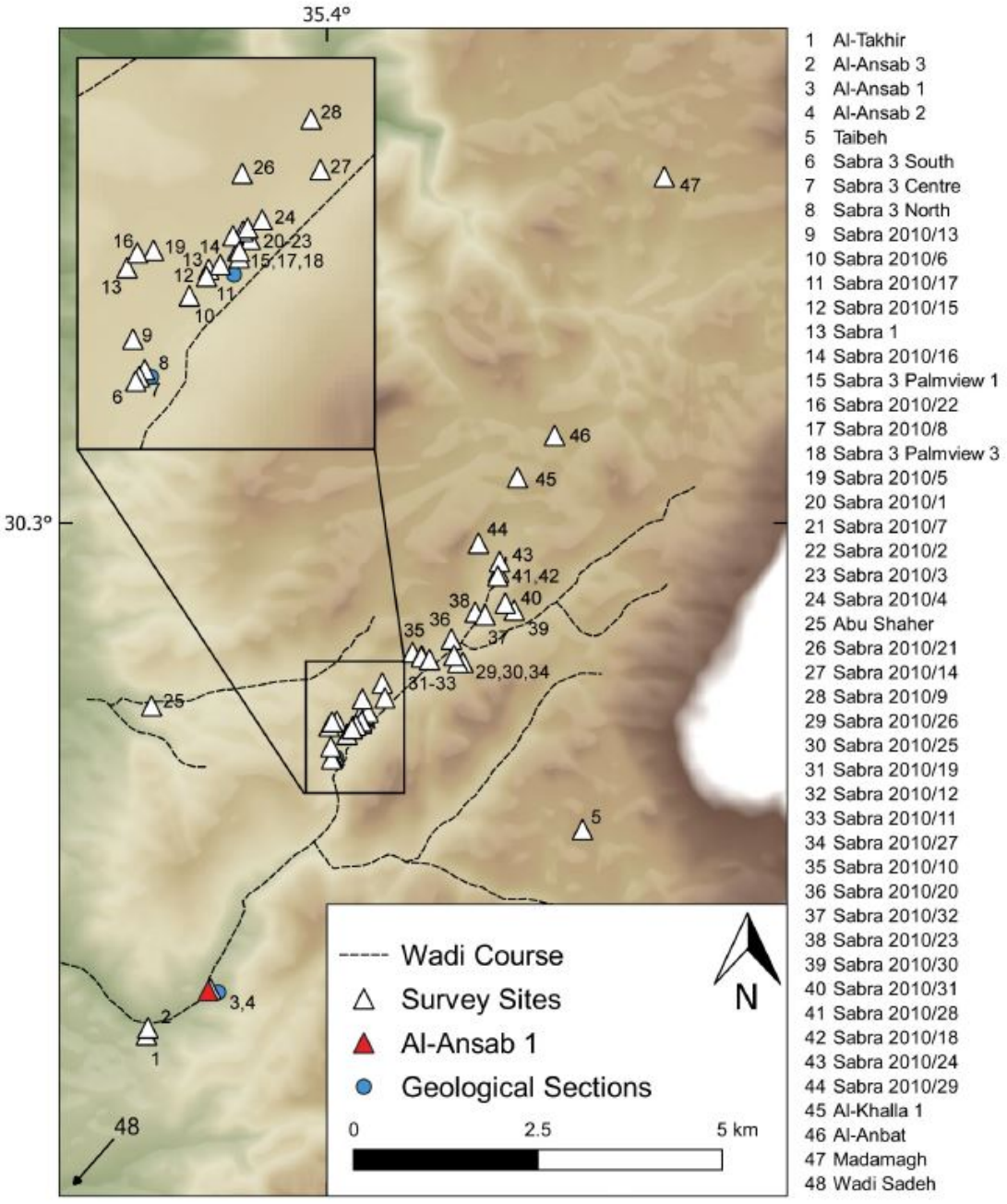


FIGURE 6.2: **Palaeolithic sites discovered in Wadi Sabra during the CRC 806 archaeological survey from 2009 to 2019.** Coordinate system used: WGS 84/EPSG 4326. (Richter et al., 2020).

The author took part in the excavation campaign in 2015 which focus on Al-Ansab 1 and 2. During this campaign, a series of samples were collected to complete the Al-Ansab chronology. It includes 5 heated flint samples and 6 stones showing potential signs of

heating (all from Al-Ansab 1) and 6 sediment samples (five from the Al-Ansab 1 and one from the Al-Ansab 2). A series of charcoal samples were also collected among the different remains of fireplaces for radiocarbon dating.

6.2 Previous Age estimation for Al-Ansab 1, Jordan

In 2013, a series sediment samples were collected for luminescence dating (Klasen et al., 2013). Using the central age model to calculate equivalent doses, the age estimations yield results in the range of 30 to 48 ka (see Table 6.1 and Fig. 6.3).

Site	Location	Sample	Depth (m)	age (ka)
Al-Ansab 1	Section 6	ANS 6-3	0.15	45 ± 3
Al-Ansab 1	Section 6	Ansab 1	0.30	32 ± 2
Al-Ansab 1	Section 6	Ansab 2	0.30	37 ± 3
Al-Ansab 1	Section 6	ANS 6-2	0.75	34 ± 3
Al-Ansab 1	Section 6	ANS 6-1	1.25	35 ± 3
Al-Ansab 1	Section 3	ANS 3-3	2.00	32 ± 3
Al-Ansab 1	Section 3	ANS 3-2	2.25	36 ± 3

TABLE 6.1: **Age estimation for the sediment sample collected during the 2013 archaeological campaign** (Klasen et al., 2013).

These first age estimations indicate that radiocarbon ages will have to be treated carefully. They are close to the absolute limit of radiocarbon dating and may have to be considered as *minimum* age rather than *absolute* age estimation. They are also consistent with a plateau on the ^{14}C calibration curve which may increase the uncertainties on radiocarbon age estimations. These luminescence ages also indicate a relatively short period of sedimentation for the existing 20 m of sandy deposits.

A series of charcoal samples were also collected from the archaeological layers of Al-Ansab 1 between 2011 and 2013 for radiocarbon dating. Seven of them, coming from several locations in the excavation area, place the occupation of the site between 36 ka and 38 ka cal BP (see Table 6.2).

Both the radiocarbon and the luminescence age are consistent with each other. They are also consistent with the general chronology for Early Ahmarian occupation sites.

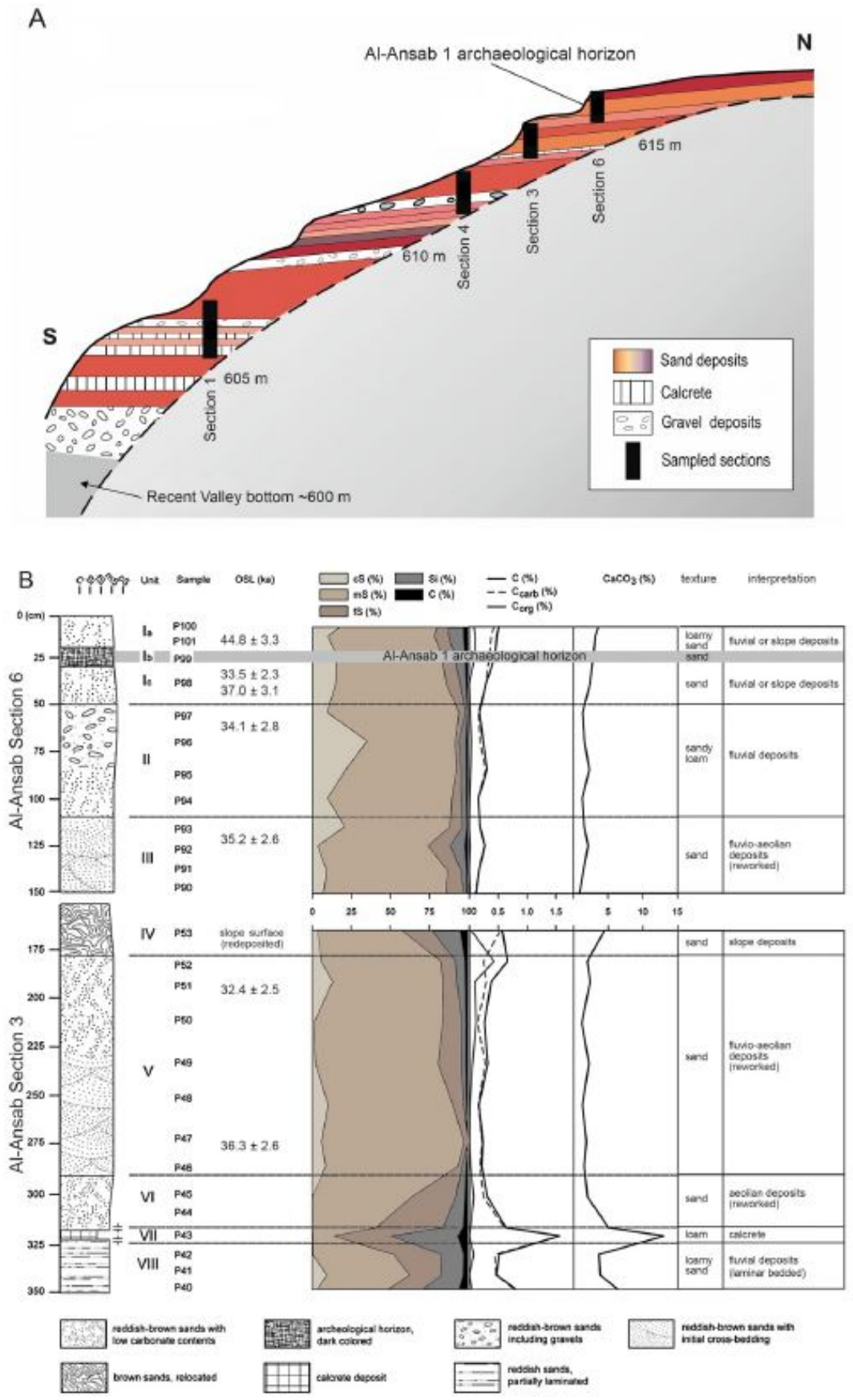


FIGURE 6.3: **Local geological sequence of the pleistocene wadi fill around the Al-Ansab 1 Early Ahmarian settlement site.** (A) South-to-North schematic section through the Pleistocene sediment remnant bearing the Al-Ansab 1 site, from the base of the present Wadi Sabra dry-river channel to the top of the wadi fill ; (B) Selected data resulting from sediment analysis of geological sections 6 and 3. (Klasen et al., 2013, Richter et al., 2020).

Site (date)	Location	Sample	Depth (m)	age (2σ, cal BP)
Al-Ansab 1 (2013)	N-S trench, layer 2/3	AN001	0.25	37182 ± 1105
Al-Ansab 1 (2013)	168-17, layer 3	AN002	0.25	37316 ± 1083
Al-Ansab 1 (2011)	184A, Pos.3, layer 3	AN003	0.25	37494 ± 1093
Al-Ansab 1 (2011)	184A, Pos.2, layer 3	AN004	0.25	37741 ± 1167
Al-Ansab 1 (2013)	N-S Trench	AN005	1.25	37730 ± 1197
Al-Ansab 1 (2013)	N-S Trench	AN006	1.25	37231 ± 1138
Al-Ansab 1 (2013)	N-S Trench	AN007	1.25	37623 ± 1130

TABLE 6.2: **Radiocarbon age estimations for charcoal samples collected during the 2011 and 2013 archaeological campaigns.** Calibration was conducted using the IntCal13 calibration curve provide by the OxCal 4.3 software package. ^{14}C measurements provided by CologneAMS and realised using a Acid-Alkani-Acid (AAA) pretreatment (Richter et al., 2020).

6.3 New age estimations for Al-Ansab 1 and 2, Jordan

During the 2015 excavation campaign of Al-Ansab, a series of samples were collected by the author to complete the Al-Ansab chronology. These includes sediment, heated flint, heated stones and charcoal samples.

6.3.1 Sediment sample dating

For the sediment samples, the D_e estimations were made using the SAR protocol on small aliquots. HP-Ge γ-spectrometry was used to estimate the radionuclide concentration of the sediment sample and therefore the $\dot{D}$. The final age estimations were consistent with those previously obtained (see table 6.3).

Site	Section	Sample	D_e (Gy)	$\dot{D}$ (Gy)	Age (ka)
Al-Ansab 1	Lower profile	ANS S1	38.85 ± 1.04	1.08 ± 0.03	35.98 ± 1.39
Al-Ansab 1	Lower profile	ANS S2	30.46 ± 1.17	0.90 ± 0.03	33.97 ± 1.64
Al-Ansab 1	Lower profile	ANS S3	29.61 ± 1.35	0.92 ± 0.03	32.29 ± 1.77
Al-Ansab 2	Middle profile	ANS S4	36.35 ± 1.77	0.86 ± 0.03	42.27 ± 2.45
Al-Ansab 1	Upper layer	ANS S6	16.15 ± 0.84	0.65 ± 0.03	24.73 ± 1.80
Al-Ansab 1	Layer 2	ANS S7	41.14 ± 1.68	1.13 ± 0.03	36.49 ± 1.78

TABLE 6.3: **D_e, $\dot{D}$ and age estimations for the Al-Ansab sediment samples collected during the 2015 field campaign**.

The age estimation for the sample coming from the occupation layer (ANS S7) is fully consistent with the previous radiocarbon and OSL age estimations. The age estimation for the sample coming from the layer above the occupation layer (ANS S6) provides a minimum age to the overall stratigraphic chronology. This sample has been collected close to the actual surface layer and definitively suffered from bioturbation. Its age

estimation should be considered as a minimum age estimation and is therefore still consistent with the hypothesis that sedimentation came to a halt around 32 ka BP in the lower Wadi Sabra, i.e. where Al-Ansab 1 is located (Bertrams et al., 2012a,b).

The Al-Ansab 1 *Lower Profile* may present an inversion of the age sequence similar to the one observed in the sections 3 and 6 of Al-Ansab 1. This profile, being in a slope, could be the consequence of sediment re-deposition due to landslides. However, a rapid deposit of partially bleach sediments, as considered based on the previous OSL age estimation, also fully explained these results.

The Al-Ansab 2 section was not stable enough to collect reliable sediment samples from its lower and upper profiles. The age estimation for the ANS S4 sediment sample is consistent with the hypothesis that the middle section of Al-Ansab 2 contains the traces of an Initial Upper Palaeolithic (IUP) occupation. Radiocarbon age estimation for samples coming from this second site should definitively be considered carefully and as minimum age estimations.

6.4 Heated flint sample dating

During the 2015 excavation campaign, 11 samples were collected for TL dating (see Table 6.4). These includes 6 stone samples (ANS F1a, F1b, F4, F5, F9 and F11) and 5 flints samples (ANS F1c F2, F3, F10 and F12). Among the stones samples, two of them (ANS F1b and F11) present usual signs of heating (pot-lids), while the four others (ANS F1a, F4, F5 and F9) only present potential signs of heating (change in the colouration and texture). Among the flint samples, all have usual signs of heating (pot-lids). It has to be noted that pot lids and other usual signs of heating can also be generated by a long exposition to sunlight, especially in warm and arid region as it is the case in the Wadi Sabra, Jordan.

Three of the heated flint (ANS F1c, F2 and F3) and one of the burnt stone (ANS F1a) samples were too small or too thin to allow the extraction of their core material using the available equipment. The 2 remaining heated flint samples (ANS F10 and ANS F12) provide consistent D_e and *a-value* estimations. Unfortunately, the final age estimations were definitively too low and inconsistent with the sediment OSL age estimations (see Table 6.9). For four of the stone samples (ANS F4, F5, F9 and F11), the initial D_e estimations were especially high, i.e. above the maximum regenerative dose (see Table 6.5). It wad assumed that these samples were not reset by any human activities and their D_e accumulated through geological time. The last stone sample (ANS F1b) presents a TL signal that may be consistent with an archaeological reset. However, this signal

Site	Location	Sample	Material	Depth (m)
Al-Ansab 1	Layer 2 (sq 176, spit 4)	ANS F1a	Stone (heated?)	0.25
Al-Ansab 1	Layer 2 (sq 176, spit 4)	ANS F1b	Burnt stone	0.25
Al-Ansab 1	Layer 2 (sq 176, spit 4)	ANS F1c	Heated flint	0.25
Al-Ansab 1	Layer 2 (sq 176, spit 4)	ANS F2	Heated flint	0.25
Al-Ansab 1	Lower profile	ANS F3	Heated flint	0.50
Al-Ansab 1	Lower profile	ANS F4	Stone (heated?)	0.50
Al-Ansab 1	Lower profile	ANS F5	Stone (heated?)	0.50
Al-Ansab 1	Lower profile	ANS F9	Stone (heated?)	0.50
Al-Ansab 1	Layer 2 (sq 167, spit 5)	ANS F10	Heated flint	0.25
Al-Ansab 1	Lower profile	ANS F11	burnt stone	0.50
Al-Ansab 1	Lower profile	ANS F12	heated flint	0.50

TABLE 6.4: **List of the burnt and heated samples collected during the 2015 field campaign in Al-Ansab for TL dating.**

also presents multiple TL peaks around the usual integration interval (between 260°C and $\sim$ 400°C). Two hypothesis could explain such behaviour: (1) the sample was not properly reset by the heating and (2) it is a polymineral sample. The results of the elemental analysis is in agreement with the second hypothesis. In the end, it was not possible to provide a reliable age estimation for this last sample. Despite the lack of final age estimation for these last samples, they provide a good case study for several challenges often encountered when dating heated flint samples.

6.4.1 Sample selection and preparation

Based on the Inventory of excavated finds (2015-2018), more than 40000 flint artefacts were collected at Al-Ansab 1. Those represent 94% of the finds (chips below 1 cm excluded). Around half of them are chunks. Traces of burning occur among c. 10% of all single plotted lithics, mostly on the chunks, with around 33% that shows traces of burning or are shattered (Richter et al., 2020).

Despite this large amount of heated flint samples, only 11 of those collected during the 2015 campaign were identified as potentially datable using TL. On one hand, the large majority of the samples were just too small or too thin to extracted their core material. On the other hand, the better preserved samples need to be kept for the archaeological collections and are therefore not available for TL dating which will induce their destruction. Among the remaining samples, most did not present clear signs of heating (especially pot-lids) when they were collected. Such samples often present only a partial reset of the TL signal and are usually discarded.

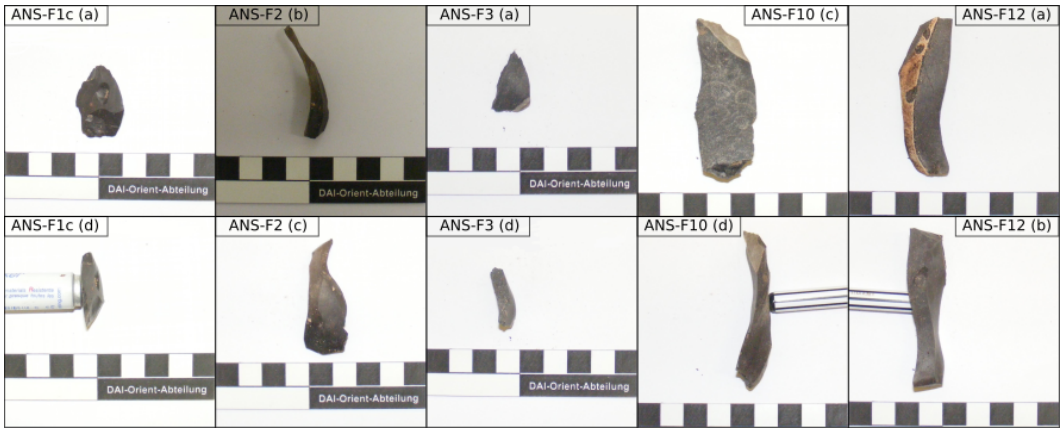


FIGURE 6.4: **Heated flint samples from Al-Ansab 1 collected in 2015 for TL dating.**

Once the 11 selected samples (5 heated flints and 6 burnt stones) were brought back to the Cologne Luminescence Laboratory, a third of them were identified as too small to be processed using the available equipment to extract their core material (ANS F1a, F1c, F2 and F3), including half of the heated flint samples (ANS F1c, F2 and F3) (see Fig. 6.4).

The 7 last samples (ANS F1b, F4, F5, F9, F10, F11 and F12) were treated using the same protocol. This protocol is similar to that presented in Chapters **??** and used on the Taibeh samples (see Chapter 4 and 5) with a few modifications.

Sample's core material extraction

First, the flint sample's external layer, especially the cortex, was removed by 2 mm. For this step, a water cooled diamond saw was used, in this case, a *Isomet 1000 precision saw* from *Buehler* (see Fig. 6.5). Before cutting, the sample was painted with white to allow the external surface and the core material to be easily distinguished.

Then, the core material was cut in two, using the same water cooled diamond saw. The smallest part, that had to be at least 200 mg, was used for the estimation of the radionuclide element concentration using elemental analysis. The largest part was used to produce the coarse grains (CG) for the D_e estimation and the fine grains (FG) for the α-efficiency (a-value) estimation.

Preparation of the fine grain fraction for elemental analysis

The smallest part of the core material was crushed using a hydraulic press, at a pressure of maximum 2 to 3 bar (see Fig. 6.5), and the artificially created grains were sieved

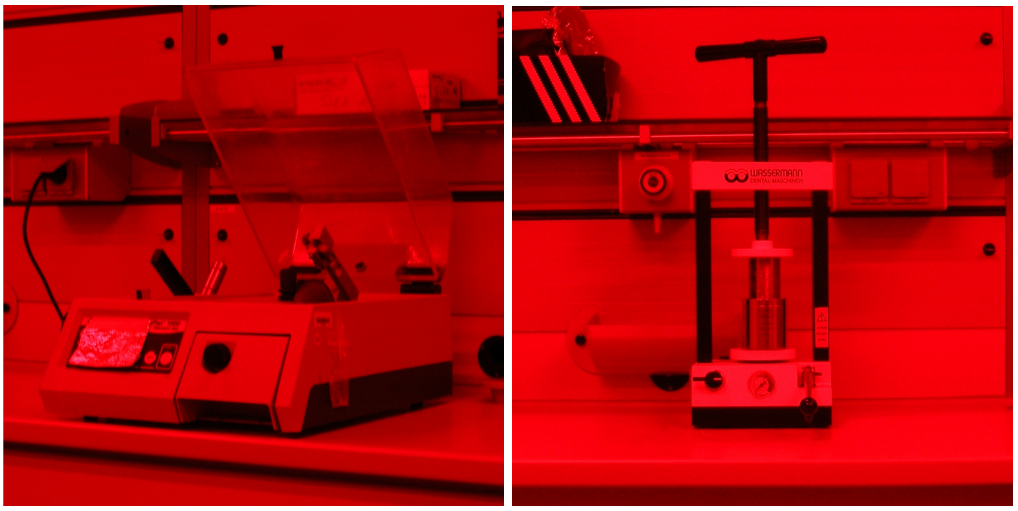


FIGURE 6.5: **Diamond saw and Hydraulic press** used for the sample's core material extraction of the Ansab flint samples.

using a mesh with a size of 63 μm. The crushing process was repeated until all the (artificially created) grains go through this mesh. These grains were then crushed again, this time using a mortar and a pestle, until a very fine and homogeneous powder was obtained.

For the Al-Ansab samples, it was decided to externalise the measurement of the radionuclide concentrations. For each of the three remaining samples (ANS F1b, ANS F10 and ANS F12), 200 mg of the obtained fine powder was sent to the external laboratory, in this case *Actlab*[1], without any additional preparation step. A known sample of 200 mg, the Nussloch loess sediment, was added to the batch as a control sample.

Preparation of the coarse grain fraction for D_e estimation

The largest part of the core material was also crushed, using the same hydraulic press and at a pressure of maximum 2 to 3 bar too (see Fig. 6.5). However, this time, the (artificially created) grains were sieved using two different mesh sizes, 100 and 200 μm. Once again, the process was repeated until all the grains went through the meshes (and, therefore, were smaller than 200 μm). Between each crushing, the grains with a diameter between the 2 mesh sizes were collected for the CG preparation and the grain smaller than 100 μm were collected for the FG preparation.

The last step of the CG fraction preparation was to treat the (artificially created) grains with HCl to remove any trace of carbonates. These carbonates were identified as the

[1] https://actlabs.com/

origin of the tribo- and spurious luminescence that were present in some samples (Valladas, 1978). For our experiments we used HCl (10%), then washed the CG three times with deionized H_2O and dry them in an oven at 50 $°C$.

Preparation of the fine grain fraction for a-value estimation

The finer fraction ($< 100\ \mu m$) of the biggest part of the core material was dedicated to the a-value estimation. The production of proper FG required a series of extra preparation steps. The grains were crushed again: first using the hydraulic press and the finest mesh available (63 μm) and then using a pestle and a mortar for around $10'$. Once a fine and homogeneous powder was obtained, wet settling was used to extract the FG fraction (i.e. the grain between 4 and 11 μm).

A first wet settling using deionized H_2O and a 7 cm water column was used to extracted the grain bigger than 11 μm. A settling time of 10'45" was defined based on the Stoke's law:

$$t = \frac{18\eta h}{(\rho_s - \rho_l)gd^2} \tag{6.1}$$

Where t is the settling time, ν the viscosity coefficient, h the height of liquid in the beaker, ρ_s the density of the grains, ρ_l the density of the liquid, g the gravitation acceleration and r the radius of the grain (Weida and Junding, 1989).

At the end of this settling time, the grains that settled were crushed again within the mortar during $5'$ and the process was repeated at least 3 times.

The solution containing the FG fraction was dried in an oven at 50 $°C$ to evaporate the deionized H_2O and collect the grains smaller than 11 μm. These grains were then treated with HCl (10%), to remove any traces of carbonates, and cleaned with deionized H_2O. We used to wait one night before removing the HCl and between each cleaning but the process can be speed up with a centrifuge.

Once we were sure to only have quartz grains finer than 11 μm, the silt was removed from the sample using a second wet settling. This time an centrifuge and deionized H_2O was used. A second settling time of 1' at a speed of 800 rounds per minute was used based on a modified Stoke's law (Weida and Junding, 1989):

$$t = \frac{\eta_0}{\pi^2(\rho_s - \rho_l)d^2U^2} \ln\left(\frac{R}{r_0}\right) 1.62 \times 10^4 \tag{6.2}$$

This step was repeated 5 times to remove as much silt as possible. To reduce the loss of FG, the solution containing the silt fraction was collected and the settling process repeated a second time.

6.4.2 Equivalent dose estimation

Sample	Material	Heating plateau ($°C$)	$\mathbf{D_e}$ (Gy)
ANS F1b	Stone	300-400	137.93 ± 11.80
ANS F4	Stone	300-450	363.09 ± 21.85
ANS F5	Stone	300-450	941.76 ± 50.93
ANS F9	Stone	300-400	498.60 ± 25.57
ANS F11	Stone	300-400	361.00 ± 18.56
ANS F10	Flint	300-400	40.36 ± 1.14
ANS F12	Flint	300-380	30.55 ± 5.29

TABLE 6.5: **Results of the heating plateau test (HPT) using an additive protocol on 4 aliquots** (2 for the natural signal and 2 for the additive one) **and first estimation of the $\mathbf{D_e}$ using a SAR protocol on 3 aliquots.** For four stones samples (ANS F4, F5, F9 and F11), the D_e estimation was above the higher regenerative dose (3200 s or 317.44 Gy). Three of the stone samples (ANS F1b, F5 and F11) present multiple TL peaks around the plateau region ($\sim 270°C$ and $\sim 370°C$) which could be indicative of polymineral samples.

For each of the prepared sample, a heating plateau test was perform on a first series of 6 CG aliquots using an additive dose protocol. All the samples present a clear plateau above 300 $°C$ and up to 375-400 $°C$. Above 400 $°C$, noise signal significantly increases, usually as a result of the black body radiation and the background subtraction pretreatment. All the samples presenting a clear heating plateau, a first estimation of the D_e was performed using a short SAR protocol. This protocol was carried out on 6 aliquots, with regenerative β irradiation time going from 200 to 3200 s. For four of the stone samples (ANS F4, F5, F9 and F11), these first D_e estimations were above the maximum regenerative dose. In this case, such results could only be consistent with a geological reset, long before any human occupation of Al-Ansab 1 (see table 6.5).

For the samples presenting a behaviour consistent with an archaeological reset (ANS F1b, ANS F10 and F12), a second series of D_e estimations were realised. These final D_e estimations were performed using (1) a MAAD protocol on twelve aliquots (8 mm) and (2) a SAR protocol on 12 aliquots (8 mm). When the new D_e estimation obtained for the flint samples (ANS F10 and F12) were relatively consistent with their first analysis (see Table 6.6), the MAAD protocol provided no reliable results for the last burnt stone samples (ANS F1b). For this last sample (ANS F1b), the D_e estimation obtained using the DP and GC approaches were never consistent and highly sensitive to any slight modification of the calculation parameters (integration interval, using weighed

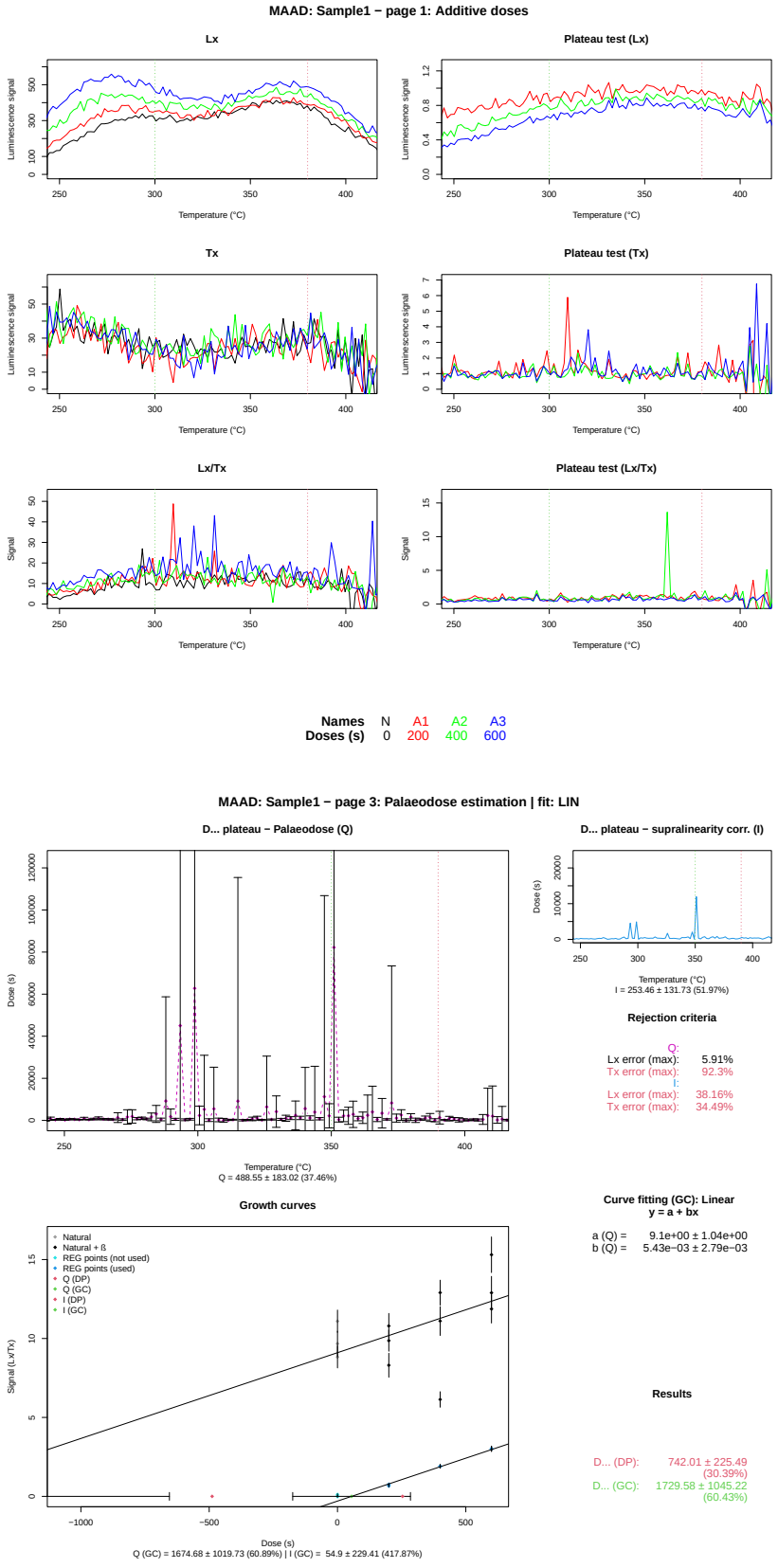


FIGURE 6.6: **Luminescence signal and Growth curve for the F1b stone sample using the MAAD protocol.** The integration interval is $320 - 390°C$. The relative uncertainty on the D_e is above 60%. Only one of the rejection criteria is validated.

or unweighed fitting, reusing the Q slope for I,...). The relative uncertainties on these estimations were also systematically around 50% (see Fig. 6.6). It was therefore decided to discard this sample.

Sample (material)	**Protocol**	**Approach**	**Integration** ($°C$)	D_e **(Gy)**
ANS F10 (flint)	MAAD	DP	320-360	42.34 ± 2.45
ANS F10 (flint)	MAAD	GC	320-370	45.14 ± 2.90
ANS F10 (flint)	SAR	DP	320-370	44.82 ± 0.46
ANS F10 (flint)	SAR	GC	320-370	41.12 ± 1.96
ANS F12 (flint)	MAAD	DP	315-370	21.34 ± 2.79
ANS F12 (flint)	MAAD	GC	315-370	28.08 ± 5.39
ANS F12 (flint)	SAR	DP	320-370	33.65 ± 6.40
ANS F12 (flint)	SAR	GC	320-370	34.29 ± 5.05

TABLE 6.6: **D_e estimations for the burnt stone sample (ANS F1b) and the two heated flint samples (ANS F10 and F12) showing an archaeological reset.** The D_e were estimated with a SAR and a MAAD protocols and, in both cases, using a dose plateau and a growth curve approach (see Chapter 4).

For both flint samples, the D_e estimations obtained using the SAR and the MAAR protocol were consistent with each other (see Table 6.6). The growth curves obtained using the SAR protocol also indicate that the natural signal was still in the linear region (see Fig. 6.7).

6.4.3 a-value estimation

For the samples providing a reliable D_e estimation, i.e. the two last heated flint samples (ANS F10 and F12), an a-value estimation was carried on fine grain 9 mm aliquots. First, these FG aliquots were heated at $280°C$ for 2 hours in a furnace to reset the natural TL signal. Second, they were irradiated using a cross calibrated α source during 400 s at 0.1968 ± 0.005 Gy/s (see Appendix E). Finally, for each sample, two a-values were estimated. The first one using a MAAD protocol on 12 aliquots and the second one using a SAR protocol on 6 aliquots (see table 6.7).

For the first heated flint sample (ANS F10), both the MAAD and SAR protocol provide an a-value of 0.2 ± 0.01. For the second heated flint sample (ANS F12), the MAAD protocol provides an unexpectedly high a-value (0.33 ± 0.04). Neglecting the supralinear correction provides an a-value much more consistent with the previous sample's values (0.21 ± 0.03). The SAR protocol provides a smaller a-value (0.16 ± 0.01). In both cases, the smaller a-value estimation was used for the $\dot{D}$ estimation (0.20 ± 0.01 for ANS F10 and 0.16 ± 0.01 for ANS F12).

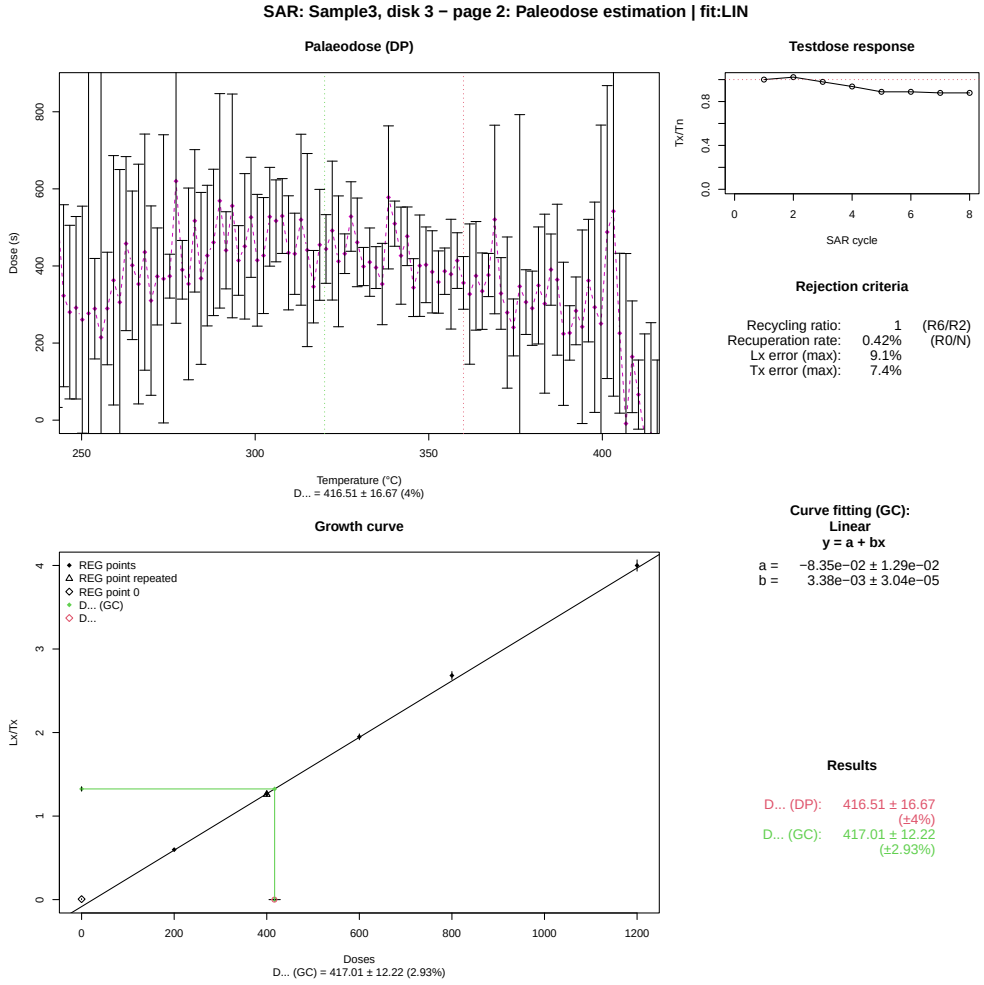


FIGURE 6.7: **D_e estimation using the dose plateau (DP) and the growth curve (GC) approaches for a representative aliquot from ANS F10.** Both D_e estimation are consistent with each other and the natural dose is in the linear region of the growth curve.

All the TL signal measurements were carried on a Risø 20 TL/OSL reader equipped with an EMI 9235GG bialkani photomultiplier. For the D_e estimation and the heating plateau test (HPT), a filter combination with *Schott HA-3*, *Schott BG-39*, *Schott GG-400* and *Corning 37-59* was applied (bandwidth 440-470 nm) (Schmidt, 2013). For the α-efficiency (a-value) estimation, a filter combination with a *Semroch Brightline HC 470/50* and *Schott BH-3* was applied (Schmidt et al., 2015b). All the luminescence data were processed on **R** using the *TLdating* package.

6.4.4 Dose rate estimation

For each of the collected stone and flint samples, surrounding sediment material was also collected (around 1 kg per sample). These sediment samples were used to estimate the environmental component of the $\dot{D}$. Their water content was determined by weighing

Sample	Protocol	α-dose (Gy)	β-dose (Gy)	a-value
ANS F10	MAAD	78.72 ± 2.01	15.68 ± 0.5	0.20 ± 0.01
	SAR	78.72 ± 2.01	16.14 ± 0.44	0.21 ± 0.01
ANS F12	MAAD	78.72 ± 2.01	34.60 ± 2.47	0.44 ± 0.03
	SAR	78.72 ± 2.01	14.61 ± 0.37	0.19 ± 0.01

TABLE 6.7: **A-value estimation for the 2 heated flint samples showing signs of a signal reset during archaeological times.** The β-dose values were estimated using a GC and a DP approaches. Only the CG values are reported here. The DP results are used to defined the integration temperature interval. The a-value obtained using the MAAD protocol for ANS F12 is definitively overestimated. Neglecting its supra-linearity correction brings it down to 0.23 ± 0.02 which is already more consistent with the other a-value estimations.

them, (1) at the opening of the sample bags in the laboratory and (2) after drying for a few days in a oven at 50 $°C$, and by estimating the ratio between the two measurements. Their radionuclide (U, Th and K) concentration were determined by γ-spectrometry using a High purity Germanium (HPGe) detector at the Cologne Luminescence Laboratory (CLL) (see table 6.8).

Sample	Location	Material	Method	K (%)	Th (ppm)	U (ppm)
TAI F1b	Layer 2	sediment	HPGe	0.36 ± 0.01	3.92 ± 0.21	1.21 ± 0.06
TAI F2	Layer 2	sediment	HPGe	0.37 ± 0.01	4.00 ± 0.21	1.18 ± 0.06
TAI F3	Lower profile	sediment	HPGe	0.28 ± 0.01	4.16 ± 0.23	1.16 ± 0.06
TAI F4	Lower profile	sediment	HPGe	0.23 ± 0.01	3.79 ± 0.21	1.09 ± 0.06
TAI F5	Lower profile	sediment	HPGe	0.23 ± 0.01	3.69 ± 0.20	1.10 ± 0.06
TAI F9	Lower profile	sediment	HPGe	0.22 ± 0.01	3.58 ± 0.20	1.08 ± 0.06
TAI F10	Layer 2	sediment	HPGe	0.32 ± 0.01	3.60 ± 0.20	1.09 ± 0.06
TAI F11	Lower profile	sediment	HPGe	0.26 ± 0.01	4.03 ± 0.22	1.14 ± 0.06
TAI F12	Lower profile	sediment	HPGe	0.28 ± 0.01	4.16 ± 0.23	1.16 ± 0.06
TAI F1b	Layer 2	stone	ICP-MS	8.19 ± 0.01	7.55 ± 0.05	3.45 ± 0.01
TAI F10	Layer 2	flint	ICP-MS	0.03 ± 0.01	< 0.05	2.27 ± 0.01
TAI F12	Lower profile	flint	ICP-MS	0.03 ± 0.01	< 0.05	1.5 ± 0.01
Nussloch	Control	loess	ICP-MS	1.34 ± 0.01	8.61 ± 0.05	3.07 ± 0.01

TABLE 6.8: **Radionuclide concentrations for the heated flint/stone samples and the surrounding sediment material.**

We can see a clear correlation between the radionuclide concentration and the collection location of the sediment samples. The sediment samples coming from the Layer 2 of Al-Ansab 1 (TAI F1b, F2 and F10) have a slightly higher K content.

As previously presented, 200 mg of fine powder from the core material of the 3 samples presenting a potential reset event during archaeological time were sent to an external laboratory to perform elemental analysis. The internal radionuclide concentrations (U, Th and K) of these three samples (TAI F1b, F10 and F12) were estimated using ICP-MS

(see table 6.8). The heated stone sample (ANS F1b) presents a very high K content (> 8%). It is therefore very likely that the TL signal may partially originate from K feldspar. Such hypothesis could explain the presence of a double peak in the TL signal.

In average, the radionuclide concentrations in the two heated flint samples (ANS F10 and F12) remain relatively low. The Th concentration is even lower than the detection limit of the measurement device used (0.05 ppm). However, all these concentration remain systematically higher than those obtained for the heated flint samples from Taibeh, Jordan (see Table 6.9 and Chapter 5).

6.4.5 Age estimation

Based on the D_e and $\dot{D}$ obtained for the two remaining heated flint samples, an age was estimated. For both samples, the SAR and the MAAD protocol provided consistent age estimation (see Table 6.9). Despite the fact that the two age estimations are consistent with each other, they are both much younger than the expected age for artefacts coming from a Early Ahmarian occupation layer.

Sample	**Protocol**	D_e **(Gy)**	$\dot{\mathbf{D}}$ **(Gy/ka)**	**Age (ka)**
ANS F10	MAAD	45.14 ± 2.9	2.51 ± 0.39	18.02 ± 3.02
	SAR	44.82 ± 0.46	2.51 ± 0.39	17.89 ± 2.78
ANS F12	MAAD	29.23 ± 7.82	1.80 ± 0.23	16.23 ± 4.83
	SAR	34.29 ± 5.05	1.60 ± 0.22	21.38 ± 4.32

TABLE 6.9: **D_e, $\dot{D}$ and age estimation for the two heated flint samples (ANS F10 and F12) from Al-Ansab 1 showing a archaeological reset.** The D_e were estimated with a SAR protocol on 12 aliquots and a MAAD protocol on 24 aliquots (12 for the Q estimation and 12 for the I estimation). In both case, a DP and a GC approaches are used. The DP results are used to define the temperature integration interval when the GC results are used for the age estimation (Strebler et al., 2017).

6.5 Discussion

When the age estimation obtained for the sediment samples are fully consistent with the existing age estimation, i.e. the sediment OSL age from Klasen et al. (2013) and the radiocarbon ages from (Richter et al., 2020), the age estimations for the heated flint samples are much younger (see table 6.9 and Fig. 6.8). Such young ages are definitively not consistent with the archaeological background. It is very unlikely that the two heated flint samples that were dated do not belong to the archaeological layers where there were found. Therefore their age estimations should probably be dismissed.

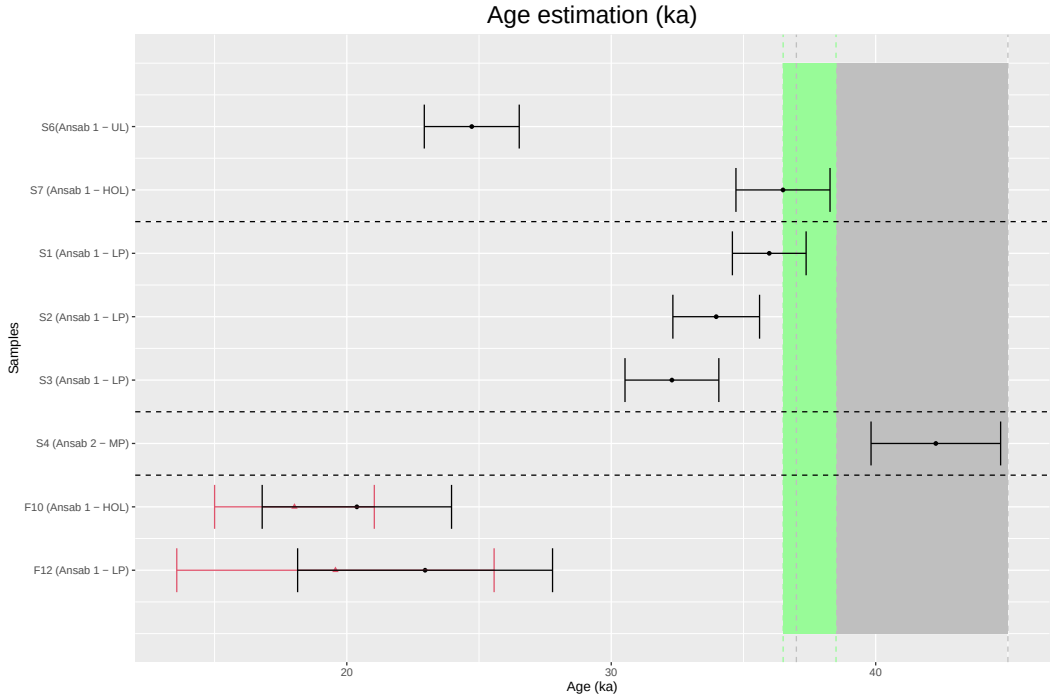


FIGURE 6.8: **Age estimation for the sediment and heated flint samples from Al-Ansab.** The green box indicates the time range of the radiocarbon age estimations for Al-Ansab 1 (Richter et al., 2020) when the grey box (and the grey doted lines) indicates the time span of the Ahmarian techno-cultural unit (Goring-Morris and Belfer-Cohen, 2018).

It has to be noted that despite a relatively low internal radionuclide concentration in the two heated flint samples (ANS F10 and F12), all concentrations remain systematically higher than those obtained for the heated flint samples from Taibeh, Jordan (see Chapter 5). An hypothesis that could easily explain the excessively young age estimations is an overestimation of the $\dot{D}$, especially the internal dose rate that represents up to 78% of the total $\dot{D}$ (see Table 6.10). The presence of an undetected hot-spot in the core material that was used for the radionuclide concentration could be the origin of such overestimation.

Section	Sample	Protocol	$\dot{D}_{flint}$ (Gy)	$\dot{D}$ (Gy)	$\dot{D}_{flint}$ (%)
Layer 2	ANS F10	MAAD	1.95 ± 0.39	2.51 ± 0.39	78%
		SAR	1.65 ± 0.39	2.2 ± 0.39	75%
Lower profile	ANS F12	MAAD	1.22 ± 0.23	1.8 ± 0.23	68%
		SAR	1.03 ± 0.22	1.6 ± 0.22	64%

TABLE 6.10: **Internal and external $\dot{D}$ components of the Ansab heated flint samples.**

A slight modification of the preparation protocol could have reduced the impact of a potential hot spot and increased the quantity of material available for elemental analysis. Rather than cutting the flint core in two before the crushing, the core material dedicated

to the elemental analysis could have been collected from the finer grain fraction ($< 68\mu m$) before the wet settling was performed. On one hand, this modified protocol reduces the material lost due to the extra cutting. On the other hand, it allows to more precisely defined the quantity of fine grains collected for the elemental analysis. We recommend to collect up to 400 μg (twice the amount needed for a single ICP-MS measurement) when possible. It allows for a second elemental analysis when needed. The crushing and mixing of all the finer grain's fraction using a mortar and a pestle will also reduce the influence of a localised hotspot on the radionuclide concentration values.

Another hypothesis to explain the underestimation of the heated flint age estimations is an underestimation of the D_e. The D_e estimations for both heated flint samples are similar to, or slightly lower than, those from the sediment samples (see Fig. 6.9). When the radionuclide concentrations in the flint matrix is lower than those of the surrounding sediments, the α and β components usually have a higher influence on the final $\dot{D}$ in heated flint than sediment samples. In the case of the Al-Ansab samples, the flint $\dot{D}$ estimations are systematically higher than the sediment $\dot{D}$ estimations. A higher D_e estimations is therefore expected for the heated flint than the sediment samples. The SAR and the MAAD protocol produce consistent results, independently of the approach (DP or GC) used. A heat sensitisation effect is therefore quite unlikely. For both heated flint samples, the luminescence signals are especially weak. The uncertainty on the

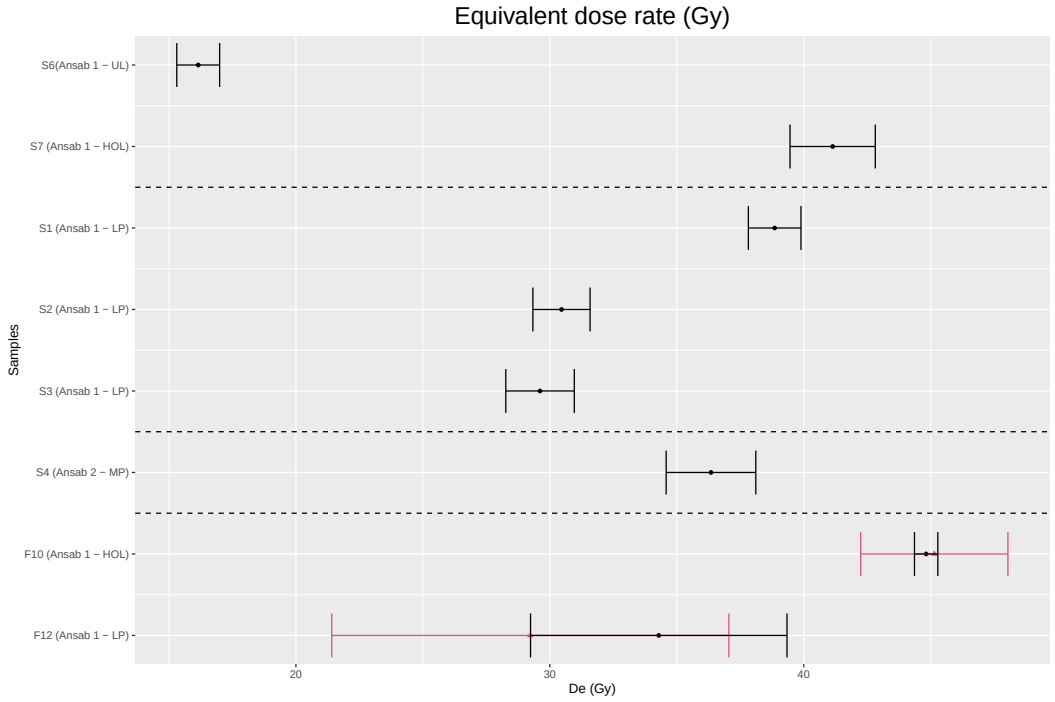


FIGURE 6.9: **D_e Estimations for the sediment and heated flint samples from Al-Ansab 1 and 2.** The D_e values estimated using the SAR protocol are in black while those estimated using the MAAD protocol are in red.

luminescence data were therefore significant. For all the aliquots, the growth curves obtained using the SAR protocol indicates that the natural doses remain in the linear region.

In conclusion, an overestimation of the internal $\dot{D}$, that represents up to 78% of the total $\dot{D}$, is the most probable explanation of the underestimation of the heated flint sample's ages. This $\dot{D}_{int}$ overestimation may have been combine to a slight underestimation of the D_e due to the weak natural luminescence signal. Therefore, the age estimation obtained for the heated flint samples are definitively minimum ages. Regardless on the hypothesis (underestimation of the D_e or overestimation of the $\dot{D}$), the age estimations for both flint samples are consistent which may indicate that they both suffer from a shared systematic shift.

The visualisation and comparison of the luminescence signals produced by the natural, additive and regenerative doses, here using the *TLdating* package, is important to assess the quality of the data that are used for the D_e and the *a-value* estimation. The use of two different protocols (SAR and MAAD) and two different approach (DP and CG) help to increase our confidence on the final results. Numerical analysing tools can help when working with data suffering from a high signal to noise ratio but the results need to be treated carefully. The results obtained for the Al-Ansab heated flint samples enlighten the importance of using multiple dating methods.

Chapter 7

Roman traces in Germania Magna: New thermoluminescence and pIRIR$_{290}$ data from a lime kiln at Bergisch Gladbach, Germany

Anja Zander[1,2], *David Strebler*[2], *Helmut Brückner*[2], *Erich Classen*[3] and *Janet Rethemeyer*[4]

Notes: The content of this chapter has been published in *Archaeometry* **61**, 2 (2019), pp. 506-518. DOI: 10.1111/arcm.12435 (Zander et al., 2019). This article was mostly written by the main author. The second author provided support for the data processing using the *TLdating* **R** package and the writing of sections 7.2 and 7.3. The remaining co-authors provided valuable input including, but not limited to, archaeological background, radiocarbon age estimations, comments, formatting and proofreading. Formatting changes were made to adopt the format of this Thesis.

Keywords: *Luminescence dating, Thermoluminescence, pIRIR$_{290}$, Polymineral, Fine grain, Roman lime kiln, Germania Magna.*

Highlights: *A Roman lime kiln and surrounding sediments were successfully dated using both TL and pIRIR.*

[1]Corresponding author: anja.zander@uni-koeln.de
[2]Institute of Geography, University of Cologne, Germany
[3]LVR-State Service for Archaeological Heritage, Overath, Germany
[4]Institute of Geology and Mineralogy, University of Cologne, Germany

Abstract

The applicability of a post-infrared infrared stimulated luminescence ($pIRIR_{290}$) protocol and two different thermoluminescence (TL) protocols—a single aliquot regeneration (SAR) and a multiple aliquot additive dose (MAAD)—was tested on six polymineral fine-grain (4–11μm) samples extracted from the wall remains of a Roman lime kiln and a Roman roof tile. These remains had been excavated close to Bergisch Gladbach, which was at that time part of Germania magna. For the $pIRIR_{290}$ measurements, no dependence of D_e on first-stimulation temperature was detectable, and the standard first stimulation temperature at 50°C was adopted. Fading tests and dose-recovery tests were made for all samples. Background subtracted glow curves were recorded up to 480°C for TL after a preheat of 220°C for 120 s. A-values were determined for all TL and pIRIR measurements. The results for all three protocols were fairly consistent, and TL and $pIRIR_{290}$ protocols are shown to be suitable to estimate reliable equivalent doses for the fired kiln walls. The resulting ages are in agreement with the expected time range—Roman Iron Age—and with independent age control provided by radiocarbon ages of animal bones and charcoal from the firing chamber.

7.1 Introduction

Roof tile remains found in a forest near Bergisch Gladbach (see Fig. 7.1) were identified as typical tegula tiles (Dasbach and Selbach 2015), which were used during the Roman Iron Age. Subsequent excavations revealed an underlying sequence of four lime kilns designed in a typical Roman style. Four 13 m long east-west oriented double pits were detected on a western slope of a little hill in the Paffrather Mulde. The bedrock consists of silty weathered loam, covering Devonian compact limestone and dolomite. The whole kiln structure was dug into the weathered bedrock material, while only the feed hole wall was masoned. The rest of the kiln structure of about 5 m diameter consists of fritted and sintered loam (Classen et al., 2016).

It is not completely understood how these kilns were operated. However, a succession of charcoal- and burnt limestone layers at the base of the kiln indicates that they were reused several times. From Roman to modern times, burnt lime was required for mortar production and used to whitewash walls and buildings. The necessary temperature to transfer natural limestone ($CaCO_3$) into burnt lime ($CaO + CO_2$) ranges between 900°C and 1200°C. This temperature was kept for a long period of time, probably several days. A thorough signal reset in the kiln walls and the surrounding sediments is hence most likely; thus, this study dates the last heating, i.e., the last use, of the

kiln. Thermoluminescence (TL) dating is usually the first choice when heated objects are unearthed in an archaeological excavation. This technique was initially developed in the early sixties (Aitken et al., 1964, Tite and Waine, 1962) as a dating tool for archaeological artefacts, like pottery and ceramics (Fleming, 1973a, Zimmerman, 1971b). An object has to be initially heated up to, at least, $500°C$ during its fabrication process to be dated by TL. This temperature treatment resets any inherited luminescence signal, like the geological signal, and allows for a new luminescence signal to grow, which is proportional to the time elapsed since the last annealing. TL dating was later successfully applied on heated lithic artefacts (Richter et al., 2017b, Schmidt et al., 2015b), architectural ceramics which included bricks and tiles (Goedicke et al., 1981, Martini and Sibilia, 2001) as well as heated sediments (Fu et al., 2010). The use of luminescence dating on architectural ceramics highlighted the importance of the reusing of material, a phenomenon which had already been well known but underestimated (Blain et al., 2010, Chruscinska et al., 2014, Guibert et al., 2009, Vieillevigne et al., 2007). This problem of relocation does not occur with luminescence dating of ancient kilns, where the last firing of the construction is dated. Kondopoulou et al. (2015) and Tema et al. (2013) applied a combination of archaeomagnetic studies and TL dating on kilns for pottery and brick fabrication in Greece and Italy; they got a good agreement for the two techniques.

An increasing number of optically stimulated luminescence (OSL) studies on heated materials was presented within the last years (Bailiff, 2008, Bailiff et al., 2010, 2013, Brass and Schwenniger, 2013, Hood and Schwenninger, 2015,). Hanebuth et al. (2013) used OSL from fine grain quartz to determine the age of salt production kilns in Bangladesh. They reported a good agreement with radiocarbon dating from mangroves and ashes. The first successful attempt with a post IRIR290 protocol was made by al Khasawneh et al. (2015) on coarse grain feldspars extracted from ceramics and heated stones from Denmark.

This paper presents here a dating study using multiple aliquot additive dose (MAAD) and a single aliquot regeneration (SAR) TL protocols as well as a $pIRIR_{290}$ protocol on polymineral fine grain (4-11 mm) samples, extracted from the remains of a Roman lime kiln.

7.1.1 Sample and independent age control

Six samples were analysed from the kiln, the attached silty sediments and a roof tile found close by. BGB 1, 2 and 3 were extracted from the platy reddish oxidised 30 cm thick fritted contact area between the packing chamber and the environmental loam (see Fig. 7.1). Hard-baked brick-like chunks were gathered in black plastic bags and



FIGURE 7.1: **Cut through the lime kiln dug into the soft weathered Devonian base rock without any further mansoning.** Three samples were taken from the fritted contact area (open circles), two from the soft sediment (filled circles) which was oxidised and fritted by temperature influence, and one typical Roman roof tile (open square). Dose rate samples were also taken from the greyish lime remains from inside the kiln, exposed in the front centre of the picture.

the outer light exposed surface of the chunks was later removed by means of a diamond saw in the dark lab under subdued red light. Samples BGB 4 and 5 were taken with steel cylinders from the reddish brown sediment beyond the fritted contact area. The fragment of the Roman roof tile (BGB 6) was found about 8 cm below the modern surface and was analysed to compare with the heated sediment samples.

Radiocarbon dating was applied on charcoal and animal bones, extracted from different layers from inside and around the kiln (Classen et al., 2016). Results range between 54-125 AD for charcoal from the base of the firing chamber, 175-390 AD for fragments of a horse skull found in front of the kiln mouth, and 997-1158 AD for charcoal from the upper backfilling of the firing chamber. Fragments of a ceramic bowl found in the same layer are attributed to Paffrather pottery, which is dated to the 11th- 13th centuries, indicating a long-time activity in the Lerbacher Forest.

7.1.2 Sample preparation and measuring equipment

Sample preparation was carried out in the Cologne luminescence lab (CLL) under subdued red light for the fine grain technique (Zimmerman, 1971a). Samples BGB 1, 2, 3

and 6 (hard-fired kiln walls and roof tile) were cut with a water cooled diamond saw, making sure that all bleached surfaces were removed. They were sampled with a slow turning cordless electric screwdriver (Stoneham, 1991); then the drill dust was collected and treated with 10% hydrochloric acid, $0,01N$ sodium oxalate and 10% hydrogen peroxide to remove carbonates, organic material and aggregates. After settling and extraction of the $4-11\mu m$ fraction in acetone the polymineral fine grain material was pipetted from a suspension of demineralised water ($1.0mg/ml$) on steel discs. Sample preparation of BGB 4 and BGB 5 (soft loam) was conducted as described in Frechen et al. (1996), using water for settling.

An automated TL-DA 15 Risø Reader with a calibrated 90Sr/90Y beta source delivering $7.284Gy/min$ was used for luminescence measurements and a blue filterpack (4 mm Schott BG39 + 2 mm Corning 7-59) to detect TL signals. For all TL measurements, the OSL unit was detached from the Risø reader to increase the signal yield by reducing the distance between sample and photomultiplier (PM). All OSL measurements were made on the same reader using IR diodes centred at about 870 nm FWHM 40 for stimulation and a LOT D410/30x interference filter for signal detection. All measurements were made on polymineral fine grains. Optical bleaching for dose recovery test was carried out with a SOL2 solar simulator for 24 hrs.

7.2 Material and methods

7.2.1 Application of the TL-MAAD protocol

Six aliquots per samples (see Fig. 7.2a) were measured for the multiple aliquot additive dose (MAAD) protocol. The process included heating to $480°C@5°C/s$ after a preheat of $120s@220°C$ to extract the stable high temperature TL peaks (Aitken, 1985a). The signals of two natural and two dose steps with two aliquots each were recorded (see Fig. 7.2a1), followed by a second TL measurement to determine the background signal for subtraction. After a hot bleach ($480°@5°C/s$, no preheat) and a uniform test dose of $\sim 20Gy$, the resulting TL and background signals of all discs were measured after a preheat of $120s@220°C$ for normalisation. For detailed information about the protocol, see F.1.

An equivalent dose (D_e) plateau (see Fig. 7.2a2) was defined to determine the appropriate integral, and a linear function was fitted for D_e determination. The corresponding supra-linearity test was made on 6 discs each after a hot bleach ($480°C@5°C/s$). Small beta doses of max. $6.7Gy$ were applied to generate the second glow TL dose response curve (see Fig. 7.2a3).

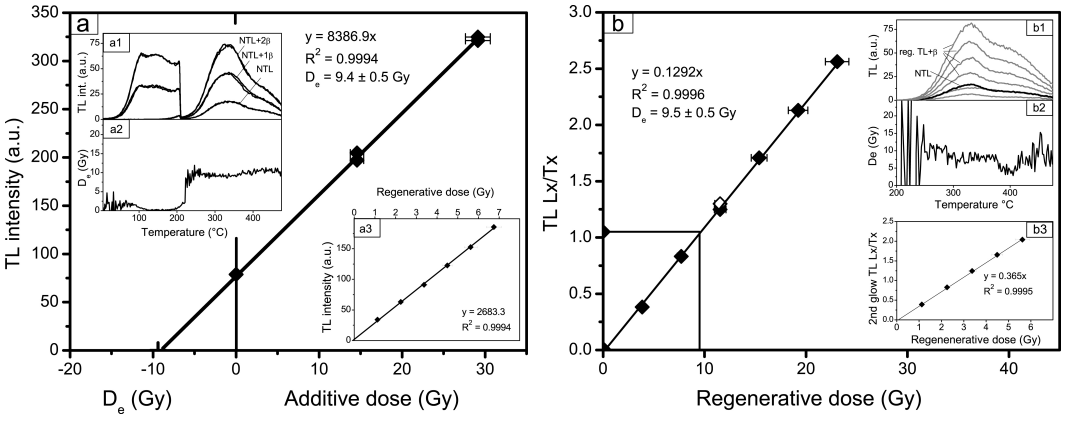


FIGURE 7.2: **Typical dose response curve of a polymineral fine grain sample (BGB 3) measured with the multiple aliquot additive dose (MAAD) TL protocol (a) and a single aliquot regeneration dose (SAR) TL protocol (b).** The insets show glow curves after background subtraction (a1 and b1), the associated De plateau (a2 and b2) and the corresponding 2nd glow TL dose response curve after applying low doses to check for supra-linearity (a3 and b3).

Routine tests for anomalous fading (fle, 1979, Wintle, 1973) were made for all 6 samples, though we do not expect any volcanic input in these sediments. After depleting the natural signal by a TL measurement, four discs received a laboratory dose of $\sim 25Gy$ and were stored at room temperature in a lightproof container. After 64 days, a second set of samples was irradiated with the same activity-corrected beta dose, and the TL of both sets was measured after a preheat ($120s@220°C$) simultaneously to compensate for potential sensitivity changes of the photomultiplier. After background subtraction and a second glow normalisation, the $300 - 400°C$ integral of both data sets was compared and the quotient taken as an indicator for signal loss.

7.2.2 Application of the TL-SAR protocol

TL measurements with a single aliquot regeneration (SAR) protocol (see Table F.2) were made on 12 discs per sample using the modified protocol with five dose steps described by Bluszcz and Bøtter-Jensen (1995) and using the **R** package called *TLdating* (Strebler et al., 2017) for peak alignment and D_e determination (see Fig. 7.2b). The appropriate integral was determined by means of the maximum peak range and a D_e plateau test (see Fig. 7.2b1 and 7.2b2), and the growth curve approach was used for final D_e determination. A linear function was fitted to determine the D_e. The regenerative dose interval was defined between the 1st and the 5th dose points (between 40 and 200 s) to avoid any potential nonlinear part of the growth curve. A linearity correction is not implemented in the programme, but was made separately on three discs of each sample using 5 small regenerative doses of max. 5.7 Gy (see Fig. 7.2b3). Rejection criteria for recycling ratio, recuperation rate, maximum palaeodose error and test dose error were

defined to 10%. Dose recovery tests were performed after a hot bleach at 480°C and 1 month delay between signal depletion and irradiation.

7.2.3 Application of the pIRIR$_{290}$ and IR$_{50}$ protocols

With regard to the promising approach presented by al Khasawneh et al. (2015), we also applied a $post-IR-IRSL_{290}$ ($pIRIR_{290}$) protocol (Buylaert et al., 2012, 2009, Thiel et al., 2011) for D_e determination. After a preheat of 60s@320°C and a first IR measurement for 200s@50°C, a post-IR stimulation for 200s@290°C and a hot IR bleach for 40s@320°C followed (see Table F.2). Twelve aliquots per sample were measured (see Fig. 7.3).

Given that the initial reset of the luminescence signal occurred by heat, dose recovery tests were made on bleached (Sol 2 for 24 hrs) and on thermally reset (5°C/s to 480°C) samples, using 4 and 5 discs each. A first IR stimulation temperature test was performed for all samples to check for temperature dependence of the D_e (see Fig. 7.3b). Four sets of four aliquots were measured with the preheat temperature and the pIRIR stimulation temperature fixed at 320°C and 290°C, respectively. The temperature of the first IR stimulation varied, starting at 50°C with, an increase of 50°C for each set.

Acceptance criteria for D_e determination were defined as for TL-SAR, i.e. 10% for recycling ratios, recuperation and test dose uncertainties. A standard IR_{50} SAR protocol (200s@50°C) combined with a preheat plateau test was applied to samples BGB 4 and BGB 5. Four sets of 4 discs were measured using preheat temperatures between 210°C and 270°C for 10s and an IR shine down for 200s at 50°C. The D_e was then determined by averaging the individual $D_e s$ from the stable temperature range.

Fading tests for IR_{50} and $pIRIR_{290}$ were conducted according to Auclair et al. (2003). The natural signal of five discs each was reset by a hot bleach (100sIR@320°C) and the discs subsequently irradiated to $\sim$ 20Gy. Storage times after irradiation ranged between 50 min and 27 hrs. The fading correction for the IR_{50} ages was made according to Huntley and Lamothe (2001) with the R-package software (Kreutzer, 2017, Kreutzer et al., 2012).

7.2.4 Determination of dose rate

Dose rate (D_0) measurements were made on an Ortec Profile M-Series GEM Coaxial P-type high-precision Germanium Gamma-Ray detector in the Cologne luminescence Lab (CLL). Samples were dried at 50°C, crushed in a jaw breaker where necessary, homogenised and stored in sealed 200g PP capsules for 4 weeks to compensate for radon

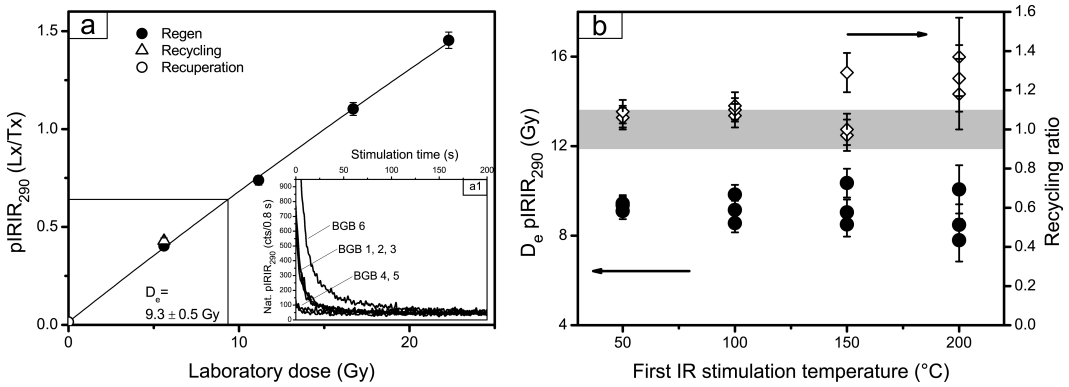


FIGURE 7.3: **Typical $pIRIR_290$ growth curve of sample BGB 1, natural $pIRIR_{290}$ signal intensity of all six samples (a1) and a check for temperature dependence of De and recycling ratio (b).** Recycling ratios match the 10% acceptance criterion at least for the lower temperature range.

loss induced by sample preparation. The internal dose rate of the roof tile was calculated from an element analysis, carried out at the VKTA Rossendorf by means of gamma-ray spectrometry.

Up to three gamma dose rate samples were measured per luminescence sample to account for differences in water content and radioactive element concentration between the silty sediment, the fritted kiln wall and the remains of the limestone filling of the kiln. These variations in gamma dose rate were calculated according to (Aitken, 1985a)Appendix H, using the multi-layer gamma spreadsheet of Ian Bailiff, Durham University (pers. comm.). DRAC v1.2 (Durcan et al., 2015) was used to calculate internal and external alpha and beta dose rates, and to correct them for water content. Conversion factors for gamma and beta dose rates are based on Guerin et al. (2011). Alpha and beta grain size attenuation factors of Brennan et al. (1991) and Guerin et al. (2012), respectively, were applied. The effective water contents (in relation to dry mass) given in Table F.3 represent the measured moisture content of the samples and the averaged values used for age calculation.

Alpha efficiency values, necessary to correct the alpha contribution to the annual dose rate, were determined for each sample by comparing the artificial signals induced by a calibrated ^{2}41Am alpha source (Lexsyg research TL/OSL reader, Freiberg Instruments) and a 90Sr beta source (Risø TL DA 15) for TL, $pIRIR_{290}$ and IR_{50} measurements. A set of 5 discs per sample received a 78.8 Gy alpha dose after a hot bleach ($5°C/s$@$480°C$ or $100sIR$@$320°C$) and were stored for 24 h, before the accumulated alpha dose was determined by the standard dating protocol as used for TL, $pIRIR_{290}$ and IR_{50}.

7.3 Results and discussion

Table 7.1 shows the results obtained for all six polymineral fine grain samples. All ages and dose rates were calculated with the DRAC v1.2 (Durcan et al., 2015) software.

7.3.1 TL-MAAD

All samples reveal a stable D_e plateau between $280°C$ and at least $360°C$ (see Fig. 7.2a2) and no significant supra-linearity of the growth curve in the low-dose region (see Fig. 7.2a3 and Table 7.1). The values are close to zero and a linearity correction was therefore omitted. D_es from the kiln range between $9.4 \pm 0.5Gy$ for BGB 3, and $10.7 \pm 0.7Gy$ for BGB 2. The lowest D_e value was obtained for the roof tile, giving $8.0 \pm 0.5Gy$. The results obtained for the fading tests are congruent within the 1 sigma error, indicating no systematic signal loss within 2 months of storing at room temperature. A-values range between 0.09 and 0.10, and the resulting ages range from $1860 \pm 170a$ to $2530 \pm 230a$ for the kiln and the surrounding sediments, and $1700 \pm 157a$ for the roof tile. Within the margin of errors, four of five kiln samples cover the same age range, confirming a Roman age for the lime kiln. Sample BGB 5 from the soft sediment gives a slightly higher age, but the result is still close to the Roman period. This sample was taken about 40 cm off the fritted kiln wall, which might have resulted in an insufficient thermal resetting. A slight increase of the D_e plateau beyond $400°C$ seems to confirm this explanation. Deeper traps of poorly fired minerals still contain electrons accumulated during geological times, leading to an increase of the artificial TL signal above the D_e plateau value at higher temperatures (Aitken, 1985a).

The lowest age was determined for the typical Roman roof tile. This sherd was excavated a few metres away from the kiln and about 8 cm below the modern surface between the roots of a tree. Dose rate calculation included the internal dose of the tile, sediment dose rate, specific water content and reduced radiation according to the low depth. However, it is not clear if and when the sherd was last relocated and if the assumed dosimetry context is valid for the time since tile production.

7.3.2 TL-SAR

The TL results were determined with the so called "growth curve approach" included in the *TLdating* **R** package. Dose rates are the same as for TL-MAAD. Compared with the TL-MAAD results, the TL-SAR results (see Table 7.1) show a considerably larger scatter and the D_e plateau range is more variable. They all show a minimum

D_e plateau between 300°C and 350°C (see Fig. 7.2b2), and the equivalent doses range between $9.4 \pm 0.6Gy$ for the roof tile and $16.9 \pm 0.9Gy$ for sample BGB 5. Within the margins of the confidence interval, the resulting ages are in agreement with the MAAD ages, except for sample BGB 5, which overestimates the MAAD date by about 40%. The ages range between 1910 ± 260 a and $2240 \pm 210a$ for the kiln samples, and $1820 \pm 170a$ for the roof tile. BGB 5 yielded an age of $3620 \pm 320a$.

Dose recovery tests match or nearly match the 10% acceptance limit, but they mainly range in the lower part of the range between 0.89 ± 0.03 and 0.94 ± 0.04. Only BGB 5 gives a dose recovery ratio above 1 with a very large confidence interval. The recycling ratios of all samples meet the expected limits, and recuperation is below 1% (see Table F.4). The supra-linearity test revealed negligible values for five of the six samples (see Table 7.1). BGB 5 showed an average value of $0.61 \pm 0.06Gy$, but a correction was also omitted here.

7.3.3 pIRIR$_{290}$ and IR$_{50}$

Figure 3 shows a typical growth curve of sample BGB 1 and the natural $pIRIR_{290}$ of all six samples. The samples taken from the kiln walls show a comparably brighter elevated temperature signal than the samples from the soft sediment. D_e values range between $9.3 \pm 0.5Gy$ for BGB 1 and $9.5 \pm 0.5Gy$ for BGB 2 and 3. Recuperation values are below 5%, and recycling ratios vary between 1.06 and 1.1. First IR stimulation temperature tests (see Fig. 7.3b) did not show any dependence of the D_e on the first IR stimulation temperature between 50°C and 150°C. A-values range between 0.094 and 0.092 for the samples from the kiln walls. The resulting ages range from $1740 \pm 150a$ to 1880 ± 170 a for the last heating of the kiln. Fading is negligible as g-values range between -0.61 ± 1.48 and 0.71 ± 1.43% for the $pIRIR_{290}$ protocol.

The comparably low $pIRIR_{290}$ signal intensity obtained from samples BGB 4 and BGB 5 (see Fig. 7.3a1) prevented a reliable D_e- and a-value determination and produced bad recycling ratios. For young samples with low signal intensities, low temperature pIRIR protocols can deliver satisfactory results, if applied on coarse grain potassium feldspar, as demonstrated by Madsen et al. (2011), Reimann and Tsukamoto (2012) and Riedesel et al. (2018). Our tests with reduced preheat temperatures and reduced IR stimulation temperatures (preheat 160°C, $pIR_{50/130}$ and preheat 180°C, $pIR_{50/150}$) applied on our fine grain samples from BGB 4 and BGB 5 did not improve the signal yield and did not allow to determine a reliable D_e. For the standard IR_{50} SAR protocol (see Table F.2), the signal yield was sufficient, recycling ratios were close to unity and dose recovery tests were within 10%. Preheat plateau tests with preheat temperatures between 210°C

and $270°C$ have shown that the IR_{50} D_e is not dependent on the preheat temperature, but that a preheat of $270°C$ for 10 s already reduces the signal intensity significantly and leads to a large D_e scatter (see Fig. 7.4). D_es of $7.4 \pm 0.5Gy$ and $8.1 \pm 0.4Gy$, and dose rates of $4.7 \pm 0.3Gy/ka$ for both samples resulted in IR_{50} ages of $1680 \pm 150a$ and $1810 \pm 160a$, respectively. However, fading tests have shown a significant signal loss within 27 hours and resulted in g-values of $2.58 \pm 0.83\%$ and $3.65 \pm 1.05\%$ (see Table F.4). After a fading correction (Huntley and Lamothe, 2001) using the luminescence R package (Kreutzer et al., 2021), the IR_{50} ages are in perfect agreement with the TL results.

With regard to the initial thermal resetting of the natural luminescence signal in the kiln walls, dose recovery tests were made by thermal and optical reset prior to administering the given dose (see Fig. F.1). al Khasawneh et al. (2015) demonstrated valid dose recovery tests for both optical and thermal resetting methods applied to ceramics and heated stones from Denmark. In our study, we obtained a mean measured to given dose ratio of 0.97 ± 0.04 for the samples from the kiln, if the reset occurred thermally, demonstrating that the $pIRIR_{290}$ protocol can measure a known laboratory dose, if the natural signal is reset by a temperature treatment comparable to the initial signal reset. On the contrary, an optical signal reset in a Solar simulator for 24 hrs always resulted in significant underestimations of $\sim 20\%$. For sample BGB 6, none of the two tests was successful. Dose recovery ratios of 0.83 ± 0.03 and 0.76 ± 0.02 were obtained for the thermal and the optical signal reset, demonstrating that it was not possible to recover an artificial laboratory dose with the $pIRIR_{290}$ protocol, a D_e was hence not determined. For the IR_{50} protocol applied on BGB 4 and BGB 5, the method of signal reset had no influence on the dose recovery ratio. They were all within the same range.

7.4 Conclusions

TL ages and $pIRIR_{290}$ ages obtained from the walls of the Roman lime kiln at Bergisch Gladbach are fairly concordant. They are in good agreement with the archaeological age control and with radiocarbon ages of charcoal from the burning chamber, covering the time of the Roman occupation period in the Rhineland (see Fig. 7.5 and Table F.5). Samples BGB 4 and BGB 5 from the weathered loam surrounding the kiln remains were taken to examine, how far the temperature had penetrated the sediments during the firing process.

They both failed to match the standard quality criteria like recycling ratio and dose recovery tests for the $pIRIR_{290}$ approach. Low signal intensities for low ($pIRIR_{130}$ and

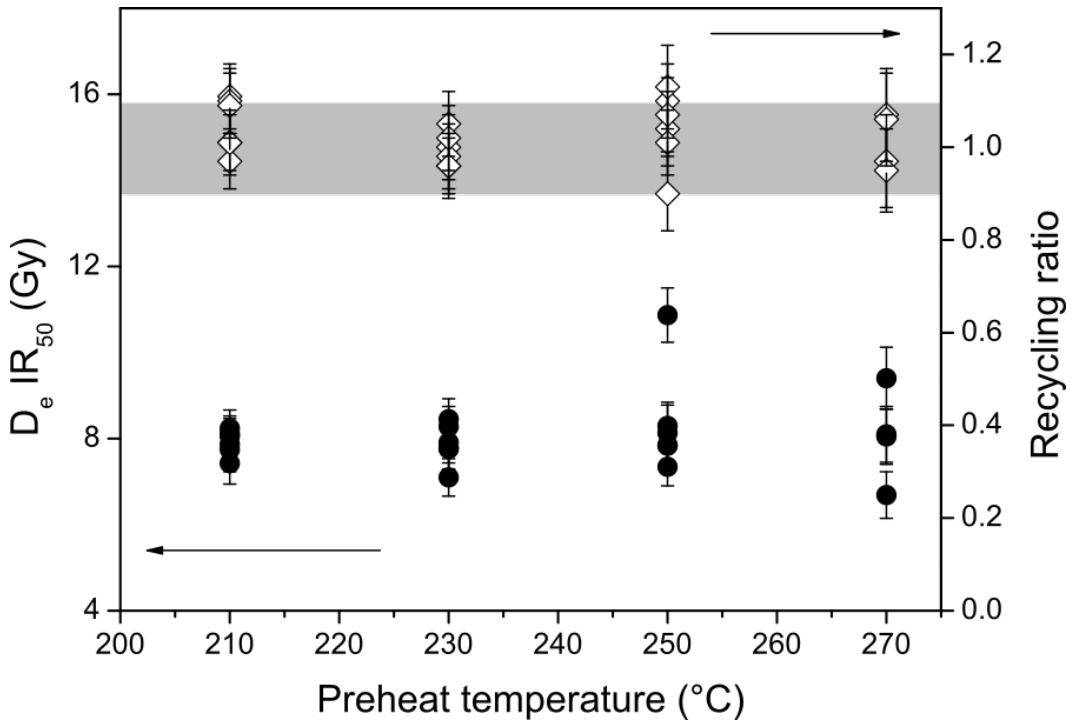


FIGURE 7.4: **Preheat plateau test for sample BGB 5 from the soft sediment surrounding the kiln structure using a standard SAR $IRSL_{50}$ protocol with a 60 s preheat and a 200 s IR stimulation.** The D_e shows no dependence on the preheat temperature, but the scatter increases due to reduced signal intensities. Recycling ratios are within the 10% acceptance range.

pIR_{180}) and high temperature ($pIRIR_{290}$) protocols prevented a reliable De determination. This could be attributed to a lower sensitisation of the feldspar minerals as a consequence of lower thermal affection. However, the thermal impact from the kiln on the surrounding sediments was strong enough to reset the TL signals at least from sample BGB 4, which was taken close to the kiln structure. The results for the TL-MAAD protocol and the TL-SAR protocol are in agreement with the average dating results of the kiln. BGB 5 gives higher ages for both TL approaches and the fading corrected IR_{50} approach, indicating an insufficient signal reset for the sediments about 50 cm beyond the fritted zone of the kiln.

The dating approach on the Roman roof tile fragment with $pIRIR_{290}$ failed due to an insufficient sensitivity change correction, resulting in a mean recycling ratio of 1.14 ± 0.03. The sensitivity correction of the TL-SAR protocol was satisfactory, giving a mean recycling ratio of 1.0. The ages obtained for the roof tile, however, must be considered with caution. The fragment was found about 15 cm below the soil surface some metres away from the trench. A displacement combined with changes of the water content and environmental radiation conditions is hence conceivable. Partial reheating or a temporary use in another context within the archaeological history is also likely.

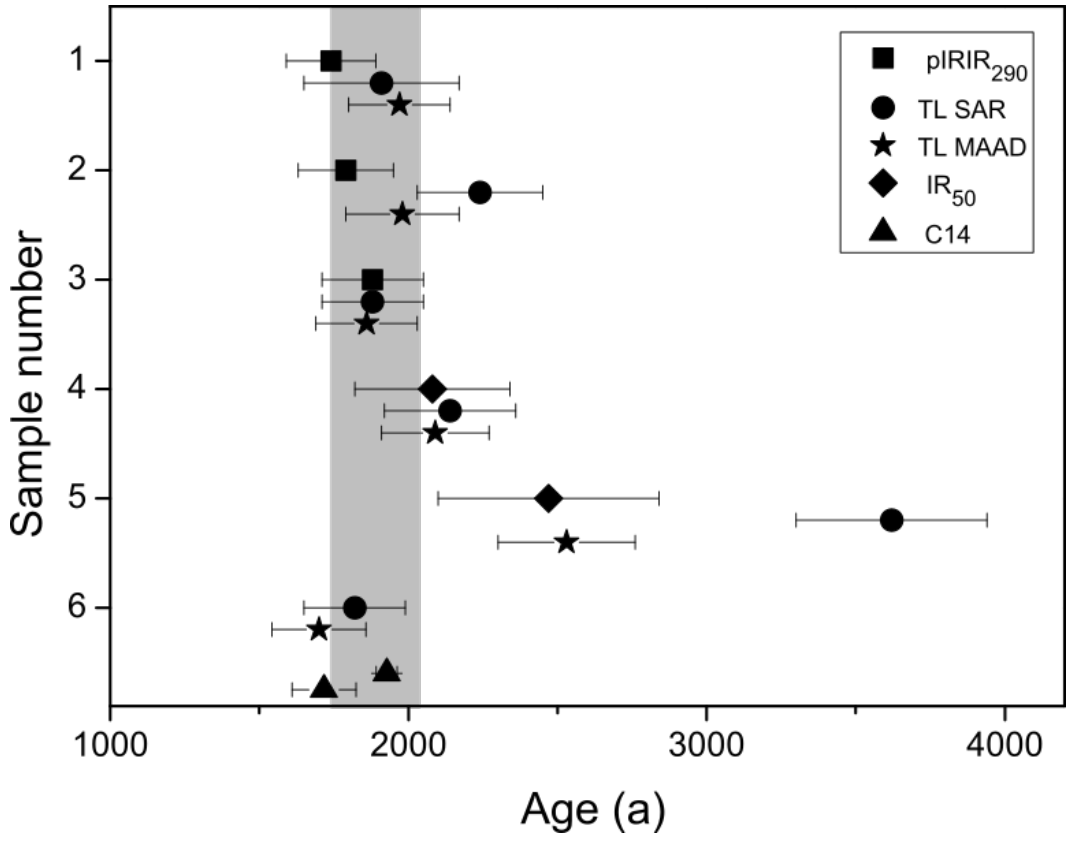


FIGURE 7.5: **Age compilation of OSL and TL results.** Except for sample 5, all age estimates match the expected Roman age range within 1σ confidence interval. They are also in good agreement with two radiocarbon ages (cal. AD, 2σ), obtained for a horse scull which was excavated in a working pit in front of the kiln, and charcoal remains from the kiln area (see Table F.5).

Acknowledgements

We thank Svenja Riedesel (now at Aberystwyth University, UK) for fruitful discussions about dose rate determination within thin layer environments. Prof. Ian Bailiff (Durham University, UK) is thanked for providing the spreadsheet used to correct for layer-to-layer variations in gamma dose rate according to Aitken (1985a). Prof. R. Gerlach is thanked for support in the field. Dating and fieldwork of this project was funded by the LVR-State Service for Archaeological Heritage.

Protocol	**Sample ID**	**Intercept** (Gy)	**D_e-Plateau** ($^\circ C$)	**Dose rate** $\mathbf{D_0}$ (Gy/ka)	**Equivalent dose** $\mathbf{D_e}$ (Gy)	**Age** (a)	**Fading corrected** $\mathbf{IR_{50}}$ **age** (a)
TL-MAAD	BGB 1	0.29 ± 0.04	$280 - 400$	5.3 ± 0.3	10.5 ± 0.5	1970 ± 170	
	BGB 2	0.04 ± 0.31	$280 - 400$	5.4 ± 0.3	10.7 ± 0.7	1980 ± 190	
	BGB 3	0.14 ± 0.08	$280 - 400$	5.0 ± 0.3	9.4 ± 0.5	1860 ± 170	
	BGB 4	-0.25 ± 0.32	$280 - 350$	4.7 ± 0.3	9.9 ± 0.5	2090 ± 180	
	BGB 5	0.61 ± 0.06	$280 - 390$	4.7 ± 0.3	11.8 ± 0.8	2530 ± 230	
	BGB 6	0.03 ± 0.05	$300 - 400$	5.2 ± 0.4	8.8 ± 0.5	1700 ± 160	
TL-SAR	BGB 1	-0.11 ± 0.09	$300 - 380$	5.3 ± 0.3	10.2 ± 1.2	1910 ± 260	
	BGB 2	0.06 ± 0.08	$300 - 380$	5.4 ± 0.3	12.1 ± 0.7	2240 ± 210	
	BGB 3	-0.10 ± 0.05	$290 - 350$	5.0 ± 0.3	9.5 ± 0.6	1880 ± 170	
	BGB 4	-0.05 ± 0.08	$300 - 380$	4.7 ± 0.3	10.2 ± 0.8	2140 ± 220	
	BGB 5	0.25 ± 0.08	$280 - 350$	4.7 ± 0.3	16.9 ± 0.9	3620 ± 320	
	BGB 6	0.03 ± 0.05	$280 - 400$	5.2 ± 0.4	9.4 ± 0.6	1820 ± 170	
$pIRIR_{290}$ &IR_{50}	BGB 1			5.3 ± 0.4	9.3 ± 0.5	1740 ± 150	
	BGB 2			5.3 ± 0.4	9.5 ± 0.5	1790 ± 160	
	BGB 3			5.1 ± 0.4	9.5 ± 0.5	1880 ± 170	
	BGB 4			$^*4.4 \pm 0.3$	$^*7.4 \pm 0.5$	$^*1680 \pm 150$	2080 ± 260
	BGB 5			$^*4.5 \pm 0.3$	$^*8.1 \pm 0.4$	$^*1810 \pm 160$	2470 ± 370
	BGB 6			4.9 ± 0.4	-	-	-

TABLE 7.1: **Compilation of dose rate results and dating results** of polymineral fine grain samples obtained by multiple aliquot additive dose (MAAD) and single aliquot regenerated (SAR) TL protocols and by IRSL. The $pIRIR_{290}$ protocol was used for BGB 1, 2, 3 and the IR_{50} protocol (*) for BGB 4, 5 because the $pIRIR_{290}$ signal intensity was too low for a reliable D_e determination.

Chapter 8

Discussion

This chapter intends to summarise and discuss the main results of the present PhD thesis. It is divided in three sections. The first section is dedicated to the **R** packages developed in the frame of this project and how they respond to the objectives defined in Chapter 1. The second section explores the contribution of this thesis to heated flint dating within a broader perspective. It reviews the new age estimation proposed in the frame of the **CRC 806** but also the new preparation protocol proposed in chapter 6. Finally, the last section goes beyond the dating of heated flint samples and examines the contribution of this project to the TL dating of other archaeological settings.

8.1 From the design of the experiment to the age estimation using R

As we have seen in section 2.5, numerous software solutions are used in luminescence dating. However, when various options exist for the D_e and the age estimation using OSL, there is a lack of solutions specifically dedicated to the D_e estimation using TL.

In this section, we also saw the limitations of stand-alone software solutions which are often the leading choice for manufacturing companies. Those solutions allow to keep the control on the source code while ensuring compatibility with the equipment produced and distributed. However, they often suffer from a lack of flexibility which encourages the development of home-brew alternatives. When companies can usually provide support and some version tracking for the stand-alone software solution that they still distributed, it is rarely the case for home-brew solutions and abandonware. Numerous home-brew software solutions are written as scripts for computing environment like

Matlab or as spreadsheets. They are generally shared between laboratories and updated by multiple people over time, which made the version tracking nearly impossible.

A possible solution to this problem was proposed with the publication of the *Luminescence* package for the **R** free software environment for statistical computing and graphics (Kreutzer et al., 2012). **R** natively embedded version tracking solutions. Moreover the publication and update of a new package requires the respect of a series of good practices. Over time, the *Luminescence* package gathers all the tools needed for the estimation of an age for sediment samples using OSL dating. Nowadays, it is not only a fully functional alternative to stand-alone software solutions like *Analyst* but it also includes tools for the $\dot{D}$ estimation or the treatment of OSL dosimeter measurements. Following this original **R** package, numerous other packages were developed to explore other aspects of luminescence dating. Among those are the *TLdating* and *LumReader* packages.

8.1.1 The *TLdating* package

The *TLdating* package was the first package developed in the frame of this thesis. It was destined to fill the lack of up-to-date solutions dedicated to TL dating when the project started. On one hand, *Analyst* was able to assess equivalent dose for TL measurement using both MAAD of SAR protocols but was lacking the tools needed to do the preprocessing; on the other hand, the *Luminescence* package included a function for the D_e using TL and the SAR protocol but had no function for multi-aliquot protocols. We could have written new functions to add to the *Luminescence* package and addressing the protocols and signal treatment not yet included in the package. However, we quickly realised that some of the treatments that are routinely made on TL curves required to handle the uncertainties slightly differently than what is done with CW-OSL dating. Therefore, we decide to write a independent package whose functions could be implemented in the *Luminescence* package at a later stage if required.

When writing our new package, we tried to keep a number of key features in mind:

- Our package should (re)use the code already existing as much as possible.
- It should include a complete workflow for an age estimation.
- It should be flexible and easy to update.
- It should be user-friendly.

This last feature leads us to include not only the various functions needed to process TL dating data in the package but also a series of scripts combining them and a graphical user interface (GUI) for the users which are not used to software programming.

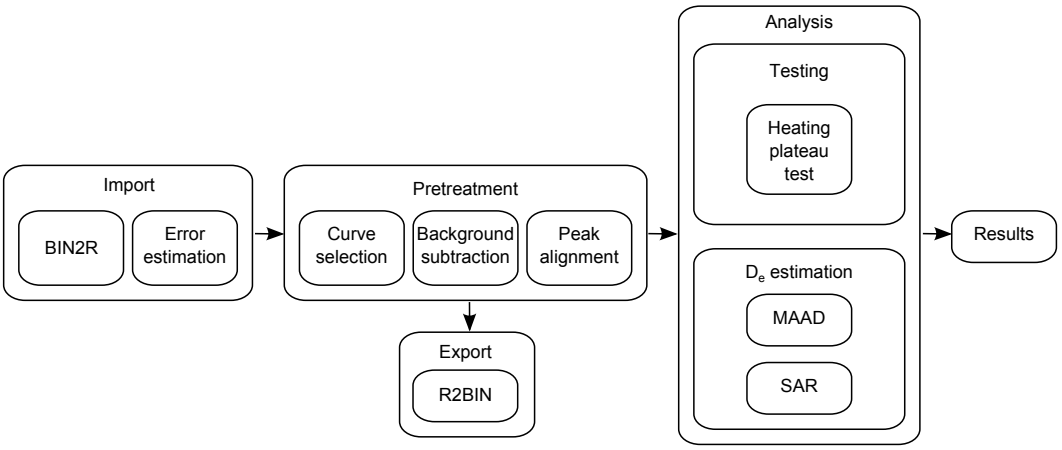


FIGURE 8.1: **Workflow for the D_e estimation using the TLdating package.** First, the luminescence signal data are imported into **R**. Second, the luminescence data are reorganised, modified and combined to allow for their analysis. It is the pretreatment step. Third, the data are analysed either to fulfil the desired test or to estimate an equivalent dose using the MAAD or the SAR protocol (Strebler et al., 2017).

The different functionalities of the package are described in chapters 4 and 5. In its current version the *TLdating* package includes tools to estimate (1) the D_e, (2) the *a-value* and (3) the $\dot{D}$. Those results are then combined to provide (4) an *age* estimate.

D_e (1) and *a-value* (2) estimation are based on the estimation of an equivalent dose using TL and therefore on the same set of functions (see Fig. 8.1): (1) is the *β-dose equivalent* to the natural palaeodose accumulated through time and (2) is the ratio between the *β-dose equivalent* to an artificial α-dose and this same artificial α-dose. The *TLdating* package allows to estimate these *equivalent doses* using either a SAR or a MAAD protocol.

In both cases, two estimations of the *equivalent dose* are provided for each set of aliquots. The first estimation is made using the usual *growth curve* approach (Aitken, 1985a). The second estimation is made using a *dose plateau* approach (Wintle, 1997). While the *growth curve* method provides robust results, the *dose plateau* allows for a better determination of the integration temperature interval. Using a recursive process, the combination of these two approaches improves our confidence on the final D_e estimation.

In the end, both approaches should provide consistent results. An inconsistency between the results could be the consequence of insufficiently heated material or second order kinetics (Grün, 1994). Therefore, it indicates that the materials should probably be discarded or, at least, required further analyses. As for the *growth curve* approach, being the one used for most publications, it is recommended to use its results for the final *age* or *a-value* estimations, for consistency.

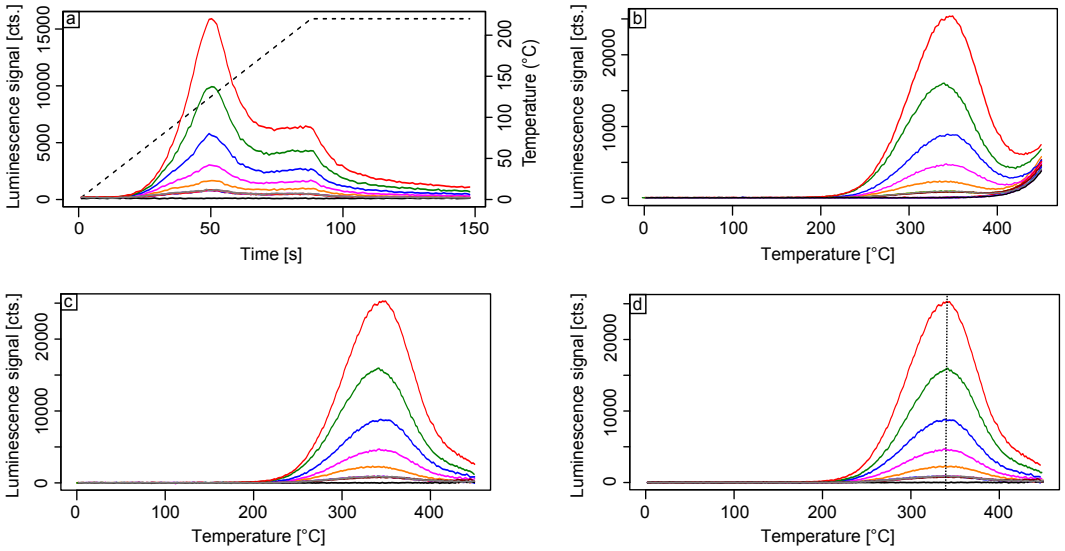


FIGURE 8.2: **Pretreatment of TL signal from a heated flint sample (NS2).** (a) Preheat curves, (b) Luminescence curves (before any modification), (c) background subtraction and (d) peak alignment (Strebler et al., 2017).

One of the main differences between the estimation of an equivalent dose using OSL or TL signals is the pre-processing of the data curves. The *TLdating* package includes three of these TL signal pre-processing procedures: (a) the identification and removal of the preheat curves, (b) the subtraction of the background signal and (c) the alignment of the TL peak maxima (see Fig 8.2).

(a) The recording of TL and OSL signals often requires a preheat, a first heating of the sample at lower temperature that removes the signal unstable in time. When the signal is recorded during this preheat it will always be as a TL curve. When OSL is used to estimate the D_e, such data can easily be identified and discarded. However, in the case of TL dating, they need to be properly identified and isolated from the curves that will be used for the D_e estimation. It has to be noted that some of the TL dating techniques are using these preheat curves for the D_e estimation, it is the case for the *predose technique* which relies on the 110 $°C$ peak (Fleming, 1973a). Currently, the predose technique is not supported by the *TLdating* package. However, the pretreatment functions are designed in a way that also allows to gather the preheat curves rather than discard them. Once again, the package was designed to be as flexible as possible. A function dedicated to the $\dot{D}_e$ estimation using the pre-dose technique can always be implemented when needed.

(b) The background signal of OSL curves is relatively uniform and can be estimated based on the signal remaining at the end of the stimulation. The background signal of the TL curses is temperature dependant. It needs to be recorded independently and properly subtracted from the luminescence signal. Currently, the package considers that

a background curve is recorded for each signal curve. Alternative protocols propose to record the background only once per additive/regenerative cycle, the same background curve being used for the additive/regenerative and the test dose signal. These protocol variants can easily be implemented in future versions of the package when needed.

(c) TL curves often show slight variations in their peak maximum positions. These variations can be measurement artefacts or the sign of an undesirable behaviour of the sample. To provide a reliable and robust age estimation, the peaks need to be properly aligned. It has to be noted that, contrary to the growth curve approach, the dose plateau approach may help to identify the presence of such undesirable behaviours after the peak maximum alignment. The presence of second order kinetics will generate a gradient of the D_e estimation around the peak position rather than a dose plateau as expected for first order kinetics (Grün, 1994).

Two of these signal pretreatments require to combine multiple luminescence curves and therefore impact on the uncertainties associated to the signal data. When it comes to data processing, this is one of the main differences between the estimation of an equivalent dose using TL and OSL dating. The tracking of these uncertainties was the main motivation to develop a new **R** package independent to the existing *Luminescence* package. The *TLdating* package is structured in a way that, if any other pretreatment needs to be done on the luminescence curves, the appropriate functions can easily be added to the package without compromising the operation of existing functions.

Currently, when estimating an equivalent dose using the *TLdating* package only linear fitting is available for the growth curve estimation. When the MAAD protocol is applied, it is recommended that the palaeodose is still in the linear region of the growth curve and not in the saturation region. When the SAR protocol is applied, it is recommended to reduce the number of irradiation steps as much as possible (Richter and Krbetschek, 2006). By choosing the β-dose steps carefully to frame the palaeodose signal, a linear regression is already sufficient to provide a reliable estimation of the *equivalent β-dose*. However, once again, functions allowing to apply other fitting curves, for example *exponential* or *exponential + linear*, can easily be added to the package.

When it comes to estimating the $\dot{D}$ (3), the calculation procedure is similar for TL and OSL dating. Any existing stand-alone software solution for $\dot{D}$ estimation could have been used as long as the adequate setting was selected. However, we desire to provide a solution which does not require the user to navigate between multiple software solutions to calculate an age. When this project started, the *Luminescence* package was only including functions to estimate a $\dot{D}$ for sediment setting using *DRAC* (Durcan et al., 2015).

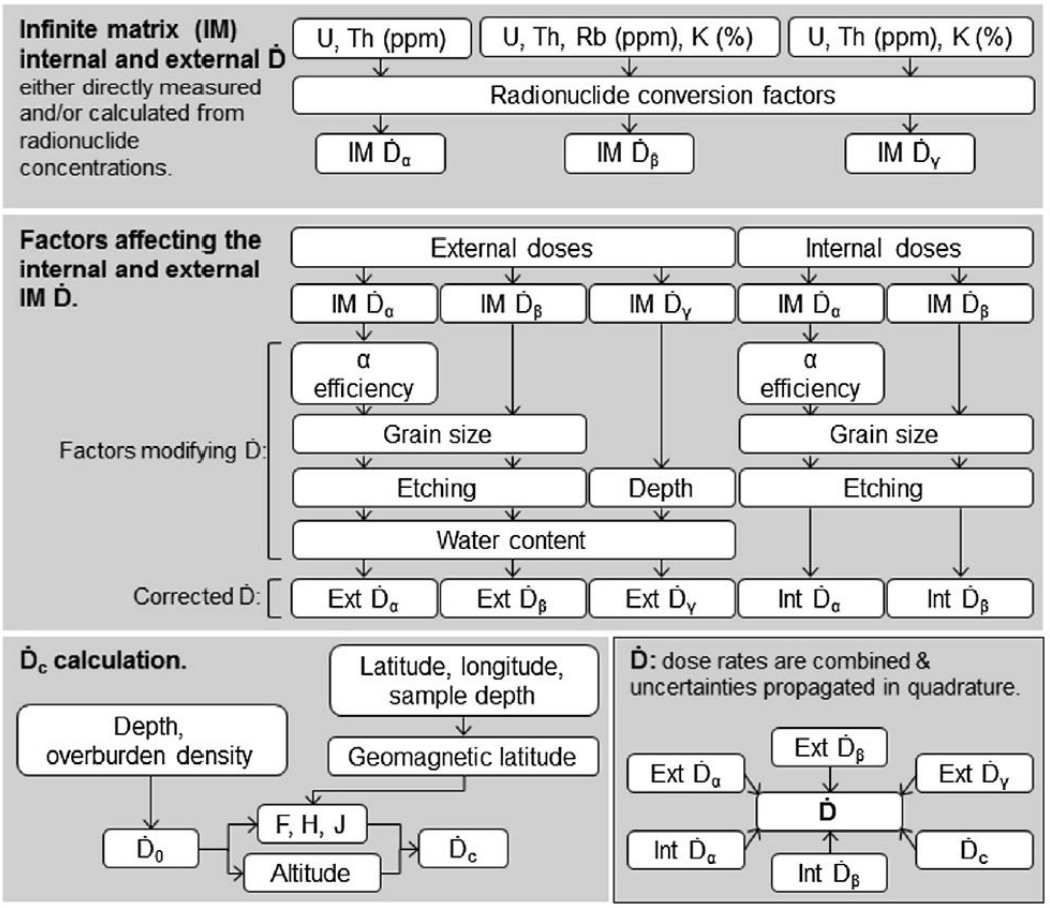


FIGURE 8.3: **Overview of the workflow for the Ḋ calculation using the DRAC software.** (Durcan et al., 2015)

The estimation of the $\dot{D}$ mostly depends on the composition and origin of the sample, i.e. aeolian or cave sediments, heated flint, domestic or architectural ceramics, but also on the size of the grains used for the D_e estimation. The idea was to start with this existing *DRAC function* (see Fig. 8.3) but to use it in a way that allows the estimation of $\dot{D}$ for geometries more complex than the usual homogeneous sediment setting. A new function, relying on the DRAC function from the *Luminescence* package, but allowing to date heated flint and ceramics samples surrounded by a homogeneous sediment matrix, was developed. This function is presented in Chapter 5. The main interest of this approach is that the $\dot{D}$ estimation is made using information similar to that used for sediment dating. A heated flint or ceramic sample provides the dose originating from the grains themselves and from the flint or ceramic matrix surrounding them. The environmental dose is estimated using either a high resolution γ-spectrometry on a sample of the surrounding sediments, or an in-situ measurement using OSL or TL dosimeter (TLD or OSLD) or NaI γ-spectrometry. Finally, the cosmic component of the dose rate is estimated either based on the in-situ measurement or theoretically using the dedicated

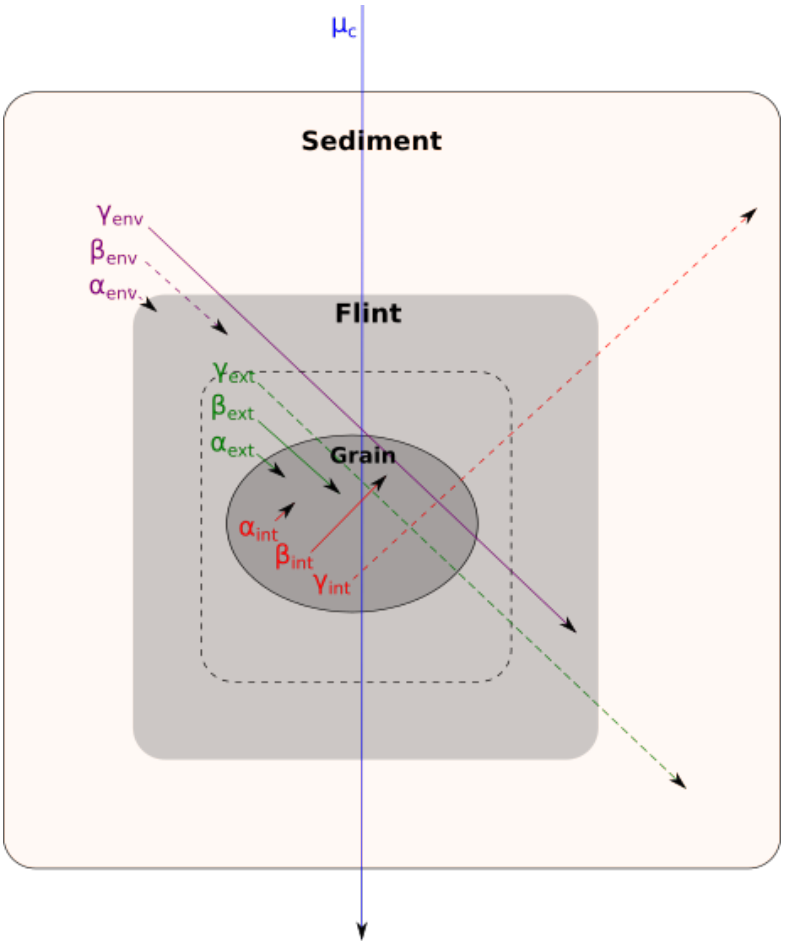


FIGURE 8.4: **Various components of the total $\dot{D}$.** The total $\dot{D}$ can be separated in four origins: (1) The internal $\dot{D}$ ($\dot{D}_{int}$) is coming from the radionuclide elements present inside the grain. It includes α and β radiations. (2) The *external* $\dot{D}$ ($\dot{D}_{ext}$) is coming from the radionuclide elements present inside flint matrix surrounding the grain. It includes α and β radiations. Its γ component is usually neglected, especially when the artefact is relatively small as it the case in this project. (3) The environmental component is coming from the radionuclide elements present in the sediment surrounding the flint sample. Since the external layer of the flint is removed, it is only composed of γ radiations. (4) The cosmic dose rate ($\dot{D}_c$) is due to the cosmic radiation reaching the earth. It is mostly composed of muon (Blain, 2009).

function from the *Luminescence* package (see Fig. 8.4).

When the α-component of the $\dot{D}$ cannot be neglected, like for heated flint sample dating, the a-value has to be estimated. This a-value is not only sample specific but also dependant on the type of luminescence signal which is recorded (OSL or TL) and wavelength dependant, i.e. red and blue TL signals will have slightly different a-values (Schmidt, 2013). As seen earlier, the data processing for the a-value estimation is similar to that for D_e value estimation. Its estimation is made using fine-grained aliquots and requires a calibrated α-source.

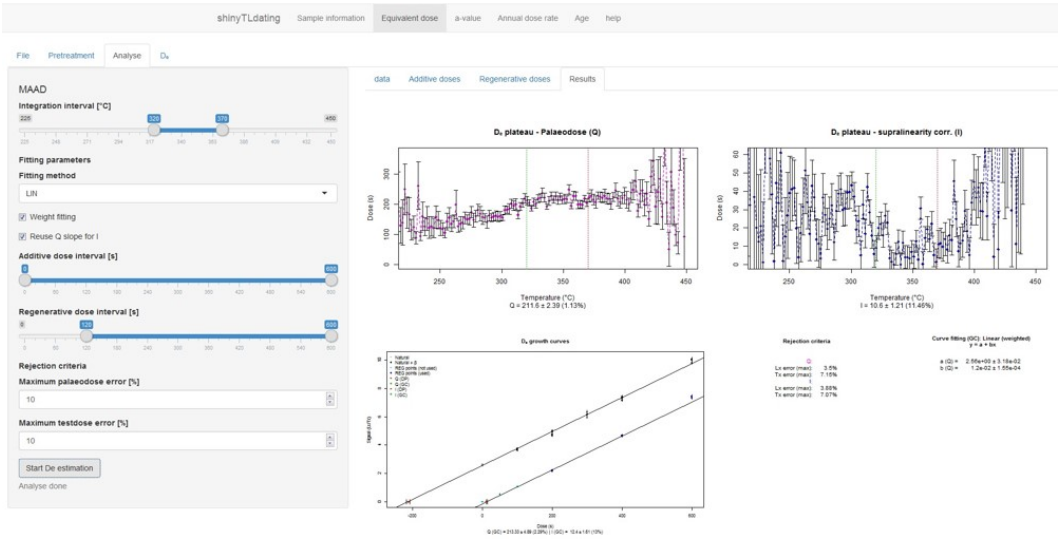


FIGURE 8.5: **The *TLdating* graphical user interface (GUI).** This screenshot shows the third step from the D_e estimation section, here, using the MAAD protocol. This GUI was developed using the *shiny* package.

A non-negligible number of luminescence specialists do not have programming experience. This is often an obstacle to the use of **R** for the processing of luminescence data. All of the functions of the *TLdating* package can be called and combined in a customised **R** script. However, the package also includes a series of scripts already combining the different functions to generate an age. Moreover, some of these all-inclusive scripts are provided with a graphical user interface (GUI). These interfaces were designed to provide to the user a experience similar to the usual stand-alone software solutions. They are composed of a series of tabs, each dedicated to a specific value estimation. The first tab is dedicated to the D_e estimation, the second to the *a-value* estimation, the third to the $\dot{D}$ estimation and, finally, the fourth one provides an *age* estimation based on the previous results (see Fig. 8.5).

As we can see, the *TLdating* package fully meets the first objective set in chapter 1. It is open source and therefore transparent and freely available. It is easy to use through its graphical interface but also to report in the scientific literature using the standard defined by the **R** framework. Finally, it can be easily updated and expansed with new functions, for example to add new data preprocessing, include more fitting curves for the D_e estimation, or adapt the usage of DRAC to other complex geometries, like bricks or cave sediments. Moreover, it is always possible to include a full set of new functions, for example to estimate the D_e using a different technique, like the predose method, or to estimate the $\dot{D}$ using TLD rather than based on the radionuclide element concentration of the samples and their surrounding material.

8.1.2 The *LumReader* package

The *LumReader* package was the second **R** package developed in the frame of this project. Over time, multiple combinations of filters and PMT have been proposed to date heated flint samples. The selection of a specific combination depends on various parameters. Among those is the luminescence signal which is recorded but also the equipment available to the laboratory making the measurement. Heated flint samples can emit a TL signal in the blue (BTL) or the orange-red region (RTL) but also an OSL signal in the UV-Blue region (BSL). The *EMI 9235 QG bialkani* photomultiplier can detect all those signals. When it is present in heated flint samples, the RTL signal should be more stable than the BTL signal and therefore allows the dating of older samples (Richter and Krbetschek, 2006). However the quantum efficiency of this PMT is very low in the orange-red region. RTL signals also suffer from a higher background noise signal due to the black body radiation than BTL signals (see Chapter 2). Depending on the signal that is used, different sets of filters but also detectors are required.

The filters usually used for OSL dating of quartz sediment samples should work perfectly for OSL dating of heated flint samples. Those filters should also allow for the detection of BTL signals as shown in Chapter 3 (see Fig. 8.6). However, a non-negligible part of the signal is then lost. The $\dot{D}$ is often lower in heated flint than in sediment samples. This means that the palaeodose accumulated, even over a long period of time, remains limited. Therefore, the luminescence signal of a heated flint sample can be quite low. It is not uncommon that this luminescence signal remains close to the detection limit. Improving the filter selection increases the signal-to-noise ratio and allows for the measurement of dimmer signals. For RTL dating of heated flint samples, not only the filter selection should be modified, but using a PMT with a better quantum efficiency in the orange-red region is definitively recommended as well.

The question is obviously not limited to the dating of heated flint. For just over a decade, luminescence dating has been undergoing a period of diversification. The luminescence dating properties of new materials is explored, including volcanic quartz (Tsukamoto et al., 2007), gypsum (Aydas et al., 2011, Mahan and Kay, 2012, Nagar et al., 2010), halite (Zhang et al., 2005), apatite (Kitis et al., 2013) or calcium carbonate from different origins (Pagonis et al., 2009, Polikreti et al., 2003, Polymeris et al., 2016, Stirling et al., 2012). OSL dating techniques using wavelengths different than the usual blue (BSL), green (GSL) and infrared (IRSL) are proposed, i.e. yellow stimulated luminescence (YSL) (Lauer et al., 2011, 2012, Lüthgens et al., 2011) and violet stimulated luminescence (VSL) (Ankjaergaard et al., 2016, 2015, 2013, Jain, 2009). All these new applications of luminescence dating requires their own filter combinations, some also required the use of specific PMT to optimise the signal detection.

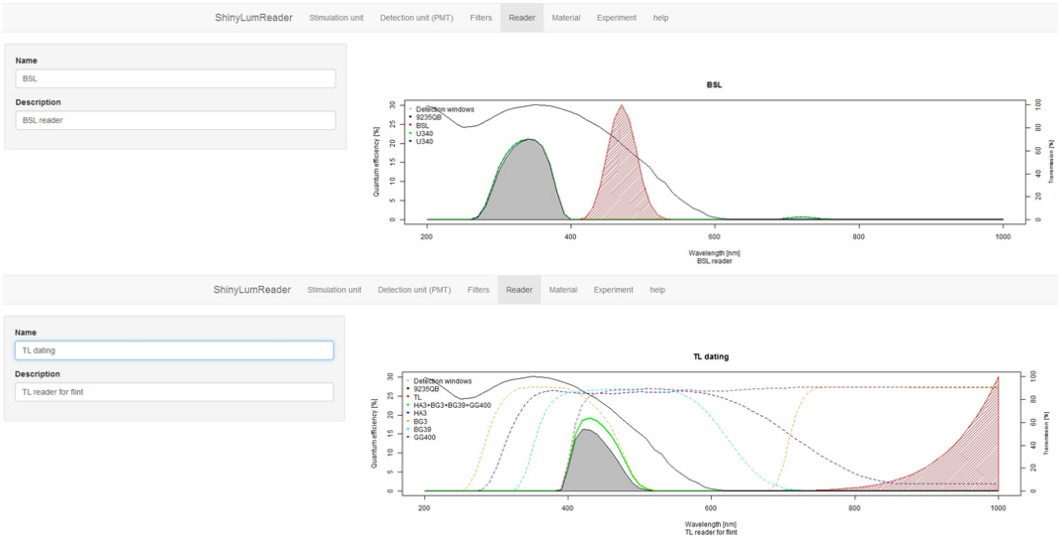


FIGURE 8.6: **Detection windows for the 'usual' reader configuration for BSL and BTL.** The red curves represent the stimulation signal (up) and the black body radiation signal (down). The black continued curves are the PMT quantum efficiency. The green curves are the filters' detection windows. The grey area are the final detection windows for both reader configurations.

Manufacturers already proposed tools to combine filters. However, such tool are most of the time stand-alone solutions that cannot be modified and the filter selection is usually limited. The filters that are no longer produced or those distributed by a different company are rarely included. The collection of filters available in a research laboratory grew over time and trough multiple research projects. It generally includes filters from different manufacturers and some older one that are not produced any more. Discontinued equipment is also ubiquitous is older publications. Moreover, as seen previously, when it comes to luminescence dating, filters are only a part of a more complex setting.

The key features that drive the development of the *TLdating* package were also present during the writing of the *LumReader* package. This second package should include (1) a series of functions (2) easy to combine and (3) creating a complete workflow, but also (4) easy to update and (5) user-friendly. Unfortunately, it was not really possible to rely on existing codes for the data import in **R**. As for the *TLdating* package, the *LumReader* package includes a graphical user interface developed with the *shiny* package (see Fig. 8.7).

For a long time, the technical data were only provided by the manufacturers as graphs. Nowadays, most of them are also available as spreadsheets. However, most manufacturers also have their own specific spreadsheet templates; so to be as user-friendly as possible, we would have to write a specific import function for each of them. We rather decided to focus on a collection of text files already containing the technical data of most

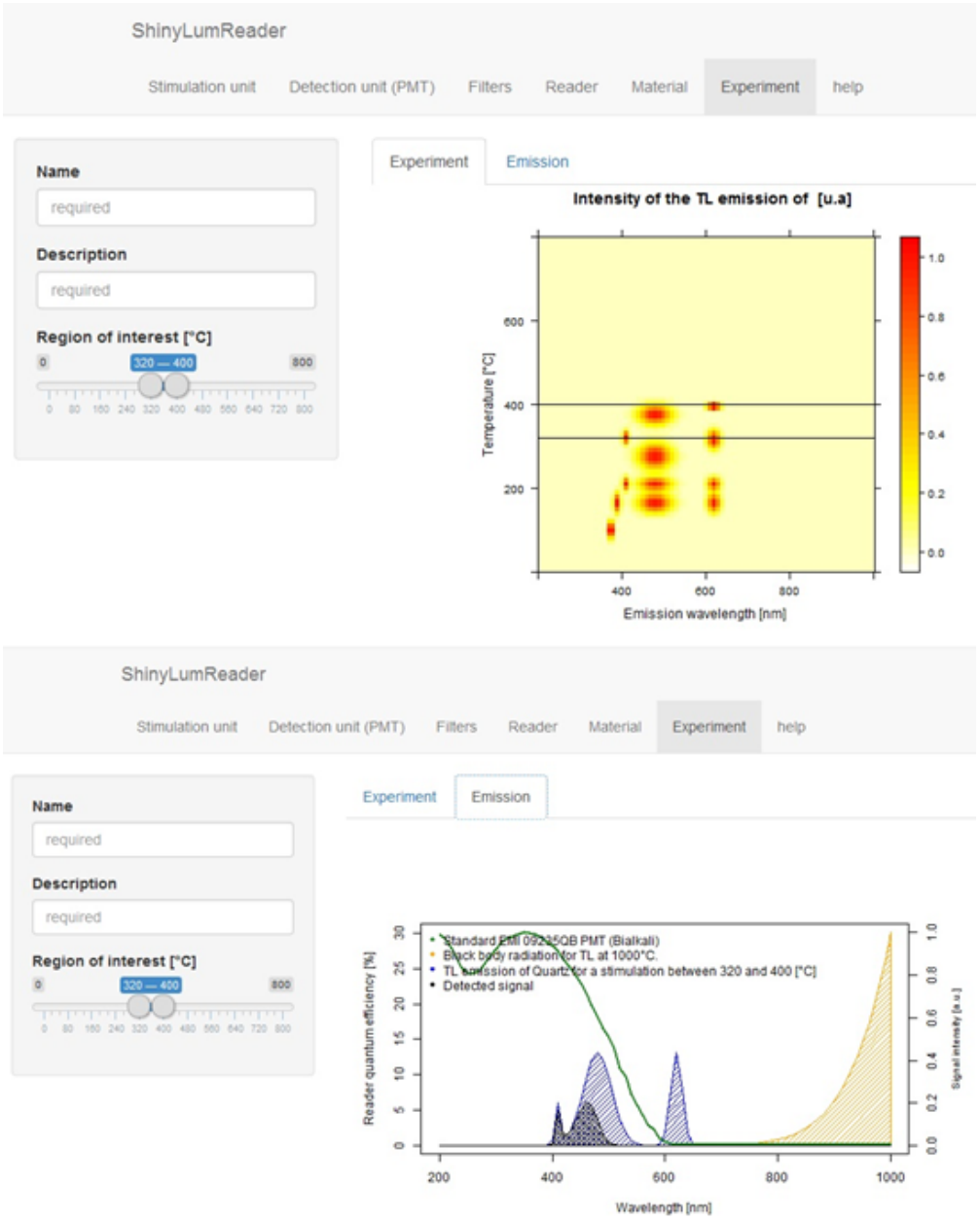


FIGURE 8.7: **Graphical user interface of the *LumReader* package.** The upper figure shows the visualisation of the TL properties of the material emitting the luminescence signal, i.e. quartz. The lower graph combins the stimulation signal with the reader detection window. The blue dashed area is the emitted signal while the black dashed area is the detected signal. The red dashed area represents the black body radiation signal.

filters available at the Cologne Luminescence Laboratory (CLL). **R** natively provides functions to extract data out of text files and spreadsheets. Using a home-made script, it was possible to automatically convert all of these text files into filter objects in our new package. Using the import functions that are included in the *LumReader* package and basic knowledge in **R** programming, the same approach can be used to convert

any other collection of files containing the properties of specific objects (filters, PMT, material luminescence emissions).

The data of the *EMI 9235 QG bialkani* PMT were originally presented as a graph. First, an online tool[1] was used to extract the values and create a spreadsheet. This spreadsheet was then converted using an import function of the *LumReader* package. The stimulation signals and the quartz luminescence properties presented in Chapter 3 were generated in **R** using a home-made script and, once again, converted using the *LumReader* package import functions. These luminescence properties are based on data provided by Krbetschek et al. (1997). Such approach, on a case-by-case basis, is time-consuming. It highlights the importance of collaborative work to create a comprehensive collection of objects (filters, detection and stimulation unit, material luminescence properties) compatible with the *LumReader* package.

Two case studies are presented in Chapter 3. In this section, we focus on the comparison of different filter sets for heated flint dating. This case study shows that a simplistic approach, removing some of the filters, increases the detected signal as expected but is accompanied by undesired side effect, here a reduction of the signal-to-noise ratio and therefore the quality of the data. On a second thought, replacing the complete set of filters by a single filter specifically selected based on the material luminescence properties should have been the perfect solution. However, the signal lost due to the detection geometry change almost completely negates the gain from the improved detection window. As often, there is no perfect solution. For a bright luminescence signal, the improvement of the signal-to-noise ratio is required but, for a dim luminescence signal, the detection of a signal should be prioritised. Using the *LumReader* package it was possible to compare, explain and quantify experimental observations. It is also possible to explore new filter combinations and visualise the results using technical data available online.

The *LumReader* package was developed as a research tool, but also as a teaching tool. It allows the simulation of routine luminescence dating experiments as easily as research applications. Multiple working hypotheses can be explored and their outputs visualised. It is easy to create multiple reader simulations and study the impacts of modification made on a reader setting. It is possible to visualise the consequence of an improper setting or to identify when the filter lets the stimulation signal reach the detection unit.

The *LumReader* package still requires the implementation of a database containing the properties of the filters, detection unit (PMT and CCD camera) and material that are relevant not only for luminescence dating but luminescence research in general. However, it already provides a solid framework to solve numerous research and teaching questions. It is user-friendly, transparent, freely available and easy to update. It therefore fulfils our

[1] http://www.graphreader.com/

objective of developing a software to help for the configuration of the TL/OSL readers (see Chapter 1).

8.2 Age estimations of heated flint samples in the context of the CRC 806: Our Way to Europe

During the first phase of the *CRC 806: Our Way to Europe*, a series of heated flint sample were dated using TL and OSL. They were collected in several archaeological excavations including the open-air site of Românești-Dumbrăviţa I (Romania) (Schmidt et al., 2013b), Sodmein Cave (Egypt) (Schmidt et al., 2015b), Las Palomas cave (Spain) and the rockshelter of Vale Boi (Portugal) (Schmidt, 2013). A series of heated flint samples were also collected in the collapsed rockshelter of Taibeh 3 (Jordan).

During its second phase, several other archaeological sites investigated by the CRC were considered as potential sources of heated flint samples. Those include the open-air site of At near Vrsac (Serbia), Ifri N'Ammar cave (Morocco) and the open-air sites of Al-Ansab 1 and 2 (Jordan).

The author joined the Vrsac field campaign in 2014. In addition to the absence of heated flint artefacts, most of the digging was done on disturbed layers which would have seriously increased the uncertainty on any environmental dose estimation. The author should have joined the Ifri N'Ammar field campaign in 2015. However this campaign concentrated on the peripheral areas of the cave were no heated material was expected or found. The author's participation was therefore cancelled. Finally, the author joined the Al-Ansab field campaign in 2015. It was the only one that allowed for the collection of new heated flint samples potentially suitable for dating during the second phase of the CRC.

8.2.1 Taibeh 3, Jordan

The collapsed rockshelter of Taibeh 3 is located south of Wadi Musa, Jordan. The excavation took place in 2010. 12 geological horizons were identified including 5 with traces of human occupation (see Fig. 8.8).

A total of 2793 artefacts were discovered in the two first occupation layers, 804 in layer AH 1 (stratigraphic layer B) and 1989 in layer AH 2 (stratigraphic layer C). They were identified as related to the late Ahmarian, or Masraqan, technocomplex (Hussain and Richter, 2015). These artefacts include 20 heated flints that were collected to be dated using luminescence dating. Several charcoal samples were also collected for radiocarbon

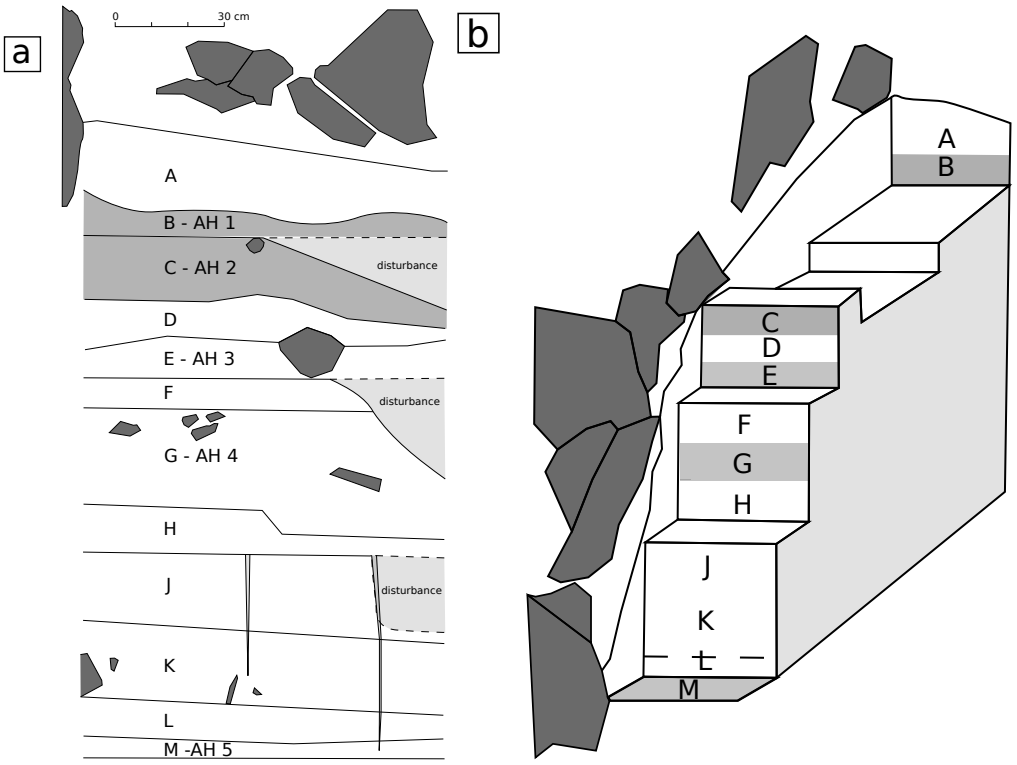


FIGURE 8.8: **(a) Stratigraphic sequence and (b) schematic representation of the test trench with geological (A-M) and archaeological (AH 1-5) horizons.** The flint samples are from the layers B (AH-1) and C (AH-2).

dating in these two layers and their surrounding. A total of 93 artefacts were discovered in the three lower human occupation layers, 42 in layer AH 3 (stratigraphic layer E), 43 in layer AH 4 (stratigraphic later G) and 8 in later AH 5 (stratigraphic layer M). None of them were heated flint artefacts (Hussain and Richter, 2015). Three sediment samples were collected at various depths for OSL dating. Unfortunately, these sediment samples were compromise during transport and potentially exposed to sunlight, making their dating impossible. They were, however, used to estimate the environmental component of the $\dot{D}$ due to the sediment surrounding the heated flint samples.

Of the 20 heated flint artefacts isolated during the fieldwork, 9 were quickly identified as being too small (TAI 4, TAI 5, TAI 6 and TAI 9) or too flat (TAI 7, TAI 8, TAI 10, TAI 12 and TAI 16) to be processed for luminescence dating. Once in the laboratory, 5 additional samples (TAI 2, TAI 11, TAI 13, TAI 14 and TAI 17) were also discarded. They were too small to allow the extraction of their core material using the available tools, an *Isomet 1000 precision saw* from *Buehler*. Of the 6 remaining samples, five (TAI 1, TAI 15, TAI 18, TAI 19 and TAI 20) provided enough core material for a D_e and an *a-value* estimation using both the SAR and the MAAD protocols. The last sample (TAI 3) only provided core material for a D_e estimation using the SAR protocol on a reduced

number of aliquots. It was decided to only make a $\dot{D}$ estimation for the 5 samples that provided a reliable D_e estimation (see table 8.1).

Layer	Sample	Protocol	D_e (Gy)	Age (ka)
C	TAI 1	MAAD	20.77 ± 1.24	15.6 ± 1.9
C	TAI 1	SAR	24.19 ± 0.34	18.1 ± 2.6
C	TAI 3	SAR		-
C	TAI 15	MAAD	22.52 ± 1.41	25.6 ± 3.8
C	TAI 15	SAR	24.05 ± 0.76	23.9 ± 2.9
C	TAI 18	MAAD	26.48 ± 0.85	17.3 ± 2.3
C	TAI 18	SAR	28.66 ± 0.51	19.1 ± 2.4
B	TAI 19	MAAD	23.90 ± 0.49	15.8 ± 2.1
B	TAI 19	SAR	22.45 ± 0.47	14.7 ± 1.9
C	TAI 20	MAAD	18.35 ± 0.55	20.2 ± 2.1
C	TAI 20	SAR	14.09 ± 0.77	15.6 ± 2.1

TABLE 8.1: **Age of the Taibeh heated flint samples** (see Table 5.1).

The 5 final TL ages were consistent with the radiocarbon ages (see Fig. 8.9). TAI 19 is the only heated flint sample coming from layer B and, as expected, the youngest of the series. TAI 1, TAI 18 and TAI 20 (layer C) provide ages consistent with the expected time range, i.e. the Masraqan technocomplex which is usually dated between 18 and 25 ka BP (Goring-Morris and Belfer-Cohen, 1998, 2017). However, their age estimatess are systematically younger than the TB3-14 radiocarbon sample that was collected in layer B. TAI 15 provides the oldest age. Despite being roughly 3 ka older than the expected age for an Masraqan artefact, its age is consistent with the radiocarbon age from the TB3-7 charcoal sample that was also collected in layer C.

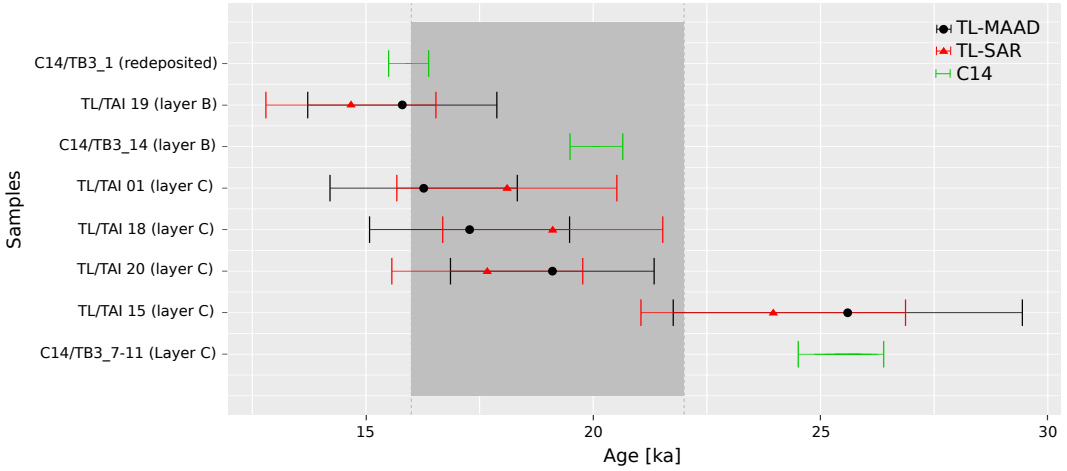


FIGURE 8.9: **Comparison of the age estimates using the MAAD and the SAR protocols.** All of the ages are in the expected range for Masraqan artefacts except for TAI 15 which seems slightly older. The TL ages are also in good agreement with the radiocarbon ages (see Fig. 5.2).

The exposition of the sediment samples to sunlight during transport was a significant loss for dating the complete sequence. Currently, everything seems to indicate that if the three lower layers can be associated with the Masraqan they may be the oldest traces of this technocomplex discovered in the region until now. A new sampling campaign is however needed to validate this hypothesis.

Until now, the chronology for the Masraqan technocomplex was exclusively based on radiocarbon ages. Despite the larger uncertainty on the results, having independent TL ages for heated flint samples that are consistent with the radiocarbon ages definitively increases our confidence in the current Masraqan chronology. The presence of potentially older occupation layers related to the Masraqan also underline the importance of having more age estimates, including some using different dating techniques, especially when the ages estimates reach time ranges in which the reliability of radiocarbon starts to drop. With this in mind, TL dating of heated flint and OSL dating of sediments are the best candidates for extending the dating methods used to date this technocomplex.

The consistency between TL and ^{14}C age estimates is also a strong indication of the viability and reliability of the tools that were used, i.e. the *TLdating* package. This reliability is strengthened by the consistency between the different D_e estimations made for each sample. Those were not only estimated using both the SAR and the MAAD protocols, as said previously, but also using, in both cases, a dose plateau and a growth curve approach (see Chapter 4).

It has to be noted that a slight discrepancy remains between the TL and the OSL ages. The mean values of the TL ages seem systematically younger than the associated ^{14}C ages. Three phenomena could easily explain this difference:

- The ^{14}C ages could have been overestimated. It may, e.g., be due to some unknown reservoir effect. The probability of making such a systematic error is not negligible but it is quite unlikely that this alone explains a difference of several millenia.
- The bridging events between the heated flint and the charcoal sample are not direct. Nothing indicates that they are coming from a single firing event; on the the contrary, they may all be related to different human activity events. Several disturbances in the geological strata were identified during the field campaign. It is not impossible that the discrepancies in the chronology are the result of such disturbances.
- As the radionuclide concentration of the flint samples are very close to the detection limit, it is quite probable that the mean $\dot{D}$ estimates are slightly overestimated. This leads to an underestimation of the mean age estimates and an increase in the uncertainties which is consistent with the final chronology.

As often, the internal $\dot{D}$ estimation of the different heated flint samples constitutes a serious challenge for the final age calculations. In the case of the Taibeh heated flint samples, 50 to 70 % of the total $\dot{D}$ originates from the radionuclides present in the flint matrix (see Table 8.2). This also means that an *a-value* needs to be estimated for each heated flint sample.

Layer	Sample	a-value	$\dot{D}_{flint}$ (Gy)	$\dot{D}_{tot}$ (Gy)	$\dot{D}_{flint}$ (%)
C	TAI 1	0.24 ± 0.01	1.01 ± 0.18	1.48 ± 0.18	68%
C	TAI 15	0.14 ± 0.02	0.44 ± 0.12	0.92 ± 0.12	48%
C	TAI 18	0.2 ± 0.01	0.94 ± 0.14	1.42 ± 0.19	66%
B	TAI 19	0.22 ± 0.01	1.07 ± 0.19	1.55 ± 0.20	69%
C	TAI 20	0.17 ± 0.01	0.45 ± 0.11	0.93 ± 0.11	43%

TABLE 8.2: **The a-value and the corresponding internal and external $\dot{D}$ components for the Taibeh 3 heated flint samples.** For this table, only the results obtained using the MAAD protocol are presented (see Chap. 5, Table 1 for the SAR data).

Despite their dominance in the $\dot{D}$ estimation, the radionuclide concentration values of the flint samples were also close to the detection limits of the instrument used for their estimation. In this case, the measurements provide values between 0.4 and 1.4 ppm for U, between 0.02 and 0.07 ppm for Th and around 0.01-0.02 % for K concentrations (see Table 8.3). Unfortunately, this situation is quite common when dating heated flint samples using luminescence. On the one hand, the *internal* $\dot{D}$ can represent up to 80, sometimes even 90 %, of the total dose (Richter, 2007, Valladas, 1992). On the other hand, the radionuclide elements that generate these radiation have very low concentrations.

Layer	Sample	Material	U (ppm)	Th (ppm)	K (%)
C	TAI 1	flint	1.21 ± 0.12	0.02 ± 0.01	0.02 ± 0.01
C	TAI 15	flint	0.8 ± 0.01	0.03 ± 0.01	0.01 ± 0.01
C	TAI 18	flint	1.28 ± 0.01	0.03 ± 0.01	0.02 ± 0.01
B	TAI 19	flint	1.4 ± 0.01	0.03 ± 0.01	0.01 ± 0.01
C	TAI 20	flint	0.38 ± 0.01	0.07 ± 0.01	0.02 ± 0.01
C	TAI 20-1	sediment	0.83 ± 0.05	3.25 ± 0.19	0.24 ± 0.01
E	TAI 2010-3-2	sediment	0.7 ± 0.05	2.83 ± 0.18	0.16 ± 0.01
G	TAI 2010-3-1	sediment	0.81 ± 0.05	3.27 ± 0.02	0.2 ± 0.01
J	TAI 2010-1	sediment	0.59 ± 0.04	2.47 ± 0.16	0.12 ± 0.00

TABLE 8.3: **Radionuclide concentrations for the Taibeh heated flint and sediment samples.**

For this project, the radionuclide concentration values were estimated using Inductively Coupled Plasma Mass Spectrometry (ICP-MS) at the Institute of Geology and Mineralogy of the University of Cologne. The analysis was performed on the grains obtained

during the crushing of the core material that were between 100 μm and 11 μm, i.e. the grain size that could be used neither for the D_e nor the *a-value* estimation. These *middle* grains were crushed again using a mortar and a pestle to obtain a powder as fine as possible. They were then prepared using a protocol specifically designed to separate the trace elements from the quartz matrix (see Appendix A). Finally, the resulting solutions were sent to the laboratory where the ICP-MS measurements were carried out.

8.2.2 Al-Ansab 1 and 2, Jordan

In 2013, a series of sediments samples were collected from the archaeological site of Al-Ansab, Jordan, for luminescence dating (Klasen et al., 2013). Using the central age model (CAM) to calculate equivalent doses, the age estimations yielded results in the range of 30 to 48 ka (see Table 8.4 and Fig. 8.10).

These first age estimates indicate that radiocarbon ages may not be reliable for samples coming from the oldest layers. Moreover, radiocarbon ages for samples coming from the younger layers may have an unusually high uncertainty due to the presence of a plateau in the calibration curve.

Site	Section	Sample	Depth (m)	age (ka)
Al-Ansab 1	Ansab 6	ANS 6-3	0.15	45 ± 3
Al-Ansab 1	Ansab 6	Ansab 1	0.30	32 ± 2
Al-Ansab 1	Ansab 6	Ansab 2	0.30	37 ± 3
Al-Ansab 1	Ansab 6	ANS 6-2	0.75	34 ± 3
Al-Ansab 1	Ansab 6	ANS 6-1	1.25	35 ± 3
Al-Ansab 1	Ansab 3	ANS 3-3	2.00	32 ± 3
Al-Ansab 1	Ansab 3	ANS 3-2	2.25	36 ± 3

TABLE 8.4: **Age estimation for the sediment samples collected during the 2013 archaeological campaign** (Klasen et al., 2013).

The author took part to the excavation campaign in 2015 which focused on two sections, Al-Ansab 1 and 2. During this campaign a series of fireplaces and a large number of lithic artefacts were excavated (Richter et al., 2020). A series of samples was also collected to complete the Al-Ansab chronology. It includes 6 sediment samples (five from Al-Ansab 1 and one from Al-Ansab 2), 5 heated flint samples and 6 burnt stones (all from Al-Ansab 1). Finally, a series of charcoal samples for ^{14}C dating was collected from different fireplaces.

For the sediment samples, the D_e estimations were made using the SAR protocol on small aliquots. HP-Ge γ-spectrometry was used to determine the radionuclide concentration

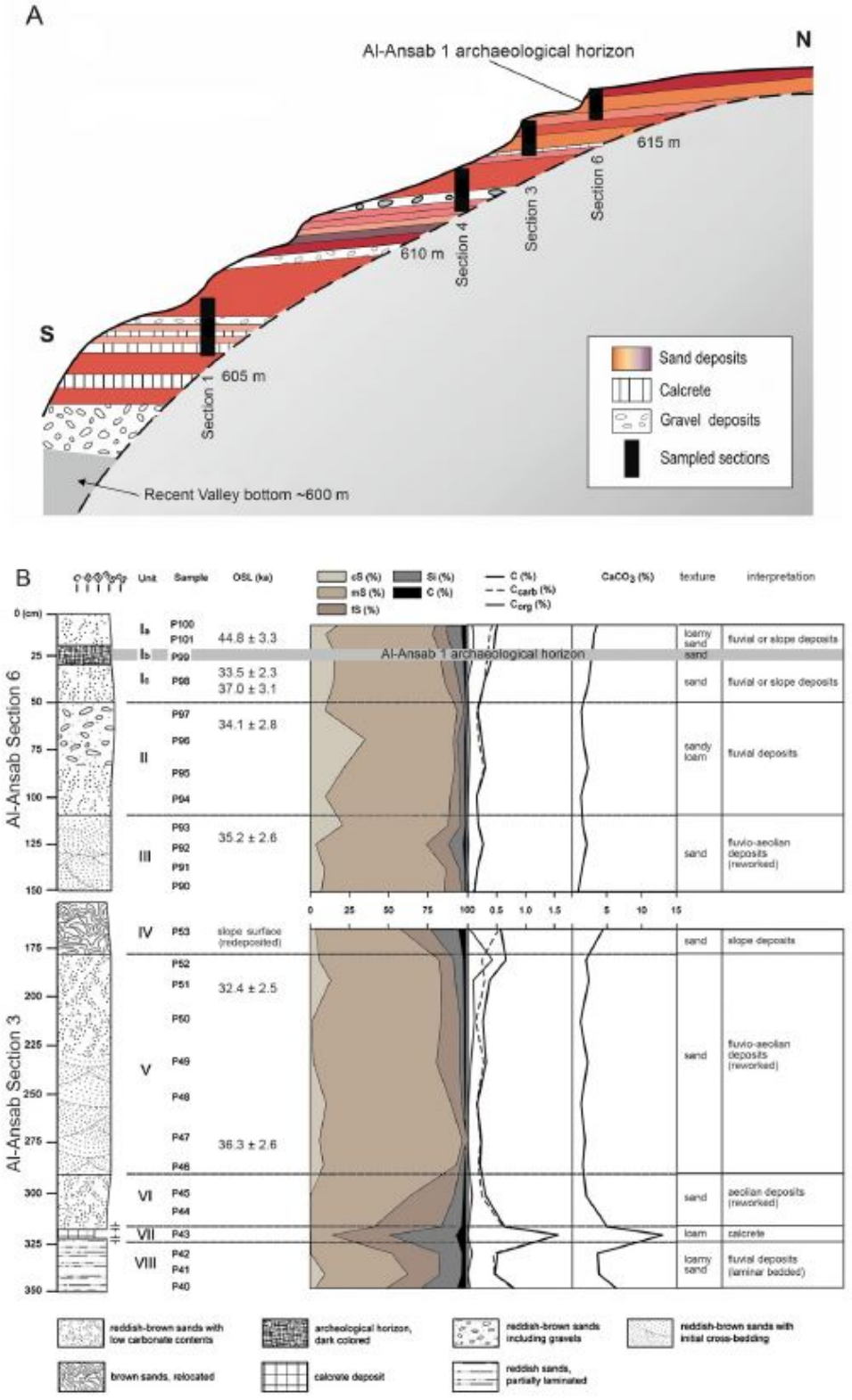


FIGURE 8.10: **Local geological sequence of the pleistocene wadi fill around the Al-Ansab 1 Early Ahmarian settlement site.** (A) South-to-North schematic section through the Pleistocene sediment remnant bearing the Al-Ansab 1 site, from the base of the present Wadi Sabra dry-river channel to the top of the wadi fill; (B) Selected data resulting from sediment analysis of geological sections 6 and 3. (Klasen et al., 2013, Richter et al., 2020).

of the sediment samples and therefore their $\dot{D}$. The calculated ages were consistent with those previously obtained (see table 8.5).

Site	Section	Sample	D_e (Gy)	$\dot{D}$ (Gy)	Age (ka)
Al-Ansab 1	Lower profile	ANS S1	38.854 ± 1.036	1.080 ± 0.030	35.98 ± 1.39
Al-Ansab 1	Lower profile	ANS S2	30.458 ± 1.126	0.897 ± 0.028	33.97 ± 1.64
Al-Ansab 1	Lower profile	ANS S3	29.614 ± 1.349	0.917 ± 0.028	32.29 ± 1.77
Al-Ansab 2	Middle profile	ANS S4	36.346 ± 1.765	0.86 ± 0.027	42.27 ± 2.45
Al-Ansab 1	Upper layer	ANS S6	16.152 ± 0.844	0.653 ± 0.033	24.73 ± 1.80
Al-Ansab 1	Layer 2	ANS S7	41.138 ± 1.679	1.127 ± 0.03	36.49 ± 1.78

TABLE 8.5: **D_e and age estimates for the Al-Ansab sediment samples collected during the 2015 field campaign in Wadi Sabra** (see table 6.3).

This second series of OSL ages confirms that, with the exception of Al-Ansab 1 upper layer, in this case, the radiocarbon ages should probably be considered as unreliable. Al-Ansab 1 *lower profile* may present an inversion of the age sequence similar to the one observed in the Al-Ansab 3 and 6 sections. Being on a slope, this profile could be the consequence of sediment redeposition due to landslides. In any case, the hypothesis of a fast sediment deposition remains the most consistent with the rest of the findings (Richter et al., 2020). The Al-Ansab 2 section was not stable enough to collect reliable sediment samples from its lower and upper profiles. ^{14}C ages from samples collected in any layer of the section should be considered with caution.

Three of the heated flint (ANS F1c, ANS F2 and ANS F3) and one of the burnt stone (ANS F1a) samples were too small to allow the extraction of their core material. The two remaining heated flint samples (ANS F10 and ANS F12) provide consistent D_e and *a-value* estimations. Unfortunately, the final age estimations were definitively too young and inconsistent with the sediment OSL ages (see Table 8.6). The TL profile of the remaining burnt stone (ANS F1a) indicates that it is a polymineral sample and that it may not have been properly reset by heating. It was therefore not possible to provide a reliable age estimate for this last sample either.

The main hypothesis for the underestimation of the two remaining heated flint ages is an overestimation of the $\dot{D}$. The internal component of the $\dot{D}$ reaches up to 76% of the total $\dot{D}$ (see Table 8.7). Its overestimation will therefore have a significant impact on the final age calculation.

The *a-values* are relatively similar to those from the Taibeh's samples (see Tables 8.2 and 8.7). However those were already relatively high compared to the literature (Schmidt, 2013). The only exception is the estimation of the *a-value* from ANS F12 using the

Sample	Protocol	D_e (Gy)	$\dot{D}$ (Gy/ka)	Age (s)
ANS F10 (flint)	MAAD	45.14 ± 2.9	2.51 ± 0.39	18.02 ± 3.02
	SAR	44.82 ± 0.46	2.51 ± 0.39	17.89 ± 2.78
ANS F12 (flint)	MAAD	29.23 ± 7.82	1.80 ± 0.23	16.23 ± 4.83
	SAR	34.29 ± 5.05	1.60 ± 0.22	21.38 ± 4.32

TABLE 8.6: **D_e, $\dot{D}$ and age estimation for the two heated flint samples (ANS F10 and F12) from Al-Ansab 1 showing a archaeological reset.** The D_e were estimated with a SAR protocol on 12 aliquots and a MAAD protocol on 24 aliquots (12 for the Q estimation and 12 for the I estimation). In both cases, a DP and a GC approach are used. The DP results are used to define the temperature integration interval when the GC results are used for the age estimation (Strebler et al., 2017) (see Table 6.9.

Sample	Protocol	a-value	$\dot{D}_{flint}$ (Gy)	$\dot{D}$ (Gy)	$\dot{D}_{flint}$ (%)
ANS F10	MAAD	0.20 ± 0.01	1.95 ± 0.39	2.51 ± 0.39	**78 %**
	SAR	0.21 ± 0.01	1.65 ± 0.39	2.2 ± 0.39	75%
ANS F12	MAAD	$\mathbf{0.44 \pm 0.03}$	1.22 ± 0.23	1.8 ± 0.23	68%
	SAR	0.19 ± 0.01	1.03 ± 0.22	1.6 ± 0.22	64%

TABLE 8.7: **Internal and external $\dot{D}$ components for the Al-Ansab heated flint samples.** The *a-value* estimated for ANS F12 using the MAAD protocol is clearly overestimated. When the supra-linearity correction is neglected, the value becomes similar to the SAR estimation (~ 0.20). The internal doses represent up to 78% of the total dose rate. Therefore, any $\dot{D}_{int}$ overestimation has a strong effect on the final age estimate.

MAAD protocol which is clearly overestimated (see Table 8.7). Neglecting the supra-linear correction allows to obtain a value similar to the one estimated using the SAR protocol (~ 0.20).

As for the Taibeh heated flint samples, the internal $\dot{D}$ was estimated based on the radionuclide concentrations in the flint matrix (see Table 8.8). However, unlike the Taibeh samples, it was decided to rely entirely on an external laboratory for the ICP-MS measurement. Only the crushing of the core material into a fine powder was archieved at the CLL before the samples were sent to a commercial laboratory. This decision was partially motivated by practical considerations including the complexity of the preparation protocol, its hazardousness, and the small amount of core material available for the radionuclide concentration estimation (see Appendix A).

The radionuclide concentration values of the burnt stones are quite similar to those of the sediment samples. The radionuclide concentrations of the Al-Ansab heated flint samples are systematically higher than those from the Taibeh heated flint samples. This is especially the case for the uranium concentration values in ANS F10 (see Tables 8.8 and 8.3). In addition to the stone and flint samples, a known sediment sample was also sent to the external laboratory. The radionuclide concentration values obtained for

Sample	Location	Material	Method	U (ppm)	Th (ppm)	K (%)
TAI F1b	Layer 2	stone	ICP-MS	3.45 ± 0.01	7.55 ± 0.05	8.19 ± 0.01
TAI F10	Layer 2	flint	ICP-MS	2.27 ± 0.01	< 0.05	0.03 ± 0.01
TAI F12	Lower profile	flint	ICP-MS	1.5 ± 0.01	< 0.05	0.03 ± 0.01
Nussloch	Control	loess	ICP-MS	3.07 ± 0.01	8.61 ± 0.05	1.34 ± 0.01

TABLE 8.8: **Radionuclide concentrations for the heated flint/stone samples from Al-Ansab 1** (see Table 6.8 for the radionuclide concentrations in the surrounding sediments).

this reference samples were consistent with the expected values. It is therefore quite unlikely that the unexpected values can be explained by a calibration issue. The final radionuclide concentration value remains very close to the detection limits. It is also lower than those from the sediment sample as expected. In the end, two main hypotheses could explain such high values:

- The presence of an undetected *hot spot* in the core material that was used.
- The contamination of the sample either during its crushing in the CLL or during its preparation in the external laboratory.

Due to the lack of extra material to make a second estimation of the radionuclide concentration values, none of these hypotheses can be definitively excluded. It is technically possible to make a second estimation of the radionuclide concentration value using material from the external layer of the flint samples. However, the risk of contamination of this external material by the surrounding sediment is very high. It was therefore decided to exclude this possibility.

While the dating of the sediment samples confirms the first age estimations for the human occupation of Al-Ansab, no reliable TL age estimations could be produced for the heated flint samples (see Fig. 8.11). It sheds light on one of the well-known challenges of dating heated flint artefacts using TL: most of them have to be discarded during the process. Of the several thousand artefacts collected during the 2015 field campaign in Al-Ansab, there were only 5 heated flints and less than half of them were large enough to extract core material. Moreover, while most of the focus remains on the estimation of the D_e, the $\dot{D}$ estimation is just as important. A solution that could have solved the problem encountered during the dating of the Al-Ansab heated flint samples is a more systematic use of LA-ICP-MS to estimate the radionuclide concentrations for small heated flint samples. This technique does not require the specific sample preparation needed to apply *Liquid chromatography* ICP-MS on flint samples. LA-ICP-MS needs a minimum amount of material. It allows for multiple measurements that enables the

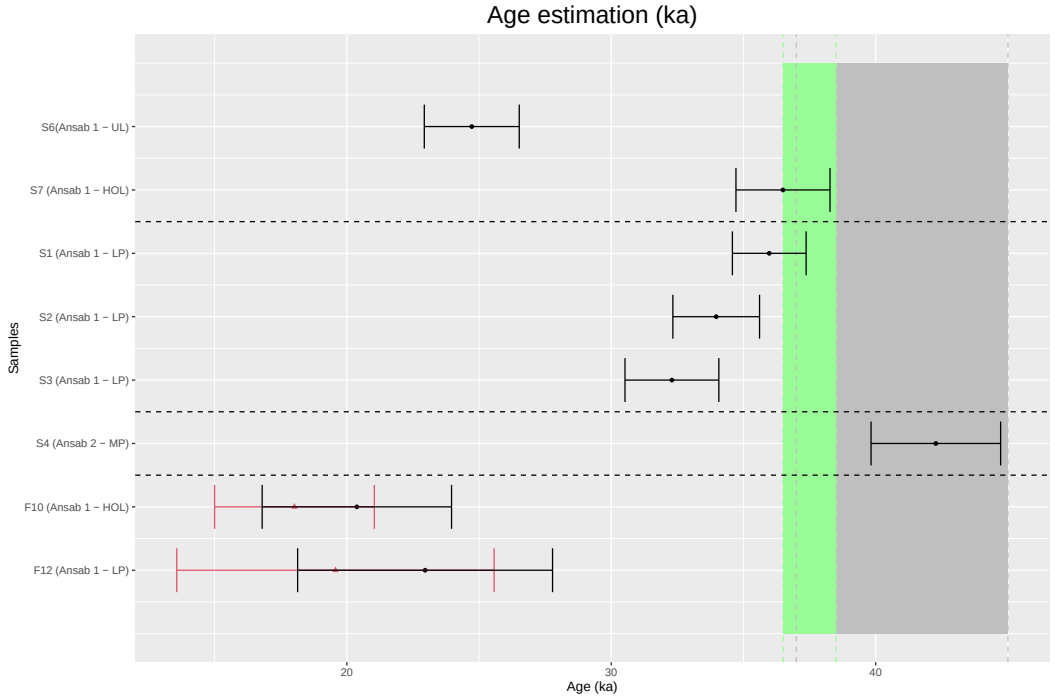


FIGURE 8.11: **Age estimation for the sediment and heated flint samples from Al-Ansab.** The green box indicates the time range of the radiocarbon age estimations for Al-Ansab 1 (Richter et al., 2020), while the grey box (and the grey doted lines) indicates the time span of the Ahmarian techno-cultural unit (Goring-Morris and Belfer-Cohen, 2018).

identification of hot spots. The possibility to perform these analyses on the internal side of the external layer of the flint sample should also be explored. In the absence of LA-ICP-MS, collecting core material from homogenised fine grains rather than dedicate a specific part of the flint's core to the elemental analysis would also have been a better approach to reduce the influence of a potential hot-spot. Such collection can be done just before the first wet sieving of the fine grain fraction used to estimate the *a-value*.

8.3 Applying the new TL software solutions to other settings

The primary focus when developing the *LumReader* and the *TLdating* packages was to produce a series of tools to ease and improve TL dating of heated flint samples. However, the research applications of these two **R** package are much broader.

8.3.1 TL emission spectra from feldpar samples

As seen earlier in this chapter and in Chapter 3, the *LumReader* package was designed for research and teaching applications. It allows the visualisation of common filter/PMT combinations, assessing the function of each piece of equipment and their effects on the detected luminescence signal. It also allows the simulation of poor equipment configurations, including those that could damage the detection unit, without actually risking damage to the equipment. Finally, it allows the exploration of new filter combinations for specific research applications, including the detection of luminescence signals outside the usual UV-blue and IR spectra.

In Chapter 3, the *LumReader* package was used to visualise the TL emission spectra from two feldspar samples (F1 and NB139). Both of them have been studied previously (Clark and Sanderson, 1994, King et al., 2016, Riedesel et al., 2019, Sanderson and Clark, 1994). They are sand-sized perthitic alkali feldspar containing orthoclase, albite and anorthite. Sample F1 contains a relatively high concentration of albite (33.4%) and its spectrum is dominated by a yellow emission around 560 nm. Sample NB139 contains much less albite (9.4%) and its spectrum is dominated by the blue emission of the orthoclase. The LumReader package was used to explore two filter combinations proposed by Sohbati et al. (2013) when exploring the potential of Na-rich feldspar for rock surface dating. On the one hand, the authors used the combination of a Schott BG39 and a Corning 7-59 to isolate the blue emission. On the other hand, they used the combination of an OG 515, a 730 IK, two 660 IK and a band-pass interference filter with FWHM 511-563 nm to isolate the yellow emission. For sample F1, only a low emission sensitivity was obtained within the blue-filter stack window when a brighter yellow could be isolated with the second filter combination. Unless an internal K content is assumed, this yellow signal could be used for dating purposes. For sample NB139, it is the opposite. A bright blue emission can be isolated when the yellow signal is very dim. It has to be noted that, for this blue signal, an internal dose rate from K_2O should be assumed.

8.3.2 Bergisch Gladbach, Germany

The *TLdating* package includes functions to estimate a D_e regardless of the setting that is dated. In Chapter 7, these functions were used to date heated sediments and a roof tile coming from a Roman lime kiln at Bergisch Gladbach, Germany (see Fig. 8.12). Three different measurement protocols were used. Two of them were TL measurements and the last one was an OSL measurement, more specifically pIRIR_{290} or IR_{50} depending



FIGURE 8.12: **Archaeological section from Bergish Gladbach, Germany.** Cut through the lime kiln dug into the soft weathered Devonian base rock without any further mansoning. Three samples were taken from the fritted contact area (open circles), two from the soft sediment (filled circles), which was oxidised and fritted by temperature influence, and one typical Roman roof tile (open rectangle). Dose rate samples were also taken from the greyish lime remains from inside the kiln, exposed in the front centre of the image (Zander et al., 2019).

on the samples. They all provide consistent results, which were also in good agreement with ^{14}C ages of a horse mandible and a charcoal sample (see Fig. 8.13).

The two TL measurements were made using the SAR and the MAAD protocols. They were made on polymineral fine grains and carried out in the Cologne Luminescence Laboratory (CLL) by Anja Zander. The D_e estimates were calculated using the dedicated functions from the *TLdating* package. In both cases, the growth curve approach was used for the final D_e estimation. The values obtained for TL-SAR measurements show a considerably larger scatter than those from the TL-MAAD measurements (see Table 8.9). Their D_e plateau ranges were also more variable.

The calculation of the internal $\dot{D}$ of the roof tile relied on an element analysis carried out at the VKTA Rossendorf using γ-spectrometry. The calculation of the external $\dot{D}$ relied on element analysis carried out on surrounding sediment samples using HPGe γ-spectrometry. Up to three γ-dose samples were measured per luminescence sample to account for difference in water content and radioactive element concentration between the silty sediment, the fritted kiln wall and the remains of the limestone filling of the kiln. An *a-value* was also measured for each sample. The γ component of the external $\dot{D}$

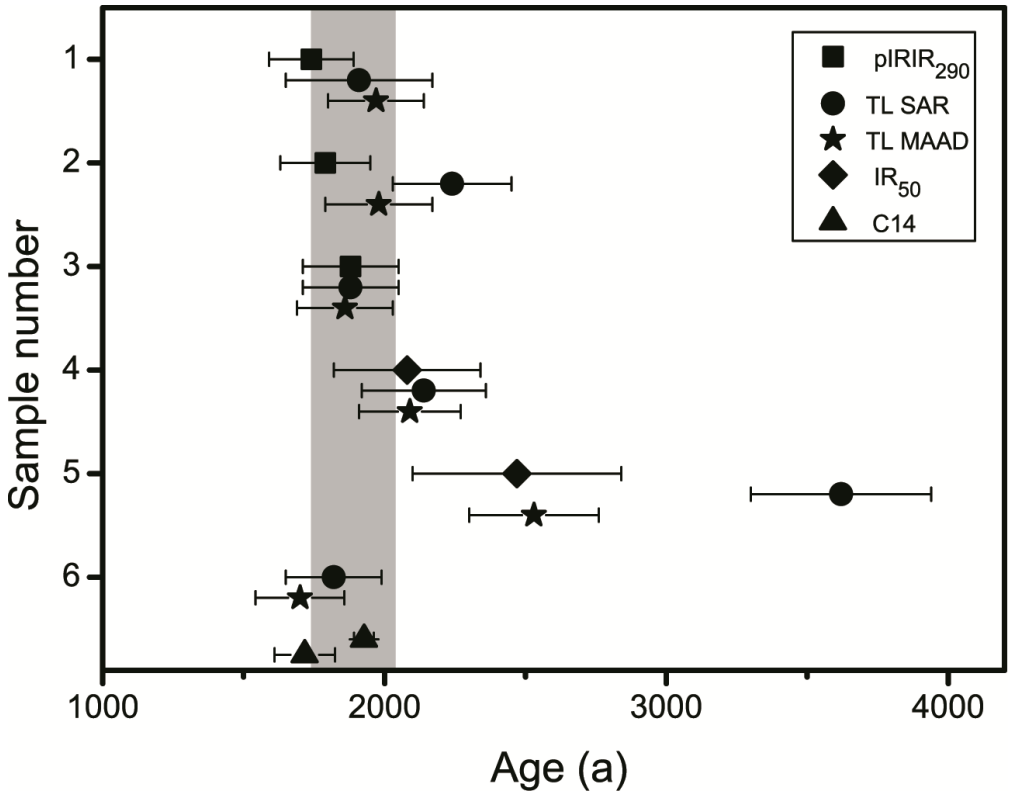


FIGURE 8.13: **Age compilation of OSL and TL results for the samples from the Roman lime kiln at Bergisch Gladbach.** Except for sample 5, all age estimates match the expected Roman age range within a 1σ confidence interval. They are also in good agreement with the two radiocarbon ages obtained for a horse skull excavated in a working pit in front of the kiln and charcoal remains from the kiln area (Zander et al., 2019).

was calculated using a spreadsheet provided by Ian Bailiff, Durham University (personal communication). The α and β components of the internal and external $\dot{D}$ were calculated using DRAC (Durcan et al., 2015), more specifically its dedicated function from the *Luminescence* package (Kreutzer et al., 2021).

The *TLdating* package also includes a function to estimate the $\dot{D}$ for more complex geometries than a homogeneous sediment setting. In Chapter 5, this approach is used to estimate the $\dot{D}$ for heated flint samples but it can easily be applied to other similar settings, especially for dating domestic and architectural ceramics. As with heated flint, when dating ceramic samples it is necessary to distinguish between the internal dose coming from the grains themselves, the external dose coming from the surrounding ceramic matrix and the environmental dose coming from the material surrounding the ceramic artefact and the cosmic radiation.

For domestic ceramics, the surrounding material is usually sediment. When both the internal and external $\dot{D}$ rely on the same radionuclide concentrations for dating heated flint samples, they will require two separated measurements for domestic ceramic samples:

Sample	Protocol	D_e (Gy)	$\dot{D}$ (Gy)	Age (a)
BGB 1	MAAD	10.5 ± 0.5	5.3 ± 0.3	1970 ± 170
	SAR	10.2 ± 1.2		1910 ± 260
BGB 2	MAAD	10.7 ± 0.7	5.4 ± 0.3	1980 ± 190
	SAR	12.1 ± 0.7		2240 ± 210
BGB 3	MAAD	9.4 ± 0.5	5.0 ± 0.3	1860 ± 170
	SAR	9.5 ± 0.6		1880 ± 170
BGB 4	MAAD	9.9 ± 0.5	4.7 ± 0.3	2090 ± 180
	SAR	10.2 ± 0.8		2140 ± 220
BGB 5	MAAD	11.8 ± 0.8	4.7 ± 0.3	2530 ± 230
	SAR	16.9 ± 0.9		3620 ± 320
BGB 6	MAAD	8.8 ± 0.5	5.2 ± 0.4	1700 ± 160
	SAR	9.4 ± 0.6		1820 ± 170

TABLE 8.9: **Compilation of the D_e and $\dot{D}$ results for the TL-MAAD and TL-SAR measurements and the resulting ages.**

(1) the determination of the radionuclide concentrations in the grains themselves (they are often considered negligible for quartz grain dating, but it is not the case for K-rich feldspar and therefore most polymineral samples); (2) the determination of the radionuclide concentrations in the ceramic matrix.

For architectural ceramics, the surrounding material can be sediment but also architectural ceramics, depending on the context. As seen for the tile dated in Chapter 7, the surrounding material geometry can be very complex, with multiple layers of material having different radionuclide concentration values. In that case, the environmental component of the $\dot{D}$ cannot be assessed using DRAC or the approach presented in Chapter 5. However, a large part of architectural ceramics comes from bricks collected inside large walls thicker than 60 cm. The gamma component of the external $\dot{D}$ can then be considered as originated from a homogeneous setting. The approach presented in Chapter 5 can be applied to this configuration. The internal $\dot{D}$ will be defined by the radionuclide concentration values of the grains. The external and the environmental $\dot{D}$ will depend on the radionuclide concentration values of the bricks.

Chapter 9

Conclusion and Outlook

As seen in Chapters 2 and 8, TL dating of heated flint is a technique that occupies a unique place in the construction of prehistoric chronologies. On the one hand, it complements radiocarbon dating which remains the reference dating method. TL dating makes it possible to date archaeological material with no trace of carbon, in particular the widely used heated flint artefacts, but also to reach older time periods, up to 500 ka compared to 50 ka for radiocarbon dating. On the other hand, the TL dating of heated flint samples is also complementary to OSL dating of sediments. While estimating the age gap between a specific human occupation and the deposition of the surrounding sediment can be ambiguous, the complete resetting of the TL signal from a heated flint sample is usually a direct consequence of a human activities, especially when the artefact is found close to the remains of a fireplace. The TL dating of heated flint provides an age for a direct anthropological event.

In this PhD thesis, we have presented new tools designed to improve and modernise TL dating, namely the *TLdating* and *LumReader* **R** packages. These tools were primarily developed to assist in the dating of heated flint samples but, as shown by several examples, have also been used in other geological and archaeological settings.

This project provided new luminescence ages were provided for four archaeological sites: Taibeh 3 (Jordan) provided TL ages for five heated flint samples; Bergisch Gladbach (Germany) provided TL and OSL ages for five heated sediment samples and one architectural ceramic sample; and Al-Ansab 1 and 2 (Jordan) provided OSL ages for six sediment samples.

Not all the heated flint samples collected for TL dating provide an age estimate. At Taibeh 3, fifteen of the heated flint samples collected for TL dating were discarded, i.e. 75% of the samples sent to the luminescence dating laboratory. At Al-Ansab 1, eleven

heated flint or stone samples were collected for dating, but none provided a reliable age estimate. However, they provided a good opportunity to highlight and investigate some of the challenges encountered when dating heated flint samples using TL dating. The latter case study will assist in the development of a preparation protocol to reduce the loss of archaeological material and the consumption of chemicals.

Where heated lithic materials are frequent in archaeological settings, Chapter 6 and the case study of Al-Ansab 1 showed that often only a very small fraction can be TL dated. Due to the required removal of 2 mm of the outer layer of the heated flint, only thicker artefacts (greater than 7-8 mm thick) can be processed. Numerous heated flint samples are often flat, bent or irregular, reducing the number of possible samples. Thus, the cutting equipment available to a laboratory has a major impact on the possible sample pool. High precision water-cooled saws are required for accurate cuts, reducing waste. Finally, painting the outer surface of the samples white creates a visual distinction between the outer surface and core materials, facilitates cutting and reduces core material loss.

The *TLdating* **R** package, presented in Chapters 4 and 5, provides reliable tools for estimating D_e and $\dot{D}$ values. Despite these tools, the process remains highly dependent on an accurate estimation of the radionuclide concentration values and the presence of a sufficient luminescence signal, as seen in Chapters 6 and 8.

Most of the $\dot{D}$ is produced by the radionuclide elements present within the flint matrix. Internal $\dot{D}$ typically accounts for more than 70% of the total $\dot{D}$, and in some case studies it is as high as 90%. Despite generating most of the total dose rate, radionuclide concentrations in flint sample are generally very low. Inductively Coupled Plasma Mass Spectrometry (ICP-MS) is among the most efficient and reliable methods to estimate nuclide concentrations. Even then, the internal concentrations of uranium and thorium in some heated flint samples can be close to the instrument's detection limit, i.e. around 0.01 ppm for U and 0.05 ppm for Th. If the radionuclide concentration is estimated from a sub-sample of the core material, it is also recommended that grains are collected from the finest fraction produced after the crushing of this core material. This reduces the loss of material due to unnecessary cutting of core material and allows mitigation of the influence of undetected *hotspots* on the $\dot{D}$ estimate.

Low radionuclide concentrations also mean a reduced $\dot{D}$ and therefore a relatively weak natural luminescence signal. Proper selection of the filters and the PMT that are used based on the luminescence characterics of the dated material is key to maximising the luminescence signal and minimising the signal-to-noise ratio. The *LumReader* **R** package, presented in Chapter 3, is designed to assist in the configuration of the TL/OSL readers. The Taibeh heated flint case study shows that, in addition to the choice of

filters, their diameters and the geometry of the reader can have a significant effect on luminescence signal reaching the PMT.

Outlook

As already proposed by Schmidt et al. (2012), laser ablation inductively coupled plasma mass spectrometry (LA-ICP-MS) could be an interesting alternative to more classical ICP-MS methods for the estimation of the radionuclide concentrations. In particular, it may open up the possibility of estimating these concentrations using the external layer of the flint, which is currently discarded. LA-ICP-MS collects material on a few μm, whereas the external layer fragments should be at least 2 mm thick (minus the blade width). The application of this method to the inner surface of the external layer fragments without any trace of cortex should therefore not only provide reliable estimates for the radionuclide concentration, but also allow the measurement values to be multiplied by repeating the procedure on different fragments, thus reducing their uncertainties.

Both the *TLdating* package and the *LumReader* package are designed to allow the addition of new tools and features.

It would have been interesting to include additional options for the growth curve estimation, especially the exponential and the exponential plus linear fits. However, this was not necessary in this project because the measured natural signals were still in the linear region of their respective growth curves. In fact, as seen earlier, most of the $\dot{D}$ from a heated flint sample comes from the internal radionuclide concentrations, which are very low compared to those from sediment samples. Therefore, only the oldest heated flint samples reach the non-linear region of the growth curve.

During this project, we focused on the most commonly used methods, i.e. linearly modulated thermoluminescence (LM-TL or TL) using the SAR and MAAD protocols. The inclusion of tools dedicated to isothermal thermoluminescence (ITL) dating could have been a compelling addition to the package, especially since it already provides interesting results for heated flint samples (Tribolo and Mercier, 2012). As no automated data processing software for ITL appears to be currently available, this is one of the most promising developments for the package.

All of the heated flint samples dated during this project were relatively small, usually less than a few centimetres. For larger flint samples, it is necessary to consider the effect of their shape and size on the estimation of their $\dot{D}$. Indeed, it is no longer possible to neglect the γ component of their internal dose rate and it also affects the γ component of their environmental dose rate. Some of these variations were studied by Valladas

(1985a), who proposed corrective factors that could be included in a later version of the package.

As far as the *LumReader* package is concerned, the next extension to be developed would be a module to automatically estimate the effect of the filter size and reader geometry on the detected signal. However, the main limitation of the *LumReader* package at present is the lack of a database containing the luminescence properties of all materials regularly dated and investigated using luminescence (TL and OSL). Without such a database, the use of the package will mostly remain limited to simulating luminescence readers rather than complete luminescence experiments. While the TL properties of many minerals relevant to luminescence dating have already been investigated by Krbetschek et al. (1997), the characterisation of the OSL properties of these materials requires the use of spatially resolved luminescence analysis, EM-CCD cameras, and a variety of stimulation sources. The creation of this database will be a collaborative effort between several research teams.

Both the *LumReader* and the *TLdating* packages are available online. The LumReader package can be found on Github[1] and on CRAN[2]. The Cologne Luminescence Laboratory (CLL) hosts an online version of the Shiny application based on the package freely available to all[3]. The *TLdating* package can be found on Github[4] and on CRAN[5]. Again, the CLL hosts an online version of the Shiny application based on the package freely available to all[6].

[1] https://github.com/dstreble/LumReader
[2] https://CRAN.R-project.org/package=LumReader
[3] http://rlum.geographie.uni-koeln.de:9418/packages/LumReader/inst/shinyLumReader/
[4] https://github.com/dstreble/TLdating
[5] https://CRAN.R-project.org/package=TLdating
[6] http://rlum.geographie.uni-koeln.de:9418/packages/shiny_TLdating/shinyTLdating/

Appendix A

Flint samples preparation for radionuclide content estimation

The following protocol for the preparation of Silicate based sample, including flint sample, for ICP-MS analysis was proposed by H.U Kasper in 2005, based on personal communication of P, DUlski in 2003. The full protocol requires at least 2 days of laboratory works.

First day

1. Collect exactly 200 mg of sample material (as a fine powder).
2. First acidic treatment:
   - Put the sample in a pressure digestion vessel.
   - Add 3 ml of HF (40%) and 3 ml of $HClO_4$ (70%).
   - Heat the pressure digestion vessel (closed) for 12 to 24 hours in a oven at $180°C$.
   - Let the pressure digestion vessel (closed) cool down to room temperature (around $30°C$).

Second day

3. Evaporation of the added solutions:
   - Evaporate the solution by heating the pressure digestion vessel (open) in a fume hood using a heating plate at $160°C$ (max $180°C$) for ~ 4 hours.
   - Only a tear drop of solution should remains at the end of the process.
   - Let the sample cool down to room temperature.

4. Removal of the remaining traces of HF and $HClO_4$:
   - Add 5 ml of HCl (30%) in the pressure digestion vessel.
   - Evaporate the solution by heating the pressure digestion vessel (open) in a fume hood using a heating plate at $160°C$ for ~ 2 hours.
   - Only a tear drop of solution should remains at the end of the process.
   - Let the sample cool down to room temperature.
5. Second acidic treatment:
   - Add 5 ml of HCl (30%) to the sample.
   - Heat the pressure digestion vessel (closed) for 12 hours in a oven at $130°C$.
   - Let the pressure digestion vessel (closed) cool down to room temperature.

   Third day
6. Evaporation of the added solution:
   - Evaporate the solution by heating the pressure digestion vessel (open) at $160°C$ on a heating plate in a fume hood for ~ 2 hours.
   - Let the sample cool down to room temperature.
7. Preparation of the final solution for ICP-MS analysis:
   - Add 2 ml of HCl (30%) and 10 ml of H_2O.
   - Transfer the solution in a sample tube using HNO_3 (2%).
   - Add HNO_3 (2%) to the sample tube until there is 50 ml of solution.

This protocol requires to manipulate dangerous chemical including HF and $HClO_4$.

- *A very short exposure* to HF *could cause death or major residual injury* (NFPA 704 - blue:4).
- HF is *Normally stable, but can become unstable at elevated temperatures and pressures* (NFPA 704 - Yellow:1).
- *Short exposure* to $HClO_4$ *could cause serious temporary or moderate residual injury* (NFPA 704 - blue:3).
- $HClO_4$ is *capable of detonation or explosive decomposition but requires a strong initiating source, must be heated under confinement before initiation, reacts explosively with water, or will detonate if severely shocked* (NFPA 704 - Yellow:3).

Appendix B

LumReader: Designing your luminescence experiment with R - Online supplement

B.1 Source files

```
Name: HA3
Description: Ha-3
Thickness [mm]: 1
Reflexion (1-P) [%]: 1
Transmission (T) [nm ; %]:
200 ; 1e-05
210 ; 1e-05
(...)
540 ; 0.8665
550 ; 0.8735
560 ; 0.8735
(...)
1200 ; 0
```

FIGURE B.1: **.FLT file for the Huya *U340* filter.**

```
Name: 9235QB
Description: Standard EMI 09235QB PMT (Bialkali)
Quantum efficiency (QE) [nm ; %]:
100 ; 0.00473
110 ; 0.00474
(...)
260 ; 0.24297
(...)
1200 ; 0.0011
```

FIGURE B.2: **.PMT file for the *9235QB* PMT.**

```
Name: TL
Description: Black body radiation at 500 C.
Type: TL
emission (s) [nm ; mA/W]:
100 ; 2.05e-69
110 ; 2.83e-62
120 ; 2.43e-56
(...)
1180 ; 0.84
1190 ; 0.91
1200 ; 1
```

FIGURE B.3: **.EXI file for a TL stimulation**

```
Name: imaginary
Description: TL properties of an imaginary material.
TL emission [nm ; C ; a.u.]:
200 ; 0  ;  1
200 ; 10  ;  1
(...)
200 ; 800  ;  1
210 ; 0  ;  1
(...)
1200 ; 790  ;  1
1200 ; 800  ;  1
```

FIGURE B.4: **.TL file for an imaginary material.**

```
Name: imaginary
Description: OSL properties of an imaginary material.
OSL emission [nm ; nm ; a.u.]:
200 ; 200  ;  1
200 ; 210  ;  1
(...)
200 ; 1000  ;  1
210 ; 200  ;  1
(...)
1200 ; 990  ;  1
1200 ; 1000  ;  1
```

FIGURE B.5: **.OSL file for an imaginary material.**

Appendix C

Using R for thermoluminescence dating - Online supplement

C.1 Tables

	Functions	Mandatory input parameters	**Description**
(1)	*TLum.BIN.file*		Object containing the information present in *.BINX* file
	TLum.Data.Curve		Objet gathering the information linked to a record
	TLum.Analysis		List of *TLum.Data.Curve*.
	TL.Results		Results provided by *Analyse_** function
(2)	*Risoe.BINfileData2TLum.BIN.file*	[*Risoe.BINfileData*] object	Converts *Risoe.BINfileData* object into *TLum.BIN.file* object
	Tlum.BIN.file2Risoe.BINfileData	[*Tlum.BIN.file*] object	Converts *TLum.BIN.file* object into *Risoe.BINfileData* object
	Tlum.BIN.file2Tlum.Analysis	[*Tlum.BIN.file*] object	Converts *Tlum.BIN.file* object into *TLum.Analysis* object
	RLum.Analysis2TLum.Analysis	[*TLum.Analysis*] object	Converts *RLum.Analysis* object into *TLum.Analysis* object
(3)	*mod_extract.TL*	[*TLum.Analysis*] object	Extracts TL curve from *TLum.Analysis*
	mod_update.dType	[*TLum.Analysis*] object	Updates *data-type* metadata of *TLum.Analysis*
	mod_remove.aliquot	[*TLum.Analysis*] object, [*list*] list	Removes specified aliquots from *TLum.Analysis*
	mod_remove.preheat	[*TLum.Analysis*] object	Removes preheat curves from *TLum.Analysis*
	mod_subtract.background	[*TLum.Analysis*] object	Subtracts background from associated TL curve in *TLum.Analysis*
	mod_align.peaks	[*TLum.Analysis*] object	Aligns TL peaks from *TLum.Analysis*
(4)	*analyse_TL.plateau*	[*TLum.Analysis*] object	Performs the heating plateau test for *TLum.Analysis* object
	analyse_TL.MAAD	[*TLum.Analysis*] object, [*numeric*] eval.Tmin, [*numeric*] eval.Tmax	Estimates D_e using the MAAD protocol for *TLum.Analysis* object
	analyse_TL.SAR	[*TLum.Analysis*] object, [*numeric*] eval.Tmin, [*numeric*] eval.Tmax	Estimates D_e using the SAR protocol for *TLum.Analysis* object
(5)	*script_TL.import*	[*character*] file.name	Creates *TLum.Analysis* from *.BINX* file
	script_TL.export	[*TLum.Analysis*] object, [*character*] file.name	Creates *.BINX* file from *TLum.Analysis*
	script_TL.pretreatment	[*character*] file.name	Gathers series of data pretreatments
	script_TL.plateau	[*character*] file.name	Gathers heating plateau test estimation and series of data pretreatments
	script_TL.MAAD	[*character*] file.name, [*numeric*] eval.Tmin, [*numeric*] eval.Tmax	Gathers complete workflow to estimate D_e using MAAD protocol
	script_TL.SAR	[*character*] file.name, [*numeric*] eval.Tmin, [*numeric*] eval.Tmax	Gathers complete workflow to estimate D_e using SAR protocol

TABLE C.1: **Summary of the main functions of the *TLdating* package.** (1) Class object containing the data; (2) functions converting a class object into another one; (3) functions manipulating the data; (4) functions making the data analysis; and (5) scripts gathering a predefined set of functions.

Protocol	**Sample**	Δt (**R**) [$^\circ C$]	DP (**R**) [s]	GC (**R**) [s]	Δi (A) [out of 250]	Before PT (A) [s]	After PT (A) [s]	Dose rate [Gy/s]
MAAD	TAI 1	$320-370$	222.2 ± 2.68	225.73 ± 5.15	$180-210$	176.6 ± 9.9	174.1 ± 10.1	0.1058
	TAI 15	$370-410$	215.51 ± 2.9	216.25 ± 10.69	$200-230$	152.1 ± 29.6	152.1 ± 29.6	0.1058
	TAI 18	$350-390$	248.83 ± 2.54	250.24 ± 7.72	$190-220$	285 ± 26.1	274.4 ± 24.3	0.1058
	TAI 19	$340-380$	224.14 ± 1.99	225.91 ± 4.64	$190-220$	213.7 ± 10.3	214.5 ± 10	0.1063
	TAI 20	$350-390$	170.65 ± 2.74	173.1 ± 6.07	$190-220$	104 ± 12.1	104.1 ± 12.9	0.1063
SAR	TAI 1	$320-370$	227.06 ± 5.56	227.38 ± 3.76	$180-210$	228.5 ± 5.54	225.5 ± 12.26	0.1058
	TAI 15	$350-390$	227.41 ± 8.65	230.14 ± 7.49	$190-220$	235.4 ± 9.22	227.3 ± 7.93	0.1058
	TAI 18	$350-390$	268.53 ± 5.18	269.06 ± 4.2	$190-220$	267.5 ± 5.19	267.9 ± 5.51	0.1054
	TAI 19	$340-380$	213.58 ± 4.53	213.3 ± 4.43	$190-220$	215.9 ± 6.57	210.7 ± 5.36	0.1061
	TAI 20	$340-390$	135.6 ± 3.07	135.42 ± 3.74	$190-220$	133.2 ± 7.86	136.6 ± 7.25	0.1063

TABLE C.2: **Comparison of the D_e estimation (in s) for 5 burnt flint sample from Taibeh, Jordan**, using the *TLdating* package (**R**) and *Analyst* (A) with the SAR & MAAD protocols. DP = dose plateau approach, GC = Growth curve approach, and PT = pretreatment.

Id.	Protocol	$\Delta T[^\circ C]$	Approach	(UI0)	(UQ0)	(WI0)	(WQ0)	(UI150)	(UQ150)	(WI150)	(WQ150)
TAI 1	MAAD	320 − 370	DP	211.11 ± 3.55	222.61 ± 3.42	213.16 ± 2.41	213.12 ± 2.4	211.11 ± 3.55	218.18 ± 6.29	240.27 ± 3.48	222.2 ± 2.68
			GC	211.25 ± 3.55	211.6 ± 3.42	213.42 ± 2.41	213.71 ± 2.4	211.25 ± 3.55	215.67 ± 6.29	242.68 ± 3.48	225.73 ± 2.68
	SAR	320 − 370	DP	//	222.21 ± 4.47	//	225.65 ± 4.43	//	227.23 ± 5.72	//	227.06 ± 5.56
			GC	//	223.72 ± 4.47	//	225.86 ± 4.43	//	228.13 ± 5.72	//	227.38 ± 5.56
TAI 15	MAAD	370 − 410	DP	159.51 ± 4.78	191.06 ± 4.26	169.73 ± 2.63	170.48 ± 2.61	159.51 ± 4.78	206.24 ± 6.98	222.45 ± 4.47	215.51 ± 2.9
			GC	159.91 ± 4.78	188.65 ± 4.26	169.51 ± 2.63	169.53 ± 2.61	159.91 ± 4.78	207.85 ± 6.98	221.31 ± 4.47	216.25 ± 2.9
	SAR	350 − 390	DP	//	217 ± 5.88	//	226.49 ± 7.35	//	227.83 ± 7.99	//	227.41 ± 8.65
			GC	//	219.6 ± 5.88	//	227.41 ± 7.35	//	230.49 ± 7.99	//	230.14 ± 8.65
TAI 18	MAAD	350 − 390	DP	219.95 ± 3.84	226.27 ± 3.52	215.97 ± 2.31	217.63 ± 2.29	219.95 ± 3.84	238.1 ± 6.15	259.17 ± 3.53	248.83 ± 2.54
			GC	220.2 ± 3.84	227.94 ± 3.52	217.35 ± 2.31	216.89 ± 2.29	220.2 ± 3.84	239.94 ± 6.15	260.81 ± 3.53	250.24 ± 2.54
	SAR	350 − 390	DP	//	260.95 ± 5.01	//	271.11 ± 5.77	//	269.52 ± 5.39	//	268.53 ± 5.18
			GC	//	261.1 ± 5.01	//	271.17 ± 5.77	//	269.28 ± 5.39	//	269.06 ± 5.18
TAI 19	MAAD	340 − 380	DP	192.71 ± 3.3	192.75 ± 2.84	183.93 ± 1.77	183.48 ± 1.75	192.71 ± 3.3	222.99 ± 5.15	224.98 ± 2.98	224.14 ± 1.99
			GC	193.9 ± 3.3	211.72 ± 2.84	184.95 ± 1.77	184.44 ± 1.75	193.9 ± 3.3	223.42 ± 5.15	226.72 ± 2.98	225.91 ± 1.99
	SAR	340 − 380	DP	//	207.76 ± 4.72	//	212.04 ± 4.48	//	215.66 ± 4.75	//	213.58 ± 4.53
			GC	//	210.16 ± 4.72	//	212.91 ± 4.48	//	216.41 ± 4.75	//	213.3 ± 4.53
TAI 20	MAAD	350 − 390	DP	134.8 ± 4.98	166.79 ± 6.77	133.12 ± 2.39	128.42 ± 2.34	134.8 ± 4.98	182.93 ± 8.27	157.72 ± 4.18	170.65 ± 2.74
			GC	132.66 ± 4.98	163.31 ± 6.77	135.13 ± 2.39	133 ± 2.34	132.66 ± 4.98	179.05 ± 8.27	160.72 ± 4.18	173.1 ± 2.74
	SAR	340 − 390	DP	//	131.75 ± 5.05	//	132.94 ± 5.57	//	134.01 ± 3.55	//	135.6 ± 3.07
			GC	//	133.16 ± 5.05	//	132.81 ± 5.57	//	134.09 ± 3.55	//	135.42 ± 3.07

TABLE C.3: **Comparison of the age estimation using the MAAD and the SAR protocols.** All the age are in the expected range for Masraqan artefacts except for TAI 15 which seems a little bit older. The TL ages are also in good agreement with the radiocarbon ages. (UI0) unweighted average, all doses & independent I; (UQ0) unweighted average, all doses & reusing Q slope; (WI0) weighted average, all doses & independent I; (WQ0) weighted average, all doses & reusing Q slope; (UI150) unweighted average, only higher doses & independent I; (UQ150) unweighted average, only higher doses & reusing Q slope ; (WI150) weighted average, only higher doses & independent I; (WQ150) weighted average, only higher doses & reusing Q slope. For the SAR protocol, there is no supralinear correction, therefore columns (UI0) and (UQ0), columns (WI0) and (WQ0), columns (UI150) and (UQ150) and columns (WI150) and (WQ150) provide the same results (this is indicated by slashes in the table). All the doses are provided in s, the dose rates are the same as in Table C.2.

Appendix D

Using DRAC in complex geometries: TL dating heated flints from Taibeh, Jordan - Online supplement

D.1 Calibration of the α-source

The α-source in the lexsyg research reader in the Cologne Luminescence Laboratory (CLL) was cross-calibrated against the *Heidelberg Littlemoore* α-irradiation facility. For the calibration procedure, fine grain (4-11 μm) quartz was used, from which the natural signal was reset by heating the grain in a furnace at 360 $^{\circ}C$ for 2 h. The material was divided into two subsets of 24 aliquots each, which received two different α-doses (corresponding to 30 and 60 min irradiation time). These doses were recovered by means of a SAR protocol using α-regeneration and α-test doses. Optimal measurement parameters for this protocol were determined beforehand according to the results of performance tests such as a preheat plateau test. Dose response curves constructed from the signal of the first $\sim$ 1.3 s of the OSL decay curve (minus a background averaged from the last $\sim$ 8.3 s) were fitted with a single-saturating exponential function. Averaged results of recovered equivalent irradiation times for the two α-doses received in Heidelberg were then taken to calculate the dose rate of the α-source to be calibrated.

D.2 Measurement Protocols

D_e estimation

Multiple aliquot additive dose (MAAD) protocol

	Step	**β-dose/Temperature max.**	**β-dose/Heating rate**	**Plateau**
1	*additive* dose	Nat + 0/200/400/600 [s]	0.1058 [Gy/s]	-
2	Preheat	220 [$°C$]	2 [$°C$/s]	10 [s]
3	TL Signal (L_x)	450 [$°C$]	2 [$°C$/s]	-
4	TL Background	450 [$°C$]	2 [$°C$/s]	-
5	*test* dose	180 [s]	0.1058 [Gy/s]	-
6	Preheat	220 [$°C$]	2 [$°C$/s]	10 [s]
7	TL Signal (T_x)	450 [$°C$]	2 [$°C$/s]	-
8	TL Background	450 [$°C$]	2 [$°C$/s]	-
9	*bleach+additive* dose	Bleach + 0/200/400/600 [s]	0.1058 [Gy/s]	-
10	Preheat	220 [$°C$]	2 [$°C$/s]	10 [s]
11	TL Signal (L_x)	450 [$°C$]	2 [$°C$/s]	-
12	TL Background	450 [$°C$]	2 [$°C$/s]	-
13	*test* dose	180 [s]	0.1058 [Gy/s]	-
14	Preheat	220 [$°C$]	2 [$°C$/s]	10 [s]
15	TL Signal (T_x)	450 [$°C$]	2 [$°C$/s]	-
16	TL Background	450 [$°C$]	2 [$°C$/s]	-

The steps 9 to 16 were performed on the aliquots used for the D_e estimation and on aliquots that were bleached at 380 $°C$ for 2 h. Both produce consistent estimations for the supralinearity correction.

Single aliquot regenerative dose (SAR) protocol

	Step	**β-dose/Temperature max.**	**β-dose/Heating rate**	**Plateau**

1	*regenerative* dose	Nat, 100, 200, 400, 600, 800, 0, 200 [Gy]	0.1058 [Gy/s]	-
2	Preheat	220 [°C]	2 [°C/s]	10 [s]
3	TL Signal (L_x)	450 [°C]	2 [°C/s]	-
4	TL Background	450 [°C]	2 [°C/s]	-
5	*test* dose	180 [Gy]	0.1058 [Gy/s]	-
6	Preheat	220 [°C]	2 [°C/s]	10 [s]
7	TL Signal (T_x)	450 [°C]	2 [°C/s]	-
8	TL Background	450 [°C]	2 [°C/s]	-

a-value estimation

Multiple aliquot additive dose (MAAD) protocol

	Step	**Dose/Temperature max.**	**Dose/Heating rate**	**Plateau**
1	Bleach (TL)	450 [°C]	5 [°C/s]	-
2	Bleach (BG)	450 [°C]	5 [°C/s]	-
3	*Artificial* dose (α)	400 s	0.197 [Gy/s]	-
4	*additive* dose (β)	*Nat* + 0/200/400/600 [s]	0.1058 [Gy/s]	-
5	Preheat	220 [°C]	2 [°C/s]	10 [s]
6	TL Signal (L_x)	450 [°C]	2 [°C/s]	-
7	TL Background	450 [°C]	2 [°C/s]	-
8	*test* dose (β)	180 [s]	0.1058 [Gy/s]	-
9	Preheat	220 [°C]	2 [°C/s]	10 [s]
10	TL Signal (T_x)	450 [°C]	2 [°C/s]	-
11	TL Background	450 [°C]	2 [°C/s]	-
12	*bleach+additive* dose (β)	0/200/400/600 [s]	0.1058 [Gy/s]	-
13	Preheat	220 [°C]	2 [°C/s]	10 [s]
14	TL Signal (L_x)	450 [°C]	2 [°C/s]	-
15	TL Background	450 [°C]	2 [°C/s]	-

16	*test* dose (β)	180 [s]	0.1058 [Gy/s]	-
17	Preheat	220 [$°C$]	2 [$°C$/s]	10 [s]
18	TL Signal (T_x)	450 [$°C$]	2 [$°C$/s]	-
19	TL Background	450 [$°C$]	2 [$°C$/s]	-

The aliquots were bleached twice (at 450 $°C$) to allow the recording of the *natural* signal of each aliquot.

Single aliquot regenerative dose (SAR) protocol

	Step	**Dose/Temperature max.**	**Dose/Heating rate**	**Plateau**
1	Bleach (TL)	450 [$°C$]	5 [$°C$/s]	-
2	Bleach (BG)	450 [$°C$]	5 [$°C$/s]	-
3	*Artificial* dose (α)	400 s	0.197 [Gy/s]	-
4	*regenerative* dose (β)	*Nat*, 100, 200, 400, 600, 800, 0, 200 [Gy]	0.1058 [Gy/s]	-
5	Preheat	220 [$°C$]	2 [$°C$/s]	10 [s]
6	TL Signal (L_x)	450 [$°C$]	2 [$°C$/s]	-
7	TL Background	450 [$°C$]	2 [$°C$/s]	-
8	*test* dose (β)	180 [Gy]	0.1058 [Gy/s]	-
9	Preheat	220 [$°C$]	2 [$°C$/s]	10 [s]
10	TL Signal (T_x)	450 [$°C$]	2 [$°C$/s]	-
11	TL Background	450 [$°C$]	2 [$°C$/s]	-

The aliquots were bleached twice (at 450 $°C$) to allow for the recording of the *natural* signal of each aliquot.

D.3 Filter combinations for the estimation of the De value and the a-value.

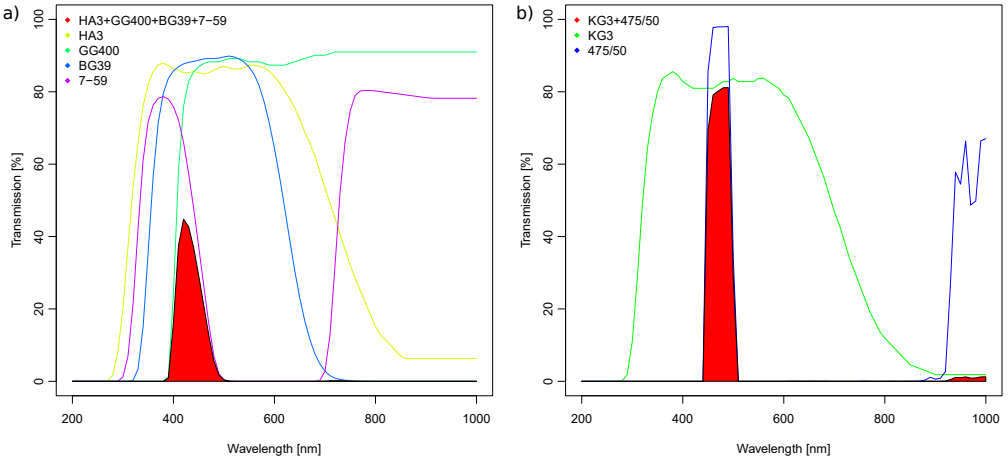


FIGURE D.1: **(a) Filter combination for the D_e value estimation (bandwidth 400-470 [nm]) and (b) filter combination for the *a-value* estimation (bandwidth 450-500 [nm]).**

D.4 Radio-element concentration tables

Sample	**U [ppm]**	**Th [ppm]**	**K [%]**	**Depth [m]**	$\dot{\mathbf{D}}_{\mathbf{ext2}}$ **[Gy/ka]**
TAI 2010/1	0.59 ± 0.04	2.47 ± 0.16	0.12 ± 0.01	1.5 ± 0.1	0.20 ± 0.02
TAI 2010/3-1	0.81 ± 0.05	3.27 ± 0.20	0.20 ± 0.01	1.1 ± 0.1	0.28 ± 0.02
TAI 2010/3-2	0.70 ± 0.05	2.83 ± 0.18	0.16 ± 0.01	0.8 ± 0.1	0.24 ± 0.02
TAI 20 (sediment)	0.83 ± 0.05	3.25 ± 0.19	0.24 ± 0.01	0.4 ± 0.2	0.29 ± 0.02
TAI (average)	0.73 ± 0.12	2.95 ± 0.40	0.18 ± 0.06	0.4 ± 0.2	0.25 ± 0.04

TABLE D.5: **Radio-element concentrations for the Taibeh sediment samples.** The radio-element concentration are relatively low which allows to use an average for the flint $\dot{D}_{ext2}$ estimation.

Sample	**U [ppm]**	**Th [ppm]**	**Rb [ppm]**	**K [%]**	**Depth [m]**
TAI 1	1.21 ± 0.01	0.02 ± 0.01	0.21 ± 0.01	0.02 ± 0.01	0.5 ± 0.1
TAI 15	0.80 ± 0.01	0.03 ± 0.01	0.17 ± 0.01	0.01 ± 0.01	0.5 ± 0.1
TAI 18	1.28 ± 0.01	0.03 ± 0.01	0.24 ± 0.01	0.02 ± 0.01	0.5 ± 0.1

TAI 19A	1.40 ± 0.01	0.03 ± 0.01	0.14 ± 0.01	0.01 ± 0.01	0.3 ± 0.1
TAI 19B	1.44 ± 0.01	0.04 ± 0.01	0.16 ± 0.01	0.01 ± 0.01	0.3 ± 0.1
TAI 19 (average)	1.42 ± 0.01	0.04 ± 0.01	0.15 ± 0.01	0.01 ± 0.01	0.3 ± 0.1
TAI 20	0.68 ± 0.01	0.07 ± 0.01	0.55 ± 0.01	0.02 ± 0.01	0.5 ± 0.1

TABLE D.6: **Radio-element concentrations for the Taibeh heated flint samples.**

D.5 Dose rate table

Sample	$\dot{D}_\alpha$ **[Gy] (flint)**		$\dot{D}_\beta$ **[Gy] (flint)**	$\dot{D}_\gamma$ **[Gy] (sediment)**	$\dot{D}_c$ **[Gy]**
	MAAD	**SAR**			
TAI 1	0.82 ± 0.1	0.71 ± 0.09	0.19 ± 0.17	0.25 ± 0.04	0.22 ± 0.02
TAI 15	0.31 ± 0.05	0.44 ± 0.05	0.13 ± 0.11	0.25 ± 0.04	0.22 ± 0.02
TAI 18	0.74 ± 0.09	0.86 ± 0.1	0.2 ± 0.18	0.25 ± 0.04	0.22 ± 0.02
TAI 19	0.73 ± 0.09	0.86 ± 0.11	0.21 ± 0.19	0.25 ± 0.04	0.22 ± 0.02
TAI 20	0.34 ± 0.04	0.34 ± 0.04	0.12 ± 0.1	0.25 ± 0.04	0.22 ± 0.02

TABLE D.7: α, β **and** γ **Dose rates for the Taibeh heated flint samples.**

D.6 Radiocarbon ages

COL #	**Sample ID**	**Conv. Age [years BP]**	$\delta^{13}C$ [‰]	**calBP** (2σ)	**Pretreatment**
2820.0.1	TB3_1	14705 ± 75	-17.7	17666 -18101	AAA
2826.1.2	TB3_7	23637 ± 133	-32.5	27516-27968	AAA
2833.1.1	TB3_14	18145 ± 96	-17.6	21727-22304	AAA

TABLE D.8: **Radiocarbon ages.** All samples are charcoal samples. The calibrated radiocarbon ages were estimated using *Calib 7.2* and the *IntCal13 Northern Hemisphere atmospheric radiocarbon calibration curve.*

Reference paper

IntCal13 (Reimer et al., 2013.)

D.7 Input table for the *TLdating* package in R

code	TAI 1		TAI 15		TAI 18		TAI 19		TAI 20	
sa_gr_project_str	SFB_806_F2									
sa_gr_site_str	Taibeh									
sa_gr_year_val	2010									
sa_gr_name_str	TAI_F1		TAI_F15		TAI_F18		TAI_F19		TAI_F20	
de_in_protocol_str	MAAD	SAR	MAAD	SAR	MAAD	SAR	MAAD	SAR	MAAD	SAR
de_in_k_val	1.5									
de_pt_remDisc_bin	FALSE	FALSE	FALSE	FALSE	FALSE	FALSE	FALSE	FALSE	FALSE	TRUE
de_pt_alignPeak_bin	TRUE									
de_pt_remDisc_str	-	-	-	-	-	-	-	-	-	7
de_an_eval_min	330		350		350		340		340	
de_an_eval_max	370		390		390		380		380	
de_an_fit_str	LIN									
de_an_fitWeight_bin	TRUE									
de_an_reuseSlope_bin	TRUE									
de_an_addDose_min	0	-	0	-	0	-	0	-	0	-
de_an_addDose_max	800	-	800	-	800	-	800	-	800	-
de_an_regDose_min	150	150	150	150	150	150	150	150	150	150
de_an_regDose_max	800	800	800	800	800	800	800	800	800	800
de_an_rejMaxLxErr_val	10									
de_an_rejMaxTxErr_val	10									
de_an_rejRecycling_val	-	10	-	10	-	10	-	10	-	10
de_an_rejRecup_val	-	10	-	10	-	10	-	10	-	10
de_re_errApproach_str	GROWTH CURVE									
de_re_errMethod_str	WEIGHTED									
de_re_average_str	MEAN									
de_re_averageErr_str	SD									

code	TAI 1		TAI 15		TAI 18		TAI 19		TAI 20	
de_re_betaDr_val	0.1058									
de_re_betaDr_err	0									
av_in_protocol_str	MAAD	SAR	MAAD	SAR	MAAD	SAR	MAAD	SAR	MAAD	SAR
av_in_k_val	1.5									
av_pt_remDisc_bin	TRUE	FALSE	FALSE	FALSE	FALSE	FALSE	FALSE	FALSE	FALSE	FALSE
av_pt_alignPeak_bin	TRUE									
av_pt_remDisc_str	1, 11	-	-	-	-	-	-	-	-	-
av_an_eval_min	330		360	380	350	360	340	350	350	360
av_an_eval_max	370		420	420	390	400	380	390	390	400
av_an_fit_str	LIN									
av_an_fitWeight_bin	TRUE									
av_an_reuseSlope_bin	TRUE									
av_an_addDose_min	0	-	0	-	0	-	0	-	0	-
av_an_addDose_max	800	-	800	-	800	-	800	-	800	-
av_an_regDose_min	150	150	100	100	150	150	150	150	150	150
av_an_regDose_max	800	800	800	800	800	800	800	800	800	800
av_an_rejMaxLxErr_val	10									
av_an_rejMaxTxErr_val	10									
av_an_rejRecycling_val	-	10	-	10	-	10	-	10	-	10
av_an_rejRecup_val	-	10	-	10	-	10	-	10	-	10
av_re_errApproach_str	GROWTH CURVE									
av_re_errMethod_str	-	WEIGHTED	-	WEIGHTED	-	WEIGHTED	-	WEIGHTED	-	WEIGHTED
av_re_average_str	-	MEAN	-	MEAN	-	MEAN	-	MEAN	-	MEAN
av_re_averageErr_str	-	SD	-	SD	-	SD	-	SD	-	SD
av_re_betaDr_val	0.115									
av_re_betaDr_err	0									
av_re_alphaDose_val	400									
av_re_alphaDose_err	1									
av_re_alphaDr_val	0.1968									

code	TAI 1	TAI 15	TAI 18	TAI 19	TAI 20
av_re_alphaDr_err	0				
dr_gr_context_str	FLINT				
dr_gr_mineral_str	Q				
dr_gr_conversion_str	Liritzisetal2013				
dr_gr_alphaAttenuation_str	Brennanetal1991				
dr_gr_betaAttenuation_str	Guerinetal2012-Q				
dr_gr_etchAttenuation_str	Brennan2003				
dr_m1_U_val	1.21	0.8	1.28	1.4	0.68
dr_m1_U_err	0.005				
dr_m1_Th_val	0.02	0.03	0.03	0.03	0.07
dr_m1_Th_err	0.005				
dr_m1_K_val	0.02	0.01	0.02	0.01	0.02
dr_m1_K_err	0.005				
dr_m1_Rb_val	0.21	1.21	0.24	0.14	0.55
dr_m1_Rb_err	0.005				
dr_m1_density_val	2.65				
dr_m1_density_err	0.2				
dr_m1_grainSize_min	100				
dr_m1_grainSize_max	200				
dr_m1_grainEtch_min	0				
dr_m1_grainEtch_max	0				
dr_m2_U_val	0.73				
dr_m2_U_err	0.12				
dr_m2_Th_val	2.95				
dr_m2_Th_err	0.40				
dr_m2_K_val	0.18				
dr_m2_K_err	0.06				
dr_m2_K2Kb_bin	TRUE				
dr_m2_density_val	1.8				

code	TAI 1	TAI 15	TAI 18	TAI 19	TAI 20
dr_m2_density_err			0.1		
dr_m2_waterContent_val			5		
dr_m2_waterContent_err			3		
dr_dc_latitude_val			31.9544		
dr_dc_longitude_val			35.3003		
dr_dc_altitude_val			700		
dr_dc_depth_val			0.4		
dr_dc_depth_err			0.2		

Reference papers

Brennan2003 (Brennan, 2003)

Brennanetal1991 (Brennan et al., 1991)

Guerinetal2012-Q (Guerin et al., 2012)

Liritzisetal2013 (Liritzis et al., 2013)

D.8 Selection of plateau and growth curves

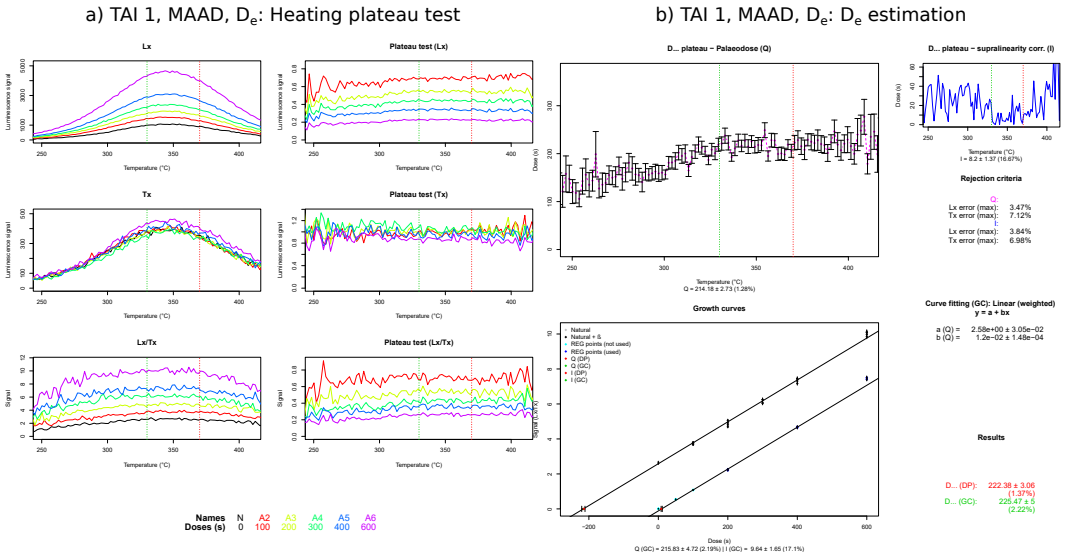


FIGURE D.2: **TL curves for the D_e estimation of the TAI 1 sample using the MAAD protocol:** (a) Average TL signal and heating plateau test curves; (b) D_e plateau and growth curves.

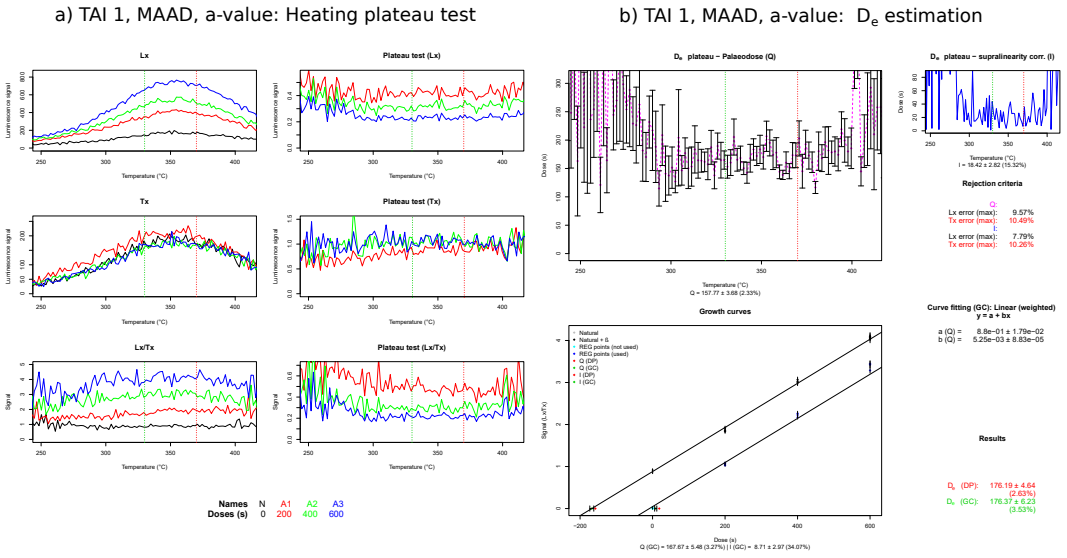


FIGURE D.3: **TL curves for the *a-value* estimation of the TAI 1 sample using the MAAD protocol:** (a) Average TL signal and heating plateau test curves; (b) D_e plateau and growth curves.

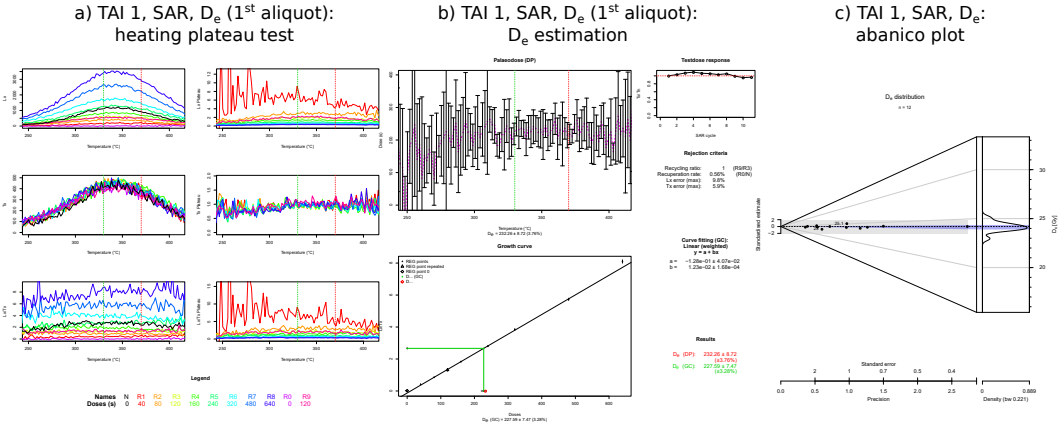


FIGURE D.4: **TL curves for the D_e estimation of the TAI 1 sample using the SAR protocol:** (a) Average TL signal and heating plateau test curves; (b) D_e plateau and growth curves.

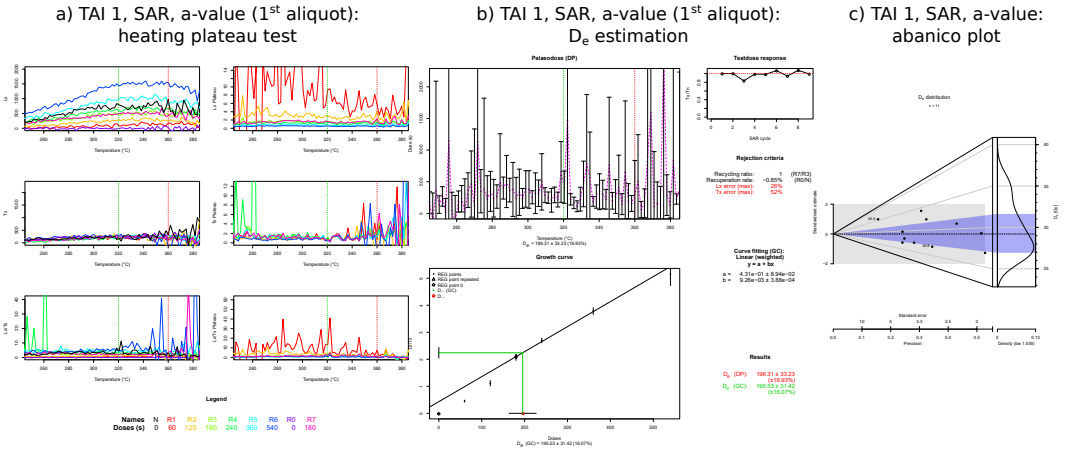


FIGURE D.5: **TL curves for the *a-value* estimation of the TAI 1 sample using the SAR protocol:** (a) Average TL signal and heating plateau test curves; (b) D_e plateau and growth curves.

Appendix E

Alpha source Calibration

The α-irradiation unit of the *Lexsyg Research Imaging TL-OSL-RF-System* from *Freiberg Instruments* of the Cologne Luminescence Laboratory (CLL) was cross calibrated using the α source from the Heidelberg Luminescence Laboratory (HLL). The irradiation took place in November 2015 and the calibration in April 2016.

The calibration was made using fine grain aliquots (0.38 mg of material/disc) from a known sediment sample (IN8). In total 100 discs were irradiated in the HLL. Half of them were irradiated during 30 min and the other half during 60 min. The two irradiation times were selected to remains in the linear section of the α growth curve. For each disc, an exact α-dose was provided by the HLL. Before being α-irradiated, the aliquots were bleached in a furnace at $280°C$ for 2 h.

Among these 100 α-irradiated discs, 2 were used for testing, 48 (24 for each of the two irradiation times) were used for the calibration and 50 were kept in case of a second calibration need to be done in the future.

The calibration was made using a SAR protocol. Prior to the calibration, a series of test were made, using IN 8 fine grain aliquots, to determine the best measurement parameters. These tests includes: (1) variation of the laser power and filter combination to check the stability of the signal and the combination providing the best signal (380 nm at 60 mW) and (2) the Preheat plateau test. The final SAR protocol integrates: (1) a Preheat (Lx) at $240°C$, (2) a Cutheat (Tx) at $220°C$ and (3) a hot bleach at $220°C$.

The dose rate was estimated using 3 different fitting and a dose plateau test was made to select the best integration interval:

- LIN (full): estimates the D_e using all data available and a weight linear fitting.

- LIN (short): estimates the D_e using only the reg. doses ¿ 2000s and a weight linear fitting.
- EXP (full) e estimates the D_e using all data available and an exponential fitting.

It was determined that integrating on the 4 first channel for the signal and using the 25 last channel for the background provide a reliable estimation of the dose rate.

Finally, the dose rate obtained when doing a linear regression base on the dose rate calculated using the EXP fitting was selected as the best approximation of the "real" dose rate reaching the FG.

$$\dot{D}_\alpha = 0.197 \pm 0.004 Gy/s \tag{E.1}$$

Sequence used for the SAR protocol

1. Enable nitrogen
2. Irradiation (Alpha - Lx)
   - Nat. : "720 s" or "1440 s" (HLL)
   - Reg. (Dose) : 360 - 720 – 1080 – 1440 – 2160 – 2880 – 0 – 720 s
3. TL (preheat)
   - Heating: $5°C/s$, $25°C - 240°C$, for 10 s, cool to $60°C$
   - Detection (TL): After 0 s, for 54 s ; channel time: 0.25 s ; H7360-02 (UV/VIS) - TL – 475 nm.
4. GSL (Lx)
   - Heating: $5°C/s$, $25°C - 125°C$, for 90 s, cool to $60°C$
   - Stimulation: $60 mW/cm^2$; After 30 s, for 80 s.
   - Detection: After 30 s, for 80 s ; channel time: 0.32 s ; H7360-02 (UV/VIS): greenOSL – 380 nm
5. Irradiation (Alpha - Tx)
   - Test: 480 s
6. TL (cutheat)
   - Heating: $5°C/s$, $25°C - 220°C$, cool to $60°C$

- Detection (TL): After 0 s, for 39 s ; channel time: 0.25 s ; H7360-02 (UV/VIS): TL – 475 nm

7. GSL (Tx)
   - Heating: $5°C/s$, $25°C - 125°C$ for 90 s, cool to $60°C$
   - Stimulation: $60mW/cm^2$; After 30 s, for 80 s.
   - Detection: After 30 s, for 80 s ; channel time 0.32 s ; H7360-02 (UV/VIS): greenOSL – 380 nm
8. GSL (Hot bleach)
   - Heating: $5°C/s$, $25°C - 280°C$ for 50 s, cool to $60°C$
   - Stimulation $60mW/cm^2$; After 61 s, for 40 s.
   - Detection: After 35 s, for 40 s ; channel time: 0.32 s ; H7360-02 (UV/VIS): greenOSL – 380 nm
9. Disable nitrogen

Appendix F

Roman traces in Germania Magna: New thermoluminescence and pIRIR$_{290}$ data from a lime kiln at Bergisch Gladbach, Germany - Online supplement

F.1 Tables

TL-MAAD					
1	Disc 1-2	Nat	Preheat 120s@220°C	TL 5°/s@480°C	TL 5°/s@480°C
2	Disc 3-4	Nat + D1 ß	Preheat 120s@220°C	TL 5°/s@480°C	TL 5°/s@480°C
3	Disc 5-6	Nat + D2 ß	Preheat 120s@220°C	TL 5°/s@480°C	TL 5°/s@480°C
4	Disc 1-6	TL 5°/s@480°C			
5	Disc 1-6	Beta dose	Preheat 120s@220°C	TL 5°/s@480°C	TL 5°/s@480°C

TABLE F.1: **Luminescence measuring protocol used for multiple aliquot additive dose (MAAD) TL dating.** Two discs each were measured for the natural signal and additive dose signal. Step 4 works as a reset, step 5 records the signal for normalisation.

	$\mathbf{IR_{50}}$		$\mathbf{pIRIR_{290}}$		**TL-SAR**	
1	Nat/Regen dose		Nat/Regen dose		Nat/Regen dose	
2	Preheat $60s$@$210-270°C$		Preheat $60s$@$320°C$		$Preheat120s$@$220°C$	
3	IR $200s$@$50°C$	Lx	IR $200s$@$50°C$		TL $5°C/s$@$480°C$	Lx
4	Test dose		pIRIR $200s$@$290°C$	Lx	TL $5°C/s$@$480°C$	
5	Preheat $60s$@$210-270°C$		Test dose		Test dose	
6	IR $200s$@$50°C$		Preheat $60s$@$320°C$		Preheat $120s$@$220°C$	
7	Repeat	Tx	IR $200s$@$50°C$		TL $5°C/s$@$480°C$	Tx
8			pIRIR $200s$@$290°C$	Tx	TL $5°C/s$@$480°C$	
9			pIRIR $40s$@$325°C$		Repeat	
			Repeat			

TABLE F.2: **Single aliquot regeneration (SAR) measuring protocols used for IRSL and TL dating.**

Sample ID	**Material**	**Water cont.**		**Depth**	**Cosmic dose**	**U**	**Th**	**K**
		meas. (%)	**used (%)**	**(mbs)**	**(Gy/ka)**	**(ppm)**	**(ppm)**	**(%)**
BGB1	kiln wall	10.1	10	1.50	182 ± 18	2.52 ± 0.12	11.16 ± 0.56	3.13 ± 0.05
BGB1	limestone mix	25.1	25	1.50	182 ± 18	1.26 ± 0.07	1.09 ± 0.12	0.32 ± 0.01
BGB2	kiln wall	10.1	10	1.45	183 ± 18	2.59 ± 0.12	11.33 ± 0.57	3.13 ± 0.05
BGB2	limestone mix	25.0	25	1.45	183 ± 18	1.26 ± 0.08	1.21 ± 0.17	0.33 ± 0.01
BGB3	kiln wall	9.4	10	1.20	188 ± 19	2.61 ± 0.12	10.45 ± 0.53	2.93 ± 0.05
BGB3	sediment	14.2	15	1.20	188 ± 19	2.27 ± 0.11	10.64 ± 0.54	2.72 ± 0.05
BGB3	limestone mix	16.9	15	1.20	188 ± 19	2.42 ± 0.12	7.66 ± 0.42	1.92 ± 0.03
BGB4	sediment	13.3	15	1.40	184 ± 18	2.24 ± 0.11	10.60 ± 0.53	2.85 ± 0.05
BGB5	sediment	14.7	15	1.80	177 ± 18	2.26 ± 0.11	10.41 ± 0.53	2.80 ± 0.05
BGB6	sediment	24.3	25	0.15	243 ± 24	2.94 ± 0.13	8.96 ± 0.57	2.09 ± 0.04
BGB6	roof tile	6.1	7	0.15	243 ± 24	2.50 ± 0.50	11.5 ± 0.80	3.10 ± 0.30

TABLE F.3: **Dose rate determination results using high resolution gamma-ray spectrometry.** To account for potential variations of the different materials, up to 3 dose rate samples were measured. Water contents are given in relation to dry mass.

	Labcode	**Sample ID**	**Recycling Ratio**	**Recuperation (%)**	**a-value**	**Dose recovery ratio#**	**Dose recovery ratio&**	**g-value**
$TL - SAR$	C-L3849	BGB 1	1.00	0.07	0.094	0.93 ± 0.05		
	C-L3850	BGB 2	1.00	0.33	0.100	0.94 ± 0.04		
	C-L3851	BGB 3	1.02	0.87	0.090	0.91 ± 0.01		
	C-L3852	BGB 4	1.05	0.04	0.090	0.89 ± 0.03		
	C-L3853	BGB 5	1.00	0.02	0.090	1.08 ± 0.08		
	C-L3854	BGB 6	1.00	0.05	0.094	0.90 ± 0.01		
$IRSL - SAR$	C-L3849		1.06	4.1	0.094	0.99 ± 0.03	-	0.71 ± 1.43
	C-L3850		1.08	2.9	0.092	0.98 ± 0.05	0.81 ± 0.02	0.20 ± 1.49
	C-L3851		1.10	4.6	0.092	0.94 ± 0.04	0.80 ± 0.07	-0.61 ± 1.48
	C-L3852		*1.03	*3.2	*0.065	$^*0.97 \pm 0.05$	$^*1.01 \pm 0.06$	$^*2.58 \pm 0.83$
	C-L3853		*1.01	*6.2	*0.062	$^*1.00 \pm 0.04$	$^*1.00 \pm 0.05$	$^*3.65 \pm 1.05$
	C-L3854		-	-	-	0.83 ± 0.03	0.76 ± 0.02	-

TABLE F.4: **Results of the quality check measurements for the TL-SAR and $pIRIR_{50\&290}$ protocols**. # = discs were thermally reset by a $480°C$ TL measurement & = discs were reset in an SOL2 solar simulator for 24 hrs * measurements made by an IR50 protocol (pIRIR290 unsuccessful).

COL#	**Material**	**F ^{14}C**	**Conv. Age (yrs BP)**	δ^{13}**C*** (‰)	**Calendar age**, 2σ **(cal. AD)**
COL3203.1.1	Bone	0.804 ± 0.003	1751 ± 34	-23.6	$175 - 390$
COL3453.1.1	Charcoal	0.782 ± 0.004	1976 ± 40	-20.4	$54 - 125$

TABLE F.5: **Radiocarbon ages were calibrated using OxCal V 4.2.3.**

F.2 Figures

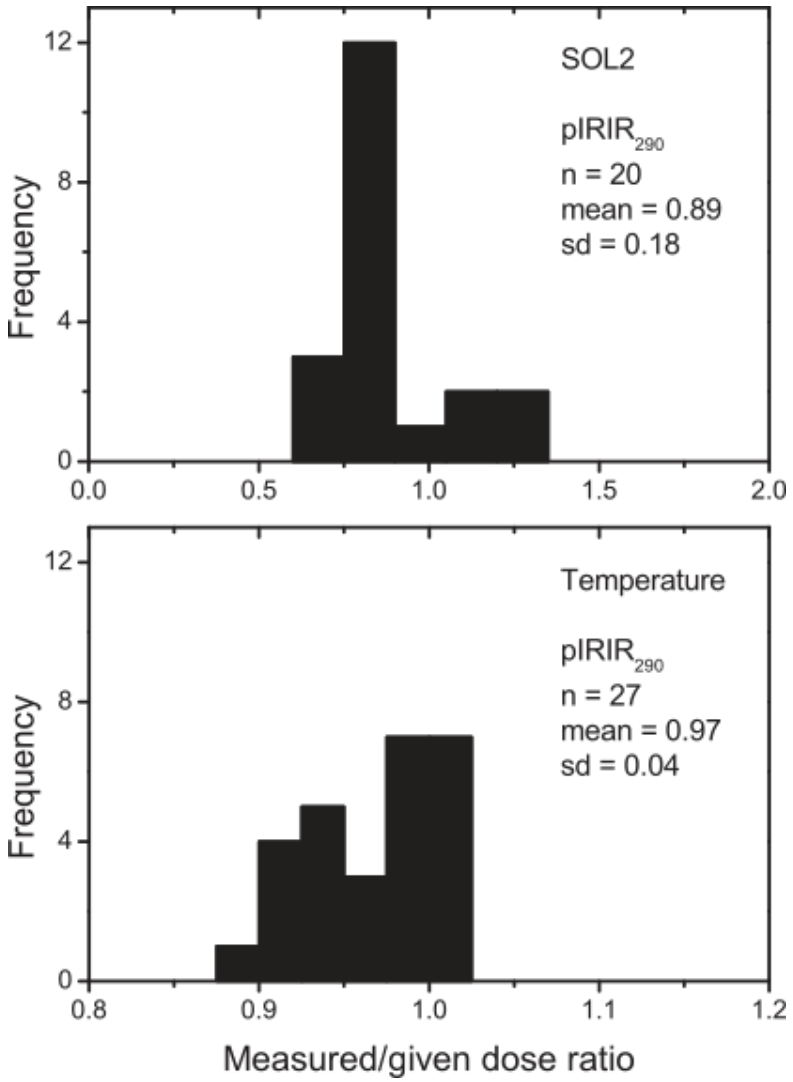


FIGURE F.1: **IRSL dose recovery tests obtained for the pIRIR290 protocol (BGB 1, 2, 3) and the IR50 protocol (BGB 4, 5).** # = discs were thermally reset by a $480°C$ TL measurement. & = discs were reset in an SOL2 solar simulator for 24 hr. * = measurements were made by an IR_{50} protocol ($pIRIR_{290}$ unsuccessful).

Bibliography

, 1979. Thermoluminescence techniques in archaeology, Clarendon Press, Oxford, pp. 1–233.

Adamiec, G., Aitken, M., 1998. Dose rate conversion factors : update. Ancient TL 16 (2), 37–50.

Adamiec, G., Heer, A.J., Bluszcz, A., 2012. Statistics of count numbers from a photomultiplier tube and its implications for error estimation. Radiation Measurements 47, 746 – 751. URL: http://www.sciencedirect.com/science/article/pii/S1350448711005750, doi:http://dx.doi.org/10.1016/j.radmeas.2011.12.009.

Agam, A., Azuri, I., Pinkas, I., Gopher, A., Natalio, F., 2021. Estimating temperatures of heated lower palaeolithic flint artefacts. Nature Human Behaviour 5, 221–228.

Aitken, M., 1969. Thermoluminescence dosimetry of environmental radiation on archaeological sites. Archaeometry 11, 109–114.

Aitken, M., 1985a. Thermoluminescence Dating. Academic Press, Oxford.

Aitken, M. (Ed.), 1990. Science-based dating in archaeology. Longman, London.

Aitken, M., 1998. An Introduction to Optical Dating. The Dating of Quaternary Sediments by the Use of Photon-stimulated Luminescence. Oxford University Press, Oxford.

Aitken, M., Reid, J., Tite, M., 1964. Thermoluminescence dating of ancient ceramics. Nature 202, 1032–1033. doi:10.1038/2021032b0.

Aitken, M., Wintle, A., 1977. Thermoluminescence dating of calcite and burnt flint: the age relation for slices. Archaeometry 1, 100–105.

Aitken, M.J., 1985b. Thermoluminescence Dating: past progress and future trends. Nucl. tracks. 10, 3–6.

Ankjaergaard, C., Guralnik, B., Buylaert, J.P., Reimann, T., Yi, S.W., Wallinga, J., 2016. Violet stimulated luminescence dating of quartz from Luochuan (Chinese

Loess Plateau): agreement with independent chronology up to 600 ka. Quaternary Geochronology , –URL: http://www.sciencedirect.com/science/article/pii/S1871101416300115, doi:http://dx.doi.org/10.1016/j.quageo.2016.03.001.

Ankjaergaard, C., Guralnik, B., Porat, N., Heimann, A., Jain, M., Wallinga, J., 2015. Violet stimulated luminescence: geo- or thermochronometer? Radiation Measurements 81, 78 – 84. URL: http://www.sciencedirect.com/science/article/pii/S1350448715000128, doi:http://dx.doi.org/10.1016/j.radmeas.2015.01.011.

Ankjaergaard, C., Jain, M., Wallinga, J., 2013. Towards dating Quaternary sediments using the quartz Violet Stimulated Luminescence (VSL) signal. Quaternary Geochronology 18, 99 – 109. URL: http://www.sciencedirect.com/science/article/pii/S1871101413000617, doi:http://dx.doi.org/10.1016/j.quageo.2013.06.001.

Auclair, M., Lamothe, M., Huot, S., 2003. Measurement of anomalous fading for feldspar irsl using sar. Radiation Measurements 37, 487–492. doi:10.1016/S1350-4487(03)00018-0.

Aydas, C., Engin, B., Aydin, T., 2011. Radiation-induced signals of gypsum crystals analysed by ESR and TL techniques applied to dating. Nuclear Istruments and Methods in Physics Research B 269, 417–424.

Bailiff, I., 2007. Methodological developments in the luminescence dating of brick from English late medieval and post medieval buildings. Archaeometry 49, 827–851.

Bailiff, I., 2008. New developments in the scientific dating of bricks, in: Medieval brick architecture in Flanders and Northern Europe: the question of the Cistercian origin,. Gent: Academia Press, Koksijde, Belgium, p. 133–144.

Bailiff, I., Blain, S., Graves, C., Gurling, T., Semple, S., 2010. Uses and recycling of brick in medieval English buildings: insights from the application of luminescence dating and new avenues for further research. The Archaeological Journal 167, 165–196.

Bailiff, I., Holland, N., 2000. Dating Bricks of the two millennia from Newcastle upon Tyne : a preliminary study. Radiation Measurements 32, 615–619.

Bailiff, I., Lacey, H., Coningham, R., Gunawardhana, P., Adikari, G., Davis, C., Manuel, M., Strickland, K., 2013. Luminescence dating of brick stupas: an application to the hinterland of Anuradhapura, Sri Lanka. Antiquity 87, 189–201.

Bailiff, I.K., Morris, D.A., Aitken, M.J., 1977. A rapid-scanning interference spectrometer: application to low-level thermoluminescence emission. Journal of Physics E: Scientific Instruments 10, 1156–1160. URL: https://doi.org/10.1088%2F0022-3735%2F10%2F11%2F019, doi:10.1088/0022-3735/10/11/019.

Bartz, M., Duval, M., Brill, D., Zander, A., King, G., Rhein, A., Walk, J., Stauch, G., Lehmkuhl, F., Brückner, H., 2020. Testing the potential of k-feldspar pir-irsl and quartz esr for dating coastal alluvial fan complexes in arid environments. Quaternary International doi:10.1016/j.quaint.2020.03.037.

Bassinet, C., Mercier, N., Miallier, D., Pilleyre, T., Sanzelle, S., Valladas, H., 2006. Thermoluminescence of heated quartz grains: Intercomparisons between SAR and multiple-aliquot additive dose techniques. Radiation Measurements 41, 803–808. URL: http://www.sciencedirect.com/science/article/pii/S1350448706000333, doi:http://dx.doi.org/10.1016/j.radmeas.2006.04.013.

Bateman, M.D., Frederick, C.D., Jaiswal, M.K., Singhvi, A.K., 2003. Investigations into the potential effects of pedoturbation on luminescence dating. Quaternary Science Reviews 22, 1169–1176. URL: https://www.sciencedirect.com/science/article/pii/S0277379103000192, doi:https://doi.org/10.1016/S0277-3791(03)00019-2. lED 2002.

Belfer-Cohen, A., Goring-Morris, A., 2007. From the Beginning: Levantine Upper Palaeolithic Cultural Change and Continuity, in: Mellars, P., Boyle, K., Bar-Yosef, O., Stringer, C. (Eds.), Rethinking the human revolution. McDonald Institute for Archaeological Research, Cambridge, Cambridge, UK, pp. 199–206.

Bell, W., 1976. The assessment of the radiation dose-rate for thermoluminescence dating. Archaeometry 18, 107–111.

Bell, W., 1980. Alpha attenuation in quartz grains for thermoluminescence dating. Ancient TL 12, 4–8.

Benazzi, S., Douka, K., Fornai, C., Bauer, C.C., Kullmer, O., Svoboda, J., Pap, I., Mallegni, F., Bayle, P., Coquerelle, M., Condemi, S., Ronchitelli, A., Harvati, K., Weber, G.W., 2011. Early dispersal of modern humans in europe and implications for neanderthal behaviour. Nature 479, 525–528. doi:10.1038/nature10617.

Bertrams, M., Protze, J., Löhrer, R., Schyle, D., Richter, J., Hilgers, A., Klasen, N., Schmidt, C., Lehmkuhl, F., 2012a. Multiple environmental change at the time of the modern human passage through the middle east: First results from geoarcheological investigations on upper pleistocene sediments in the wadi sabra (jordan). Quaternary International 274, 55–72. doi:10.1016/j.quaint.2012.02.047.

Bertrams, M., Protze, J., Schyle, D., Klasen, N., Richter, J., Lehmkuhl, F., 2012b. A preliminary model of upper pleistocenelandscape evolution in the wadi sabra (jordan) based on geoarchaeological investigations. ETopoi J Anc Stud. 3, 229–236.

Blain, S., 2009. Les terres cuites architecturales des églises du haut Moyen age dans le nord-ouest de la France et le sud-est de l'Angleterre. Ph.D. thesis. Sciences archéologiques Bordeaux 3 2009. URL: http://www.theses.fr/2009BOR30038. phD Thesis directed by Bailiff, Ian and Guibert, Pierre.

Blain, S., Bailiff, I.K., Guibert, P., Bouvier, A., Baylé, M., 2010. An inter-comparison study of luminescence dating protocols and techniques applied to medieval brick samples from Normandy (France). Quaternary Geochronology 5, 311 – 316. URL: http://www.sciencedirect.com/science/article/pii/S1871101409000405, doi:http://dx.doi.org/10.1016/j.quageo.2009.02.016.

Blain, S., Guibert, P., Bouvier, A., Vieillevigne, E., Bechtel, F., Sapin, C., Baylé, M., 2007. TL-dating applied to building archaeology: The case of the medieval church Notre-Dame-Sous-Terre (Mont-Saint-Michel, France). Radiation Measurements 42, 1483 – 1491. URL: http://www.sciencedirect.com/science/article/pii/S1350448707003149, doi:http://dx.doi.org/10.1016/j.radmeas.2007.07.015.

Blair, M., Kalchgruber, R., McKeever, S., 2007. Developing luminescence dating for extraterrestrial applications: Characterization of martian simulants and minerals. Radiation Measurements 42, 392–399.

Bluszcz, A., Bøtter-Jensen, L., 1995. Dosimetric properties of natural quartz grains extracted from fired materials. Radiation Measurements 24, 465 – 468. URL: http://www.sciencedirect.com/science/article/pii/135044879500005Y, doi:http://dx.doi.org/10.1016/1350-4487(95)00005-Y.

Bortolot, V., 2000. A new modular high capacity osl reader system. Radiation Measurements 32, 751 – 757. URL: http://www.sciencedirect.com/science/article/pii/S135044870000038X, doi:https://doi.org/10.1016/S1350-4487(00)00038-X.

Botter-Jensen, L., Agersnap Larsen, N., Mejdahl, V., Poolton, N., Morris, M., McKeever, S., 1995. Luminescence sensitivity changes in quartz as a result of annealing. Radiation Measurements 24, 535–541.

Bowman, S., 1975. Dependance of supralinearity on pre-dose : some observations. Archaeometry 17, 129–132.

Bowman, S., Seeley, M.A., 1978. The BritishMuseum Flint Dating Project. PACT Spec. Semim. Thermolumin. Dating 1-2, 151–164.

Bowman, S., Sieveking, G.d.G., 1983. Thermoluminescence dating of burnt flint from Combe Grenal. PACT 9, 253–268.

Boyle, S.R., 1664. Experiments and Considerations upon Colours - with Observations on a Diamond that shines in the Dark.

Brass, M., Schwenniger, J.L., 2013. Jebel moya (sudan): new dates from a mortuary complex at the southern meroitic frontier, azania. Archaeological Research in Africa 48, 455–472. doi:,10.1080/0067270X.2013.843258.

Brennan, B., 2003. Beta doses to spherical grains. Radiation Measurements 37, 299–303.

Brennan, B., Lyons, R., Phillips, S., 1991. Attenuation of alpha particle track dose for spherical grains. international journal of radiation applications and instrumentation. Part D. Nuclear Tracks and Radiation Measurements 18, 249–253.

Brown, F.H., McDougall, I., Fleagle, J.G., 2012. Correlation of the khs tuff of the kibish formation to volcanic ash layers at other sites, and the age of early homo sapiens (omo i and omo ii). Journal of human evolution 63, 577—585. URL: https://doi.org/10.1016/j.jhevol.2012.05.014, doi:10.1016/j.jhevol.2012.05.014.

Buylaert, J., Jain, M., Murray, A., Thomsen, K., Thiel, C., Sohbati, R., 2012. A robust feldspar luminescence dating method for middle and late pleistocene sediments. Boreas 41, 435–451. doi:10.1111/j.1502-3885.2012.00248.x.

Buylaert, J.P., Murray, A.S., Thomsen, K.J., Jain, M., 2009. Testing the potential of an elevated temperature {IRSL} signal from K-feldspar. Radiation Measurements 44, 560 – 565. URL: http://www.sciencedirect.com/science/article/pii/S1350448709000316, doi:http://dx.doi.org/10.1016/j.radmeas.2009.02.007.

Bösken, J., Schmidt, C., Kolb, T., 2017. Testing the possibility of a common a-value for pIRIR290 protocols of polymineral fine grains, in: 15th International Conference on Luminescence and Electron Spin Resonance Dating, Capetown, South Africa.

Bøtter-Jensen, L., Thomsen, K., Jain, M., 2010. Review of optically stimulated luminescence (osl) instrumental developments for retrospective dosimetry. Radiation Measurements 45, 253–257.

Cann, R.L., Stoneking, M., Wilson, A.C., 1987. Mitochondrial dna and human evolution. Nature 325, 31–36.

Chacon, S., Straub, B., 2014. Pro Git. 2nd ed., Apress, USA.

Chang, W., Cheng, J., Allaire, J.J., Xie, Y., McPherson, J., 2016. shiny: Web Application Framework for R. URL: https://CRAN.R-project.org/package=shiny.

Chapot, M.S., Roberts, H.M., Duller, G.A.T., Lai, Z.P., 2016. Natural and laboratory TT-OSL dose response curves: Testing the lifetime of the TT-OSL signal in nature. Radiation Measurements 85, 41 – 50. URL: http://www.sciencedirect.com/science/article/pii/S1350448715300792, doi:http://dx.doi.org/10.1016/j.radmeas.2015.11.008.

Chruscinska, A., Cicha, A., Kijek, N., Palczewski, P., Przegietka, K., Sulkowska-Tuszynska, K., 2014. Luminescence dating of bricks from the gothic saint james church in torun. Geochronometria 41, 352–360. doi:doi:10.2478/s13386-013-0165-y.

Clark, R., Sanderson, D., 1994. Photostimulated luminescence excitation ofspectroscopy of feldspars and micas. Radiation Measurements 23, 641–646.

Clark-Balzan, L., Schwenninger, J.L., 2012. First steps toward spatially resolved {OSL} dating with electron multiplying charge-coupled devices (EMCCDs): System design and image analysis. Radiation Measurements 47, 797 – 802. URL: http://www.sciencedirect.com/science/article/pii/S1350448712000820, doi:http://dx.doi.org/10.1016/j.radmeas.2012.01.018.

Classen, E., Gerlach, R., Nolde, N., Rethemeyer, J., Tegtmeier, U., Weber, H., Zander, A., 2016. Eine kalkbrennerei der römischen kaiserzeit in der germania magna. Archäologie im Rheinland 2015, 142–144.

Combès, B., Philippe, A., 2017. Bayesian analysis of individual and systematic multiplicative errors for estimating ages with stratigraphic constraints in optically stimulated luminescence dating. Quaternary Geochronology 39, 24 – 34. URL: http://www.sciencedirect.com/science/article/pii/S1871101416300838, doi:https://doi.org/10.1016/j.quageo.2017.02.003.

Daniels, F., Boyd, A., Saunders, D., 1953. Thermoluminescence as a Research Tool. Science 117, 343–349.

Dasbach, M., Selbach, M., 2015. Sensationelle entdeckungen im lehrbacher wald—waren die römer im raumbergisch gladbach? Heimat zwischen Sülz und Dhünn 21, 9–16.

Daybreak, 2001. Application software for Daybreak TL/OSL systems FirstLight 2.0. Daybreak Nuclear and Medical System, Inc.. USA.

Dean, J., 1978. Independent dating in archaeological analysis. Advances in Archaeological Method and Theory 1, 223–255.

Degering, D., Degering, A., 2020. Change is the only constant - time-dependent dose rates in luminescence dating. Quaternary Geochronology 58, 101074. doi:10.1016/j.quageo.2020.101074.

Demuro, M., Stone, A.E.C., Arnold, L.J., Creighton, D.F., Spooner, N.A., 2016. Initial results of 3D spectral measurements on handpicked quartz grains with diverse OSL behaviours, in: UK Luminescence and ESR meeting.

Detschel, M., Lepper, K., 2009. Optically stimulated luminescence dating properties of Martian sediment analogue materials exposed to a simulated Martian solar spectral environment. Journal of Luminescence 129, 393–400.

Dietze, M., Kreutzer, S., Burow, C., Fuchs, M.C., Fischer, M., Schmidt, C., 2016. The abanico plot: Visualising chronometric data with individual standard errors. Quaternary Geochronology 31, 12 – 18. URL: http://www.sciencedirect.com/science/article/pii/S1871101415300583, doi:http://dx.doi.org/10.1016/j.quageo.2015.09.003.

Dietze, M., Kreutzer, S., Fuchs, M.C., Burow, C., Fischer, M., Schmidt, C., 2013. A practical guide to the R package Luminescence. Ancient TL 31, 11–18. URL: http://www.aberystwyth.ac.uk/en/media/departmental/iges/ancienttl/pdf/vol31no1/dietze%5fatl13(1)%5f11.pdf. publisher: Aberystwyth Luminescence Laboratory, Institute of Geography and Earth Sciences, Aberystywth University (UK).

Duller, G., 1991. Equivalent dose determination using single aliquots. Nuclear Track and Radiation Measurements 18, 371–378.

Duller, G., 2003. Distinguishing quartz and feldspar in single grain luminescence measurements. Radiation Measurements 37, 161 – 165. URL: http://www.sciencedirect.com/science/article/pii/S1350448702001701, doi:https://doi.org/10.1016/S1350-4487(02)00170-1.

Duller, G., 2008. Luminescence dating: Guidelines on using luminescence dating in archaeology. English Heritage.

Duller, G., 2015a. The Analyst software package for luminescence data: overview and recent improvements. Ancient TL 33, 35–42. URL: http://www.ecu.edu/cs-cas/physics/Ancient-Timeline/upload/ATL_33-1_Duller_p35-42.pdf. place: Greenville, NC, USA.

Duller, G., 2015b. Analyst v4.31.7.

Duller, G., Murray, A., 2000. Luminescence dating of sediments using individual mineral grains. Geologos 5.

Duller, G.A.T., Bøtter-Jensen, L., Murray, A.S., Truscott, A.J., 1999. Single grain laser luminescence (SGLL) measurements using a novel automated reader.

Nuclear Instruments and Methods in Physics Research Section B: Beam Interactions with Materials and Atoms 155, 506 – 514. URL: http://www.sciencedirect.com/science/article/pii/S0168583X99004887, doi:http://dx.doi.org/10.1016/S0168-583X(99)00488-7.

Duller, G.A.T., Kook, M., Stirling, R.J., Roberts, H.M., Murray, A.S., 2015. Spatially-resolved thermoluminescence from snail opercula using an {EMCCD}. Radiation Measurements 81, 157 – 162. URL: http://www.sciencedirect.com/science/article/pii/S1350448715000153, doi:http://dx.doi.org/10.1016/j.radmeas.2015.01.014.

Duller, G.A.T., Wintle, A.G., 2012. A review of the thermally transferred optically stimulated luminescence signal from quartz for dating sediments. Quaternary Geochronology 7, 6 – 20. URL: http://www.sciencedirect.com/science/article/pii/S1871101411000525, doi:http://dx.doi.org/10.1016/j.quageo.2011.09.003.

Durcan, J.A., King, G.E., Duller, G., 2015. DRAC: Dose Rate and Age Calculator for trapped charge dating. Quaternary Geochronology 28, 54–61.

Dutkiewicz, A., Prescott, J., 1997. Thermoluminescence ages and paleoclimate from the Lake-Malata Lake-Greenly complex, Eyre Peninsula, South Australia. Quaternary science reviews 16, 367–385.

Duttine, M., Guibert, P., Perraut, A., Lahaye, C., Bechtel, F., Villeneuve, G., 2005. Effects of thermal treatment on tl and epr of flints and their importance in tl-dating: application to french mousterian sites of les forêts (dordogne) and jiboui (drôme). Radiation Measurements 39, 375 – 385. URL: http://www.sciencedirect.com/science/article/pii/S1350448704002410, doi:https://doi.org/10.1016/j.radmeas.2004.10.006.

Erlach, R., Vana, N., 1988. TL-dating of archaeological samples from carnuntum. Nuclear Track Radiation Measurements 14, 295–298.

van Es, H., Vainshtein, D., de Meijer, R., den Hartog, H., Donoghue, J., Rozendaal, A., 2002a. Mineral zircon: A novel thermoluminescence geochronometer. Radiation Effects and Defects in Solids 157, 1063–1070.

van Es, H., Vainshtein, D., Rozendaal, A., Donoghue, J., de Meijer, R., den Hartog, H., 2002b. Thermoluminescence of ZrSiO4 (zircon): A new dating method? Nuclear instruments and Methods in Physics Research B 191, 649–652.

Fairbanks, R.G., Mortlock, R.A., Chiu, T.C., Cao, L., Kaplan, A., Guilderson, T.P., Fairbanks, T.W., Bloom, A.L., Grootes, P.M., Nadeau, M.J., 2005. Radiocarbon calibration curve spanning 0 to 50,000 years bp based on paired

230th/234u/238u and 14c dates on pristine corals. Quaternary Science Reviews 24, 1781–1796. URL: https://www.sciencedirect.com/science/article/pii/S0277379105001654, doi:https://doi.org/10.1016/j.quascirev.2005.04.007.

Fattahi, M., Stokes, S., 2000. Extending the time range of luminescence dating using red TL (RTL) from volcanic quartz. Radiation Measurements 32, 479–485. URL: http://www.sciencedirect.com/science/article/pii/S1350448700001050, doi:http://dx.doi.org/10.1016/S1350-4487(00)00105-0.

Fattahi, M., Vahdani motlagh, S., 2016. The use of low-intensity led lamps for luminescence dating laboratory safe lighting. Quaternery Journal of Iran 2. arXiv:http://journal.iranqua.ir/article-1-70-en.pdf.

Feathers, J., 1997. Luminescence dating of sediment samples from White paintings Rockshelter, Botswana. Quaternary Science Reviews 16, 321–331. URL: http://www.sciencedirect.com/science/article/pii/S0277379196000832, doi:http://dx.doi.org/10.1016/S0277-3791(96)00083-2.

Fewlass, H., Talamo, S., Wacker, L., Kromer, B., Tuna, T., Fagault, Y., Bard, E., McPherron, S.P., Aldeias, V., Maria, R., Martisius, N.L., Paskulin, L., Rezek, Z., Sinet-Mathiot, V., Sirakova, S., Smith, G.M., Spasov, R., Welker, F., Sirakov, N., Tsanova, T., Hublin, J.J., 2020. A ^{14}c chronology for the middle to upper palaeolithic transition at bacho kiro cave, bulgaria. Nature Ecology & Evolution 4, 794–801. doi:10.1038/s41559-020-1136-3.

Fleagle, J., Shea, J., Grine, F., Baden, A., Leakey, R. (Eds.), 2010. Out of Africa I. Springer.

Fleming, S., 1966. Study of thermoluminescence of crystalline extracts from pottery. Archaeometry 9, 170–173.

Fleming, S., 1973a. The pre-dose technique : a new thermoluminescence dating method. Archaeometry 15, 13–30.

Fleming, S., 1973b. The subtraction technique of thermoluminescence dating. Archaeometry 15, 229–238.

Fleming, S., 1975. Supralinéarity corrections in fine grain thermoluminescence dating : a re-appraisal. Archaeometry 16, 91–95.

Fraser, J.A., Price, D.M., 2013. A thermoluminescence (TL) analysis of ceramics from cairns in Jordan: Using TL to integrate off-site features into regional chronologies. Applied Clay Science 82, 24 – 30. URL: http://

www.sciencedirect.com/science/article/pii/S0169131713001804, doi:http://dx.doi.org/10.1016/j.clay.2013.05.016.

Frechen, M., Schweitzer, U., Zander, A., 1996. Improvements in sample preparation for the fine grain technique. Ancient TL 14, 15–17.

Friedrich, J., Kreutzer, S., Schmidt, C., 2016. Solving ordinary differential equations to understand luminescence: 'RLumModel', an advanced research tool for simulating luminescence in quartz using R. Quaternary Geochronology 35, 88 – 100. URL: http://www.sciencedirect.com/science/article/pii/S1871101416300553, doi:http://dx.doi.org/10.1016/j.quageo.2016.05.004.

Fu, Q., Posth, C., Hajdinjak, M., Petr, M., Mallick, S., Fernandes, D., Furtwängler, A., Haak, W., Meyer, M., Mittnik, A., Nickel, B., Peltzer, A., Rohland, N., Slon, V., Talamo, S., Lazaridis, I., Lipson, M., Mathieson, I., Schiffels, S., Skoglund, P., Derevianko, A.P., Drozdov, N., Slavinsky, V., Tsybankov, A., Cremonesi, R.G., Mallegni, F., Gély, B., Vacca, E., González Morales, M.R., Straus, L.G., Neugebauer-Maresch, C., Teschler-Nicola, M., Constantin, S., Moldovan, O.T., Benazzi, S., Peresani, M., Coppola, D., Lari, Martina andRicci, S., Ronchitelli, A., Valentin, F., Thevenet, C., Wehrberger, K., Grigorescu, D., Rougier, H., Crevecoeur, I., Flas, D., Semal, P., Mannino, M.A., Cupillard, C., Bocherens, H., Conard, N.J., Harvati, K., Moiseyev, V., Drucker, D.G., Svoboda, J., Richards, M.P., Caramelli, D., Pinhasi, R., Kelso, J., Patterson, N., Krause, J., Pääbo, S., Reich, D., 2016. The genetic history of ice age europe. Nature 534, 200–205. doi:10.1038/nature17993.

Fu, X., Zhang, J., Mo, D., Shi, C., Liu, H., Li, Y., Zhou, L., 2010. Luminescence dating of baked earth and sediments from the qujialing archaeological site, china. Quaternary Geochronology 5, 353–359. doi:org/10.1016/j.quageo.2009.06.006.

Fuchs, M., Lang, A., 2001. Osl dating of coarse-grain fluvial quartz using single-aliqout protocols on sediments from ne peloponnese, greece. Quaternary Science Reviews 20, 783–787.

Fuchs, M.C., Kreutzer, S., Burow, C., Dietze, M., Fischer, M., Schmidt, C., Fuchs, M., 2015. Data processing in luminescence dating analysis: An exemplary workflow using the R package 'Luminescence'. Quaternary International 362, 8 – 13. URL: http://www.sciencedirect.com/science/article/pii/S104061821400408X, doi:http://dx.doi.org/10.1016/j.quaint.2014.06.034.

Furetta, C., 2008. Questions and Answers on Thermoluminescence (TL) and Optically Stimulated Luminescence (OSL). World Scientific Publishing Co. Pte. Ltd., Singapore.

Galbraith, R., 2003. A simple homogeneity test for estimates of dose obtained using osl. Ancient TL 21, 75–77.

Galbraith, R., 2005. Statistics for Fission Track Analysis. Chapman and Hall/CRC. doi:10.1201/9781420034929.

Galbraith, R., Roberts, R., Laslett, G., Yoshida, H., Olley, J., 1999. Optical dating of single grains of quartz from jinmium rock shelter, northern australia. part i: experimental design and statistical models. Archaeometry 41, 339–364.

Galbraith, R.F., Roberts, R.G., 2012. Statistical aspects of equivalent dose and error calculation and display in osl dating: An overview and some recommendations. Quaternary Geochronology 11, 1–27.

Galloway, R., Hong, D., 1996. Concerning the normalization of additive dose opticallystimulated luminescence data from quartz. Ancient TL 14, 1–5.

Ganzawa, Y., Furukawa, H., Hashimoto, T., Sanzelle, S., Miallier, D., Pilleyre, T., 2005. Single grains dating of volcanic quartz from pyroclastic flows using red tl. Radiation Measurements 39, 479–487. doi:10.1016/j.radmeas.2004.10.012.

Gilead, I., 1991. The upper paleolithic period in the levant. J World Prehist 5, 105–154.

Goedicke, C., Slusallek, K., Kubelik, M., 1981. Thermoluminescence Dating in Architectural History : Venetian Villas. Journal of the Society of Architectural Historians 40, 203–217.

Goldberg, M., 1989. Luminescence applications in biological, chemical, environmental, and hydrological sciences. Analytical Chemistry 61, 826A–826A.

Goring-Morris, N., Belfer-Cohen, A., 1998. The articulation of cultural processes and late quaternary environmental changes in cisjordan. Paléorient 23, 71–93.

Goring-Morris, N., Belfer-Cohen, A., 2017. The early and middle epipalaeolithic of cisjordan, in: Quaternary of the Levant. Cambridge University Press, pp. 639–649.

Goring-Morris, N., Belfer-Cohen, A., 2018. The Ahmarian in the Context of the Earlier Upper Palaeolithic in the Near East. Springer Singapore, Singapore. chapter 7. pp. 87–104. URL: https://doi.org/10.1007/978-981-10-6826-3_7, doi:10.1007/978-981-10-6826-3_7.

Greilich, S., Gribenski, N., Mittelstraß, D., Dornich, K., Huot, S., Preusser, F., 2015. Single-grain dose-distribution measurements by optically stimulated luminescence using an integrated EMCCD-based system. Quaternary Geochronology 29, 70 – 79. URL: http://www.sciencedirect.com/science/article/pii/S1871101415300455, doi:http://dx.doi.org/10.1016/j.quageo.2015.06.009.

Groucutt, H.S., Petraglia, M.D., Bailey, G., Scerri, E.M.L., Parton, A., Clark-Balzan, L., Jennings, R.P., Lewis, L., Blinkhorn, J., Drake, N.A., Breeze, P.S., Inglis, R.H., Devès, M.H., Meredith-Williams, M., Boivin, N., Thomas, M.G., Scally, A., 2015. Rethinking the dispersal of homo sapiens out of africa. Evolutionary anthropology 24, 149—164. URL: https://europepmc.org/articles/PMC6715448, doi:10.1002/evan.21455.

Grün, R., 1994. The kinetics of TL peaks and its effect on the dose versus temperature plot. Radiation Measurements 23, 175 – 194. URL: http://www.sciencedirect.com/science/article/pii/1350448794900345, doi:http://dx.doi.org/10.1016/1350-4487(94)90034-5.

Grün, R., 2009. The "age" program for the calculation of luminescence age estimates. Ancient TL 27, 45–46.

Guerin, G., Mercier, N., Adamiec, G., 2011. Dose-rate conversion factors: Update. Ancient TL 29, 5–8.

Guerin, G., Mercier, N., Nathan, R., Adamiec, G., Lefrais, Y., 2012. On the use of the infinite matrix assumption and associated concepts: A critical review. Radiation Measurements 47, 778–785.

Guibert, P., Bailiff, I., Blain, S., Gueli, A., Martini, M., Sibilia, E., Stella, G., Troja, S., 2009. Luminescence dating of architectural ceramics from an early medieval abbey: The St Philbert Intercomparison (Loire Atlantique, France). Radiation Measurements 44, 488–493.

Guibert, P., Schvoerer, M., 1991. TL dating : low background gamma spectrometry as a tool for the determination of the annual dose. Nuclear Track Radiation Measurements 18, 231–238.

Göksu, H., 1972. Thermoluminescence from unirradiated flints: regeneration thermoluminescence. Archaeometry 14, 127–132.

Göksu, H., Fremlin, J., Irwin, H., Fryxell, R., 1974. Age Determination of Burned flint by a Thermoluminescent Method. Science 183, 651–654.

Göksu, H., Weiser, A., Regulla, D., 1989. 110 $^{\circ}c$ tl peak records the ancient heat treatment of flint. Ancient TL 7, 15–17.

Hajdinjak, M., Mafessoni, F., Skov, L., Vernot, B., Hübner, A., Fu, Q., Essel, E., Nagel, S., Nickel, B., Richter, J., Moldovan, O.T., Constantin, S., Endarova, E., Zahariev, N., Spasov, R., Welker, F., Smith, G.M., Sinet-Mathiot, V., Paskulin, Lindsey Fewlass, H., Talamo, S., Rezek, Z., Sirakova, S., Sirakov, N., McPherron, S.P., Tsanova, T., Hublin, J.J., Peter, B.M., Meyer, M., Skoglund, P., Janet, K., Pääbo, S., 2021. Initial

upper palaeolithic humans in europe had recent neanderthal ancestry. Nature 592, 253–257. doi:10.1038/s41586-021-03335-3.

Hanebuth, T., Kudrass, H., Linstädter, J., Islam, B., Zander, A., 2013. Rapid coastal subsidence in the central ganges-brahmaputra delta (bangladesh) since the 17th century deduced from submerged salt-producing kilns,. Geology 41, 987–990. doi:doi:10.1130/G34646.1.

Hanh, H., Tuan, T., Tuat, T., Kinh, D., Dung, P., 2013. Investigation of thermoluminescence of natural zircon relevant to dating application. Radiation Measurements 48, 55–59.

Hérisson, D., Airvaux, J., Lenoble, A., Richter, D., Claud, E., Primault, J., 2016. Between the northern and southern regions of Western Europe: The Acheulean site of La Grande Vallée (Colombiers, Vienne, France). Quaternary International 411, 108–131. doi:10.1016/j.quaint.2015.12.100.

Higham, T., 2011. European middle and upper palaeolithic radiocarbon dates are often older than they look: problems with previous dates and some remedies. Antiquity 85, 235–249.

Higham, T., Compton, T., Stringer, C., Jacobi, R., Shapiro, B., Trinkaus, E., Chandler, B., Gröning, F., Collins, C., Hillson, S., O'Higgins, P., FitzGerald, C., Fagan, M., 2011. The earliest evidence for anatomically modern humans in northwestern europe. Nature 479, 521–524. doi:10.1038/nature10484.

Higham, T.F.G., Jacobi, R.M., Ramsey, C.B., 2006. Ams radiocarbon dating of ancient bone using ultrafiltration. Radiocarbon 48, 179–195. doi:10.1017/S0033822200066388.

Hong, D.G., Kim, M.J., Choi, J.H., El-Faramawy, N.A., Göksu, H.Y., 2006. Equivalent dose determination of single aliquot regenerative-dose (SAR) protocol using thermoluminescence on heated quartz. Nuclear Instruments and Methods in Physics Research Section B: Beam Interactions with Materials and Atoms 243, 174–178. URL: http://www.sciencedirect.com/science/article/pii/S0168583X05014151, doi:http://dx.doi.org/10.1016/j.nimb.2005.05.059.

Hood, A., Schwenninger, J.L., 2015,. The minimum extraction technique: A new sampling methodology for optically stimulated luminescence dating of museum ceramics. Quaternary Geochronology 30, 381–385. doi:doi:10.1016/j.quageo.2015.06.007.

Houtermans, F.G., Jäger, E., Schön, M., Stauffer, H., 1957. Messungen der Thermolumineszenz als Mittel zur Untersuchung der thermischen und der Strahlungsgeschichte

von natürlichen Mineralien und Gesteinen. Annalen der Physik 455, 283–292. URL: http://dx.doi.org/10.1002/andp.19574550129, doi:10.1002/andp.19574550129.

Hublin, J.J., 2015. The modern human colonization of western eurasia: when and where? Quaternary Science Reviews 118, 194–210. doi:10.1016/j.quascirev.2014.08.011.

Hublin, J.J., Sirakov, N., Aldeias, V., Bailey, S., Bard, E., Delvigne, V., Endarova, E., Fagault, Y., Fewlass, H., Hajdinjak, M., Kromer, B., Krumov, I., Marreiros, J., Martisius, N.L., Paskulin, L., Sinet-Mathiot, V., Meyer, M., Pääbo, S., Popov, V., Rezek, Z., Sirakova, S., Skinner, M.M., Smith, G.M., Spasov, R., Talamo, S., Tuna, T., Wacker, L., Welker, F., Wilcke, A., Zahariev, N., P., M.S., Tsenka, T., 2020. Initial upper palaeolithic homo sapiens from bacho kiro cave, bulgaria. Nature 581, 299–302. doi:10.1038/s41586-020-2259-z.

Huntley, D., 1985. On the zeroing of the thermoluminescence of sediments. Physics and Chemistry of Minerals 12, 122–127.

Huntley, D., Lamothe, M., 2001. Ubiquity of anomalous fading in k-feldspars and the measurement and correction for it in optical dating. Canadian Journal of Earth Sciences 38, 1093–1106. doi:doi:org/10.1139/e01-013.

Hurcombe, L., 2014. Perishable material culture in prehistory: Investigating the missing majority. Routledge. doi:10.4324/9781315817729.

Hussain, S.T., 2015a. The techno-logical nexus of core variability and blandelet standardisation: Rethinking late Ahmarian/Masraqan technology in Taibeh 3, in: Pleistocene Archaeology of the Petra Area in Jordan. Verlag Marie Leidorf GmbH, Rahden, Germany. volume 5 of *Kölner Studien zur Prähistorischen Archäologie*, pp. 345–360.

Hussain, S.T., 2015b. Technological conduits along the middle to upper palaeolithic transition in the southern levant: Some conceptual considerations., in: Pleistocene archaeology of the Petra area in Jordan. Kölner Studienzur rähistorischen Archäologie 5. Schyle, D. and Richter, J., pp. 233–271.

Hussain, S.T., Richter, J., 2015. The Late Ahmarian/Masraqan site of Taibeh 3, in: Pleistocene Archaeology of the Petra Area in Jordan. Verlag Marie Leidorf GmbH, Rahden, Germany. volume 5 of *Kölner Studien zur Prähistorischen Archäologie*, pp. 305–344.

Huxtable, J., 1981. Light bleaching of archaeological flint sample: a warning. Ancient TL 16, 2–4.

Huxtable, J., Jacobi, R., 1982. Thermoluminescence dating of burned flints from a british mesolithic site: Longmoor Inclosure, East Hampshire. Archaeometry 24, 164–169.

Hütt, G., Jaek, I., Tchonka, J., 1988. Optical dating: K-feldspars optical response stimulation spectra. Quaternary Science Reviews 7, 381 – 385. URL: http://www.sciencedirect.com/science/article/pii/0277379188900339, doi:http://dx.doi.org/10.1016/0277-3791(88)90033-9.

Jacobs, Z., Roberts, R.G., 2007. Advances in optically stimulated luminescence dating of individual grains of quartz from archeological deposits. Evolutionary Anthropology: Issues, News, and Reviews 16, 210–223. URL: https://onlinelibrary.wiley.com/doi/abs/10.1002/evan.20150, doi:https://doi.org/10.1002/evan.20150, arXiv:https://onlinelibrary.wiley.com/doi/pdf/10.1002/evan.20150.

Jain, M., 2009. Extending the dose range: Probing deep traps in quartz with 3.06 eV photons. Radiation Measurements 44, 445–452. URL: http://www.sciencedirect.com/science/article/pii/S1350448709000444, doi:http://dx.doi.org/10.1016/j.radmeas.2009.03.011.

Jain, M., Andersen, C., Botter-Jensen, L., Murray, A., Haack, A., Bridges, J., 2006. Luminescence dating on Mars: OSL characteristics of Martian analogue materials and GCR dosimetry. Radiation Measurements 41, 755–761.

Jain, M., Bøtter-Jensen, L., Murray, A., Denby, P., Tsukamoto, S., Gibling, M., 2005. Revisiting tl: dose measurement beyond the osl range using sar. Ancient TL 23, 9–24.

Janotta, A., Radtke, U., Czwielung, K., Heidger, M., 1997. Luminescence dating (irsl/tl) of lateglacial and holocene dune sands and sandy loesses near bonn, gifhorn and diepholz (germany). Quaternary Science Reviews 16, 349 – 355. URL: http://www.sciencedirect.com/science/article/pii/S0277379196001035, doi:https://doi.org/10.1016/S0277-3791(96)00103-5.

al Khasawneh, S., Murray, A., Bonatz, D., Freiesleben, T., 2015. Testing the application of post ir irsl dating to iron-and viking-age ceramics and heated stones from denmark. Quatemary Geochronology 30, 386–391.

King, G.E., Herman, F., Guralnik, B., 2016. Northward migration of the easternhimalayan syntaxis revealed by osl thermochronometry. Science 353 (6301), 800–804.

Kitis, G., Polymeris, G., Pagonis, V., Tsirliganis, N., 2013. Anomalous fading of OSL signals originating from very deep traps in Durango apatite. Radiation Measurements 49, 73–81.

Klasen, N., Hilgers, A., Schmidt, C., Bertrams, M., Schyle, D., Lehmkuhl, F., Richter, J., Radtke, U., 2013. Optical dating of sediments in Wadi Sabra (SW Jordan). Quaternary Geochronology 18, 9 – 16. URL: http://

www.sciencedirect.com/science/article/pii/S1871101413000721, doi:http://dx.doi.org/10.1016/j.quageo.2013.08.002.

Knoll, G., 2010. Radiation Detection and Measurement. Wiley. URL: https://books.google.be/books?id=4vTJ7UDel5IC.

Kondopoulou, D., Aidona, E., Ioannidis, N., Polymeris, G.S., Tsolakis, S., 2015. Archaeomagnetic study and thermoluminescence dating of Protobyzantine kilns (Megali Kypsa, North Greece). Journal of Archaeological Science: Reports 2, 156 – 168. URL: http://www.sciencedirect.com/science/article/pii/S2352409X15000085, doi:http://dx.doi.org/10.1016/j.jasrep.2015.01.007.

Kook, M., Lapp, T., Murray, A.S., Thomsen, K.J., Jain, M., 2015. A luminescence imaging system for the routine measurement of single-grain OSL dose distributions. Radiation Measurements 81, 171 – 177. URL: http://www.sciencedirect.com/science/article/pii/S1350448715000372, doi:http://dx.doi.org/10.1016/j.radmeas.2015.02.010.

Kook, M., Thomsen, K., Lapp, T., Murray, A., Jain, M., 2016. Resolving luminescence in spectral, spatial and compositional domains: a new approach, in: UK Luminescence and ESR meeting.

Koul, D., Chougaonkar, M., 2011. An attempt to estimate firing temperature using osl pre-dose sensitization of quartz. Geochronometria 38, 217 – 222. URL: https://content.sciendo.com/view/journals/geochr/38/3/article-p217.xml, doi:https://doi.org/10.2478/s13386-011-0034-5.

Krbetschek, M., Götze, J., Dietrich, A., Trautmann, T., 1997. Spectral information from minerals relevant for luminescence dating. Radiation Measurements 27, 695–748. URL: http://www.sciencedirect.com/science/article/pii/S1350448797002230, doi:http://dx.doi.org/10.1016/S1350-4487(97)00223-0.

Krbetschek, M., Rieser, U., 1995. Luminescence spectra of alkalifeldspars and plagioclases. Radiation Measurements 24, 473–477.

Kreutzer, S., 2017. calc_fadingcorr(): Apply a fading correction according to huntley and lamothe (2001) for a given g-value and a given tc. function version 0.4.2., in: Luminescence: Comprehensive Luminescence Dating Data Analysis. R package version 0.8.0.. Kreutzer, S., Burow, C., Dietze, M., Fuchs, M.C., Schmidt, C., Fischer, M. and Friedrich, J. URL: https://CRAN.R-project.org/package=Luminescence.

Kreutzer, S., Burow, C., Dietze, M., Fuchs, M., Fischer, M., Schmidt, C., 2017. Software in the context of luminescence dating: status, concepts and suggestions exemplified by the r package luminescence. Ancient TL 35, 1–11.

Kreutzer, S., Burow, C., Dietze, M., Fuchs, M.C., Schmidt, C., Fischer, M., Friedrich, J., Mercier, N., Philippe, A., Riedesel, S., Autzen, M., Mittelstrass, D., Gray, H.J., 2021. Luminescence: Comprehensive Luminescence Dating Data Analysis. URL: https://CRAN.R-project.org/package=Luminescence. r package version 0.9.13.

Kreutzer, S., Mauz, B., Martin, L., Mercier, N., 2019. 'rcarb': Dose rate modellingof carbonate-rich samples -an implementation of carb in r. Ancient TL 37, 1–8.

Kreutzer, S., Schmidt, C., Fuchs, M.C., Dietze, M., Fischer, M., Fuchs, M., 2012. Introducing an R package for luminescence dating analysis. Ancient TL 30, 1–8.

Lahaye, C., Guibert, P., Bechtel, F., 2012. Uranium series disequilibrium detection and annual dose determination: A case study on magdalenian ferruginous heated sandstones (la honteyre, france). Radiation Measurements 47, 786–789. URL: https://www.sciencedirect.com/science/article/pii/S1350448712000492, doi:https://doi.org/10.1016/j.radmeas.2012.02.002. proceedings of the 13th International Conference on Luminescence and Electron Spin Resonance Dating, 10–14 July, 2011, Toruń, Poland.

Lalou, C., Valladas, G., 1985. La thermoluminescence, in: Roth, E., Poty, B. (Eds.), Methode de datation par les phénomènes nucléaires naturels : applications. Masson, Paris, pp. 251–290.

Lapp, T., Jain, M., Ankjærgaard, C., Pirtzel, L., 2009. Development of pulsed stimulation and photon timer attachments to the risø tl/osl reader. Radiation Measurements 44, 571–575.

Lapp, T., Jain, M., Thomsen, K., Murray, A., Buylaert, J., 2012. New luminescence measurement facilities in retrospective dosimetry. Radiation Measurements 47, 803–808.

Lapp, T., Kook, M., Murray, A., Thomsen, K., Buylaert, J.P., Jain, M., 2015. A new luminescence detection and stimulation head for the risø tl/osl reader. Radiation Measurements 81, 178–184.

Lauer, T., Frechen, M., Klostermann, J., Krbetschek, M., Schollmayer, G., Tsukamoto, S., 2011. Luminescence dating of Last Glacial and Early Holocene fluvial deposits from the Lower Rhine - methodological aspects and chronological framework [Lumineszenzdatierung an letztglazialen und frühholozänen Flusssedimenten vom Niederrhein - methodische Aspekte und chronologischer Rahmen.]. Zeitschrift der Deutschen Gesellschaft für Geowissenschaften 162, 47–61. URL: http://www.ingentaconnect.com/content/schweiz/zdgg/2011/00000162/00000001/art00003, doi:doi:10.1127/1860-1804/2011/0162-0047.

Lauer, T., Krbetschek, M., Mauz, B., Frechen, M., 2012. Yellow stimulated luminescence from potassium feldspar: Observations on its suitability for dating. Radiation Measurements 47, 974 – 980. URL: http://www.sciencedirect.com/science/article/pii/S135044871200234X, doi:http://dx.doi.org/10.1016/j.radmeas.2012.08.002.

Lebrun, B., Frerebeau, N., Paradol, G., Guérin, G., Mercier, N., Tribolo, C., Lahaye, C., Rizza, M., 2020. Gamma: An r package for dose rate estimation from in-situ gamma-ray spectrometry measurements. Ancient TL 38, 1–5.

Linstädter, J., Eiwanger, J., Mikdad, A., Weniger, G.C., 2012. Human occupation of northwest africa: A review of middle palaeolithic to epipalaeolithic sites in morocco. Quaternary International 274, 158 – 174. URL: http://www.sciencedirect.com/science/article/pii/S1040618212000845, doi:https://doi.org/10.1016/j.quaint.2012.02.017. temporal and spatial corridors of Homo sapiens sapiens population dynamics during the Late Pleistocene and Early Holocene.

Liritzis, I., Stamoulis, K., Papachristodoulou, C., Ioannides, K., 2013. A re-evaluation of radiation dose-rate conversion factors. Mediterranean Archaeology and Archaeometry 13, 1–15.

Lüthgens, C., Böse, M., Lauer, T., Krbetschek, M., Strahl, J., Wenske, D., 2011. Timing of the last interglacial in Northern Europe derived from Optically Stimulated Luminescence (OSL) dating of a terrestrial Saalian-Eemian-Weichselian sedimentary sequence in NE-Germany. Quaternary International 241, 79–96. URL: http://www.sciencedirect.com/science/article/pii/S1040618210002612, doi:http://dx.doi.org/10.1016/j.quaint.2010.06.026.

Madsen, A., Buylaert, J.P., Murray, A., 2011. Luminescence dating of young coastal deposits from new zealand using feldspar. Geochronometria 38, 379–390. doi:doi:10.2478/s13386-011-0042-5.

Mahan, S., Kay, J., 2012. Building on previous OSL dating techniques for gypsum: A case study from Salt Basin playa, New Mexico and Texas. Quaternary Geochronology 10, 345–352.

Marks, A., Rose, J., 2014. A century of research into the origins of the Upper Paleolithic in the Levant. Editions errance. chapter 9. pp. 221–241.

Martin, L., Incerti, S., Mercier, N., 2015. Dosivox : Implementing geant4-based software for dosimetry simulations relevant to luminescence and esr dating techniques. Ancient TL 33, 1–10.

Martini, M., Sibilia, E., 2001. Radiation in archaeometry : archaeological dating. Radiation Physics and Chemistry 61, 241–246.

Martini, M., Sibilia, E., Croci, S., 1999. Glow curves and emission spectra of burnt flints. Quaternary Science Reviews 18, 287 – 292. URL: http://www.sciencedirect.com/science/article/pii/S0277379198000614, doi:http://dx.doi.org/10.1016/S0277-3791(98)00061-4.

Martini, M., Sibilia, E., Croci, S., Cremaschi, M., 2001. Thermoluminescence (TL) dating of burnt flints: problems, perspectives and some examples of application. Journal of Cultural Heritage 2, 179 – 190. URL: http://www.sciencedirect.com/science/article/pii/S1296207401011268, doi:http://dx.doi.org/10.1016/S1296-2074(01)01126-8.

McDougall, I., Brown, F.H., Fleagle, J.G., 2008. Sapropels and the age of hominins omo i and ii, kibish, ethiopia. Journal of human evolution 55, 409—420. URL: https://doi.org/10.1016/j.jhevol.2008.05.012, doi:10.1016/j.jhevol.2008.05.012.

McKeever, S., Blair, M., Yukihara, E., DeWitt, R., 2010. The effects of low ambient temperatures on optically stimulated luminescence (OSL) processes: Relevance to OSL dating of martian sediments. Radiation Measurements 45, 60–70.

Mejdahl, V., Botter-Jensen, L., 1994. Luminescence dating of archaeological materials using a new technique based on single aliquot measurements. Quaternary Science Reviews 13, 551 – 554. URL: http://www.sciencedirect.com/science/article/pii/0277379194900760, doi:http://dx.doi.org/10.1016/0277-3791(94)90076-0.

Melcher, C., Zimmerman, D., 1977. Thermoluminescent determination of prehistoric heat treatment of chert artifacts. Science (New York, N.Y.) 197, 1359–62. doi:10.1126/science.197.4311.1359.

Mercier, N., Valladas, H., 2003. Reassessment of tl age estimates of burnt flints from the paleolithic site of tabun cave, israel. Journal of human evolution 45, 401–9. doi:10.1016/j.jhevol.2003.09.004.

Mercier, N., Valladas, H., Bar-Yosef, O., Vandermeersch, B., Stringer, C., Joron, J.L., 1993. Thermoluminescence date for the mousterian burial site of es-skhul, mt. carmel. Journal of Archaeological Science 20, 169 – 174. URL: http://www.sciencedirect.com/science/article/pii/S0305440383710125, doi:https://doi.org/10.1006/jasc.1993.1012.

Mercier, N., Valladas, H., Froget, L., Joron, J.L., Reyss, J.L., Balescu, S., Escutenaire, C., Kozlowski, J., Sitlivy, V., Sobczyk, K., Zieba, A., 2003. Luminescence dates for the

palaeolithic site of Piekary IIa (Poland): comparison between TL of burnt flints and OSL of a loess-like deposit. Quaternary Science Reviews 22, 1245–1249. URL: http://www.sciencedirect.com/science/article/pii/S0277379103000258, doi:http://dx.doi.org/10.1016/S0277-3791(03)00025-8.

Mercier, N., Valladas, H., Froget, L., Joron, J.L., Reyss, J.L., Weiner, S., Goldberg, P., Meignen, L., Bar-Yosef, O., Belfer-Cohen, A., Chech, M., Kuhn, S., Stiner, M., Tillier, A.M., Arensburg, B., Vandermeersch, B., 2007a. Hayonim cave: a tl-based chronology for this levantine mousterian sequence. Journal of Archaeological Science 34, 1064 – 1077. URL: http://www.sciencedirect.com/science/article/pii/S0305440306001993, doi:https://doi.org/10.1016/j.jas.2006.09.021.

Mercier, N., Valladas, H., Froget, L., Joron, J.L., Vermeersch, P., Van Peer, P., Moeyersons, J., 1999. Thermoluminescence dating of a middle palaeolithic occupation at sodmein cave, red sea mountains (egypt). Journal of Archaeological Science 26, 1339 – 1345. URL: http://www.sciencedirect.com/science/article/pii/S0305440398903697, doi:https://doi.org/10.1006/jasc.1998.0369.

Mercier, N., Valladas, H., Joron, J.L., Reyss, J.L., Lévêque, F., Vandermeersch, B., 1991. Thermoluminescence dating of the late neanderthal remains from saint-césaire. Nature 351, 737–379.

Mercier, N., Valladas, H., Valladas, G., 1995a. Flint thermoluminescence dates from the CFR laboratory at Gif: Contributions to the study of the chronology of the middle palaeolithic. Quaternary Science Reviews 14, 351 – 364. URL: http://www.sciencedirect.com/science/article/pii/0277379195000291, doi:http://dx.doi.org/10.1016/0277-3791(95)00029-1.

Mercier, N., Valladas, H., Valladas, G., Reyss, J.L., Jelinek, A., Meignen, L., Joron, J.L., 1995b. TL Dates of Burnt Flints from Jelinek's Excavations at Tabun and their Implications. Journal of Archaeological Science 22, 495 – 509. URL: http://www.sciencedirect.com/science/article/pii/S0305440385700489, doi:http://dx.doi.org/10.1006/jasc.1995.0048.

Mercier, N., Wengler, L., Valladas, H., Joron, J.L., Froget, L., Reyss, J.L., 2007b. The rhafas cave (morocco): Chronology of the mousterian and aterian archaeological occupations and their implications for quaternary geochronology based on luminescence (tl/osl) age determinations. Quaternary Geochronology 2, 309–313. doi:10.1016/j.quageo.2006.03.010.

Michab, M., Valladas, H., Froget, L., Mercier, N., 1998. Distinguishing burnt from partly bleached unburnt quartz pebbles of pedra furada, brazil. Ancient TL 16.

Murray, A., Olley, J., 2002. Precision and accuracy in the optically stimulated luminescence dating of sedimentary quartz: A status review. Geochronometria 21.

Murray, A.S., Wintle, A.G., 2000a. Application of the single-aliquot regenerative-dose protocol to the 375°C quartz TL signal. Radiation Measurements 32, 579 – 583. URL: http://www.sciencedirect.com/science/article/pii/S1350448700000895, doi:http://dx.doi.org/10.1016/S1350-4487(00)00089-5.

Murray, A.S., Wintle, A.G., 2000b. Luminescence dating of quartz using an improved single-aliquot regenerative dose protocol. Radiation Measurements 32, 57–73. URL: http://www.sciencedirect.com/science/article/pii/S135044879900253X, doi:http://dx.doi.org/10.1016/S1350-4487(99)00253-X.

Nagar, Y., Sastry, M., Bhushan, B., Kumar, A., Mishra, K., Shastri, A., Deo, M., Kocurek, G., Magee, J., Wadhawan, S., Juyal, N., Shukla, A., Singhvi, A., 2010. Chronometry and formation pathways of gypsum using Electron Spin Resonance and Fourier Transform Infrared Spectroscopy. Quaternary Geochronology 5, 691–704.

O'Connor, V., Lepper, K., Morken, T., Thorstad, D., Podoll, A., M.J, G., 2011. A survey of the signal stability and radiation dose response of sulfates in the context of adapting optical dating for Mars. Journal of Luminescence 131, 2762–2768.

Olley, J., Murray, A., Roberts, R., 1996. The effects of disequilibria in the uranium and thorium decay chains on burial dose rates in fluvial sediments. Quaternary Science Reviews 15, 751–760.

Olley, J., Roberts, R., Yoshida, H., Bowler, J., 2006. Single-grain optical dating of grave-infill associated with human burials at lake mungo, australia. Quaternary Science Reviews 25, 2469–2474.

Pagonis, V., Chen, R., Kitis, G., 2011. On the intrinsic accuracy and precision of luminescence dating techniques for fired ceramics. Journal of Archaeological Science - J ARCHAEOL SCI 38. doi:10.1016/j.jas.2011.02.024.

Pagonis, V., Mian, S., Chithambo, M., Christensen, E., Barnold, C., 2009. Experimental and modelling study of pulsed optically stimulated luminescence in quartz, marble and beta irradiated salt. J. Phys. D: Appl. Phys. 42, 1–12.

Peng, J., Dong, Z., Han, F., 2016. tgcd: An r package for analyzing thermoluminescence glow curves. SoftwareX 5, 1–9.

Peng, J., Dong, Z., Han, F., Long, H., Liu, X., 2013. R package numOSL: numeric routines for optically stimulated luminescence dating. Ancient TL 31, 41–48. URL: http://www.ecu.edu/cs-cas/physics/Ancient-Timeline/upload/ATL_31_2-JunPeng.pdf.

Peng, J., Pagonis, V., 2016. Simulating comprehensive kinetic models for quartz luminescence using the R program KMS. Radiation Measurements 86, 63 – 70. URL: http://www.sciencedirect.com/science/article/pii/S1350448716300221, doi:http://dx.doi.org/10.1016/j.radmeas.2016.01.022.

Philippe, A., Guérin, G., Kreutzer, S., 2019. Baylum - an r package for bayesian analysis of osl ages: An introduction. Quaternary Geochronology 49, 16–24. doi:https://doi.org/10.1016/j.quageo.2018.05.009.

Philippe, A., Vibet, M.A., 2018. Analysis of archaeological phases using the cran package archaeophases. Journal of Statistical Software , 1–26.

Polikreti, K., Michael, C.T., Maniatis, Y., 2003. Thermoluminescence characteristics of marble and dating of freshly excavated marble objects. Radiation Measurements 37, 87 – 94. URL: http://www.sciencedirect.com/science/article/pii/S1350448702000884, doi:http://dx.doi.org/10.1016/S1350-4487(02)00088-4.

Polymeris, G.S., Kitis, G., Kiyak, N.G., Theodosoglou, E., Tsirliganis, N.C., Ertek, A., Erginal, A.E., 2016. Dating fossil root cast (Black Sea coast, Turkey) using thermoluminescence: Implications for windblown drift of shelf carbonates during {MIS} 2. Quaternary International 401, 184 – 193. URL: http://www.sciencedirect.com/science/article/pii/S1040618215005686, doi:http://dx.doi.org/10.1016/j.quaint.2015.05.060.

Poolton, N., Bøtter-Jensen, L., Rink, W., 1995. An optically stimulated luminescence study of flint related to radiation dosimetry. Radiation Measurements 24-, 551–555. doi:10.1016/1350-4487(94)00115-H. international Symposium on Luminescent Detectors and Transformers of Ionizing Radiation, LUMDETR'94 ; Conference date: 25-09-1994 Through 28-09-1994.

Posth, C., Renaud, G., Mittnik, M., Drucker, D., Rougier, H., Cupillard, C., Valentin, F., Thevenet, C., Furtwängler, A., Wißing, C., Francken, M., Malina, M., Bolus, M., Lari, M., Gigli, E., Capecchi, G., Crevecoeur, I., Beauval, C., Flas, D., Germonpré, M., van der Plicht, J., Cottiaux, R., Gély, B., Ronchitelli, A., Wehrberger, K., Grigorescu, D., Svoboda, J., Semal, P., Caramelli, D., Bocherens, H., Harvati, K., Conard, N., Haak, W., Powell, A., Krause, J., 2016. Pleistocene mitochondrial genomes suggest a single major dispersal of non-africans and a late glacial population turnover in europe. Current Biology 26, 827–833.

Prescott, J., Clay, R., 2000. Cosmic ray dose rates for luminescence and esr dating: measured with a scintillation counter. Ancient TL 18, 11–14.

Prescott, J., Huntley, D., Hutton, J., 1993. Estimation of equivalent dose in thermoluminescence dating - the Australian slide method. Ancient TL 11, 1–5.

Prescott, J.R., Hutton, J.T., 1994. Cosmic ray contributions to dose rates for luminescence and ESR dating: Large depths and long-term time variations. Radiation Measurements 23, 497 – 500. URL: http://www.sciencedirect.com/science/article/pii/1350448794900868, doi:http://dx.doi.org/10.1016/1350-4487(94)90086-8.

Preusser, F., Degering, D., Fuchs, M., Hilgers, A., Kadereit, A., Klasen, N., Krbetschek, M., Richter, D., Spencer, J., 2008. Luminescence dating: Basics, methods and applications. E und G Quaternary Science Journal 57, 95–149. doi:10.3285/eg.57.1-2.5.

R Core Team, 2015. R: A Language and Environment for Statistical Computing. R Foundation for Statistical Computing, Vienna, Austria. URL: https://www.R-project.org/.

Reimann, T., Tsukamoto, S., 2012. Dating the recent past (¡500 years) by post-ir irsl feldspar - examples from the north sea and baltic sea coast. Quaternary Geochronology 10, 180–187. doi:doi:10.1016/j.quageo.2012.04.011.

Reimer, P., Bard, E., Bayliss, A., Beck, J., Blackwell, P., Bronk Ramsey, C., Buck, C., Cheng, H., Edwards, R., Friedrich, M., Grootes, P., Guilderson, T., Haflidason, H., Hajdas, I., Hatté, C., Heaton, T., Hoffmann, D., Hogg, A., Hughen, K., Kaiser, K., Kromer, B., Manning, S., Niu, M., Reimer, R., Richards, D., Scott, E., Southon, J., Staff, R., Turney, C., van der Plicht, J., 2013. Intcal13 and marine13 radiocarbon age calibration curves 0–50,000 years cal bp. Radiocarbon 55, 1869–1887.

Reimer, P.J., Austin, W.E.N., Bard, E., Bayliss, A., Blackwell, P.G., Bronk Ramsey, C., Butzin, M., Cheng, H., Edwards, R.L., Friedrich, M., et al., 2020. The intcal20 northern hemisphere radiocarbon age calibration curve (0–55 cal kbp). Radiocarbon 62, 725–757. doi:10.1017/RDC.2020.41.

Richter, D., 2007. Advantages and limitations of thermoluminescence dating of heated flint from Paleolithic sites. Geoarchaeology 22, 671–683. URL: http://dx.doi.org/10.1002/gea.20180, doi:10.1002/gea.20180.

Richter, D., Angelucci, D.E., Dias, M.I., Prudêncio, M.I., Gouveia, M.A., Cardoso, G.J., Burbidge, C.I., Zilhão, J., 2014. Heated flint TL-dating for Gruta da Oliveira (Portugal): dosimetric challenges and comparison of chronometric data. Journal of Archaeological Science 41, 705 – 715. URL: http://www.sciencedirect.com/science/article/pii/S0305440313003348, doi:http://dx.doi.org/10.1016/j.jas.2013.09.021.

Richter, D., Dibble, H., Goldberg, P., McPherron, S., Niven, L., Sandgathe, D., Talamo, S., Turq, A., 2013. The late middle palaeolithic in southwest france: New tl dates for the sequence of pech de l'azé iv. Quaternary International 294, 160 – 167. URL: http://www.sciencedirect.com/science/article/pii/S1040618212003631, doi:https://doi.org/10.1016/j.quaint.2012.05.028.

Richter, D., Grün, R., Joannes-Boyau, R., Steele, T.E., Amani, F., Rué, M., Fernandes, P., Raynal, J.P., Geraads, D., Ben-Ncer, A., Hublin, J.J., McPherron, S.P., 2017a. The age of the homo sapiens fossils from Jebel Irhoud (Morocco) and the origins of the Middle Stone Age. Nature 546, 293–296. doi:10.1038/nature22335.

Richter, D., Grün, R., Joannes-Boyau, R., Steele, T.E., Amani, F., Rué, M., Fernandes, P., Raynal, J.P., Geraads, D., Ben-Ncer, A., Hublin, J.J., McPherron, S.P., 2017b. The age of the hominin fossils from Jebel Irhoud, Morocco, and the origins of the Middle Stone Age. Nature 546, 293–296. URL: http://dx.doi.org/10.1038/nature22335.

Richter, D., Krbetschek, M., 2006. A New Thermoluminescence dating thechnique for heated flints. Archaeometry 48, 695–705. URL: http://dx.doi.org/10.1111/j.1475-4754.2006.00281.x, doi:10.1111/j.1475-4754.2006.00281.x. publisher: Blackwell Publishing Ltd.

Richter, D., Krbetschek, M., 2015. The age of the lower paleolithic occupation at schoningen. Journal of human evolution , 45–56doi:10.1016/j.jhevol.2015.06.003.

Richter, D., Krbetschek, M.R., Rieser, U., Trautmann, T., Wagner, G.A., 1999. Spectral investigation of the thermoluminescence of heated flint (silex). Quaternary Science Reviews 18, 279 – 285. URL: http://www.sciencedirect.com/science/article/pii/S0277379198000602, doi:http://dx.doi.org/10.1016/S0277-3791(98)00060-2.

Richter, D., Mercier, N., Valladas, H., Jaubert, J., Texier, P.J., Brugal, J.P., Kervazo, B., Reyss, J.L., Joron, J.L., Wagner, G.A., 2007. Thermoluminescence dating of heated flint from the Mousterian site of Bérigoule, Murs, Vaucluse, France. Journal of Archaeological Science 34, 532 – 539. URL: http://www.sciencedirect.com/science/article/pii/S0305440306001269, doi:http://dx.doi.org/10.1016/j.jas.2006.06.006.

Richter, D., Schroeder, B., Rink, W., Julig, P., Schwarcz, H., 2001. The middle to upper palaeolithic transition in the levant and new tl dates for a late mousterian assemblage from jerf al-ajla cave near palmyra, syria. Paléorient 27, 29–46.

Richter, D., Temming, H., 2006. Testing heated flint palaeodose protocols using dose recovery procedures. Radiation Measurements 41, 819 – 825. URL: http:

//www.sciencedirect.com/science/article/pii/S1350448706000448, doi:http://dx.doi.org/10.1016/j.radmeas.2006.04.027.

Richter, D., Tostevin, G., Skrdla, P., Davies, W., 2009. New radiometric ages for the Early Upper Palaeolithic type locality of Brno-Bohunice (Czech Republic): comparison of OSL, IRSL, TL and 14C dating results. Journal of Archaeological Science 36, 708–720.

Richter, D., Waiblinger, J., Rink, W., Wagner, G., 2000. Thermoluminescence, electron spin resonance and14c-dating of the late middle and early upper palaeolithic site of geißenklösterle cave in southern germany. Journal of Archaeological Science 27, 71–89.

Richter, J., Hauck, T., Vogelsang, R., Widlok, T., Tensorer, J.M.L., Schmid, P., 2012a. "contextual areas" of early homo sapiens and their significance for human dispersal from africa into eurasia between 200 ka and 70 ka. Quaternary International 274, 5–24. doi:10.1016/j.quaint.2012.04.017.

Richter, J., Litt, T., Lehmkuhl, F., Hense, A., Hauck, T.C., Leder, D.F., Miebach, A., Parow-Souchon, H., Sauer, F., Schoenenberg, J., Al-Nahar, M., Hussain, S.T., 2020. Al-ansab and the dead sea: Mid-mis 3 archaeology and environment of the early ahmarian population of the levantine corridor. PLOS ONE 15, 1–36. URL: https://doi.org/10.1371/journal.pone.0239968.

Richter, J., Melles, M., Schäbitz, F., 2012b. Temporal and spatial corridors of homo sapiens sapiens population dynamics during the late pleistocene and early holocene. Quaternary International 274, 1–4. URL: https://www.sciencedirect.com/science/article/pii/S1040618212004235, doi:https://doi.org/10.1016/j.quaint.2012.06.009. temporal and spatial corridors of Homo sapiens sapiens population dynamics during the Late Pleistocene and Early Holocene.

Richter, J., Schyle, D., 2015. The final levantine aurignacian site of sabra 4 - palm view 3, in: Pleistocene Archaeology of the Petra Area in Jordan. kölner studien zur prähistorischen archäologie 5. a crc 806 monograph ed.. Marie Leidorf (Rahden/Westfalen), pp. 233–271.

Riedesel, S., Brill, D., Roberts, H., Duller, G., Garrett, E., Zander, A., King, G., Tamura, T., Burow, C., Cunningham, A., Seeliger, M., De Batist, M., Heyvaert, V., Fujiwara, O., Brückner, H., 2018. Single-grain luminescence chronology of historical extreme-wave event deposits recorded in the shirasuka lowlands, pacific coast of central japan. Quaternary Geochronology 45, 37–49. doi:doi:org/10.1016/j.quageo.2018.01.006.

Riedesel, S., King, G.E., Prasad, A.K., Kumar, R., Finch, A.A., Jain, M., 2019. Optical determination of band-tail width, depth and excited state oft he irsltrap in feldspar. Radiation Measurements 125, 40–51.

Rigaud, J.P., Texier, P.J., Parkington, J., Poggenpoel, C., 2006. Le mobilier still-bay et howiesons poort de l'abri diepkloof. la chronologie du middle stone age sud-africain et ses implications. Comptes Rendus Palevol 5, 839 – 849. URL: http://www.sciencedirect.com/science/article/pii/S1631068306000315, doi:https://doi.org/10.1016/j.crpv.2006.02.003.

Risø, 2015. Guide to The Risø TL/OSL Reader. DTU Nutech, Denmark.

Roberts, H.M., 2012. Testing Post-IR {IRSL} protocols for minimising fading in feldspars, using Alaskan loess with independent chronological control. Radiation Measurements 47, 716 – 724. URL: http://www.sciencedirect.com/science/article/pii/S1350448712000984, doi:http://dx.doi.org/10.1016/j.radmeas.2012.03.022.

Rodnight, H., 2008. How many equivalent dose values are needed to obtain a reproducible distribution? Ancient TL 26, 3–10.

Sanderson, D., Clark, R., 1994. Pulsed photostimulated luminescence of alkalifeldspars. Radiation Measurements 23, 633–639.

Sanderson, D.C., Murphy, S., 2010. Using simple portable osl measurements and laboratory characterisation to help understand complex and heterogeneous sediment sequences for luminescence dating. Quaternary Geochronology 5, 299 – 305. URL: http://www.sciencedirect.com/science/article/pii/S1871101409000235, doi:https://doi.org/10.1016/j.quageo.2009.02.001. 12th International Conference on Luminescence and Electron Spin Resonance Dating (LED 2008).

Sarkar, D., 2008. Lattice: Multivariate Data Visualization with R. Springer, New York. URL: http://lmdvr.r-forge.r-project.org. iSBN 978-0-387-75968-5.

Scharpenseel, H., Becker-Heidmann, P., 1992. Twenty-five years of radiocarbon dating soils: paradigm or erring and learning. Radiocarbon 34, 541–549.

Schmidt, C., 2013. Luminescence dating of heated silex - Potential to improve accuracy and precision and application to Paleolithic sites. Ph.D. thesis. University of Cologne. URL: http://kups.ub.uni-koeln.de/5109/.

Schmidt, C., Anghelinu, M., Hambach, U., Veres, D., Lehmkuhl, F., 2019. Reassessing the timeframe of upper palaeolithic deposits in the ceahlău basin (eastern carpathians,

romania): Geochronological and archaeological implications. Quaternary Geochronology 55, 101020. doi:10.1016/j.quageo.2019.101020.

Schmidt, C., Friedrich, J., Zöller, L., 2015a. Thermochronometry using red TL of quartz – Numerical simulation and observations from in-situ drill-hole samples. Radiation Measurements 81, 98 – 103. URL: http://www.sciencedirect.com/science/article/pii/S1350448715300056, doi:http://dx.doi.org/10.1016/j.radmeas.2015.04.004.

Schmidt, C., Kindermann, K., Peer, P.v., Bubenzer, O., 2015b. Multi-emission luminescence dating of heated chert from the Middle Stone Age sequence at Sodmein Cave (Red Sea Mountains, Egypt). Journal of Archaeological Science 63, 94 – 103. URL: http://www.sciencedirect.com/science/article/pii/S0305440315002629, doi:https://doi.org/10.1016/j.jas.2015.08.016.

Schmidt, C., Kreutzer, S., 2013. Optically stimulated luminescence of amorphous/microcrystalline SiO2 (silex): Basic investigations and potential in archeological dosimetry. Quaternary Geochronology 15, 1 – 10. URL: http://www.sciencedirect.com/science/article/pii/S187110141300006X, doi:http://dx.doi.org/10.1016/j.quageo.2013.01.005.

Schmidt, C., Kreutzer, S., Fattahi, M., Bailey, R., Zander, A., Zöller, L., 2011. On the luminescence signals of empty sample carriers. Ancient TL 29, 65–74.

Schmidt, C., Pettke, T., Preusser, F., Rufer, D., Kasper, H.U., Hilgers, A., 2012. Quantification and spatial distribution of dose rate relevant elements in silex used for luminescence dating. Quaternary Geochronology 12, 65 – 73. URL: http://www.sciencedirect.com/science/article/pii/S1871101412001057, doi:https://doi.org/10.1016/j.quageo.2012.05.006.

Schmidt, C., Rufer, D., Preusser, F., Krbetschek, M., Hilgers, A., 2013a. The assessment of radionuclide distribution in silex by autoradiography in the context of dose rate determination for thermoluminescence dating. Archaeometry 55, 407–422. URL: https://onlinelibrary.wiley.com/doi/abs/10.1111/j.1475-4754.2012.00690.x, doi:10.1111/j.1475-4754.2012.00690.x.

Schmidt, C., Sitlivy, V., Anghelinu, M., Chabai, V., Kels, H., Uthmeier, T., Hauck, T., Bălteanu, I., Hilgers, A., Richter, J., Radtke, U., 2013b. First chronometric dates (TL and OSL) for the Aurignacian open-air site of Românești-Dumbrăviţa I, Romania. Journal of Archaeological Science 40, 3740 – 3753. URL: http://www.sciencedirect.com/science/article/pii/S0305440313001258, doi:https://doi.org/10.1016/j.jas.2013.04.003.

Schyle, D., 2015. The ahmarian site of al-ansab 1, in: Pleistocene Archaeology of the Petra Area in Jordan. kölner studien zur prähistorischen archäologie 5. a crc 806 monograph ed.. Marie Leidorf (Rahden/Westfalen), pp. 91–130.

Schyle, D., H.P., U., 1988. Paleolithic sites in the petra area, in: The prehistory of Jordan. The state of research in 1986. Garrard, A.N and Gebel, H.G, pp. 39–65.

Schyle, D., Richter, J., 2015. Pleistocene Archaeology of the Petra Area in Jordan. volume 5 of *Kölner Studien zur Prähistorischen Archäologie*. Verlag Marie Leidorf GmbH.

Seguin-Orlando, A., Korneliussen, T.S., Sikora, M., Malaspinas, A.S., Manica, A., Moltke, I., Albrechtsen, A., Ko, A., Margaryan, A., Moiseyev, V., Goebel, T., Westaway, M., Lambert, David andKhartanovich, V., Wall, J.D., Nigst, P.R., Foley, R.A., Mirazon Lahr, M., Nielsen, R., Orlando, L., Willerslev, E., 2014. Genomic structure in europeans dating back at least 36,200 years. Science 346, 1113–1118. doi:10.1126/science.aaa0114.

Sievert, C., Parmer, C., Hocking, T., Chamberlain, S., Ram, K., Corvellec, M., Despouy, P., 2016. plotly: Create Interactive Web Graphics via Plotly's JavaScript Graphing Library. Https://plot.ly/r, https://github.com/ropensci/plotly.

Singhvi, A., Stokes, S., Chauhan, N., Nagar, Y., Jaiswal, M., 2011. Changes in natural OSL sensitivity during single aliquot regeneration procedure and their implications for equivalent dose determination. Geochronometria 38, 231–241. URL: http://dx.doi.org/10.2478/s13386-011-0028-3, doi:10.2478/s13386-011-0028-3. publisher: SP Versita.

Sitlivy, V., Chabai, V., Anghelinu, M., Uthmeier, T., Kels, H., Hilgers, A., Schmidt, C., Niţă, L., Baltean, I., Veselsky, A., Hauck, T., 2012. The earliest aurignacian in romania: New investigations at the open air site of româneşti-dumbrăviţa i (banat). Quartär 59, 85–130. doi:10.7485/QU59-4.

Smedley, R.K., 2015. A new R function for the Internal External Uncertainty (IEU) model. Ancient TL 33, 16–21. URL: http://www.ecu.edu/cs-cas/physics/Ancient-Timeline/upload/ATL_33-1_Smedley.pdf.

Smith, B., Rhodes, E., Stokes, S., Spooner, N., 1990. The optical dating of sediments using quartz. Radiation Protection Dosimetry 34, 75–78.

Sohbati, R., Murray, A., Jain, M., Thomsen, K., Hong, S.C., Yi, K., Choi, J.H., 2013. Na-rich feldspar as a luminescence dosimeter in infrared stimulatedluminescence (irsl) dating. Radiation Measurements 51, 67–82.

Spooner, N.A., 1994a. The anomalous fading of infrared-stimulated luminescence from feldspars. Radiation Measurements 23, 625 – 632. URL: http://www.sciencedirect.com/science/article/pii/1350448794901112, doi:http://dx.doi.org/10.1016/1350-4487(94)90111-2.

Spooner, N.A., 1994b. On the optical dating signal from quartz. Radiation Measurements 23, 593 – 600. URL: http://www.sciencedirect.com/science/article/pii/1350448794901058, doi:http://dx.doi.org/10.1016/1350-4487(94)90105-8.

Stirling, R., Duller, G., Roberts, H., 2012. Developing a single-aliquot protocol for measuring equivalent dose in biogenic carbonates. Radiation Measurements 47, 725–731.

Stoneham, D., 1991. Authenticity testing, in: Goksu, H., Oberhofer, M., Regulla, D. (Eds.), Scientific dating methods. Kluwer Academic, Dordrecht, p. 175–192.

Straus, L., 2001. Africa and iberia in the pleistocene. Quaternary International - QUATERN INT 75, 91–102. doi:10.1016/S1040-6182(00)00081-1.

Strebler, D., Brill, D., Richter, J., Brückner, H., 2019a. Using drac in complex geometries - tl dating of heated flints from taibeh, jordan. Quaternary Geochronology 49, 4–7. URL: https://www.sciencedirect.com/science/article/pii/S1871101417301905, doi:https://doi.org/10.1016/j.quageo.2018.07.002. 15th International Conference on Luminescence and Electron Spin Resonance Dating, 11-15 September 2017, Cape Town, South Africa.

Strebler, D., Burow, C., Brill, D., Brückner, H., 2017. Using R for TL dating. Quaternary Geochronology 37, 97 – 107. URL: http://www.sciencedirect.com/science/article/pii/S1871101416301182, doi:http://dx.doi.org/10.1016/j.quageo.2016.09.001.

Strebler, D., Riedesel, S., King, G., Brill, D., Brückner, H., 2019b. Lumreader: Designing your luminescence experiment with r. Radiation Measurements 129, 106143. URL: https://www.sciencedirect.com/science/article/pii/S1350448717300793, doi:https://doi.org/10.1016/j.radmeas.2019.106143.

Stringer, C., 2003. Out of ethiopia. Nature 423, 693–695. doi:https://doi.org/10.1038/423692a.

Sutton, S., Zimmerman, D., 1976. Thermoluminescence dating using zircon grains from archaeological ceramics. Archaeometry 18, 125–134.

Svetlik, I., Jull, A.J.T., Molnár, M., Povinec, P.P., Kolář, T., Demján, P., Pachnerova Brabcova, K., Brychova, V., Dreslerová, D., Rybníček, M., et al., 2019. The best possible time resolution: How precise could a radiocarbon dating method be? Radiocarbon 61, 1729–1740. doi:10.1017/RDC.2019.134.

Sze, S.M., Ng, K.K., 2006. Physics of Semiconductor Devices, 3rd Edition. Wiley.

Tema, E., Fantino, F., Ferrara, E., Lo Giudice, A., Morales, J., Goguitchaichvili, A., Camps, P., Barello, F., Gulmini, M., 2013. Combined archaeomagnetic and thermoluminescence study of a brick kiln excavated at fontanetto po (vercelli, northern italy),. Journal of Archaeological Science 40, 2025–2035. doi:doi:10.1016/j.jas.2012.12.011.

Thiel, C., Buylaert, J.P., Murray, A., Terhorst, B., Hofer, I., Tsukamoto, S., Frechen, M., 2011. Luminescence dating of the Stratzing loess profile (Austria) – Testing the potential of an elevated temperature post-IR {IRSL} protocol. Quaternary International 234, 23 – 31. URL: http://www.sciencedirect.com/science/article/pii/S1040618210002156, doi:http://dx.doi.org/10.1016/j.quaint.2010.05.018.

Thomsen, K., Kook, M., Murray, A.S., Jain, M., 2018. Resolving luminescence in spatial and compositional domains. Radiation Measurements 120, 260–266.

Thomsen, K.J., Murray, A.S., Jain, M., Bøtter-Jensen, L., 2008. Laboratory fading rates of various luminescence signals from feldspar-rich sediment extracts. Radiation Measurements 43, 1474 – 1486. URL: http://www.sciencedirect.com/science/article/pii/S1350448708003375, doi:http://dx.doi.org/10.1016/j.radmeas.2008.06.002.

Tite, M., Waine, J., 1962. Thermoluminescence dating : a re-appraisal. archaeometry 5, 53–79. URL: http://dx.doi.org/10.1111/j.1475-4754.1962.tb00554.x, doi:10.1111/j.1475-4754.1962.tb00554.x.

Tribolo, C., Mercier, N., 2012. Towards a sar-itl protocol for the equivalent dose estimate of burnt quartzites. Ancient TL 30, 17–25.

Tribolo, C., Mercier, N., Douville, E., Joron, J.L., Reyss, J.L., Rufer, D., Cantin, N., Lefrais, Y., Miller, C.E., Porraz, G., Parkington, J., Rigaud, J.P., Texier, P.J., 2013. OSL and TL dating of the Middle Stone Age sequence at Diepkloof Rock Shelter (South Africa): a clarification. Journal of Archaeological Science 40, 3401 – 3411. URL: http://www.sciencedirect.com/science/article/pii/S0305440312005225, doi:http://dx.doi.org/10.1016/j.jas.2012.12.001.

Tribolo, C., Mercier, N., Selo, M., Valladas, H., Joron, J.L., Reyss, J.L., Henshilwood, C., Sealy, J., Yates, R., 2006. Tl dating of burnt lithics from blombos cave (south

africa): further evidence for the antiquity of modern human behaviour. Archaeometry 48, 341–357. URL: https://onlinelibrary.wiley.com/doi/abs/10.1111/j.1475-4754.2006.00260.x, doi:10.1111/j.1475-4754.2006.00260.x.

Tribolo, C., Mercier, N., Valladas, H., 2001. Alpha sensitivity determination in quartzite using an osl single aliquot procedure. Ancient TL 19, 47–50.

Tribolo, C., Mercier, N., Valladas, H., 2003. Attempt at using the single-aliquot regenerative-dose procedure for the determination of equivalent doses of upper palaeolithic burnt stone. Quaternary Science Reviews - QUATERNARY SCI REV 22, 1251–1256. doi:10.1016/S0277-3791(03)00027-1.

Tsakalos, E., Christodoulakis, J., Charalambous, L., 2015. The dose rate calculator (drc) for luminescence and esr dating-a java application for dose rate and age determination. Archaeometry 58, 347–352. doi:https://doi.org/10.1111/arcm.12162.

Tsukamoto, S., Murray, A., Huot, S., Watanuki, T., Denby, P., Bøtter-Jensen, L., 2007. Luminescence property of volcanic quartz and the use of red isothermal TL for dating tephras. Radiation Measurements 42, 190–197. URL: http://www.sciencedirect.com/science/article/pii/S1350448706001260, doi:http://dx.doi.org/10.1016/j.radmeas.2006.07.008.

Urbach, F., 1930. For the luminescence of the alkali halides: Ii, in: Measurement Methods Meeting, Verinna, Austria.

Valladas, G., 1988. Stopping power and range for alpha particules in sio_2. Ancient TL 6, 7–8.

Valladas, H., 1978. Thermoluminescence dating of burnt stones from a prehistoric site. Proceedings First Specialist Seminar on Thermoluminescence Dating, Oxford 1978, PACT (2) , 180–184.

Valladas, H., 1981. Thermoluminescence de gres de foyers prehistoriques: Estimation de leur temperature de chauffe. Archaeometry 23, 221–229. URL: https://onlinelibrary.wiley.com/doi/abs/10.1111/j.1475-4754.1981.tb00309.x, doi:10.1111/j.1475-4754.1981.tb00309.x, arXiv:https://onlinelibrary.wiley.com/doi/pdf/10.1111/j.1475-4754.1981.tb00309.x.

Valladas, H., 1985a. Datation par la thermoluminescence de gisements moustériens du sud de la France. Ph.D. thesis. Museum National d'Histoire Naturelle et Université Paris VI.

Valladas, H., 1985b. Some tl properties of burnt prehistoric flints. Nuclear Tracks and Radiation Measurements (1982) 10, 785 – 788. URL: http://

www.sciencedirect.com/science/article/pii/0735245X85900912, doi:https://doi.org/10.1016/0735-245X(85)90091-2. special Issue: Thermoluminescence and Electron-Spin-Resonance Dating.

Valladas, H., 1992. Thermoluminescence dating of flint. Quaternary Science Reviews 11, 1–5.

Valladas, H., Joron, J.L., Valladas, G., Arensburg, B., Bar-Yosef, O., Belfer-Cohen, A., Goldberg, P., Laville, H., Meignen, L., Rak, Y., Tchernov, E., Tillier, A.M., Vandermeersch, B., 1987. Thermoluminescence dates for the neanderthal burial site at kebarain israel. Nature 330, 159–160.

Valladas, H., Mercier, N., Froget, L., Hovers, E., Joron, J.L., Kimbel, W., Rak, Y., 1999. Tl dates for the neanderthal site of the amud cave, israel. Journal of Archaeological Science 26, 259 – 268. URL: http://www.sciencedirect.com/science/article/pii/S030544039890334X, doi:https://doi.org/10.1006/jasc.1998.0334.

Valladas, H., Mercier, N., Froget, L., Joron, J.L., Reyss, J.L., Karkanas, P., Panagopoulou, E., Kyparissi-Apostolika, N., 2007. Tl age-estimates for the middle palaeolithic layers at theopetra cave (greece). Quaternary Geochronology 2, 303 – 308. URL: http://www.sciencedirect.com/science/article/pii/S1871101406000173, doi:https://doi.org/10.1016/j.quageo.2006.03.014. lED 2005.

Valladas, H., Reyss, J.L., Joron, J.L., Valladas, G., Bar-Yosef, O., Vandermeersch, B., 1988. Thermoluminescence dating of mousterian troto-cro-magnon' remains from israel and the origin of modern man. Nature 331, pages614–616.

Valladas, H., Wadley, L., Mercier, N., Froget, L., Tribolo, C., Reyss, J.L., Joron, J.L., 2005. Thermoluminescence dating on burnt lithics from middle stone age layers at rose cottage cave. South African Journal of Science 101, 169–174.

Veronese, I., Göksu, H., Schwenk, P., Herzig, F., 2008. Thermoluminescence dating of a mikveh in Ichenhausen, Germany. Journal of Environmental Radioactivity 99, 621–630. URL: http://www.sciencedirect.com/science/article/pii/S0265931X07002378, doi:http://dx.doi.org/10.1016/j.jenvrad.2007.09.002.

Vieillevigne, E., Guibert, P., Bechtel, F., 2007. Luminescence chronology of the medieval citadel of Termez, Uzbekistan : TL dating of Bricks masoneries. Journal of archaeological Science 34, 1402–1416.

Wang, X.L., Lu, Y.C., Wintle, A.G., 2006. Recuperated {OSL} dating of fine-grained quartz in Chinese loess. Quaternary Geochronology 1, 89 – 100. URL: http:

//www.sciencedirect.com/science/article/pii/S187110140600032X, doi:http://dx.doi.org/10.1016/j.quageo.2006.05.020.

Weida, W., Junding, X., 1989. A convenient method for preparation of fine-grain samples. Ancient TL 7, 47.

Weiner, S., Brumfeld, V., Marder, O., Barzilai, O., 2015. Heating of flint debitage from upper palaeolithic contexts at manot cave, israel: changes in atomic organization due to heating using infrared spectroscopy. Journal of Archaeological Science 54, 45–53. URL: https://www.sciencedirect.com/science/article/pii/S0305440314004300, doi:https://doi.org/10.1016/j.jas.2014.11.023.

Weninger, B., Jöris, O., 2008. A 14c age calibration curve for the last 60 ka: the greenland-hulu u/th timescale and its impact on understanding the middle to upper paleolithic transition in western eurasia. Journal of Human Evolution 55, 772–781. URL: https://www.sciencedirect.com/science/article/pii/S0047248408001693, doi:https://doi.org/10.1016/j.jhevol.2008.08.017. chronology of the Middle-Upper Paleolithic Transition in Eurasia.

Wintle, A., 1973. Anormalous fading of thermoluminescence in mineral samples. Nature 245, 143–144.

Wintle, A., 1997. Luminescence dating: laboratory procedures and protocols. Radiation Measurements 27, 769–817. URL: http://www.sciencedirect.com/science/article/pii/S1350448797002205, doi:http://dx.doi.org/10.1016/S1350-4487(97)00220-5.

Wintle, A., 2007. Thermoluminescence dating: A review of recent applications to non-pottery materials. Archaeometry 22, 113 – 122. doi:10.1111/j.1475-4754.1980.tb00936.x.

Wintle, A., 2008. Fifty years of luminescence dating. Archaeometry 50, 276–312.

Wintle, A., Oakley, K., 1972. Thermoluminescence dating of fired rock-crystal from Bellan Bandi Palassa Ceylon. Archaeometry 14, 277–279.

Wintle, A.G., Aitken, M.J., 1977. Thermoluminescence dating of burnt flint: application to a lower palaeolithic site, terra amata. Archaeometry 19, 111–130. URL: http://dx.doi.org/10.1111/j.1475-4754.1977.tb00189.x, doi:10.1111/j.1475-4754.1977.tb00189.x.

Wintle, A.G., Murray, A.S., 2006. A review of quartz optically stimulated luminescence characteristics and their relevance in single-aliquot regeneration dating protocols. Radiation Measurements 41, 369 – 391. URL: http://

www.sciencedirect.com/science/article/pii/S1350448705003227, doi:http://dx.doi.org/10.1016/j.radmeas.2005.11.001.

Woda, C., Fuchs, M., 2008. On the applicability of the leading edge method to obtain equivalent doses in osl dating and dosimetry. Radiation Measurements 43, 26–37.

Yukihara, E.G., McKeever, S.W.S., 2011. Optical stimulated Luminescence: Fundamentals and Applications. A John Wiley and Sons, Ltd.

Zander, A., Strebler, D., Brückner, H., Classen, E., Rethemeyer, J., 2019. Roman traces in germania magna: New thermoluminescence and pirir$_{290}$data from a lime kiln at bergisch gladbach, germany. Archaeometry 61, 506–518.

Zhang, J., Yan, C., Zhou, L., 2005. Feasibility of optical dating using halite. Journal of Luminescence 114, 234–240.

Zimmerman, D., 1967. Thermoluminescence from fine grains from ancient pottery. Archaeometry 10, 26–28.

Zimmerman, D., 1971a. Thermoluminescent dating using fine grains from pottery. Archaeometry 13, 29–52. doi:doi.org/10.1111/j.1475-4754.1971.tb00028.x.

Zimmerman, D., 1971b. Uranium distributions in archaeologic ceramics: dating of radioactive inclusions. Science 174, 818–819.

Zimmerman, D., 1972. Relative thermoluminescence effects of alpha- and beta-radiation. Radiation Effects 14, 81–92.

Zimmerman, D., Yuhas, M., 1974. Thermoluminescence authenticity measurements on core material from the bronze horse of the New York Metropolitan Museum of Art. Archaeometry 16, 19–30.

Zöller, L., Richter, D., Blanchard, H., Einwögerer, T., Händel, M., Neugebauer-Maresch, C., 2014. Our oldest children: Age constraints for the Krems-Wachtberg site obtained from various thermoluminescence dating approaches. Quaternary International 351, 83 – 87. URL: http://www.sciencedirect.com/science/article/pii/S1040618213002449, doi:http://dx.doi.org/10.1016/j.quaint.2013.05.003.